ENERGETICS AND MECHANISM OF BORON/OXIDANT COMBUSTION REACTIONS

BY

ALLEN JONATHAN CAREY GOODFIELD

THESIS SUBMITTED TO THE C.N.A.A. IN PARTIAL FULFILMENT OF

CANDIDATURE FOR THE DEGREE OF DOCTOR OF PHILOSOPHY

DEPARTMENT OF CHEMICAL ENGINEERING

THE POLYTECHNIC OF WALES

TREFOREST , PONTYPRIDD

MID - GLAMORGAN

THE COLLABORATING ESTABLISHMENT WAS
NOBEL'S EXPLOSIVES CO.(ICI) LTD.

MAY,1982.

CONTENTS

CONTENTS(CONTINUED)

CONTENTS(CONTINUED)

ACKNOWLEDGEMENTS

I wish to express thanks to my Academic Supervisor, Dr. G. J. Rees, for his guidance and encouragement throughout this project. Thanks are also expressed to all the staff of the collaborating body, Nobel's Explosives Co.(ICI) Ltd., Ardeer, particularly Dr. J. Morman and Mr. T. McLaughlin for their useful comments on the work.

My appreciation is expressed to the staff, technical and academic, of the Departments of Chemical Engineering and Science at the Polytechnic of Wales for help and guidance given to me during this project.

The support of the Science Research Council, Nobel's Explosives Co.(ICI) Ltd. and the Polytechnic of Wales for this work is gratefully acknowledged.

DECLARATION

This is to certify that neither this thesis nor any part of it has been presented or is being concurrently submitted in candidature for any other degrees

a.j.c. Goodfield

Candidate

Dated 26TH May 1982

Certificate of Research

This is to certify that, except where specific reference is made, the work in this thesis is the result of the investigation carried out by the candidate.

A. & C. Goodfield
Candidate

G. D. Rees
Director of Studies

Dated 26TH May 1982

ENERGETICS AND MECHANISM OF BORON/OXIDANT COMBUSTION REACTIONS

ALLEN JONATHAN CAREY GOODFIELD

ABSTRACT

A brief introduction to the field of pyrotechnic time delays is given, followed by a survey of the published work in the field up to the present time.

A description is provided of the experimental techniques, equipment and materials used.

The energetics and mechanism of reaction in the boron/lead monoxide and boron/stannic oxide systems have been investigated by comparison with the more familiar, analogous silicon fuelled systems; the emphasis being placed on the boron/lead monoxide system.

The heats of reaction of the four fuel/oxidant systems have been measured by the use of bomb calorimetry, the results being discussed in relation to the probable reactions taking place in each system. Conclusions have been drawn as to the nature of the reactions which provide heat outputs in excess of the theoretical values in the boron fuelled systems.

The propagation rates of the four fuel/oxidant systems have been measured and the relationship between heat output and propagation rate in each system is discussed. An explanation is proposed for the apparently anomalous behaviour of the boron fuelled systems. The response of the propagation rates in each system to varying consolidation pressure has been investigated. An explanation is proposed for the difference in behaviour displayed by the boron and silicon fuelled systems.

A method of non-contact temperature measurement using a recording infra-red brightness pyrometer has been investigated. The reaction temperatures of the four fuel/oxidant systems have been measured and their relationships to the response of the propagation rates of each system to consolidation pressure variations are discussed.

The boron/lead monoxide reaction in loose powder mixes has been investigated using differential scanning calorimetry. Hot stage microscopy has been used to investigate boron/lead monoxide reactions in loose powder mixes and between consolidated pellets of the individual reactants. The thermal analysis results obtained demonstrate the effect of the boron oxidation product, B_2O_3, on the reaction rate and the role which it plays in the reaction mechanism in the boron/lead monoxide system. A reaction mechanism is proposed for the non-propagative reaction between boron and lead monoxide.

The extraction and kinetic analysis of data from the differential scanning calorimetry investigation of the boron/lead monoxide system is discussed. It is demonstrated that the analysis of the dynamic data is virtually impossible due to the complexity of the peak patterns obtained.

CHAPTER 1

INTRODUCTION

At the present time no universally accepted definition of pyrotechnics exists, but that put forward recently by Blunt(1) would seem to provide a sound basis for future world-wide agreement.

"Pyrotechnics: The science of controlled exothermic chemical reactions which are used to create timing devices, sound effects, aerosol dispersions, high pressure gas, intense heat, electromagnetic radiation, or combinations of these, and produce the maximum effect from the least volume. High explosives are excluded, but initiators are included."

In civilian and military areas of application pyrotechnic devices are extensively utilised. They are found as precision time delays for use in blasting applications above and below ground; in space technology they are widely used, having proved their worth in terms of their small size, reliability and power to weight ratio. They have found many other applications including fireworks, flares and smokes for signalling, food warming devices and matches.

This thesis is concerned with pyrotechnic systems with potential for use as precision time delays in civilian blasting detonators. In this application the precise staggering of explosions in a series of boreholes reduces vibration and improves fragmentation.

Pyrotechnic systems for use as time delays basically consist of mixtures of oxidising and reducing chemicals in powder form, which when consolidated into columns of various length and cross-sectional geometry, and ignited at one end produce a controlled exothermic

reaction. This reaction manifests itself as an incandescent reaction zone which advances along the column, at a uniform rate, until all the available reactants have been consumed. The rate of advance of the reaction zone is referred to as the propagation rate.

The reducing agent in a pyrotechnic sytem is commonly referred to as the fuel and normally takes the form of a powdered metal or non-metal of which Mg, Al, Si and B are typical examples. The oxidising agent is typically represented either by a powdered oxysalt such as $K_2Cr_2O_7$, or by a powdered oxide such as Pb_3O_4, MnO_2, or Bi_2O_3. An interesting discussion of possible oxidisers for use in pyrotechnic systems is given by Shidlovskii(2).

Delay compositions can be divided into two general categories, the gasless compositions and the 'gassy' or gas-producing compositions.

The gasless compositions produce little or no gaseous products, the products being predominantly in the solid or liquid phase at reaction temperatures. These compositions are useful at high altitude or under confined conditions where the effect of atmospheric pressure variations on the propagation rate of the gas-producing compositions would be unacceptably high.

The gas-producing compositions evolve large amounts of gaseous products but leave little or no solid residue. These compositions can be used at low altitudes and under vented conditions.

The area of concern of this work is the investigation of the energetics and mechanism of the reactions which occur in ostensibly gasless delay compositions and their propagative characteristics.

The gas-producing delay compositions, such as blackpowder(S,C,KNO_3)

represent the early stages in the development of pyrotechnic time delays, which with the increasing demand for more sophisticated and specialised delays,have largely been replaced by the new generation of gasless delays.

Probably the first example of a gasless delay was that described by Hale(3) in 1931. This system was based on Pb_3O_4 and silicon and incorporated nitrocellulose as a binding agent. It is worth mentioning that this composition has withstood the test of time and remains one of the most widely used compositions for the production of blasting time delays in the millisecond delay range.

Other widely used pyrotechnic delay systems include PbO_2/Si (millisecond delays) and $KMnO_4$/Sb($\frac{1}{2}$ second and above delays)(4).

The factors which determine the propagation rate of a given pyrotechnic composition are numerous and the list given by Ellern(5) illustrates the more obvious factors in roughly their order of significance.

1) Nature of the rectants and products.
2) Particle size of the reactants.
3) Relative amounts of the reactants.
4) Ambient atmospheric pressure.
5) Ambient temperature.
6) Degree of compaction.
7) Diameter of column.
8) Nature of the entraining envelope material.

Although this list does not mention them directly it implicitly contains the thermochemical and thermophysical properties of the composition i.e. the thermal conductivity, heat capacity and heat

output of the composition. Also missing from the list is the secondary effect of the internal pressure generated within closed delay assemblies and the effect of any binding agent used on the propagation rate. However, the list does illustrate the complexity of the problem of predicting propagation rates which is a problem which has occupied workers in the field of pyrotechnics for many years.

In order to be able to meet the continually increasing demand for more specialised pyrotechnic devices, continued research effort is required. Blunt(1) identifies seven main areas for research work and support functions which would enable pyrotechnics to advance faster and more effectively than has been the case in the past:

1) Properties of materials.
2) Reaction processes.
3) Flame structure.
4) Standards.
5) Safety.
6) Formalised special education.
7) A recognised technical society to help focus efforts.

CHAPTER 2

LITERATURE SURVEY

The investigation of the chemical reactions taking place in pyrotechnic delay mixtures can be approached in various ways, depending on which aspect of the reaction is of interest.

Spice and Staveley(6) investigated the reactions occuring in compressed iron/barium peroxide and iron/potassium dichromate mixtures, with emphasis being placed on the iron - barium peroxide reaction. The progress of the reactions was determined by quantitative measurement of the disappearance of the magnetic effect due to elemental iron. In this work it was found that in both systems a non-incandescent reaction, called the pre-ignition reaction, sets in at a measurable rate at temperatures below the ignition temperatures of the mixtures.

It was shown that in the iron/barium peroxide system the rate of the pre-ignition reaction is greater, the more highly compressed the pellet and is reduced by addition of ferric oxide as a third component. The conclusion was drawn that the pre-ignition reaction is a genuine solid-solid reaction.

In further work Spice and Staveley(7) measured the linear propagation rates and the heats of reaction of compressed binary, solid mixtures of oxidisers and fuels. The thermochemical results were used to draw conclusions about the chemistry of the reactions involved and about the maximum temperatures reached during the propagation reactions.

Their findings can be summarized as follows:

(1) The maximum in the propagation rate is usually found at a higher, but never a lower, percentage of fuel than that at which the heat of reaction is found.

(2) The chemical reactions taking place may change with changing oxidiser/fuel ratio.

(3) The propagation rate is more sensitive to the chemical nature of the oxidiser than that of the fuel.

(4) The stoichiometry of the reaction taking place in an oxidiser/fuel system could be ascertained by plotting the heat evolved by that quantity of composition containing one gram mole of oxidiser versus percentage fuel(or oxidiser).

(5) Reasonable agreement was obtained between calculated and measured reaction temperatures.

In a series of papers(8-14) Hill and coworkers presented the results of investigations into the propagation characteristics of pelleted iron/barium peroxide, iron/potassium dichromate, iron/potassium permanganate, sulphur/barium peroxide, molybdenum/barium peroxide and molybdenum/potassium permanganate compositions by means of a temperature profile method. In this method a fine wire thermojunction is embedded in the pelleted mixture of reactants and is used to record temperature, as a function of time, as the reaction zone passes the thermojunction. The temperature profile obtained was analysed by means of a thermal conduction theory of combustion wave propagation.

A technique for the rapid measurement of the thermal conductivity of solids by the transient heating of a fine thermocouple junction was also developed.

Emphasis in the work was placed on the iron/potassium permanganate and the molybdenum/potassium permanganate systems with the effect of added chemically inert substances on the iron/potassium permanganate system also being investigated.

The results of the work showed excellent agreement of measured propagation rates of the systems examined with those predicted by the Maillard and Le Chatelier theory(15) of propagation controlled by thermal conduction, especially if they contained a high percentage of a good heat conductor.

In the case of the iron/potassium permanganate reaction it was found that the kinetics at low density(loose powder) are very different from those at high density(hard pellets); and that the difference can be explained on the hypothesis that at low density the reaction takes place by way of the gas phase, and at high density, where interparticle contact is better, by diffusion across solid-solid interfaces. The study of the effect of added chemically inert substances in this system where the reaction is mainly a solid-gas-solid reaction with a rate determined by the rate of decomposition of potassium permanganate is to slow the initial rate of this reaction by a factor of 10^4. A comparison of these initial rates with independently measured rates of the thermal decomposition of potassium permanganate leads to the conclusion that, in combustion, decomposition of permanganate is normally catalysed by contact with iron and that this effect is substantially inhibited by sodium fluoride.

The temperature-profile method was also applied to the molybdenum/potassium permanganate system, the reaction being found to take

place in two stages. The chemical kinetics of the first stage in the temperature range 25–110^{o}C were derived by means of a thermal conduction theory of wave propagation, as in the case of the iron/potassium permanganate system. It was observed that the activation energy decreased with temperature, from which it was deduced that there was a single reaction path having several successive energy barriers.

It was suggested that the first stage of the reaction involved only those permanganate ions which were favourably placed at the boundaries of mosaic blocks, and that these were decomposed by molybdenum ions which had diffused through the dislocation network of the potassium permanganate.

This work provided a combined mathematical and experimental approach that gave a clearer physical model for propagative reactions than was previously available.

Booth(16) developed a general theory of self propagating exothermic or layer-to-layer reactions in the solid phase. A method was described for determining the propagation rate of the reaction zone through a consolidated mixture of reactants in the form of a cylinder, in terms of the physical properties of the powder, its chemical composition and the kinetics of the slow, unlocalised reaction between its constituents.

An exact evaluation of the propagation rate from the equation developed required very tedious numerical integration. A simpler approximate method for estimating propagation rates was developed but with the approximations involved in the development and the

difficulties involved in determining the kinetics of the slow reactions occuring in any given system, the theory and the equation developed were of limited applicability.

Nakahara and Hikita(17-21) carried out a comprehensive investigation of various aspects of the propagation characteristics of several pyrotechnic delay systems including $Mn/PbCrO_4$, $Sb/KMnO_4$, $Fe-Si/Pb_3O_4$ and Fe/BaO_2, culminating in Nakahara(22) publishing, as a result of studies on the $Fe-Si/Pb_3O_4$ system, a semi-empirical theory of layer-to-layer propagation which could be used to examine the effects of atmospheric pressure, reactant particle size and initial temperature on the propagation rate.

The equation developed took the form:

$$V^2 = 2A\lambda T_2^{a+1} p^n / \left[c \varepsilon_2 \rho r_0^b (a+1)(T_2 - T_1) \right]$$

where V = propagation velocity c = specific heat

λ = thermal conductivity ρ = density

T_1 = initial temperature

T_2 = final temperature

p = atmospheric pressure

ε_2 = fraction reacted at final temperature

r_0 = radius of fuel particles

A, a, n, and b are parameters which can be determined from experimental results.

Rees(23,24) made a detailed study of the mechanism of the propagative reaction between iron and potassium dichromate(70/30%wt ratio) by means of a temperature profile method. The temperature profiles obtained were used to derive propagation rates by means

of the Maillard-Le Chatelier theory. The derived propagation rates agreed fairly well with the measured propagation rates, from which it was concluded that the thermal propagation theory provides a good representation of the behaviour of this particular composition. The kinetics at low density were found to differ greatly from those at high density. The difference was explained on the hypothesis that reaction at low density occurs by means of the gas phase, and at high density, where contact between particles is greater, by diffusion across solid-solid interfaces.

Rees(25) also investigated the effect of reduced atmospheric pressure and high speeds of rotation upon the propagation rates of pyrochemical compositions. Reduced atmospheric pressure was found to decrease the propagation rate of a 30 wt.% ferrotitanium/70 wt.% barium peroxide composition, while rotation increased,up to a point, the propagation rate of magnesium/cupric oxide and magnesium/barium sulphate compositions(both 30/70 wt.% ratio). In other respects the mode of propagation followed the mechanism of the Maillard-Le Chatelier theory.

In a further paper Rees(26) derived an expression for the propagation rate of non-gaseous layer-to-layer combustion reactions.

In a series of papers(27-29) Hardt and coworkers examined the diffusion controlled rates of exothermic condensed phase reactions, leading to binary alloy formation, with respect to the principal reaction parameters, heat and mass diffusivities, particle size and heat of reaction.

Three aspects of the reactions were considered. In (27) an analytical model relating propagation rate to the thermochemical

properties of the mixtures was developed. Computer calculations using linear geometry were carried out which gave the temperature and the extent of reaction as a function of distance from the ignition source. An explicit expression relating propagation rate to mixture characteristics was developed by a simplified treatment. Close agreement between experimentally determined and calculated propagation rates was not expected or in fact generally attained due to uncertainties in the assumed values of diffusion coefficients and corresponding activation energies used and uncertainties in measured values of particle size and thermal conductivities. The model developed should also be applicable to thermite type reactions as long as a non-gaseous reaction prevails.

In (28) the linear propagation rates of several exothermic intermetallic reactions were studied experimentally. Boron and carbon mixtures with titanium and zirconium were found to be self-propagating at room temperature but aluminide mixtures and other types of intermetallic reaction mixtures reacted only at elevated temperatures or required additives which reduced their thermal conductivities before self-sustaining reactions could be initiated. It was shown that the adiabatic reaction temperature must exceed the melting point of the alloy product in order to ensure a self-propagating reaction, and that the ignition temperature may be below the melting point of either constituent.

(29) described the experimentally and analytically determined ignition energy requirements for condensed phase binary alloy systems which were found to obey a diffusion-limited reaction model. A model was described for the evaluation of the ignition threshold input

energy either by computer calculations or by approximate formulae. It was found that ease of ignition is promoted by low thermal conductivity, low heat capacity, small particle sizes and high heat of reaction.

Patai and Hoffmann(30) studied the pre-ignition reactions of inorganic oxidants with various combustible substances. Their work showed that in most cases reaction began at a temperature at which neither combustible material nor the oxidant in isolation suffered any appreciable chemical change. They suggested that pre-ignition reactions occur in possibly all oxidant/fuel systems. They also suggested that due to the generally low thermal conductivities of the systems examined, the pre-ignition reactions could play an important role in the propagation reactions.

McLain(31,32) discusses the results of his studies of several pyrotechnic delay systems including boron/barium chromate and silicon/lead dioxide. From the results of measurements of the variation of heat output and propagation rate with oxidiser/fuel ratio in the two systems mentioned above he concludes that their behaviour conforms to the heat transfer mechanism of propagation postulated by Spice and Staveley and by Hill and coworkers. He also reaches the conclusion that the reactions taking place in the two systems are respectively:

$$4B + BaCrO_4 \longrightarrow 4BO + Ba + Cr$$

and $$PbO_2 + Si \longrightarrow Pb + SiO_2$$

Harris(33) made a detailed study of the titanium/lead chromate system. Calorimetric measurements indicated that in this system the

titanium is oxidised to the monoxide, TiO. The effect of added inert material on propagation rates was also studied and it was shown that, to a limited extent, the propagation rates obtained with any given fuel/oxidiser ratio were linearly dependent on the amount of inert material added. Also, the proportionality constant was itself dependent on the fuel/oxidiser ratio and increased as the ratio increased.

In addition it was shown that replacement of any excess oxidiser by inert material has virtually no effect on the propagation rate. This fact suggests that the rate determining step is not the thermal decomposition of the oxidiser and must therefore be the oxidation of the metal. This is consistent with the theory that was advanced that for self-propagation to be possible the reaction must be sufficiently exothermic for the reaction zone to reach the temperature at which titanium oxide melts.

In (34) Harris discusses the results of an investigation into compatibility and stability problems associated with pyrotechnic mixtures. He studied the effect of varying moisture content on the ageing of mixtures and showed that ageing could be reduced considerably by thorough drying of the mixtures. He also showed that the addition of a small percentage of very finely divided silica was very effective in preventing the aggregation of water soluble oxidisers due to crystal growth during storage.

Miller(35) studied the effect of the preparation of boron/barium chromate mixtures by a method of coprecipitation as opposed to mechanical mixing. The results showed a reduction in ignition

temperature, as indicated by DTA curves, of 70°C to 80°C for the coprecipitated mixtures, coupled with the apparent absence of a pre-ignition reaction in coprecipitated mixtures containing low levels of boron. Another effect of the coprecipitation of the mixtures was that their propagation rates were virtually unaffected by reduction of atmospheric pressure to approximately 0·07 atm. Under the same conditions the propagation rates of the mechanical mixes fell by approximately 15%.

Benge(36) also discussed the advantages of the coprecipitation technique as applied to the boron/barium chromate system.

Al-Kazraji and Rees(37) studied the silicon/red lead(Pb_3O_4) system. Calorimetric measurements indicated that the heat output reached a maximum at 10 wt.% Si, independent of the fuel particle size, whereas propagation rate measurements indicated a maximum at 30 wt.% Si for coarse silicon and at 15 wt.% Si for fine silicon. The products obtained were mixtures of SiO_2, Pb and unreacted Si, the proportions depending on the original composition.

Compositions containing less than 20 wt.% Si were found to give violent reactions, high reaction temperatures causing considerable vaporization of the products, whereas compositions containing 20 wt.% to 50 wt.% Si were of practical value with reactions producing very little vaporization.

Bradley and coworkers(38) investigated the reaction of consolidated pellets of powdered magnesium with similar pellets of various metal oxides separated by a 2mm gap in oxygen free atmospheres at temperatures from 625°C to 1000°C. From an examination

of the weight changes of each pellet after reaction they deduced that the rate of reaction was controlled by the evolution of magnesium vapour.

Collins and coworkers(39) studied the ignition of titanium subhydride/potassium perchlorate compositions by electrostatic discharge. They showed that the ignition is due to a metal-air reaction rather than to the pyrotechnic reaction as previously supposed. Compositions were more sensitive to ignition in oxygen/nitrogen atmospheres than in oxygen/argon atmospheres due to the additional propagation reaction pathway offered by the nitriding of titanium. Humidity was also observed to be a moderator in the electrostatic ignition process.

Collins(40,41) investigated the thermal ignition of titanium hydride/potassium perchlorate compositions. It was shown that the thermal ignition was controlled by titanium oxides which encapsulate the metal particles. As the titanium powder was heated the oxide coating dissolved into the bulk metal to generate a reactive surface. The surface was reoxidised immediately by oxygen gas from the surrounding atmosphere, but with insufficient heat generation for sustained combustion. Ignition was kinetically determined by the rate of dissolution of the oxide coating relative to the rate of reoxidation.

Moghaddam and Rees(42) investigated the reaction between titanium and barium chromate. Heat outputs and propagation rates were measured for various fuel/oxidiser ratios and it was found that the maxima occur at 30 wt.% and 35 wt.% Ti respectively.

The effect of preheating compositions was also investigated and it was proposed that the main cause of the reductions in heat output observed were caused by the reaction of titanium with atmospheric oxygen forming titanium dioxide. It was concluded that the reaction taking place in this system was:

$$3Ti + BaCrO_4 \longrightarrow 3TiO + BaO + Cr$$

Thomson and Wild(43) investigated the propagation characteristics of a titanium/strontium nitrate based composition with regard to the physical properties of the titanium and strontium nitrate particles. They found that the propagation rate of the composition decreased as the porosity of the titanium decreased and that of the strontium nitrate increased, and also decreased as the titanium particle size increased.

Speros and Debesis(44) have investigated the concept that the combustion of solid oxidant/fuel systems is governed by thermodynamically predictable oxidant dissociation pressures and measurable kinetics of oxygen evolution and shown this to be consistent with the experimental results obtained. A combustion model was developed which indicated that some oxidant/fuel systems should exhibit an amplification of the combustion rate. This effect was due to:

(1) oxidant/fuel coupling associated with the exponential increase in combustion rates with temperature,

(2) sequential oxidant coupling in systems, such as Zr/Co_3O_4 - $BaCrO_4$ - Fe_2O_3, containing oxidants dissociating at sequentially increasing temperatures and rates.

The net effect is that of a 'kinetic stepladder' and this was confirmed experimentally using loose powder zirconium fuelled compositions.

The preceding work was concerned almost exclusively with the investigation of consolidated compositions and the information that could be obtained by examining their propagative reactions. Pyrotechnic compositions can also be examined as loose powders using thermal analysis techniques.

Thermal analysis, in common with pyrotechnics, has a long history but in its modern form arose from the combination of pyrometry and clay mineralogy in the late nineteenth century. The work of Roberts-Austen(45), Urbain and Boulanger(46) and Honda(47) represent landmarks in the development of thermal analysis techniques.

Thermal analysis techniques are becoming of increasing interest to workers in the field of pyrotechnics. Boddington and coworkers(48) studied the reaction between tungsten and potassium dichromate(1:1) by temperature profile analysis and differential thermal analysis. From the temperature profile obtained the rate of heat evolution as a function of time was derived which indicated that the reaction takes place in two exothermic stages. Non-ignition DTA curves obtained for the reaction were very similar to the power function derived from the temperature profile analysis.

Examination of the intermediate and final products from non-ignition DTA, using chemical and X-ray analysis, indicated that the two exothermic reactions were:

$$W + 2K_2Cr_2O_7 \longrightarrow WO_3 + 2K_2CrO_4 + CrO_3 \quad ---(1)$$

$$W + WO_3 + 2K_2CrO_4 \longrightarrow 2K_2WO_4 + Cr_2O_3 \quad ---(2)$$

A third endothermic peak was also found which corresponded to the fusion of the potassium tungstate formed in reaction (2) above.

Two further papers have been published by Boddington and Laye(49,50) covering basically the same work as described above.

Laye and Tipping(51) studied by temperature profile analysis the role of heat transfer in the propagative reaction between tungsten and potassium dichromate(35/65 % wt. ratio). The results indicated that radial heat conduction ahead of the reaction zone and axial conduction behind it exert only a small influence on the combustion wave.

Charsley and Tolhurst(52) described the application of hot stage microscopy to the study of pyrotechnic systems. Direct observation of the thermal behaviour of individual components and their mixes, using a stereomicroscope, were supplemented by 35mm photomicrography and high speed and time lapse cine photography. Results were presented for magnesium nitrate and for the tungsten/potassium dichromate system.

Charsley and Ottaway(53,54) studied the reaction between boron and molybdenum trioxide using a combination of differential thermal analysis and hot stage microscopy. They found that the reaction involved sequential, exothermic reduction of the molybdenum trioxide over the temperature range 400°C to 1100°C. The reactions under non-ignition conditions could be described by the following

equations:

exotherm 1 + 2 $\quad 2B + 3MoO_3 \xrightarrow{\text{PARTIAL}} B_2O_3 + 3MoO_2$

exotherm 3 $\quad 2B + 12\ MoO_3 \longrightarrow B_2O_3 + 3Mo_4O_{11}$

exotherm 4 $\quad 2B + Mo_4O_{11} \longrightarrow B_2O_3 + 4MoO_2$

exotherm 5 $\quad 4B + 3MoO_2 \longrightarrow 2B_2O_3 + 3Mo$

They concluded that the ignition reactions differ from those under controlled conditions in that in the presence of excess boron molybdenum borides are formed which increase the overall heat output of the reaction. It was considered likely that boride formation was being observed as the glowing reaction following ignition on the hot stage microscope.

Campbell and Beardell(4) described a differential thermal analysis apparatus, developed by them, in which the sample is heated under conditions of complete volume confinement. The sample and reference material are tightly confined to their original volume during the heating cycle. The apparatus was used mainly to study a tungsten/potassium perchlorate/barium chromate(65/15/20 % wt. ratio) composition, an antimony/potassium permanganate(36/64 % wt. ratio) composition and a zirconium/ferric oxide/silicon dioxide(65/25/10 % wt. ratio) composition, the heating rate in each case being $15^{o}\ min^{-1}$.

Reaction in the tungsten fuelled composition appeared to be little affected by the degree of confinement. However, the reaction in the antimony fuelled composition appeared to be inhibited under confined conditions. They attributed the inhibition to suppression of the dissociation of MnO_2, a decomposition product of potassium permanganate, under confined conditions

the reaction yielding final products of MnO and Sb_2O_3 as opposed to Mn_2O_3 and Sb_2O_5 in the unconfined reaction.

In the case of the zirconium fuelled composition the reaction was seemingly enhanced. This was accounted for by the observation that when a consolidated column of the composition is ignited in an unconfined state, the column undergoes an apparent two-fold expansion in volume due to the porous nature of the reaction products, Fe_3O_4, SiO_2(amorphous), ZrO_2 and Fe_2O_3. Under conditions of total confinement this expansion is prevented, keeping the reacting components in close contact, thus, inhibiting heat loss from the reaction. Under these conditions the reaction products were found to be Fe_3O_4, SiO_2(α-quartz), $ZrSiO_4$ and Fe_2SiO_4.

Howlett and May(55) investigated the reactions taking place in the $B/K_2Cr_2O_7$ and $B/Si/K_2Cr_2O_7$ systems and of the individual components, in a flowing dry oxygen atmosphere, using differential scanning calorimetry. They found that ignition of the compositions was coincident with fusion of the oxidant in all cases. They concluded that ignition in both of the systems studied was dependent on liquid phase transport, the reaction zone propagating as a molten front.

Al-Kazraji and Rees(56) studied the reaction between silicon and red lead(Pb_3O_4) and the individual components by differential thermal analysis and thermogravimetry in air and nitrogen atmospheres. They reached three main conclusions:

(1) thermal decomposition of Pb_3O_4 occurs at 590°C

(2) in air three exotherms occur with all oxidiser/fuel ratios at temperatures of 590°C, 670°C and 760°C, corresponding to

reaction of Si with Pb_3O_4, oxidation of molten lead and formation of lead silicates respectively

(3) infra-red spectroscopy and X-ray diffraction measurements confirmed the presence of SiO_2 as a reaction product from DTA in a nitrogen atmosphere and PbO, Si and SiO_2 as reaction products from DTA in air.

Al-Kazraji and Rees(57) also studied the reactions between silicon and lead monoxide and between silicon and lead using differential thermal analysis in air and nitrogen. Using 70/30 (% wt. ratio) compositions they showed that the reactions follow the same pattern in temperature of occurrence and relative sizes of peaks as for the Pb_3O_4/Si reactions described in (56).

Moghaddam and Rees(58) studied the reaction of silicon with PbO and with Pb_3O_4 by differential scanning calorimetry, thermogravimetry and hot stage microscopy in flowing nitrogen atmospheres. Their main conclusion was that in both systems the main reaction was between Si and PbO, thermogravimetry showing that in the Pb_3O_4/Si system, in loose powder form, the oxygen evolved by decomposition of the Pb_3O_4 is lost from the system.

Sulacsik(59) studied the ferrosilicon(90% Si)/MnO_2 system by simultaneous DTA, TG and DTG. He found that some oxygen evolved from MnO_2 leaves the system before a temperature is reached at which the ferrosilicon becomes reactive. The maximum rate of decomposition of MnO_2 is practically independent of the constitution of the mixture. The ferrosilicon was found to become reactive at approximately 800^{o}C, the reaction being exothermic with the

most violent reaction being found in mixtures containing 72·8% MnO_2. The temperature and duration of the reaction were sufficient for completion of all reactions, the release of oxygen and oxidation of the ferrosilicon taking place simultaneously.

It was also found that below 41% and above 82% MnO_2 content the decomposition of MnO_2 and oxidation of the ferrosilicon were independent, with no coupling of the two reactions taking place.

Thermal analysis techniques have not, up to the present time, found much application in the investigation of the reaction kinetics of pyrotechnic reactions. Generally, thermal analysis techniques have been applied to reaction kinetics in other fields, mainly clay mineralogy. The following papers, although on the whole not directly related to pyrotechnics, give some idea of the approaches taken to the problem.

Murray and White(60,61) investigated the isothermal kinetics of the thermal dehydration of clays which were shown to obey a first order law. From the isothermal kinetic parameters obtained they generated theoretical DTA curves for the clay minerals examined. They drew two important conclusions from their work:
(1) The clay mineral is only 70% decomposed at the peak maximum temperature and hence the return of the curve to the baseline is not entirely due to thermal diffusivity.
(2) The heating rate has a marked effect on the peak maximum temperature obtained, it being displaced to higher temperatures as the heating rate is increased.

Kissinger(62) extended the work of Murray and White(61) and

derived an expression relating the variation of peak temperature with heating rate to the kinetics of the reaction taking place. The working equation developed was:

$$d(\ln \Theta/T_m^2)/d(1/T_m) = -\frac{E}{R}$$

where Θ = heating rate

T_m = peak maximum temperature

E = activation energy

R = universal gas constant

Therefore, by measuring the peak maximum temperature at a number of different heating rates and plotting $\ln \Theta/T_m^2$ versus $1/T_m$, a straight line of slope $-\frac{E}{R}$ is obtained.

Borchardt and Daniels(63) derived equations, applicable to homogeneous stirred conditions, which relate the shape of a DTA curve to the kinetics of the reaction giving rise to the curve. The working equation developed for a first order reaction is shown below:

$$k_t = \frac{C_p(d\Delta T/dt) + K\Delta T}{K(A - a) - C_p\Delta T}$$

where k_t = first order rate constant at time t

A = total peak area

a = partial peak area at time t

ΔT = peak height at time T

$d\Delta T/dt$ = slope of DTA curve at time t

C_p = heat capacity of sample

K = heat transfer coefficient of reactant cell

Although rate constants are calculated for particular times across the DTA peak each time has a corresponding temperature, determined by the heating rate used. Therefore, an Arrhenius plot of $-\ln k$ versus $1/T$ can be constructed from which the kinetic parameters can be obtained.

Despite having been applied in the past to reactions between solids the method is now regarded as being of very limited applicability.

Ozawa(64) has developed a method for determining kinetic parameters which does not require a knowledge of the kinetic equation appropriate to the reaction. The working equation is shown below:

$$\log \Theta_1 + 0{\cdot}457(E/R)/T_1 = \log \Theta_2 + 0{\cdot}457(E/R)/T_2$$

where temperatures T_1 and T_2 are taken at an arbitrary but identical value of fraction reacted in the two curves corresponding to heating rates Θ_1 and Θ_2. Plotting $\log \Theta$ versus $1/T$ for selected values of fraction reacted should produce straight lines, enabling activation energy, E, to be obtained.

Rogers and Morris(65) suggested a method of estimating activation energies using a differential scanning calorimeter. If sample size, heat of reaction and heat evolution rate are known, the rate constant at any temperature can be calculated. An Arrhenius plot of the data can be made and the activation energy can be determined.

Data from the DSC are in the form of distances between the reaction curve and a baseline at the associated absolute temperature.

The distance measured is proportional to the rate of heat evolution or absorption and is, therefore, proportional to the rate constant. Provided that the Arrhenius plot is a straight line the activation energy can be calculated from the expression:

$$-E = R\,\frac{\ln d_1 - \ln d_2}{1/T_1 - 1/T_2} = \frac{4{\cdot}58\log(d_1/d_2)}{1/T_1 - 1/T_2}$$

where d_1 and d_2 are any two distances from the baseline at the associated absolute temperatures T_1 and T_2. The distances enter the calculation as a ratio; therefore, the proportionality constants cancel. Neither sample weight nor heat of reaction needs to be known to calculate the activation energy.

Tang and Chaudhri(66,67) provide a critical and comprehensive review of the methods for the analysis of isothermal and dynamic kinetic data from solid-state reactions, which covers all the preceding methods, together with their theoretical backgrounds.

CHAPTER 3

SCOPE OF THE WORK

In order to provide information of interest to the cooperating body, as well as of purely academic interest, it was decided that rather than carry out a detailed examination of a single pyrotechnic delay system, more useful information could be obtained by examining in reasonable detail several related systems. Towards this end it was decided to carry out a study of two boron fuelled systems and to compare them with the more familiar, corresponding silicon fuelled systems. In this way it was hoped that any significant differences in behaviour or common characteristics could be identified and related to the energetics and mechanisms of the reactions taking place.

The four pyrotechnic systems selected for examination were PbO/B, PbO/Si, SnO_2/B and SnO_2/Si. The pairs of oxidisers and fuels provide interesting comparisons in terms of their physical and chemical properties. Also, the two oxidisers do not display any low temperature decomposition reactions and it was hoped that it would be possible to deal exclusively with condensed phase reactions.

The work can be divided into two main areas; the first is an examination of the four pyrotechnic systems under propagative conditions by means of propagation rate measurements, heat output measurements and reaction temperature measurements under operating conditions. The second is an examination of the PbO/B system under non-propagative conditions by thermal analysis techniques. Supportive techniques used include X-ray diffraction and I.R. spectroscopy.

CHAPTER 4

EXPERIMENTAL TECHNIQUES, EQUIPMENT AND MATERIALS

4.1 SAFETY PRECAUTIONS

It is necessary to take appropriate safety precautions when preparing and working with pyrotechnic compositions as they tend to be sensitive to ignition by impact, friction and static electricity. Spark free tools and equipment are used throughout the mixing, drying, delay element loading and delay assembly firing operations, which are also carried out behind armoured safety screens. Safety clothing including gloves, face mask, goggles and electrically conducting shoes are used when carrying out all potentially hazardous operations.

All pyrotechnic compositions are prepared and loaded into delay elements in a small laboratory, located outside the main laboratory area, with all electric points and switches externally positioned. The pyrotechnic compositions are stored in sealed glass containers, in an earthed brass cupboard in this building. The temperature of the preparation, delay element loading and storage laboratory is thermostatically maintained at approximately $25^{o}C$.

A comprehensive review of the hazards and safety precautions associated with the preparation, handling, storage and transport of pyrotechnic materials is given by McLain(32).

4.2 SURFACE AREA DETERMINATIONS

The specific surface areas($m^2\ g^{-1}$) of the materials used in this work were determined using a Strohlein area meter (Model OPI). The operation of the apparatus depends on the method of low temperature nitrogen adsorption according to Brunauer, Emmet and Teller. With this apparatus the determination of surface area has been considerably simplified as only a single point on the adsorption isotherm is determined and the samples are outgassed in a heating block so that no expensive vacuum equipment is required.

The measuring principle is based on the use of two glass adsorption vessels of the same volume; one of them is filled with the sample (measuring vessel) while the other remains empty (reference vessel). Both vessels are filled at ambient temperature with dry nitrogen at atmospheric pressure; the two vessels are then cooled in the cold bath to the temperature of liquid nitrogen. The adsorption of the nitrogen on the sample results in a pressure difference between the measuring and reference vessels which is indicated on the differential manometer.

The specific surface area of the sample is calculated from the equation given below:

$$S_g = \frac{A\Delta h}{m}$$

where A = numerical factor

Δh = manometer pressure difference (mm of manometer liquid)

m = sample weight (g)

S_g = specific surface area ($m^2\ g^{-1}$)

The numerical factor, A, depends only on the measured manometer pressure difference and the atmospheric pressure at the time of the determination, and is obtained by the use of a nomogram.

Description of the heating block and preparation of samples

The heating block is metallic with an infra-red heating facility and is insulated against heat loss by a casing consisting of several shells. The block is equipped to take eight adsorption vessels at the same time.

The heating block is illustrated in Figure 4.1 with the main components indicated as follows:

a - nitrogen gas inlet with regulating valve

b - silica gel drying tube

c - flow meter

d - connector

e - drying tube clamp screw

f - nitrogen gas outlet

g - connecting tube

h - purging capillaries

i - vessel supports

k - support pins

l - thermostat

m - indicating lamps

The heating block is used to dry the sample and to remove any foreign molecules which may already be adsorbed, by purging with dry nitrogen gas while the sample is heated to 150^{o}C. In this work

FIGURE 4.1

SURFACE AREA METER HEATING BLOCK

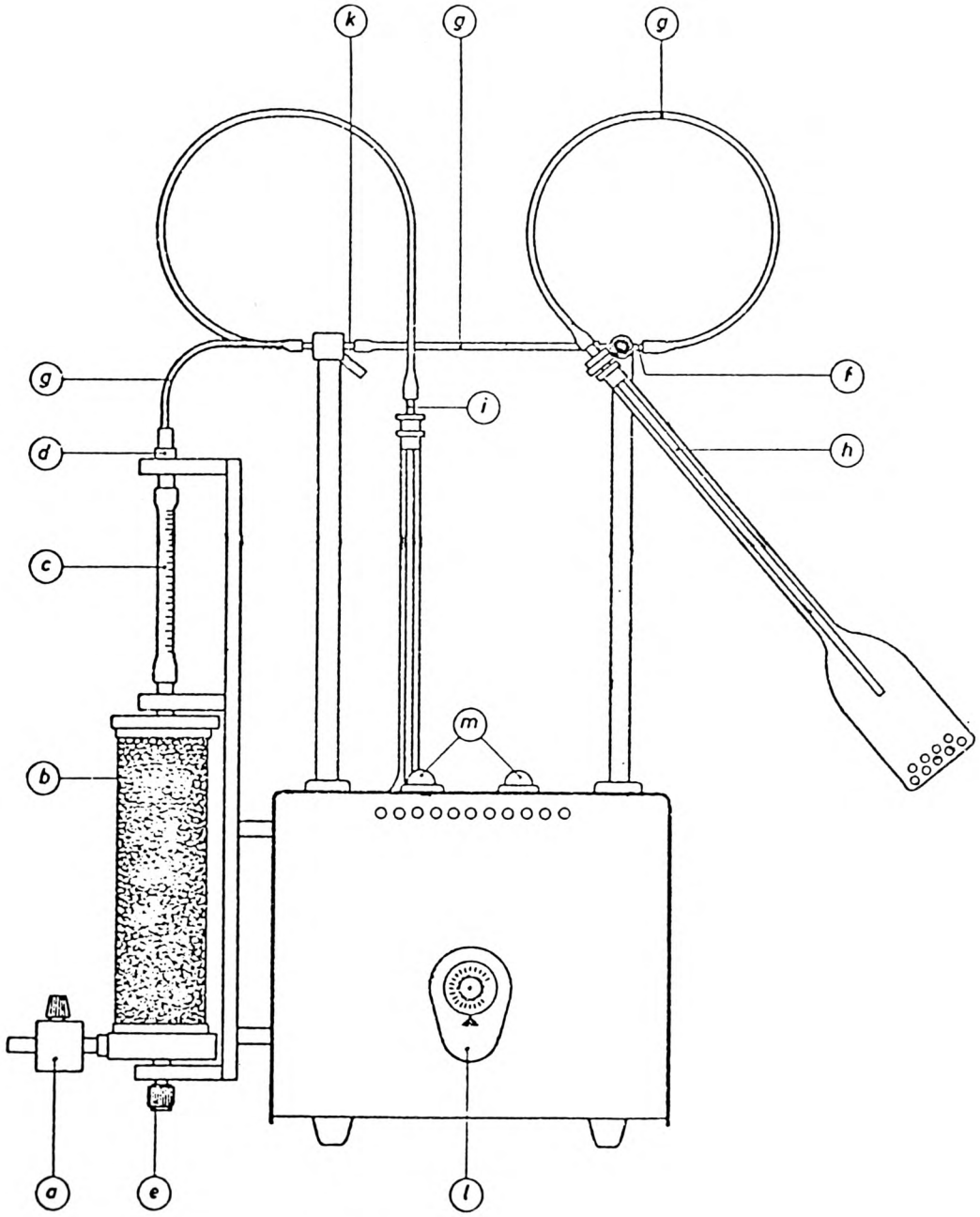

FIGURE 4·2

SCHEMATIC DIAGRAM OF SURFACE AREA METER ADSORPTION APPARATUS

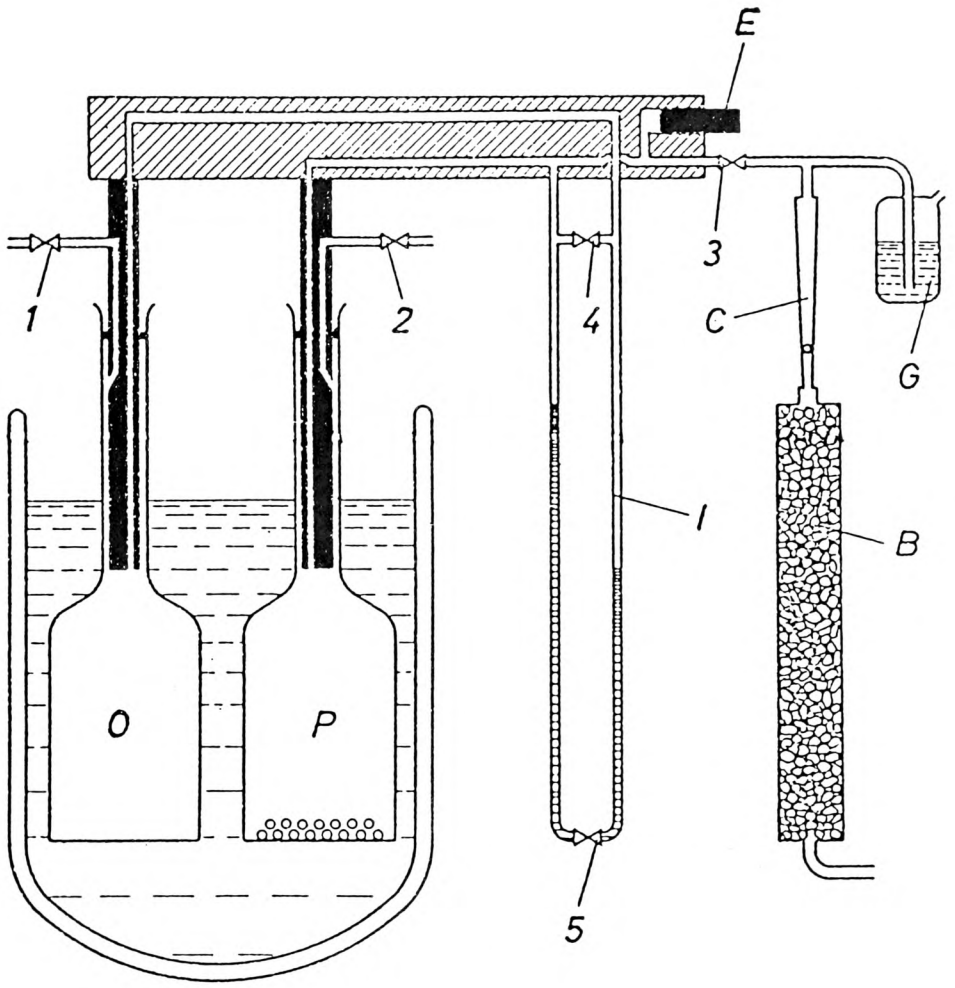

the samples were held at the elevated temperature and purged for one hour, or until a constant sample weight was obtained. Before removing the samples from the heating block they are allowed to cool to room temperature while maintaining the flow of purge gas, at which time they are either tightly stoppered or placed immediately into position on the measuring apparatus.

Description of the measuring apparatus and measuring procedure

Figure 4.2 is a schematic diagram of the adsorption apparatus. The arrangement and function of the various valves (1-5) can readily be seen, also that the adsorption vessel (P), which contains the sample, is connected to the left-hand manometer limb which is also connected to the adjustable balancing volume (E). The empty adsorption vessel (O) which serves as a reference volume is connected to the right hand manometer limb.

Figure 4.3 shows the measuring apparatus with its main components indicated as follows:

A - nitrogen gas inlet with regulating valve

B - silica gel drying tube

C - flow meter

D - protection tube

E - adjustment screw for volume balancing

F - cover

G - over-pressure vessel

H - manometer connectors

I - differential manometer

J - adjustable scale

K - adjustment knob for scale

FIGURE 4·3

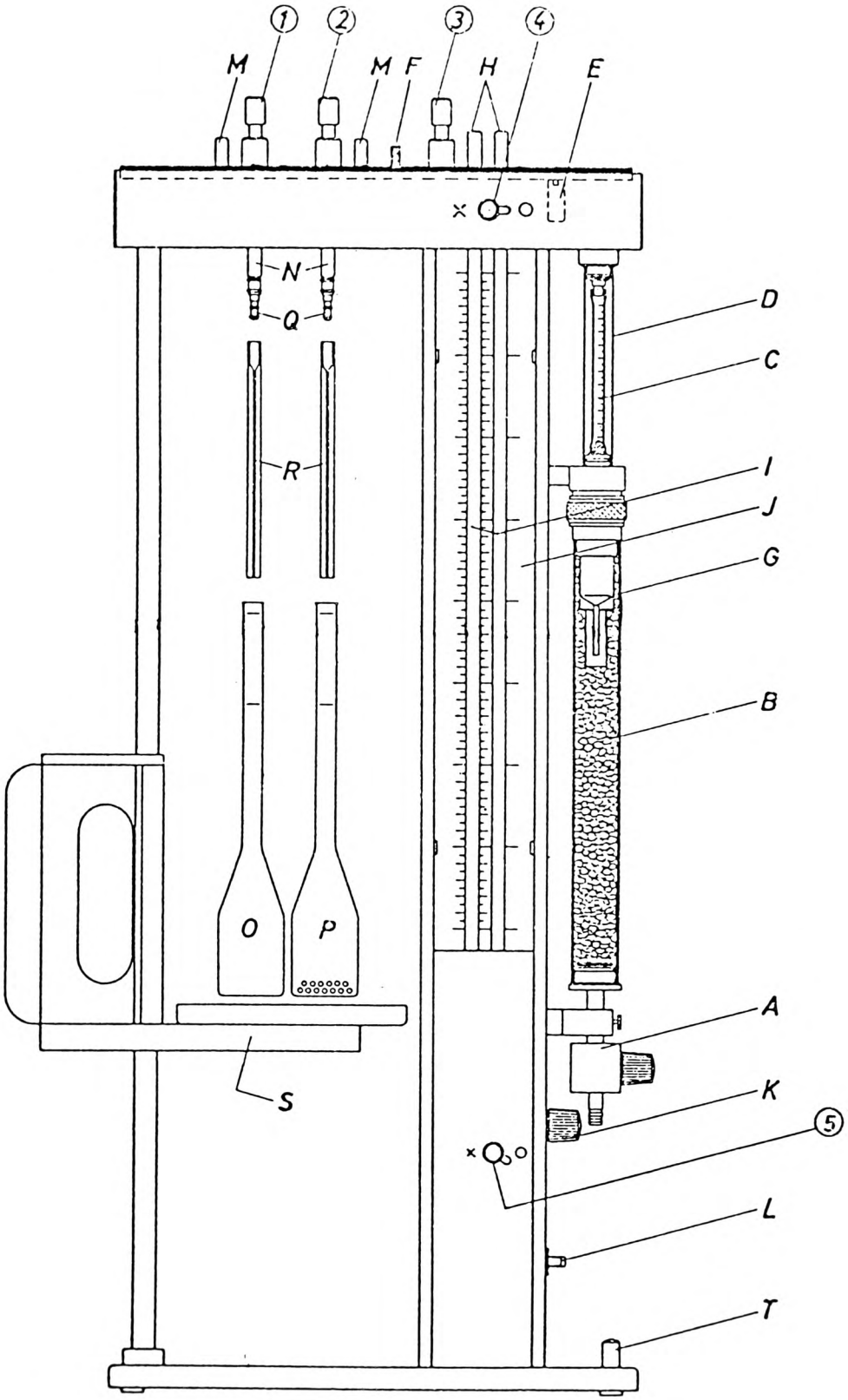

SURFACE AREA MEASURING APPARATUS

L - switch for scale illumination

M - nitrogen gas outlet

N - nipples for adsorption vessels

O - empty adsorption vessel as reference

P - adsorption vessel with sample

Q - connectors for displacement capillaries

R - displacement capillaries

S - adjustable table for baths

T - levelling screw

1 - outlet valve (reference vessel)

2 - outlet valve (sample vessel)

3 - inlet valve

4 - manometer valve

5 - stop valve

Before carrying out a surface area measurement it is necessary to check the volume balance of the sample and reference sides of the apparatus. This check is carried out by performing a blank test with no sample present.

An empty adsorption vessel is placed on each of the two nipples; the upper mark on the neck of the vessel coinciding with the lower sealing ring. The apparatus is then purged with nitrogen gas by opening all five valves. During purging the adsorption vessels are immersed in a water bath at room temperature up to the upper mark on the neck of the vessels. This procedure balances the temperatures of the two vessels. The purging and temperature equilibration is normally completed in ten minutes. The five valves are closed, the apparatus then being closed against the atmosphere, and the two

adsorption vessels are separated from each other and each connected to one of the manometer limbs.

The two vessels are then removed from the room temperature water bath, dried and immersed in a liquid nitrogen bath up to the lower mark on the necks. After cooling for five minutes the stop valve (5) is very slowly opened, thus linking the two vessels by way of the manometer. If a pressure difference is observed it is necessary to balance the volumes of the two sides of the apparatus by use of the volume adjustment screw (E). However, no adjustment is normally necessary.

The procedure for determining the surface areas of the materials used is identical to that followed in the blank test except that the weighed sample is placed in the right hand adsorption vessel and no volume balancing is required.

To obtain the greatest accuracy with this technique the sample weight is chosen so that a pressure difference of between 100 and 300 mm is obtained on the manometer.

4.3 PREPARATION OF COMPOSITIONS, DELAY ASSEMBLIES AND MEASUREMENT OF DELAY TIME

4.3.1 PREPARATION OF COMPOSITIONS

Before mixing, the individual components of the pyrotechnic compositions were passed through a 106 micron sieve to remove any large aggregates present. The required amounts of oxidiser and fuel were then accurately weighed, a maximum of 20g of composition being prepared at any one time. Larger quantities were prepared by blending of 20g lots to a maximum of 100g.

The compositions were then mixed by hand, on paper, using a horn spatula; passed twice through a 300 micron sieve and once through a 106 micron sieve. At this stage the compositions were slurried with an aqueous solution of an organic binder. For stannic oxide containing compositions the binding agent used was sodium carboxymethyl cellulose, while for lead monoxide containing compositions starch was used as the binding agent.

It was necessary to use starch as the binding agent with the lead monoxide containing compositions as with carboxymethyl cellulose they produce slurries which gel, also losing large amounts of water and causing separation of the two components.

The slurries produced were then partially dried in an oven at $80^{o}C$, the resulting 'cake' being broken up and passed through an 850 micron sieve to produce granules of composition. The granules were then returned to the oven for half an hour to complete the drying process. When completely dry the granules were gently sieved in a 106 micron sieve to remove any fine fractions which might

not flow easily from the hopper of the delay element loading press.

All compositions were used within one week of preparation to avoid the effect of ageing processes on the propagation rates.

The amount of starch incorporated in the compositions containing lead monoxide was 0·8%(wt/wt), while the amount of carboxymethyl cellulose incorporated in the stannic oxide containing compositions was 0·5%(wt/wt). The difference in binder levels was necessary because of the lower viscosity, and hence the lower slurrying ability, of the starch solutions relative to that of the carboxymethyl cellulose solutions.

4.3.2 LOADING OF DELAY ELEMENTS

The granulated compositions were loaded into zinc die-cast delay elements(normally of 10mm length) using a pneumatically operated press. The consolidation pressure of the composition in the delay element can be varied and the compositions loaded and pressed in small increments to give a more evenly consolidated column.

The air supply pressure to the press is indicated by a gauge reading in lbs/in^2. Figure 4.4 illustrates the relationship between the displayed gauge pressure and the consolidation pressure obtained in the loaded delay element, which was obtained by the use of a statimeter.

The dwell time of the pressing head on the composition was set at two seconds for all compositions, while unless otherwise stated, the consolidation pressure in all cases was $6·1 \times 10^4$ kN m^{-2}.

FIGURE 4.4 GAUGE PRESSURE VERSUS CONSOLIDATION PRESSURE IN DELAY ELEMENT FOR INCREMENTAL FILLER

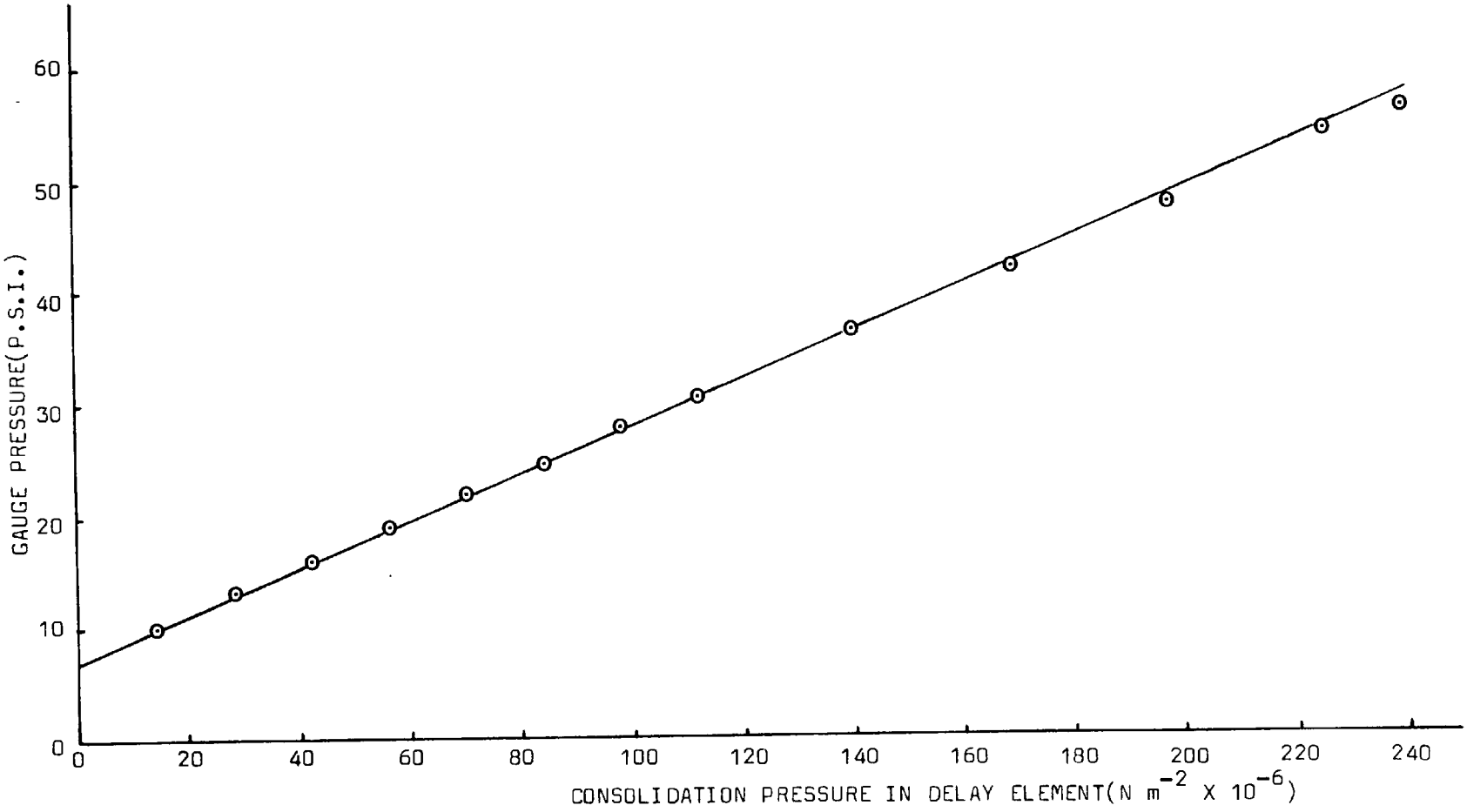

A detailed description of the pneumatic press is given by Al-Kazraji(68).

4.3.3 PREPARATION OF DELAY ASSEMBLIES

The loaded delay elements were placed inside aluminium detonator tubes, containing a hole sealed by a perspex plug at one end, and rammed hard home using a hand operated press. An electrical igniter was then crimped into position at the other end to give a gas-tight delay assembly.

The completed delay assembly is similar to the delay detonator illustrated in Figure 6.1, except that the tube is punctured at the detonating end and the base charge and the priming charge are replaced with a perspex plug.

4.3.4 MEASUREMENT OF DELAY TIME

Delay times for the four oxidiser/fuel systems examined have been measured using a Racal Universal Counter timer, Model No. 9901. The timer was linked to the firing circuit in such a way that timing was started when the firing switches were depressed and stopped when a photoelectric cell detected the light emitted by the reaction zone as it reached the end of the delay element and was transmitted through the perspex plug.

A schematic diagram of the delay time measuring apparatus is shown in Figure 4.5.

FIGURE 4·5

BLOCK DIAGRAM OF DELAY TIME MEASURING APPARATUS

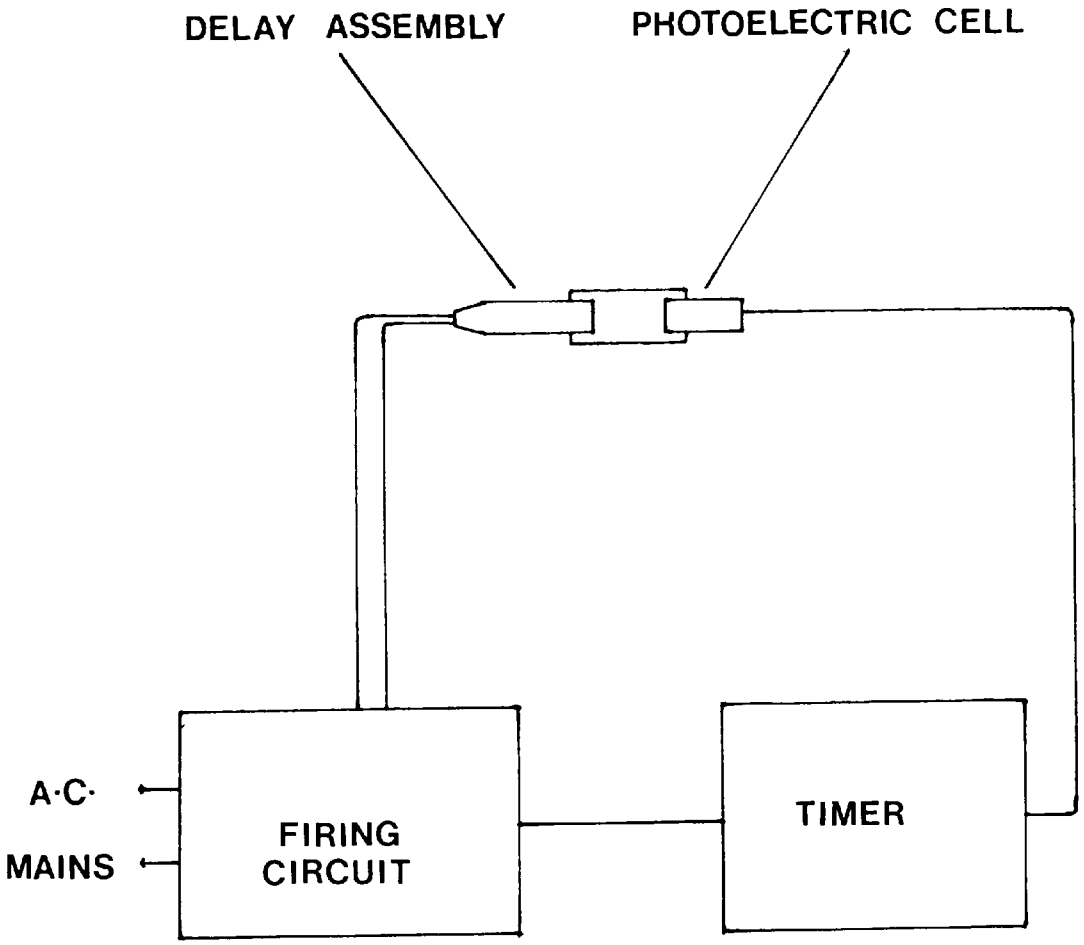

4.4 CALORIMETRY

The heats of reaction of the pyrotechnic systems examined have been determined using a Parr 1421 Semimicro Bomb Calorimeter in a nitrogen atmosphere at atmospheric pressure. This instrument has a working temperature range of 20^{o} to 30^{o}C. Temperature sensing is achieved by the use of a thermistor thermometer in the water jacket. The calorimeter is capable of measuring energy changes from approximately 200J to 5kJ. The bomb has a volumetric capacity of 22ml.

A cross-sectional diagram of the bomb with identification of the main parts is shown in Figure 4.6.

At the start of a test in this calorimeter the bomb, containing the sample and with the ignition lead attached, is immersed in a glass Dewar flask containing 400 +/- 0·1g of demineralised water which is situated in a thermally insulated air can. In all tests carried out the calorimeter water was initially at a temperature of approximately 23^{o}C.

The air can cover, containing the mechanical stirrer, is then fitted and the thermistor probe is inserted into the calorimeter water through the hole in the cover. The stirrer drive belt is then fitted and the stirrer motor started.

Temperature sensing throughout the calorimetric run is provided by the thermistor probe and an electronic bridge which is built into the calorimeter air can. The electronic bridge can be balanced to produce a zero voltage output at any temperature between 20^{o} and 30^{o}C. Within this range the thermistor output is linear with

FIGURE 4.6

CROSS-SECTIONAL DIAGRAM OF PARR SEMIMICRO CALORIMETER BOMB

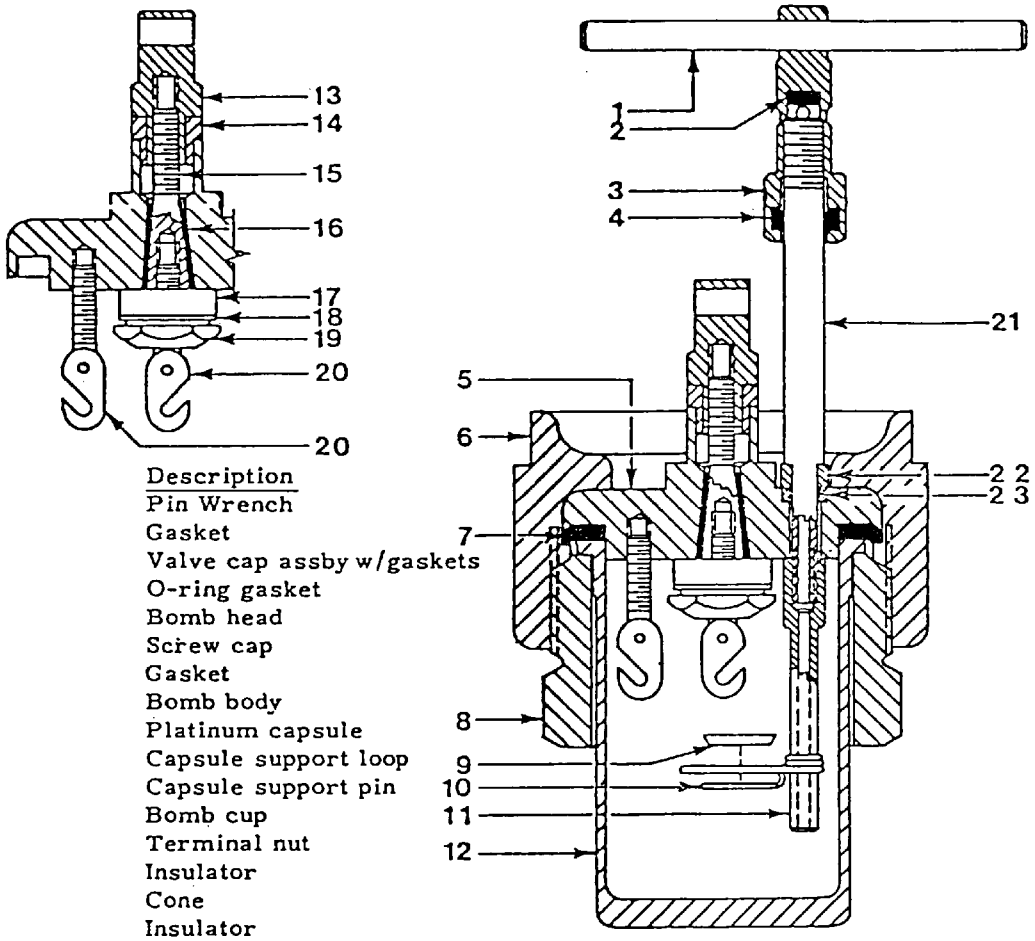

Ref.	Description
1	Pin Wrench
2	Gasket
3	Valve cap assby w/gaskets
4	O-ring gasket
5	Bomb head
6	Screw cap
7	Gasket
8	Bomb body
9	Platinum capsule
10	Capsule support loop
11	Capsule support pin
12	Bomb cup
13	Terminal nut
14	Insulator
15	Cone
16	Insulator
17	Mica washer
18	Monel washer
19	Lock nut
20	Electrode hook
21	Gas tube
22	Bushing
23	O-ring gasket

each 100 microvolt change representing a temperature change of exactly $0{\cdot}001^{o}C$. The voltage output from the electronic bridge is fed to a potentiometric strip chart recorder. In this work the chart recorder was set at a sensitivity of 100mV(full scale deflection) representing a full scale deflection of $1^{o}C$. In all tests the temperature rise was arranged to be approximately $0{\cdot}5^{o}C$.

When sufficient time has been allowed for the calorimeter to come to thermal equilibrium, indicated by linearity of the temperature trace, the reaction is initiated by electrically igniting a fuse which in turn ignites the sample. The reaction then proceeds to completion and the heat produced by the reaction raises the temperature of the calorimeter. The temperature rise produced is recorded on the strip chart recorder and when the trace again becomes linear, indicating that the calorimeter has once again achieved thermal equilibrium, the temperature recording is terminated.

A typical example of the type of temperature recording, which is described as a thermogram, is illustrated in Figure 4.7. This figure also indicates the method used for measuring the recorded temperature rise on the thermogram. In Figure 4.7 R is the midpoint vertical distance between the extrapolated preperiod and postperiod portions of the temperature trace, while ΔT_c is the corrected temperature rise measured at 0·63R.

The energy change, Q, measured in this calorimeter is calculated by multiplying the net corrected temperature rise, ΔT_c, by the energy equivalent, e, of the calorimeter. If ΔT_c is measured in

FIGURE 4·7

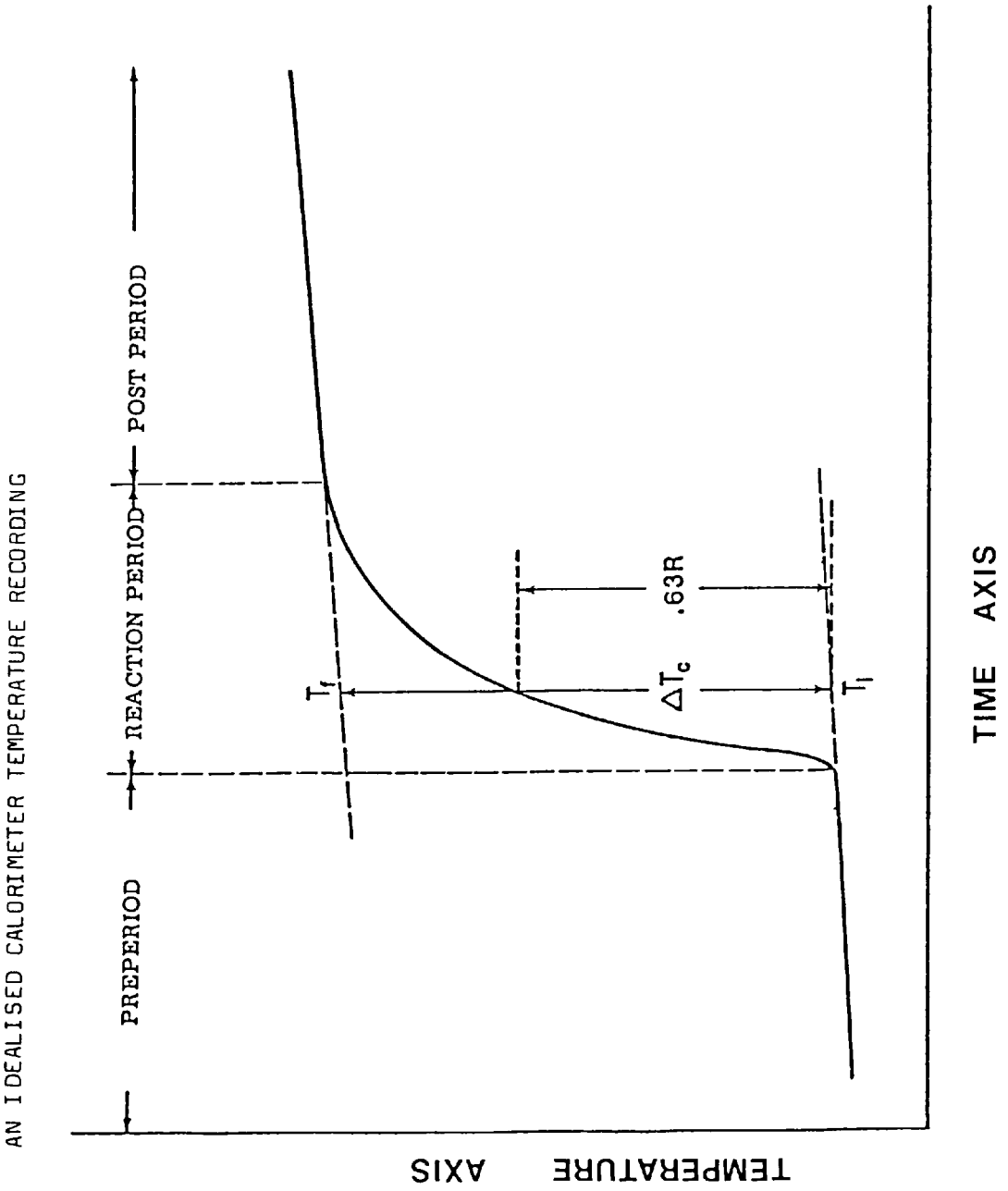
AN IDEALISED CALORIMETER TEMPERATURE RECORDING
PREPERIOD
REACTION PERIOD
POST PERIOD
T_f
ΔT_c
.63R
T_i
TEMPERATURE AXIS
TIME AXIS

^{o}C and e is expressed in J $^{o}C^{-1}$, Q is obtained in joules.

The energy equivalent of the calorimeter, which is simply the effective heat capacity of the calorimeter, is obtained by running the calorimeter with a known weight of calorimetry standard benzoic acid in the bomb under an oxygen atmosphere at 30 atmospheres pressure. Under these conditions the heat of combustion of benzoic acid is known accurately and from the temperature rise obtained the energy equivalent of the calorimeter can be calculated quite simply.

Several calibration experiments were performed which gave a mean value for the calorimeter energy equivalent of 2034·3 J $^{o}C^{-1}$ +/- 0·8%. In keeping with the IUPAC convention the error limits for this and all other calorimetric measurements reported in this thesis are given as +/- 2 standard deviation units about the mean value.

Separate experiments were performed to determine the contribution of the heat released by the electrical igniters to the overall heat of reaction measurements. These determinations were carried out under conditions identical to those used in the actual heat of reaction measurements.

4.5 MEASUREMENT OF REACTION TEMPERATURE

Reaction temperature measurements on the four oxidiser/fuel systems examined have been made using an IRCON Modline II Series 220 infra-red transducer system supplied by Sirius Instruments Limited. The equipment is illustrated in block diagram form in Figure 4.8.

The sensing head(Type 22A01) contains a silicon infra-red detector and an optical focussing system. The silicon detector operates in a narrow spectral band centred on 0·9 micrometre, thus avoiding interference from absorption bands due to atmospheric water vapour and carbon dioxide. The sensing head has a fixed focal distance of 12·7cm and a minimum target diameter of 0·13cm.

The signal from the sensing head is fed to the electronics module where it is amplified and linearized. The module also has facilities for detecting and storing the maximum sensed temperature, processing the signal with regard to target emittance, varying circuitry response time and stored signal decay time.

The equipment can be used in various temperature ranges, utilizing plug-in, integrated circuit, range change modules which automatically provide linearization of the detector output for the chosen temperature range, and scaling for the mV/degree output to the digital display meter. The system is capable of measuring temperatures from approximately 870K to 3300K, although the meter actually displays temperatures in ^{o}C.

Temperature measurements were obtained by focussing the sensing head onto the end of the delay element, through the perspex plug

FIGURE 4·8

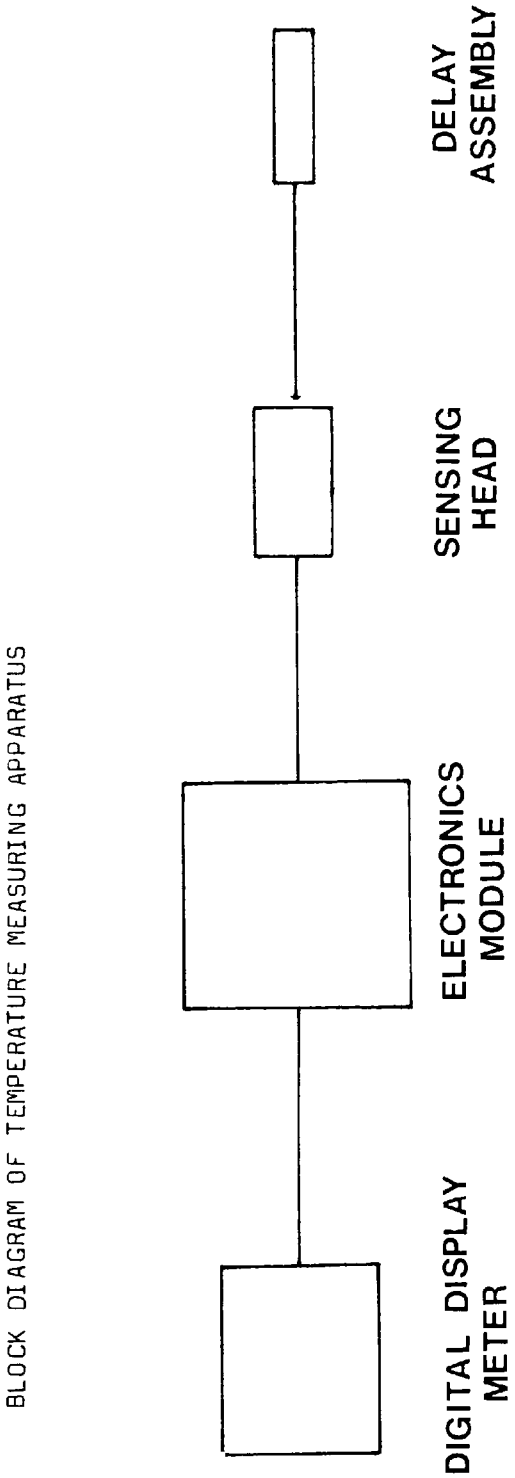
BLOCK DIAGRAM OF TEMPERATURE MEASURING APPARATUS
DELAY ASSEMBLY
SENSING HEAD
ELECTRONICS MODULE
DIGITAL DISPLAY METER

shown in Figure 4.8, setting the required emittance on the electronics module, electrically igniting the composition and reading the temperature from the digital display meter.

The emittance values for the reaction products, which were set on the electronics module, were obtained by heating samples of the reaction products to approximately 900K under a nitrogen atmosphere in a Stanton-Redcroft HSM-5 microfurnace. The samples were held in 6mm diameter inconel crucibles which were seated in the vertical furnace tube on a sample holder plate which forms the sensing head of a Pt versus Pt-Rh 13% thermocouple. The output of this thermocouple was fed to a strip chart recorder, via a $0^{o}C$ cold junction, to give a constant indication of the sample temperature. The thermocouple itself was calibrated in the normal manner using ICTA standard materials.

The sensing head was then focussed on the sample and the emittance control on the electronics module adjusted until the correct temperature was displayed on the digital meter.

Radiation losses due to the perspex window material were obtained by measuring the percentage transmission of samples of the window material at wavelengths of 2·5 and 5·0 micrometres using a Perkin-Elmer 580 infra-red spectrophotometer. The wavelengths were selected so as to avoid strong atmospheric absorption bands and were at the low wavelength limit of the instrument.

The measured radiation losses for the original samples of window material tested lay between 40% and 50% at both wavelengths. The bulk of this radiation loss could be attributed to scattering

of radiation from the rough machined ends of the perspex plugs. A later batch of plugs manufactured with smoother ends gave consistent radiation losses of approximately 35%. Results obtained with this later batch of plugs are quoted in this thesis.

To obtain the emittance values set on the electronics module the measured emittance values are multiplied by the fractional transmission value of the window material, in this case 0·65.

4.6 THERMAL ANALYSIS EQUIPMENT

4.6.1 DIFFERENTIAL SCANNING CALORIMETER

Differential scanning calorimetry (DSC) is fundamentally different from the older thermal analysis technique of differential thermal analysis (DTA). The difference can easily be understood by examining the definitions of the two techniques given by the Nomenclature Committee of the International Confederation for Thermal Analysis(69).

DTA --- 'A technique in which the temperature difference between a substance and a reference material is measured as a function of temperature whilst the substance and reference material are subjected to a controlled temperature programme.'

DSC --- 'A technique in which the difference in energy inputs into a substance and reference material is measured as a function of temperature whilst the substance and reference material are subjected to a controlled temperature programme.'

The DSC traces of the pyrotechnic compositions examined were obtained using a Perkin-Elmer DSC-2 instrument. This instrument is of the power compensation type, the sample and reference materials being contained in separate furnaces supplied with separate heaters. The two furnaces are maintained at nominally the same temperature by a servo system, operated by platinum resistance thermometers, which controls the amount of heat supplied to each furnace.

A schematic, block diagram of the DSC-2 showing the temperature control system and recorder inputs is given in Figure 4.9.

FIGURE 4·9

BLOCK DIAGRAM OF THE PERKIN-ELMER DSC-2 TEMPERATURE CONTROL SYSTEM

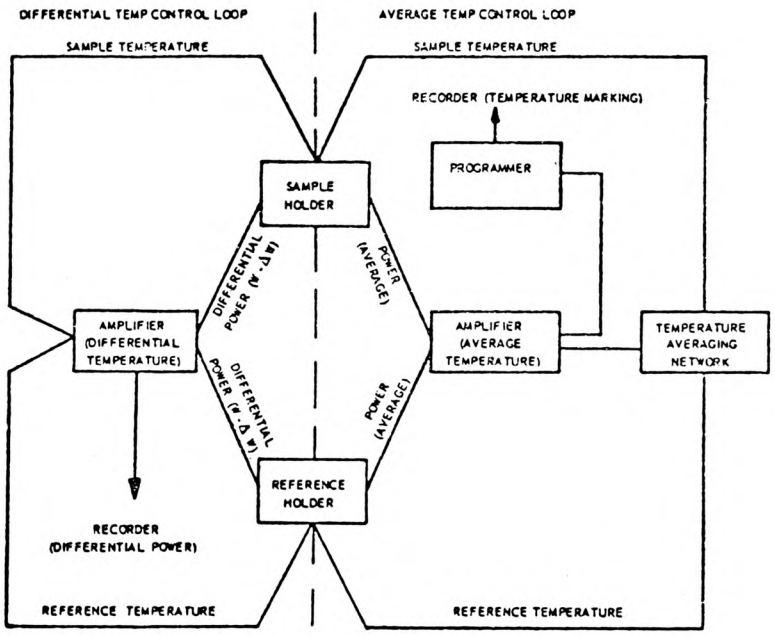

The working temperature range of the DSC-2 ranges from ambient to 1000K, the temperature programming being completely digital, with thirty digital steps per degree. It is possible to select heating and cooling rates independently in eleven discrete steps from $0{\cdot}312^{o}$ to 320^{o} min^{-1}. The instrument can be programmed to heat to and hold at the selected upper temperature, cool to the selected lower temperature, or automatically cycle at predetermined linear programme rates between the selected temperature limits. Eight sensitivities, from 20 to 0·1 mcal s^{-1}, can be selected to correspond with the full scale deflection of the recorder pen.

When an endothermic or exothermic reaction takes place in the sample the change in power required to maintain the sample holder at the same temperature as the reference holder, that is its programmed temperature, during the reaction is recorded as a peak. The chart abscissa indicates the temperature at which the reaction takes place and the peak area indicates the total energy transfer to or from the sample. The temperature calibration of the instrument is adjustable and is checked by the use of I.C.T.A. temperature standards. The maximum deviation of the indicated temperature from the actual temperature is maintained at less than $+/- 1^{o}$.

The size of samples used in DSC equipment is smaller than that used in DTA equipment, being approximately 5 to 10mg as opposed to the approximately 100mg samples used in DTA equipment.

To prevent contamination of the furnaces the samples are contained in 6mm diameter shallow pans. A choice of pan material

is available, graphite, aluminium or inconel, the choice of pan material will depend on the nature of the sample being examined and the temperature range being used.

In this work the instrument is purged with an inert gas, either nitrogen or argon, to eliminate any contribution to the oxidation-reduction reactions examined by atmospheric oxygen.

The operating conditions for all the DSC traces presented in Chapter 8 are listed in Appendix 1 at the end of the thesis.

4.6.2 HOT STAGE MICROSCOPE

Hot stage microscopy (HSM) is a complementary technique to DSC, allowing either visual observation of the sample combined with 35mm photomicrography or visual observation combined with recording of the intensity of reflected light from the sample under controlled heating and cooling programmes in a controlled atmosphere. Both modes of operation are accomplished using a long working distance stereoscopic microscope fitted with a trinocular head.

A block diagram of the complete apparatus is given in Figure 4.10.

The hot stage apparatus can conveniently be divided into two parts for ease of description:

a) Hot Stage Furnace and Temperature Programmer

b) Microscope Assembly (microscope, camera and photometer)

FIGURE 4-10

BLOCK DIAGRAM OF THE HOT STAGE MICROSCOPE APPARATUS

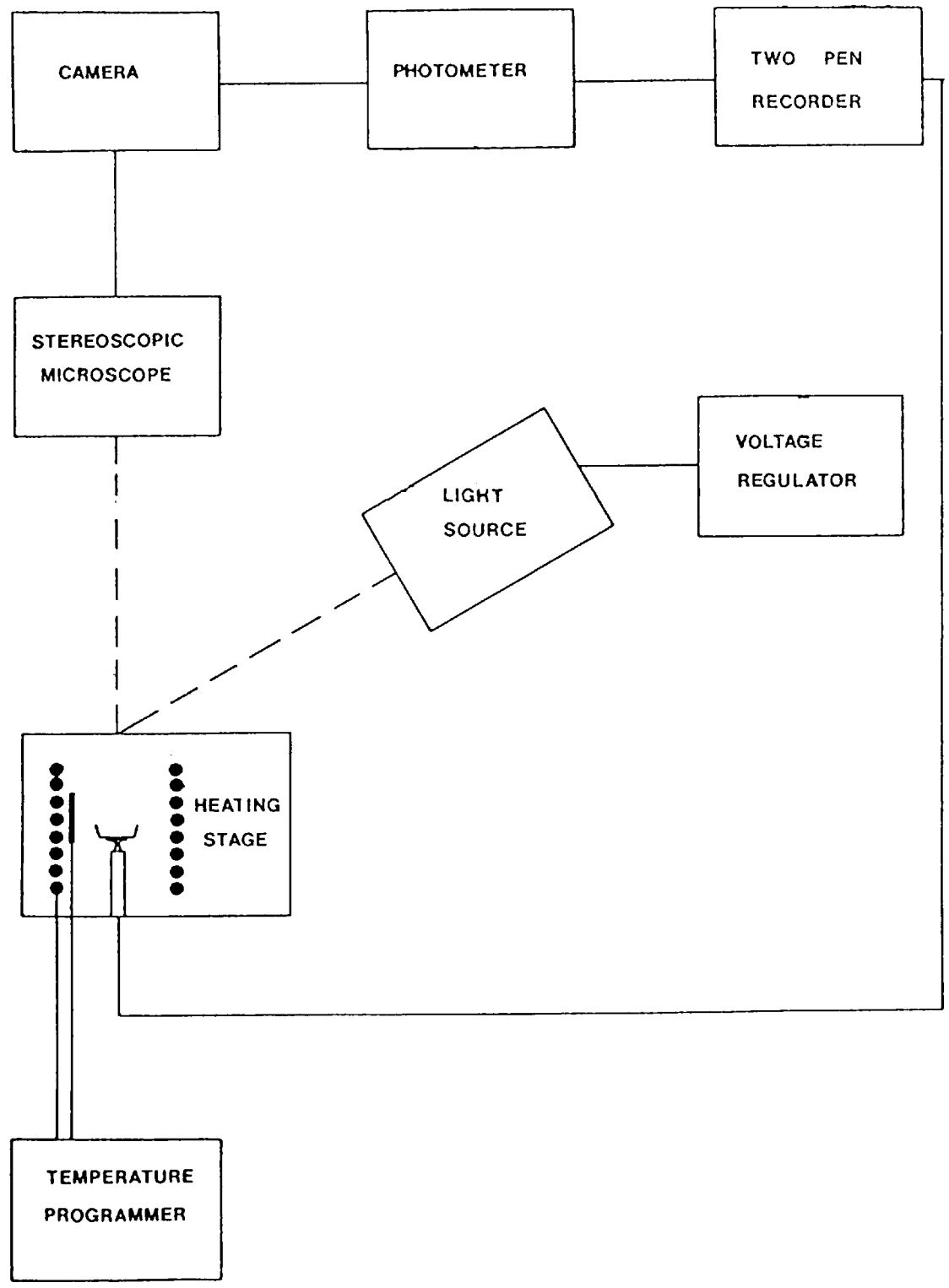

a) Hot Stage Furnace and Temperature Programmer

The hot stage furnace and temperature programmer used in this work is a Stanton-Redcroft HSM-5 unit. A cross-sectional diagram of the furnace is given in Figure 4.11. The body of the furnace unit is water cooled for safe high temperature handling. The furnace itself is a low thermal mass, microfurnace type, high heating and cooling rates being easily achieved. A chromel-alumel control thermocouple is positioned in contact with the furnace and is used to control the temperature programmer. The furnace sample chamber contains a plate-type thermocouple(Pt versus Pt-13% Rh) on which the sample, contained in a 6mm diameter, inconel sample pan can be seated.

Access to the sample chamber is made via a removable lid, fitted with a quartz window through which the sample is viewed. The lid can be rotated through 360^{o} whilst maintaining a gas-tight seal, assuring an unobstructed view of the sample at all times. The sample chamber atmosphere can be controlled and in this work the sample chamber is purged with nitrogen gas.

The furnace temperature is controlled by the programmer unit which provides a temperature range from ambient to $1000^{o}C$ with heating or cooling rates of 1,2,3,5,10,20,30,50 and 100^{o} min^{-1}. The furnace can be programmed to heat or cool and hold isothermally at a required temperature, or, heat or cool and switch off at a required temperature.

The sample temperature can be continuously monitored by means of the sample support, plate thermocouple whose output is fed

FIGURE 4·11

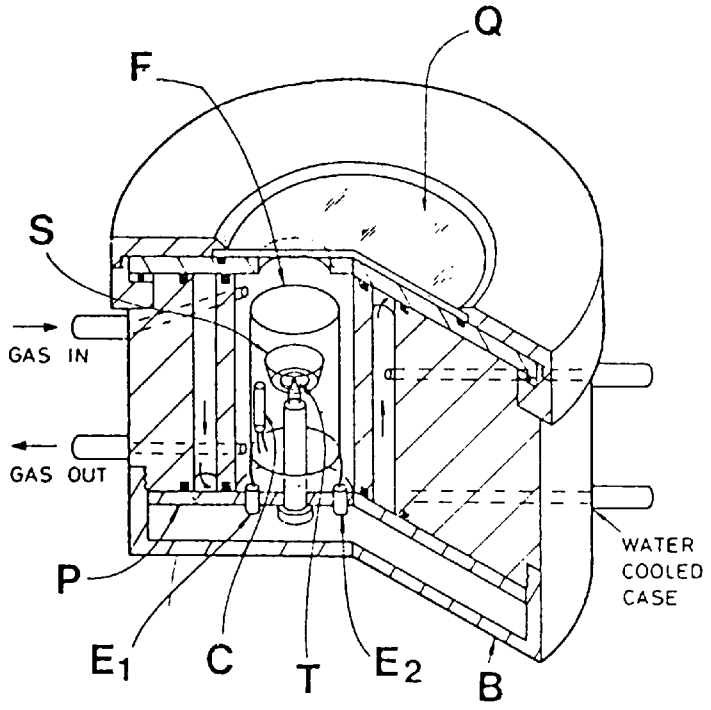

Schematic cross-section through hot stage

Key Q = quartz window
F = furnace
S = sample container
P = baseplate
E_1 & E_2 = furnace connections
C = control thermocouple
T = Pt v Pt-13% Rh thermocouple
B = removable base plate

to one channel of a two channel chart recorder. The temperature calibration of the furnace is checked by the use of I.C.T.A. temperature standards.

b) Microscope Assembly

The microscope used in this work is an Olympus X-Tr model, which is a stereoscopic model fitted with a trinocular head for photomicrography. The range of magnifications available with this microscope are shown in Table 4.1.

For photomicrography an Olympus PM 6 35mm camera is attached to the microscope, it being possible to take photographs of the sample at any time without interrupting visual observation.

By replacing the camera with a Vickers M030500 photometer unit it is possible to record changes in the intensity of reflected light from the sample. The photometer output is fed to one channel of a two channel recorder, the second channel recording sample temperature.

TABLE 4·1 Optical specifications of Olympus Stereoscopic Microscope

Drum Position	Objectives	Eyepieces	Total Magnification	Field Diameter mm	Working Distance mm
6.3	1 X (f = 100)	10 X	6.3 X	32	86
10			10 X	20	
16			16 X	12.5	
25			25 X	8	
40			40 X	5	
12.5		20 X	12.5 X	19.4	
20			20 X	12.2	
31.5			31.5 X	7.6	
50			50 X	4.9	
80			80 X	3.1	
6.3	2 X (f = 50)	10 X	-	-	45
10			-	-	
16			31.5 X	7.6	
25			50 X	4.9	
40			80 X	3.1	
12.5		20 X	-	-	
20			40 X	6.1	
31.5			63 X	3.9	
50			100 X	2.4	
80			160 X	1.5	

4.7 MATERIALS

4.7.1 OXIDISERS

Two main samples of lead monoxide have been used in this work. One supplied by Fisons had a specific surface area of 0·58 $m^2\ g^{-1}$, the other supplied by BDH Ltd. had a specific surface area of 0·42 $m^2\ g^{-1}$. The purity of both samples was 98% minimum, the main impurities in both cases being iron oxides and higher lead oxides. Where other lead monoxide samples have been used details of their physical characteristics can be found either in the text as they occur, or in Appendix 1 at the end of this thesis. Unless otherwise stated the sample supplied by BDH Ltd. is the lead monoxide used.

The stannic oxide, SnO_2, used in this work was supplied by BDH Ltd.. The sample was of 99% purity, the main impurity being lead monoxide, and possessed a specific surface area of 7·37 $m^2\ g^{-1}$.

4.7.2 FUELS

The boron used in this work was of the amorphous, microcrystalline type and was supplied by Hermann C. Starck of Berlin. It was of 95% to 97% purity, the main impurities being B_2O_3 and magnesium borides, and possessed a specific surface area of 7·96 $m^2\ g^{-1}$.

Unless otherwise stated the silicon sample used in this work was one possessing a specific surface area of 7·27 $m^2\ g^{-1}$. Where other silicon samples are used their physical characteristics are either presented in the text as they occur or can be found in Appendix 1. The purity of all samples was 98%, the main impurity in all cases being metallic iron. All samples were supplied by Nobel's Explosives Company(ICI) Ltd..

CHAPTER 5

HEATS OF REACTION

5.1 INTRODUCTION

Heat outputs are of considerable interest in the study of pyrotechnic compositions as they can provide useful information on the nature of the reactions taking place. It is, however, necessary to exercise caution in the interpretation of experimentally determined heat output/oxidiser or fuel level curves in order to, for instance, be able to discriminate between a deflection in the position of a heat output maximum due to a physical cause and that due to a fundamental difference in the nature of the chemical reactions taking place relative to the theoretical assumed reaction. As an example, incomplete reaction of the components is a physical effect which will cause a deflection in the position of the heat output maximum. Therefore, before discussing in detail the heat outputs obtained for the oxidiser/fuel systems of interest in this work it is worth placing them in context by examining the physical and chemical properties of the various reactants and their reaction products.

Silicon is a Group IVb element and in the solid state, in its compounds with oxygen, normally exhibits its group valency of 4. Silicon itself possesses a low volatility and a high melting(1683K) and boiling(2628K) points. Only one oxide is commonly found, SiO_2, although it can be obtained in several different crystal modifications. Silicon monoxide, SiO, is known but is only found in significant quantities in the vapour phase at high temperatures, while silicon

dioxide is a low volatility, refractory oxide. It should therefore be expected that SiO_2 would be found as the major oxidation product of silicon under propagative conditions where the rise and fall in temperature is extremely rapid and there is very little time for high temperature, vapour phase equilibria to be established.

Boron is a Group IIIb element and forms one commonly found oxide, B_2O_3, in which it exhibits its group valency of 3. Boron has a low volatility and a high melting(2573K) and boiling(2823K) points, whereas, B_2O_3 has a high volatility with poor refractory properties. It is also commonly found in the form of a glass, the crystalline variety being quite difficult to obtain. Because of the glassy nature of B_2O_3 its melting point is not well defined but is normally quoted as 723K.

In the vapour phase at high temperatures two suboxides are known, namely BO and B_2O_2. Boron monoxide disproportionates at low temperatures to give a mixture of B_2O_3 and elemental boron(70), while B_2O_2 gives a polymeric solid of general formula $(BO)_n$ at low temperatures, which contains B-O and B-B bonds(71).

Given the high volatility of B_2O_3 when compared with SiO_2, a greater contribution to the overall heat output should be expected from vapour phase suboxide producing reactions in boron fuelled compositions than in silicon fuelled compositions. Overall though, the same arguements should apply to the predominance of the B_2O_3 producing reaction as that for SiO_2 production in silicon fuelled compositions, the major oxidation product of boron should be expected to be B_2O_3, although to a somewhat lesser extent than for SiO_2.

With regard to the oxidisers present in the compositions, the evidence available would appear to point to the fact that their reduction is an 'all or nothing' process, that is, they are usually completely reduced to the parent metal.

A factor which must be taken into account is interaction between reaction products and the initial reactants. If chemical reaction is possible between an initial reactant and a reaction product this can contribute to the overall heat of reaction of the composition, given an appropriate excess of that reactant in the composition. Valuable information on this type of reaction can be obtained by the use of various thermal analysis techniques.

In arriving at the assumed reaction equations for each oxidiser/fuel system, given in the discussion which follows, consideration has been given only to the oxidation-reduction reactions deemed most likely to take place, taking into account the chemical and physical characteristics of the reactants and products discussed above.

The physical and thermochemical constants of the reactants and products are given in Table 5.1.

TABLE 5.1 STANDARD PHYSICAL AND THERMOCHEMICAL CONSTANTS OF THE REACTANTS AND PRODUCTS

SUBSTANCE	DENSITY ($g\ cm^{-3}$)	M.PT. (K)	B.PT. (K)	C_p ($J\ g^{-1}\ K^{-1}$)	ΔH_f ($kJ\ mol^{-1}$)	STATE
B	2·35	2573	2823	1·030	1·7	amorph.
B_2O_3	1·8 – 2·5	~723	~2000	0·892	1246·0	glass
Pb	11·34	600·5	2013	0·130	0	cryst.
PbO	8·0 – 9·5	1163	----	0·757	218·6	cryst.
Sn	5·8 – 7·3	~504·9	~2538	0·222	0	cryst.
SnO_2	6·95	1903 SUBLIMES	~2120 SUBLIMES	0·335	580·8	cryst.
Si	2·33	1683	2628	0·703	0	cryst.
SiO_2	2·2 – 2·3	1883	~2670	0·737	910·7	cryst.

5.2 ASSUMED REACTION EQUATIONS AND THEORETICAL HEAT OUTPUTS

The theoretical heat outputs for the four oxidiser/fuel systems examined have been calculated using the method described by Al-Kazraji and Rees(37). Thermochemical data used in the calculations was obtained from reference(72), CODATA recommended values being used wherever possible.

The calculated heat outputs of the four systems, in terms of J g^{-1} of composition and kJ mol^{-1} of oxide are shown in Figures 5.1 to 5.4 and Tables 5.2 to 5.5.

The assumed reaction equations from which the theoretical heat outputs have been calculated are given below:

$$3PbO_{cr} + 2B_{am} \longrightarrow B_2O_{3gl} + 3Pb_{cr} \quad (96{\cdot}9/3{\cdot}1)$$

$$2PbO_{cr} + Si_{cr} \longrightarrow SiO_{2cr} + 2Pb_{cr} \quad (94{\cdot}1/5{\cdot}9)$$

$$3SnO_{2cr} + 4B_{am} \longrightarrow 2B_2O_{3gl} + 3Sn_{cr} \quad (91{\cdot}3/8{\cdot}7)$$

$$SnO_{2cr} + Si_{cr} \longrightarrow SiO_{2cr} + Sn_{cr} \quad (84{\cdot}3/15{\cdot}7)$$

The values in parenthesis alongside the reaction equations represent the stoichiometric % wt. oxidiser/fuel ratios for each reaction.

The theoretical curves follow the expected pattern as described by Spice and Staveley(7), the maximum heat of reaction being obtained at the stoichiometric point as the percentage oxidiser level is reduced from 100%.

5.3 PbO/B HEATS OF REACTION

Figure 5.1 shows the theoretical and experimentally determined heats of reaction for a series of PbO/B compositions in terms of J g^{-1} of composition and kJ mol^{-1} of oxide. The results are summarized in Table 5.2.

The main characteristic of the experimentally determined heat output curve, which is immediately apparent, is the excess heat output at oxidiser levels above and below the theoretical stoichiometric level. This type of behaviour is not unusual in boron fuelled systems. Miller(35) has commented on this phenomenon in relation to the $BaCrO_4$/B system and McLain(32) in relation to the $BaCrO_4$/B and $CaCrO_4$/B systems.

McLain(32) cites the excess heat output in the above systems, together with the displacement of the maximum in the experimental heat output curves to higher fuel levels than predicted theoretically, the high reaction temperatures achieved during the reaction and the identification of boron monoxide in the combustion zone of composite solid propellants, as evidence that the main reaction taking place does not form B_2O_3 but the monoxide, BO. Even if this is the case, as stated earlier, boron monoxide exists only in the vapour phase at high temperatures, giving on condensation a mixture of B_2O_3 and elemental boron by way of a disproportionation reaction. This makes the assertion impossible to prove by analysis of the reaction products at room temperature.

Work by Gremyachkin et al.(73) indicates that the equilibrium combustion products of a boron particle are gaseous only if the

FIGURE 5·1

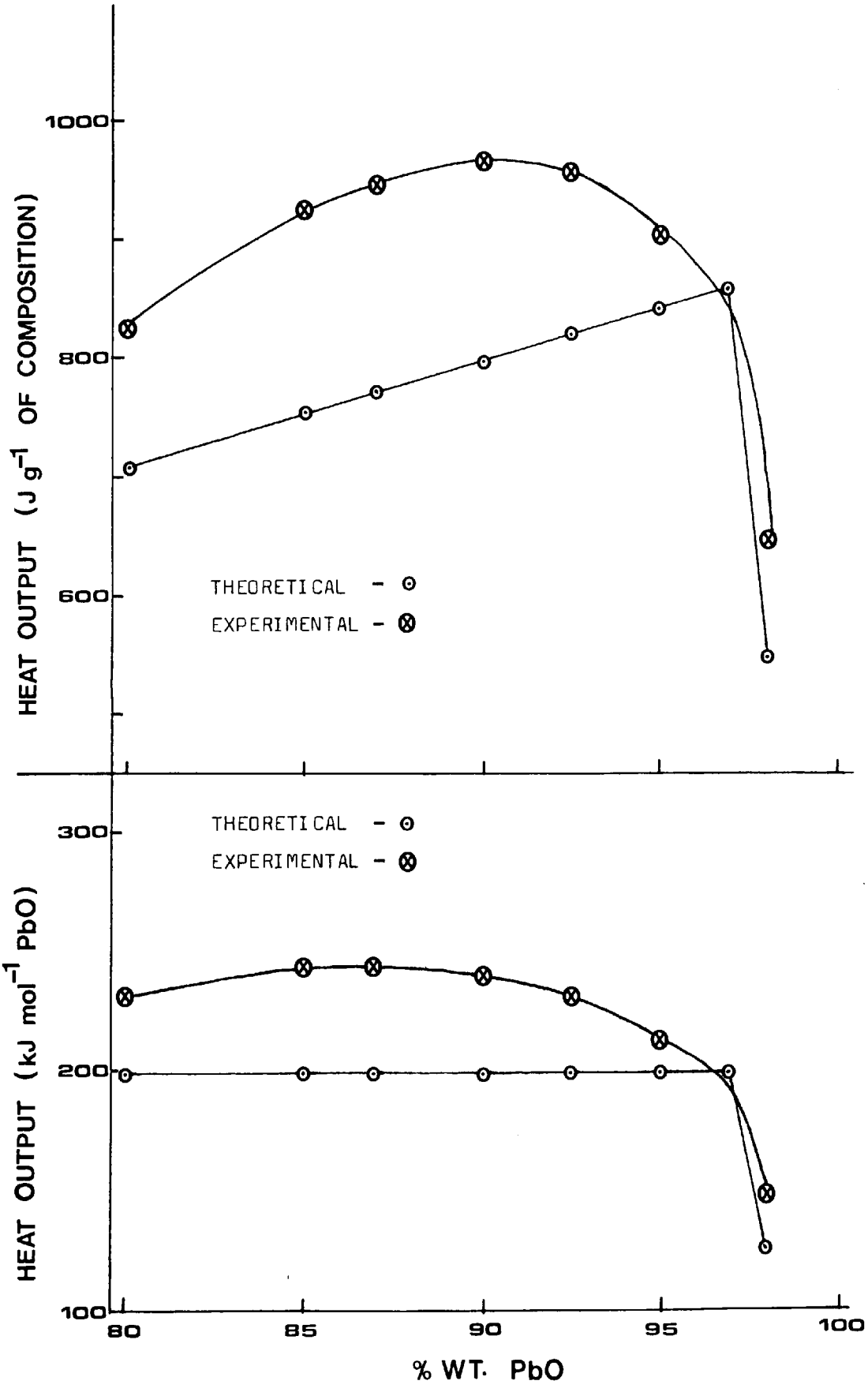

HEAT OUTPUTS OF PbO/B COMPOSITIONS

particle is burned in an atmosphere that is at an initial temperature higher than the boiling point of B_2O_3(approx. 1800K-2200K). An appreciable presence of boron monoxide in the combustion products should only occur at much higher temperatures(3000K-4000K). Under intermediate conditions the principal product from the combustion of boron particles is B_2O_2.

Thermal analysis studies(Chapter 8) have shown that the reaction between lead monoxide and boron initiates at a temperature (approx. 750K) which is considerably below the boiling point of B_2O_3. In addition , measurement of the reaction temperatures of PbO/B compositions(Chapter 7) indicates temperatures of approximately 950K at 80 wt.% PbO and approximately 1700K at 92·5 wt.% PbO, again considerably lower than the boiling point of B_2O_3. It should be stressed that measurement of reaction temperatures using an infra-red pyrometer gives an average temperature for the reaction products, which should approach the value for the calculated reaction temperature(33) after adjustment for heat losses to the entraining envelope material. It is possible that the localised, instantaneous temperatures at the points of reaction could be considerably higher, high enough in fact to produce some vapourisation of B_2O_3 and to favour the production of small amounts of boron suboxides(B_2O_2 and BO).

It must be appreciated that in order to achieve the high temperatures required for boron suboxide production in these compositions, a substantial proportion of the oxidation-reduction reaction must already have taken place close to the initiation

temperature; therefore, the main oxidation product of boron should be expected to be B_2O_3.

The boron suboxides require a higher boron to oxygen ratio for their production than B_2O_3, consequently the discrepancy between the theoretical heat output curve and the experimental heat output curve would be expected to increase as the boron level increases above the assumed stoichiometric level. This effect can be seen in Figure 5.1, the discrepancy increasing from the assumed stoichiometric ratio to approximately 90% PbO whereafter there is a decrease in the discrepancy, the experimental heat output curve gradually returning to the theoretical curve.

To explain this decrease in the discrepancy between the theoretical and experimental heat output curves, it is necessary to consider the reaction temperatures achieved at the various oxidiser/fuel ratios. Although the fuel level increases from right to left in Figure 5.1, favouring boron suboxide production, the overall reaction temperature tends to decrease from right to left, as indicated earlier. Therefore, although the increasing boron to oxygen ratio favours the production of boron suboxides, the increasing amount of excess fuel will tend act as a heat sink and the decreasing temperature will tend to discriminate against boron suboxide production in favour of B_2O_3 production. The combination of these two opposing effects would be expected to give rise to the experimental curve obtained on the high fuel side of the stoichiometric point.

It should be pointed out that the amorphous(microcrystalline) boron used in this work, which is produced by the magnesium

reduction of boric oxide, B_2O_3, contains several percent of magnesium borides as impurities. However, even if the magnesium, present as boride, is assumed to be available for reduction of the lead monoxideand the purity of the boron is taken into account by adjustment of the PbO/B ratio, this will only account for 20% to 25% of the observed excess heat output. It is also known that lead does not form a boride, it is one of the very few elements that does not, so that this type of reaction cannot explain the excess heat output(71).

Figure 5.1.A shows the infra-red reflectance spectra of an 80/20 PbO/B reaction product(obtained under propagative conditions) and a B_2O_3 sample, while Figure 5.1.B shows the DSC traces of the same 80/20 PbO/B reaction product and an ICTA lead(Pb) temperature standard, scanned between 590K and 610K. These two figures indicate the presence of B_2O_3 and lead in the reaction product at room temperature.

All the available evidence would seem to indicate that the main reaction in this system produces B_2O_3, while side reactions, of a limited but unknown extent, involving vapour phase production of boron suboxides(probably B_2O_2), are responsible for the excess heat output at fuel levels above the stoichiometric level and deflection of the heat output maximum to higher fuel levels.

The excess heat output observed at lead monoxide levels above the stoichiometric level is somewhat easier to explain. The solubility of PbO in B_2O_3 is well established(74), glasses being formed over a wide range of compositions with the viscosity of the melts decreasing as the PbO content is increased.

FIGURE 5.1.A

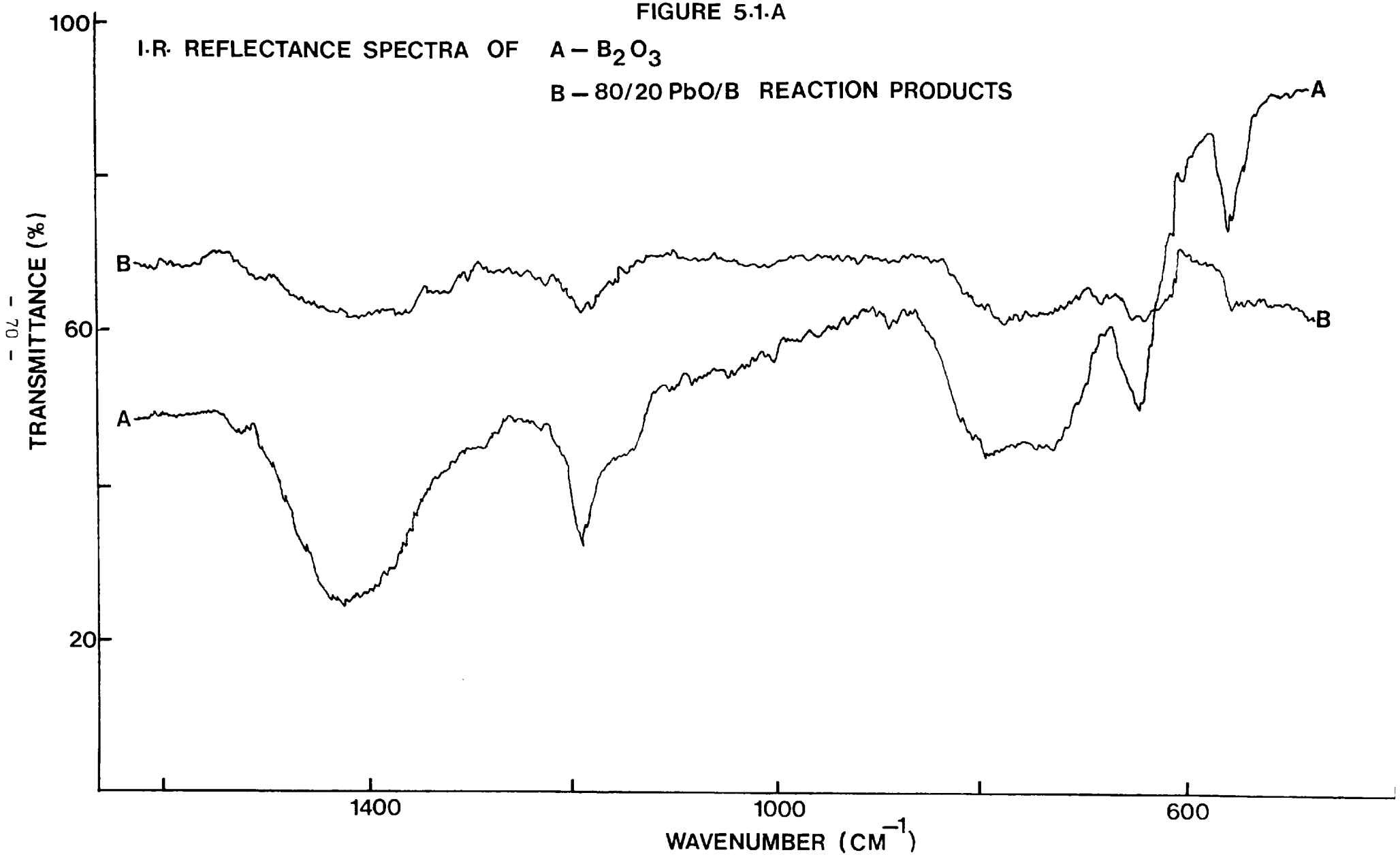
I.R. REFLECTANCE SPECTRA OF A – B_2O_3
B – 80/20 PbO/B REACTION PRODUCTS
100
60
20
TRANSMITTANCE (%)
A
B
A
B
1400
1000
600
WAVENUMBER (CM^{-1})

FIGURE 5·1·B

DSC TRACES OF A— 80/20 PbO/B REACTION PRODUCTS

B— I·C·T·A· STANDARD LEAD SAMPLE

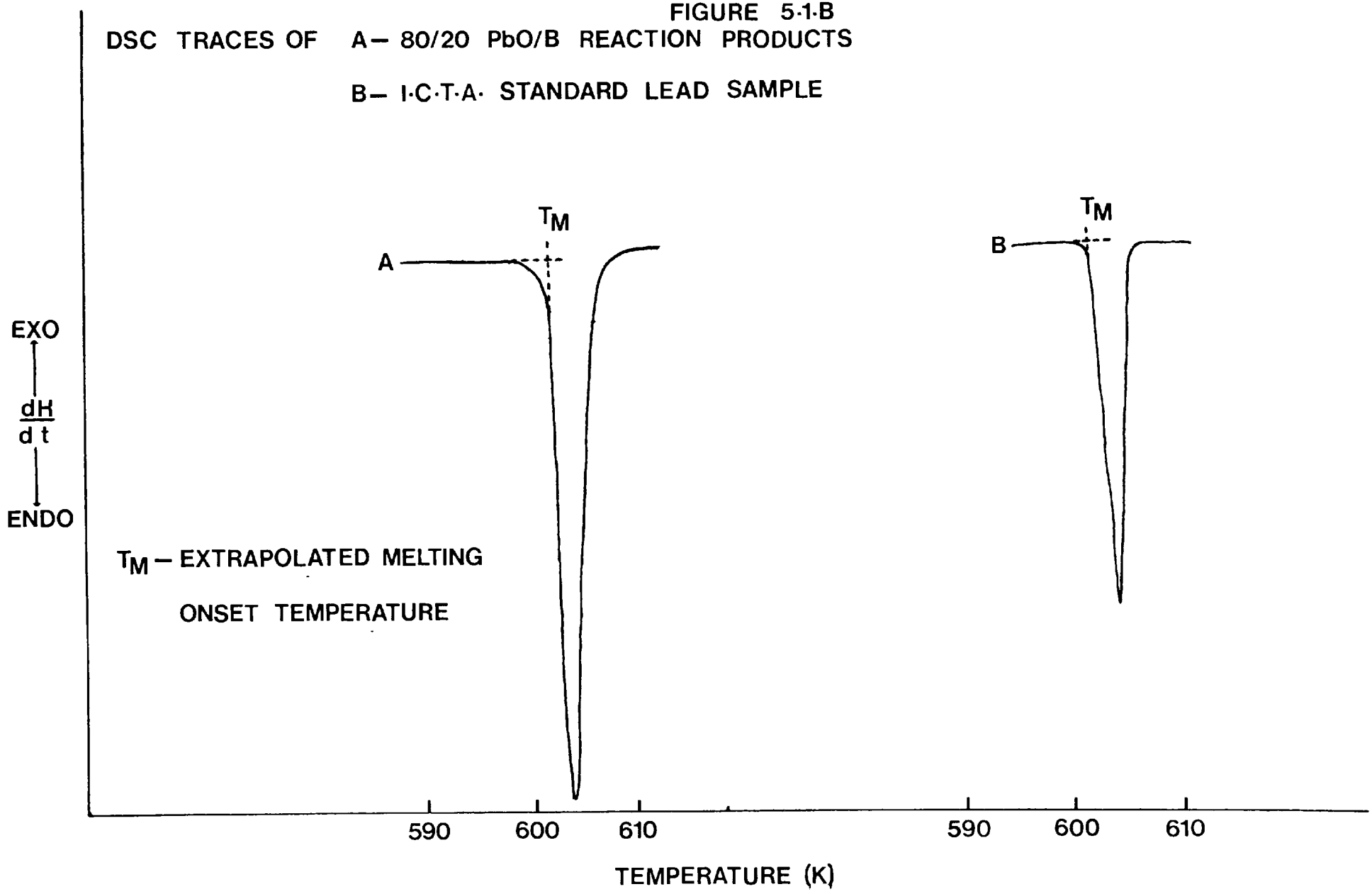

Shartsis and Newman(75) determined the heats of formation of PbO/B_2O_3 glasses containing from 30% to 95% PbO. The heats of formation varied from approximately -160J g^{-1} at 30% PbO, reaching a maximum of approximately -240J g^{-1} at approximately 65% PbO, to approximately -80J g^{-1} at 95% PbO.

In the PbO/B system, at PbO levels above the stoichiometric level, excess PbO is present which is available for reaction with B_2O_3 produced in the main oxidation-reduction reaction. The reaction products, from compositions containing excess PbO, do contain large amounts of slightly yellow coloured, glassy materials together with metallic lead globules. The heats of formation of the PbO/B_2O_3 glasses are quite adequate to explain the excess heat outputs of these compositons.

The results of thermal analysis studies(Chapter 8) on the PbO/B system would seem to confirm these conclusions.

5.4 SnO_2/B HEATS OF REACTION

Figure 5.2 shows the theoretical and experimentally determined heat outputs of a series of SnO_2/B compositions, in terms of J g^{-1} of composition and kJ mol^{-1} of oxide. The results are summarized in Table 5.3. In common with the PbO/B system, the SnO_2/B system exhibits a large excess heat output over that predicted from the assumed reaction equation. The system also exhibits the deflection of the heat output maximum to a higher fuel level than predicted, and the gradual return to the theoretical heat output levels as the fuel level is increased above that giving the maximum heat output.

The percentage excess heat output tends to be higher in the SnO_2/B system than in the PbO/B system. If the assumption is made that the excess heat output can be attributed to vapour phase, boron suboxide producing side reactions, the explanation is relatively simple. Stannic oxide, despite possessing a very high melting point(greater than 2100K) also exhibits a very high volatility at temperatures well below its melting point. This property precludes the use of stannic oxide in refractory oxide ceramics(76). Therefore, at the reaction temperatures achieved in the two systems, the SnO_2/B system displaying the higher reaction temperature, it should be expected that the SnO_2/B system would exhibit a greater degree of vapour phase reaction.

X-ray diffraction studies on SnO_2/B reaction products have indicated the presence of unreacted, but decreasing amounts

FIGURE 5·2

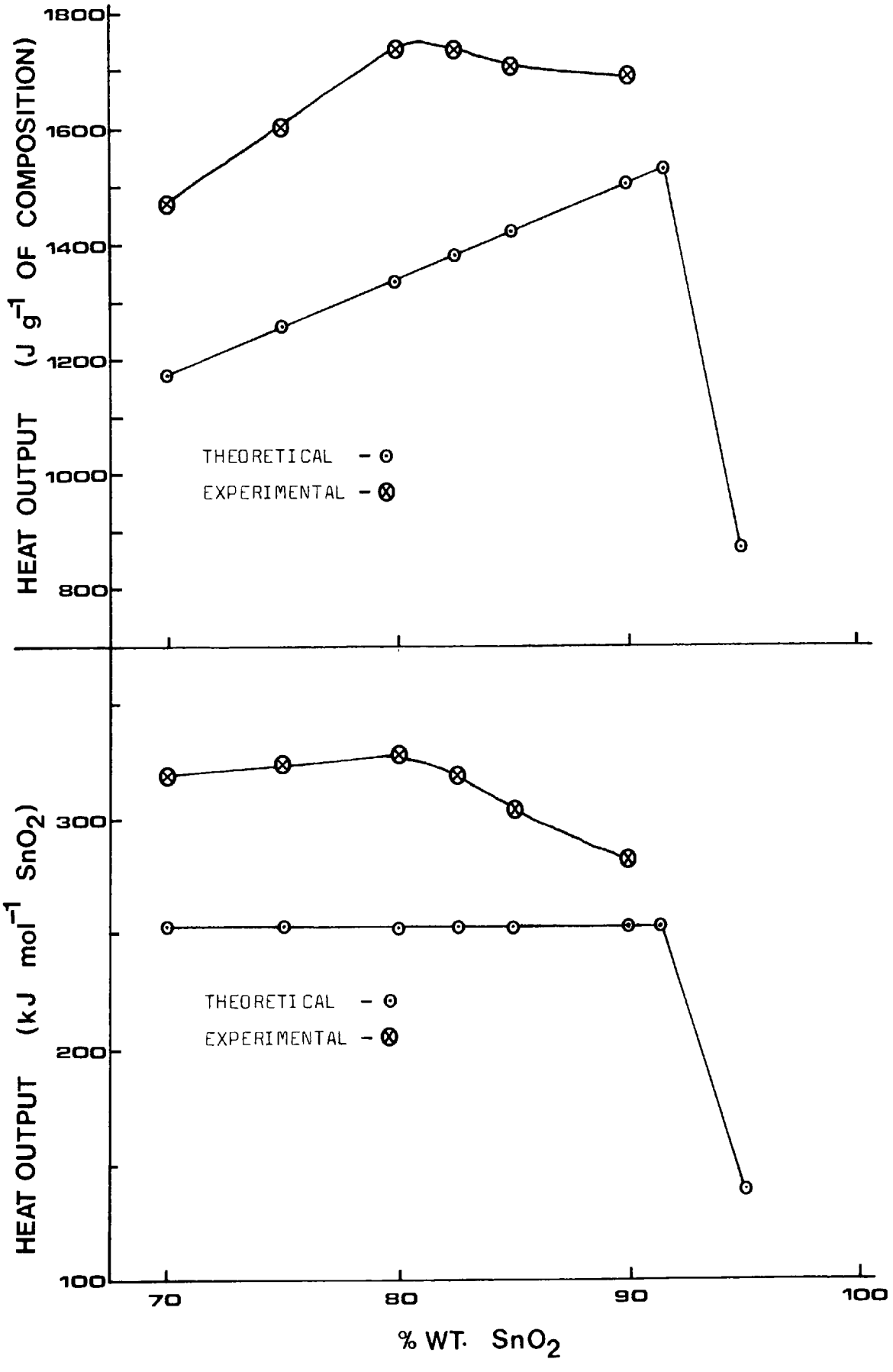

HEAT OUTPUTS OF SnO_2/B COMPOSITIONS

of SnO_2 at oxidiser levels from 90% down to the heat output maximum at approximately 80% SnO_2. This factor will explain the difference in appearance of the heat output curves of the two systems at fuel levels higher than the stoichiometric levels.

Mellor(74) states that SnO_2 is completely insoluble in B_2O_3 and hot stage microscopy studies of the SnO_2/B_2O_3 system confirm this statement. The B_2O_3 produced in the reaction between stannic oxide and boron will therefore act as an efficient diffusion barrier, making this reaction much slower than the reaction between lead monoxide and boron and contributing to the incomplete reaction between SnO_2 and boron.

It can therefore be seen that incomplete reaction of stannic oxide, probably due to its insolubility in B_2O_3, coupled with the occurrence of vapour phase reactions cause the deflection of the heat output maximum to higher fuel levels than expected. Reaction between SnO_2 and B_2O_3 will of course make no contribution to the overall heat outputs of the compositions. As in the case of lead it is known that tin does not form a boride(71) so that this reaction can be discounted as a source of the excess heat output.

5.5 PbO/Si HEATS OF REACTION

The heat outputs of PbO/Si compositions have previously been determined by Moghaddam(77), but it was felt that remeasurement was justified in this work as a different calorimeter has been used. The theoretical and experimentally determined heat outputs for a series of PbO/Si compositions, in terms of J g^{-1} of composition and kJ mol^{-1} of oxide, are shown in Figure 5.3. The results are summarized in Table 5.4.

The heat output curves obtained are similar in form to the heat output curves obtained by Al-Kazraji for the reactions between Pb_3O_4 and silicon, and PbO_2 and silicon(68). The heat output curves also agree relatively well with that obtained for the PbO/Si system by Moghaddam(77) when the relative particle sizes of the reactants and ignition fuse heat output values are taken into account.

X-ray diffraction studies of PbO-Si reaction products by Moghaddam(77) have shown that the reaction follows the course described by the assumed reaction equation given in section 5.2. This being the case, then interpretation of the kJ mol^{-1} of oxide - % wt. of oxidiser plot must be made carefully.

The poor agreement between the theoretical and experimental curves at the theoretical stoichiometric oxidiser/fuel ratio in Figure 5.3 need not indicate that the chemical reaction taking place is radically different from the assumed theoretical reaction. It is quite possible for the apparent stoichiometric point to be shifted to considerably higher fuel levels, or simply

FIGURE 5·3

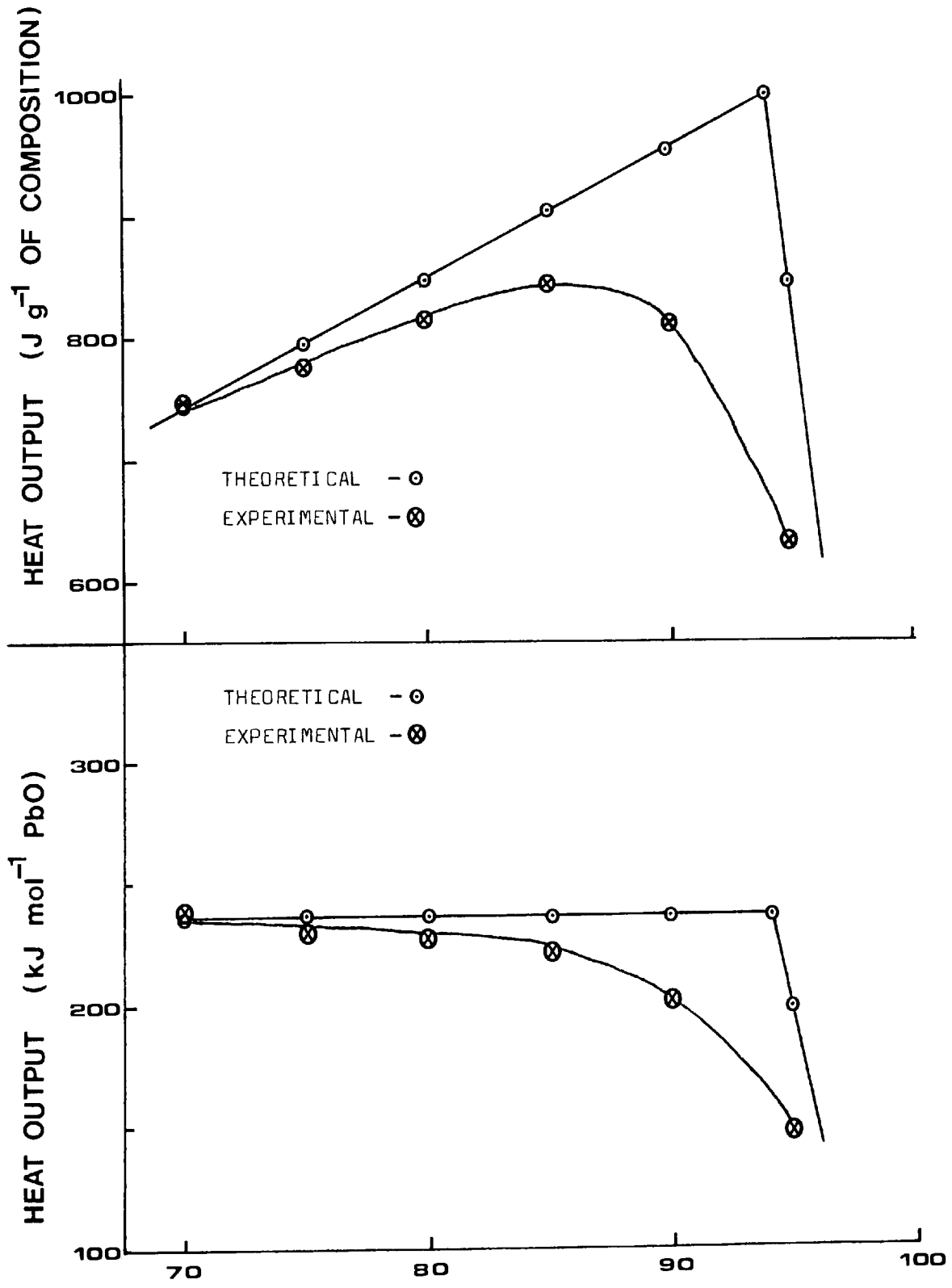

HEAT OUTPUTS OF PbO/Si COMPOSITIONS

obscured, by incomplete reaction of the fuel because of the physical barriers to reaction presented by the formation of the initial reaction products.

The results presented by Al-Kazraji(68) for the PbO_2/Si system support the view presented above, showing that as the average particle size of the fuel is decreased the experimental curve more closely approximates the theoretical curve. Perhaps more importantly, it is believed that the most telling aspect of these 'Q' plots is the final plateau value which the plot attains, where the relationship between the theoretical and experimental curves is most simply observed. In the final analysis, the limiting plateau value of the heat output mol^{-1} of fuel or oxidiser, as the reactant particle sizes are reduced, is a much more reliably determined characteristic of the oxidation-reduction reaction than the position of the inflexion point of the experimental curve. The position of this point can be affected by physical, as well as minor chemical, effects in addition to the more subjective factor of the way in which the heat output curve is drawn through the experimental points. These effects will tend to obscure the inflexion point of the curve, to the point where it no longer has the theoretical importance assigned to it.

At fuel levels considerably in excess of the stoichiometric level the experimental heat output will approach the theoretical level as the available oxidiser can be consumed in the initial surface reaction with the fuel, the fuel being present in excess. This phenomenon will tend to lessen the effectiveness of the

initial reaction product as a barrier to reaction. The point at which the theoretical maximum heat output of the system begins to be approached, in terms of the oxidiser/fuel ratio, will depend upon the degree of inhibition of the reaction by the reaction products.

5.6 SnO_2/Si HEATS OF REACTION

Figure 5.4 shows the theoretically and experimentally determined heat outputs for a series of SnO_2/Si compositions, in terms of J g^{-1} of composition and kJ mol^{-1} of oxide. The results are summarized in Table 5.5.

The forms of the heat output curves obtained are similar to the curves obtained for the PbO/Si system. The main difference between the curves of the two systems is that the shortfall in heat output in the SnO_2/Si system is greater than that observed in the PbO/Si system.

A contributing factor to the observed shortfall in heat output is most likely to be found in the physical nature of the stannic oxide particles. The stannic oxide used in this work is formed by the dehydration of stannic acid, hydrated stannic oxide, which is gelatinous or amorphous in form. On dehydration the stannic oxide produced possesses a large surface area, 7·37 m^2 g^{-1} S.S.A., and a low powder or bulk density, approximately 0·65 g cm^{-3}. These values of specific surface area and bulk density are suprising in view of the rather high material density of stannic oxide, 6·95 g cm^{-3}.

The low bulk density of the stannic oxide, compared with its rather high material density, means that relative to each fuel particle the quantity of oxide in close proximity will be small and the volume of oxide required to consume the entire fuel particle will be large. This means that material must be transported over greater distances before reaction can take

FIGURE 5·4

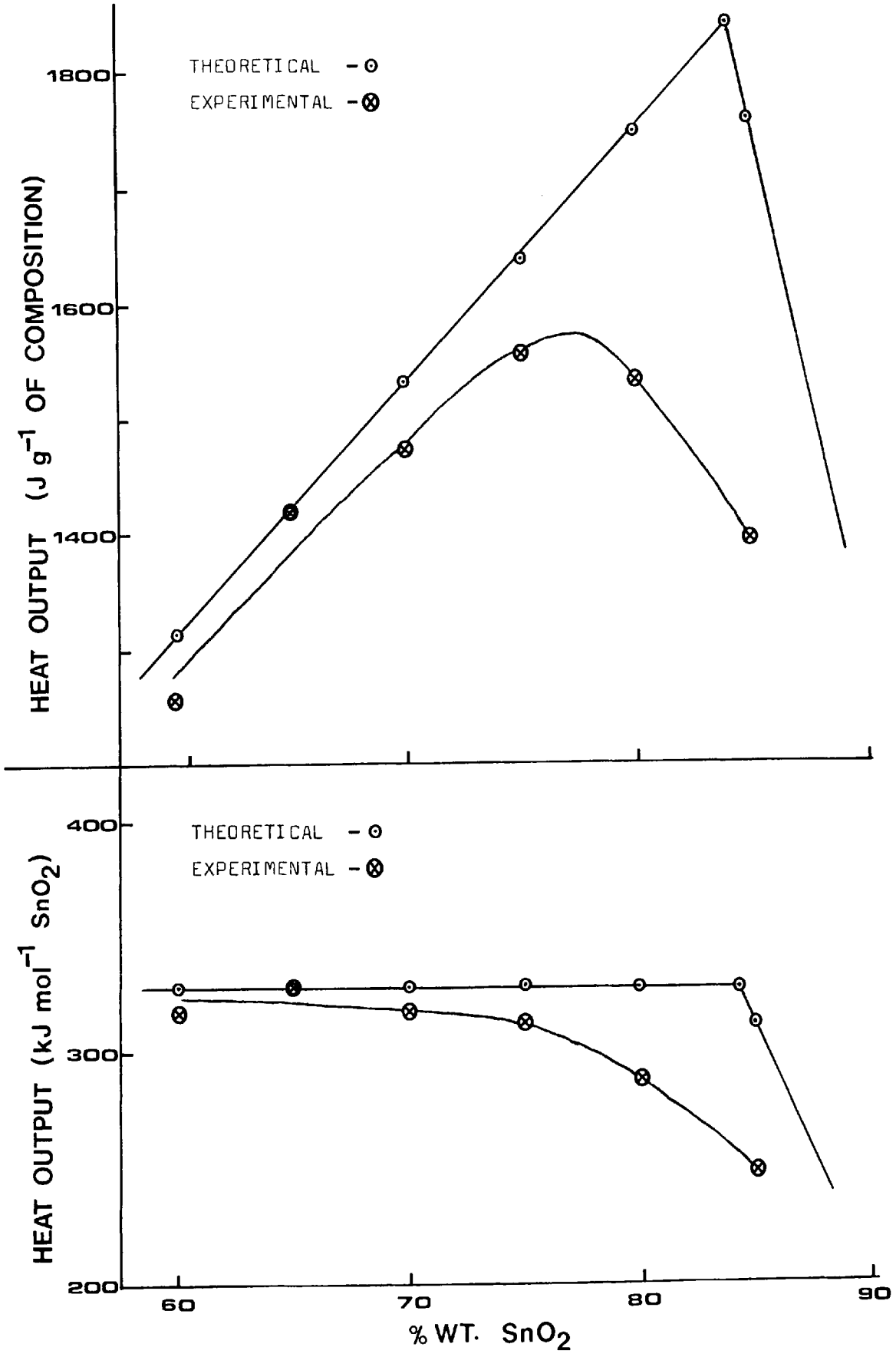

HEAT OUTPUTS OF SnO_2/Si COMPOSITIONS

place and that the heat output/unit volume will be low. It is believed that the inaccessibility of the oxide contributes to the incompleteness of the reaction in this system, until the concentration of fuel particles/unit volume reaches a level whereby a large proportion of the oxide can be consumed in reaction with the surface layers of the fuel particles.

TABLE 5.2

HEAT OUTPUTS OF PbO/B COMPOSITIONS

PbO/B RATIO % wt.	q(J g^{-1}) Theoretical	q(J g^{-1}) Experimental	Q(kJ mol^{-1} PbO) Theoretical	Q(kJ mol^{-1} PbO) Experimental
80/20	709·5	826·4 ± 1·3%	197·8	230·4
85/15	753·8	926·5 ± 4·0%	197·8	243·1
87/13	771·6	947·6 ± 4·4%	197·8	242·9
90/10	798·2	966·4 ± 3·4%	197·8	239·5
92·5/7·5	820·4	954·7 ± 8·3%	197·8	230·2
95/5	842·5	901·0 ± 2·8%	197·8	211·5
98/2	549·4	648·0 ± 2·1%	125·0	147·5

TABLE 5.3

HEAT OUTPUTS OF SnO_2/B COMPOSITIONS

SnO_2/B RATIO % wt.	q(J g^{-1}) Theoretical	q(J g^{-1}) Experimental	Q(kJ mol^{-1} PbO) Theoretical	Q(kJ mol^{-1} PbO) Experimental
70/30	1171·5	1478·6 ± 3·7%	252·2	318·3
75/25	1255·1	1604·6 ± 2·5%	252·2	322·4
80/20	1338·8	1738·5 ± 1·6%	252·2	327·5
82·5/17·5	1380·6	1735·8 ± 4·0%	252·2	317·1
85/15	1422·5	1706·7 ± 2·7%	252·2	302·6
90/10	1506·2	1687·2 ± 5·3%	252·2	282·5

TABLE 5.4

HEAT OUTPUTS OF PbO/Si COMPOSITIONS

PbO/Si RATIO % wt.	q(J g^{-1}) Theoretical	q(J g^{-1}) Experimental	Q(kJ mol^{-1} PbO) Theoretical	Q(kJ mol^{-1} PbO) Experimental
70/30	742·2	745·9 ± 6·8%	236·7	237·8
75/25	795·2	773·8 ± 13·5%	236·7	230·8
80/20	848·2	816·0 ± 3·0%	236·7	227·7
85/15	901·3	842·4 ± 2·0%	236·7	221·2
90/10	954·3	811·3 ± 2·9%	236·7	201·2
95/5	842·5	631·8 ± 3·1%	197·9	148·4

TABLE 5.5

HEAT OUTPUTS OF SnO_2/Si COMPOSITIONS

SnO_2/Si RATIO % wt.	q(J g^{-1}) Theoretical	q(J g^{-1}) Experimental	Q(kJ mol^{-1} SnO_2) Theoretical	Q(kJ mol^{-1} SnO_2) Experimental
60/40	1313·6	1257·8 ± 10·0%	329·9	315·9
65/35	1423·0	1423·6 ± 5·8%	329·9	330·0
70/30	1532·5	1476·7 ± 3·2%	329·9	317·9
75/25	1641·2	1559·5 ± 0·6%	329·9	313·3
80/20	1751·4	1537·0 ± 2·9%	329·9	289·5
85/15	1761·7	1398·1 ± 1·7%	312·3	247·9

CHAPTER 6

PROPAGATION STUDIES

6.1 INTRODUCTION

The study of the propagation characteristics of pyrotechnic systems represents the area of greatest concern to pyrochemists working in the field of commercial pyrotechnic delays.

In blasting applications, at the surface and below ground, the precise staggering of explosions in a series of boreholes is of the utmost importance. The staggering of the explosions reduce vibration, improve fragmentation of the rock and make the blasting process much more controllable.

The staggering of the explosions is brought about by the use of time delay detonators, the basic construction of which is shown in Figure 6.1. All detonators in a series of boreholes are ignited electrically at the same moment, but the timing of the final detonation in each borehole is determined, in general terms, by the length of the delay column of pyrotechnic composition interposed between the ignition source and the small charge of detonating explosive.

Most manufacturers produce two series of delay detonators, one of which progresses from virtually zero delay time to approximately one second in increments of 25 to 30 milliseconds; the other covers the delay range from half a second to approximately four seconds in increments of half a second.

In order to be able to ensure that the precise value of the delay time required for each delay column length is obtained, it is

FIGURE 6.1

A TYPICAL ELECTRIC DELAY DETONATOR

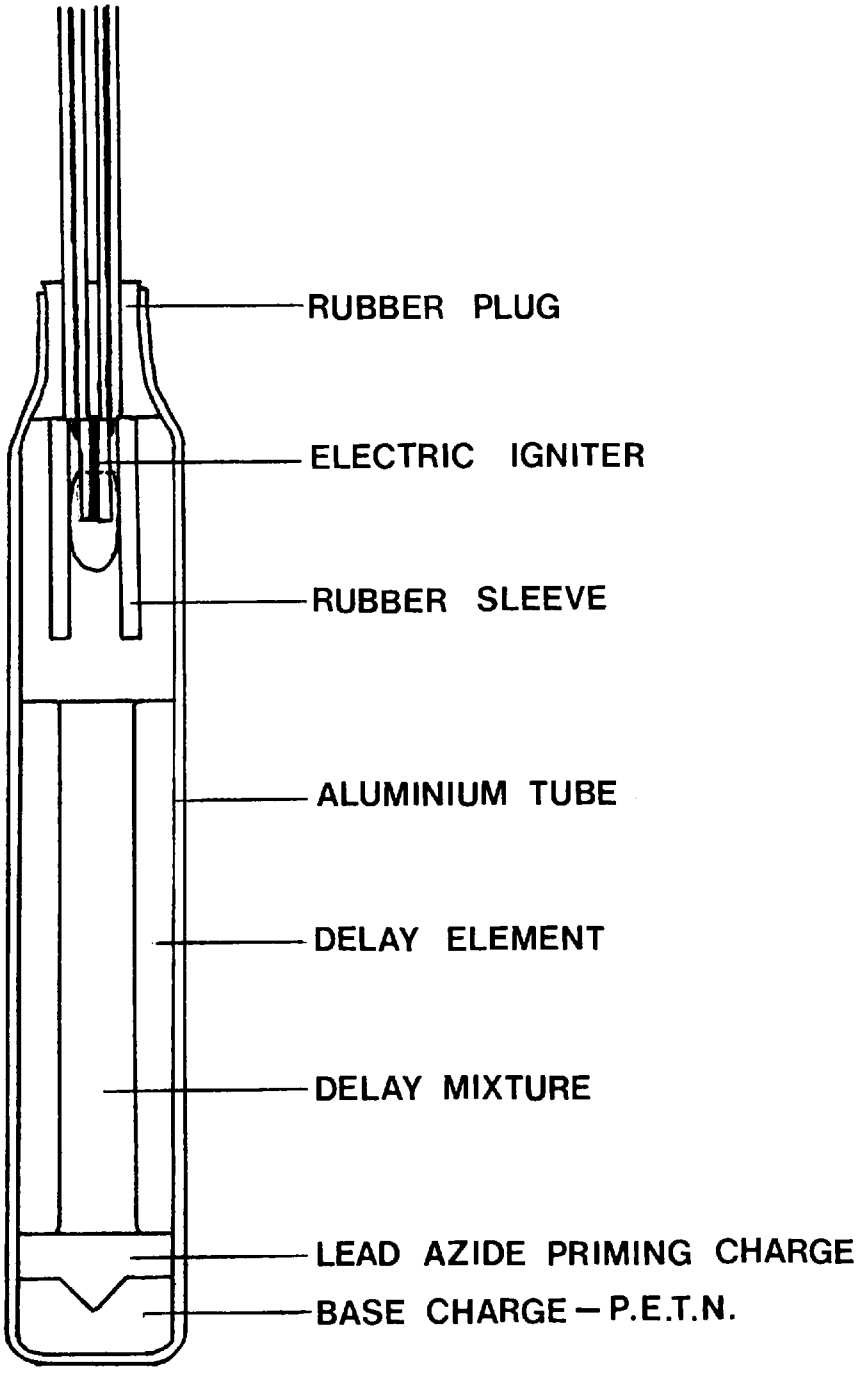

necessary that the response of the pyrotechnic composition used to all factors which affect its propagation rate, and which can be controlled during production, be known in detail.

The control and precision of the delay time in the zero to one second delay series obviously needs to be much greater than for the half to four second delay series where the incremental spacing between consecutive members of the delay series is much larger.

The characterisation of the delay time for any member of a delay series is approached statistically. The delay times of a large number(up to 100 or more) of samples of a member of the series are measured, a statistical distribution of delay times being obtained, from which a value of the mean delay time and the standard deviation of the population can be estimated.

By a comparison of the mean delay time and the standard deviation obtained for consecutive members of a delay series it is possible to tell whether significant overlap in delay times between the consecutive members of the series will be obtained in practice. If this is found to be the case it would mean that if the full delay series of detonators were set up for use,individual members of the series would detonate out of sequence effectively reducing the overall efficiency of the blasting operation.

If the mean delay time obtained for any member of a series is correct but the standard deviation is found to be too large due to poor mixing of the constituents of the composition, this will lead to considerable overlap in delay time with adjacent

members of the series. In this case very little can be done to rectify the situation. However, if the standard deviation is acceptable and the problem is a discrepancy in the mean delay time obtained relative to the nominal value of the delay time required for that member of the series it is possible to adjust the mean value of the delay time obtained, within limits, by varying the consolidation pressure of the composition in the delay element, or by varying the total enclosed volume of the detonator assembly.

As mentioned previously(Chapter 1), the factors which determine the propagation rate of any given pyrotechnic composition are numerous. To determine the detailed response of all the compositions of the four oxidiser/fuel systems examined in this work to variations in all the factors was considered to be beyond the scope of this investigation. What has been attempted is to examine the general propagation characteristics of the four oxidiser/fuel systems in a comparative way so that any differences or similarities between the boron fuelled and silicon fuelled systems can be identified.

6.2 RELATIVE PROPAGATION RATES OF THE BORON AND SILICON FUELLED SYSTEMS

Before discussing in more detail the propagation rates obtained for the four oxidiser/fuel systems examined,it is worth discussing in more general terms their relative propagation rates.

Figure 6.2 shows the variation of delay time(ms) in delay elements of 10mm length with oxidiser level(% wt.) for the four oxidiser/fuel systems examined. The data presented in Figure 6.2 are summarized in Table 6.1 together with some additional data, such as the standard deviation obtained with each measurement. The compositions used to obtain the above data were prepared with the use of organic binders.

The curves of Figure 6.2 show some interesting characteristics. One point that is immediately apparent is that the minimum delay times(maximum propagation rates) obtained for the PbO/B and PbO/Si systems are similar, as are the minimum delay times of the SnO_2/B and SnO_2/Si systems. This would seem to indicate that the oxide component plays a greater part in determining the overall propagation rate of the system than does the fuel component. This conclusion is in accord with the statement of Spice and Staveley(7) where they state that the propagation rate is 'more sensitive to the chemical nature of the oxidising agent than to that of the metal'.

Another point which is easily observed in Figure 6.2 is that the general form of the delay time - oxidiser level curve would appear to depend to a greater extent on the nature of the fuel component present in the system than on the nature of the oxide component. The form of the PbO/B curve is very similar to that

FIGURE 6.2

A COMPARISON OF DELAY TIMES IN THE BORON AND SILICON FUELLED SYSTEMS

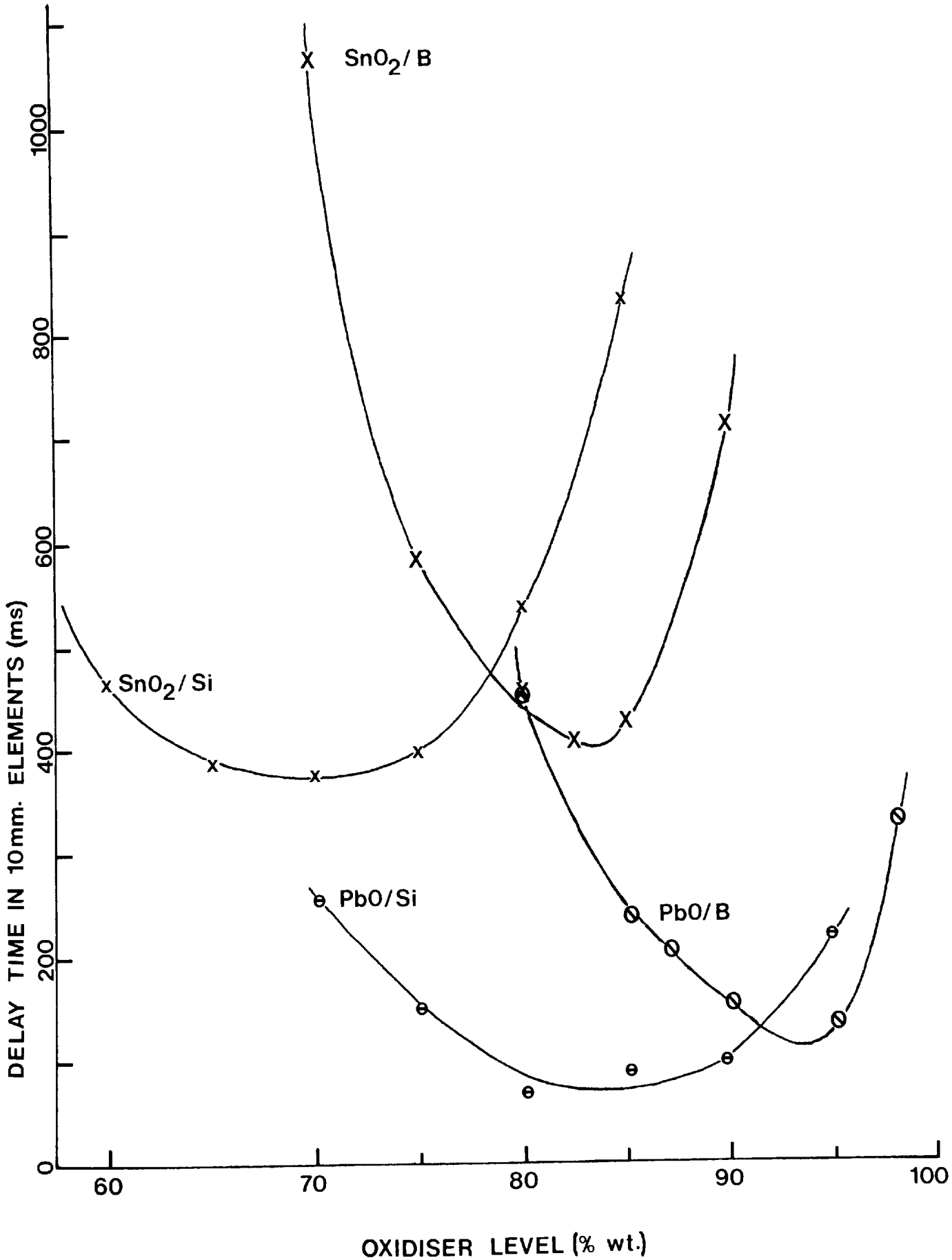

TABLE 6.1

DELAY TIMES IN 10mm. DELAY ELEMENTS AT VARIOUS OXIDE/FUEL RATIOS FOR THE OXIDISER/FUEL SYSTEMS EXAMINED

SYSTEM	OXIDE/FUEL RATIO(% wt.)	DELAY TIME(ms)	STANDARD DEVIATION(ms)	PROPAGATION RATE(cm/s)
PbO/B	80/20	458·3	39·3	2·18
	85/15	239·3	33·1	4·18
	87/13	206·3	20·5	4·85
	90/10	151·3	11·2	6·61
	95/5	133·2	4·9	7·51
	98/2	327·8	31·9	3·05
PbO/Si	70/30	256·2	10·4	3·90
	75/25	150·7	25·9	6·63
	80/20	69·1	13·5	14·47
	85/15	85·6	13·8	11·68
	90/10	99·8	12·3	10·02
	95/5	220·0	17·2	4·55
SnO_2/B	70/30	1066·1	43·0	0·94
	75/25	581·9	25·9	1·72
	80/20	458·6	12·5	2·18
	82·5/17·5	405·6	17·6	2·47
	85/15	425·7	25·2	2·35
	90/10	712·4	79·6	1·40
SnO_2/Si	60/40	465·4	8·3	2·14
	65/35	388·1	7·4	2·58
	70/30	375·2	5·5	2·67
	75/25	398·6	13·9	2·51
	80/20	539·8	34·8	1·85
	85/15	835·0	37·7	1·20

CONSOLIDATION PRESSURE IN ALL CASES = $6{\cdot}1 \times 10^4$ kN m^{-2}

of the SnO_2/B curve, the same being true of the curves of the PbO/Si and SnO_2/Si systems. It would also appear that the range of oxidiser/fuel ratios over which the system will propagate is to a large extent determined by the nature of the fuel component.

6.3 THE RELATIONSHIP BETWEEN HEAT OUTPUTS AND PROPAGATION RATES

Figures 6.3 to 6.6 illustrate the relationship between propagation rates and heat outputs, both theoretical and experimental, for the four oxidiser/fuel systems examined. The data used for these figures can be found in Tables 5.2 to 5.5 and Table 6.1. The consolidation pressure of the compositions was in all cases $6{\cdot}1 \times 10^4$ kN m^{-2}.

Spice and Staveley(7) concluded from their work that the propagation rate 'usually reaches its maximum at a higher, and never a lower, percentage of reducing agent than that at which the heat of burning has its greatest value'. An examination of Figures 6.3 to 6.6 indicates that for the two silicon fuelled systems examined this is indeed the case.

The deflection of the propagation rate maximum to higher fuel levels, relative to the heat output maximum, can be explained by considering the rate of heat evolution rather than simply the magnitude of the heat output itself. Spice and Staveley(7) suggest that in terms of layer-to-layer propagation 'the decrease in the total amount of heat which each layer is capable of generating may be outweighed by a greater rate of evolution of the heat', so that it is possible for the propagation rate to continue to increase even when the heat output is falling.

General observations of the effect of increasing fuel content on DSC traces would tend to support this observation. As the fuel content is increased, above the stoichiometrically required level, the initial peaks in the DSC trace generally increase in size. This indicates the importance of the contribution of the surface

FIGURE 6.3

RELATIONSHIP BETWEEN HEAT OUTPUT AND PROPAGATION RATE IN THE PbO/B SYSTEM

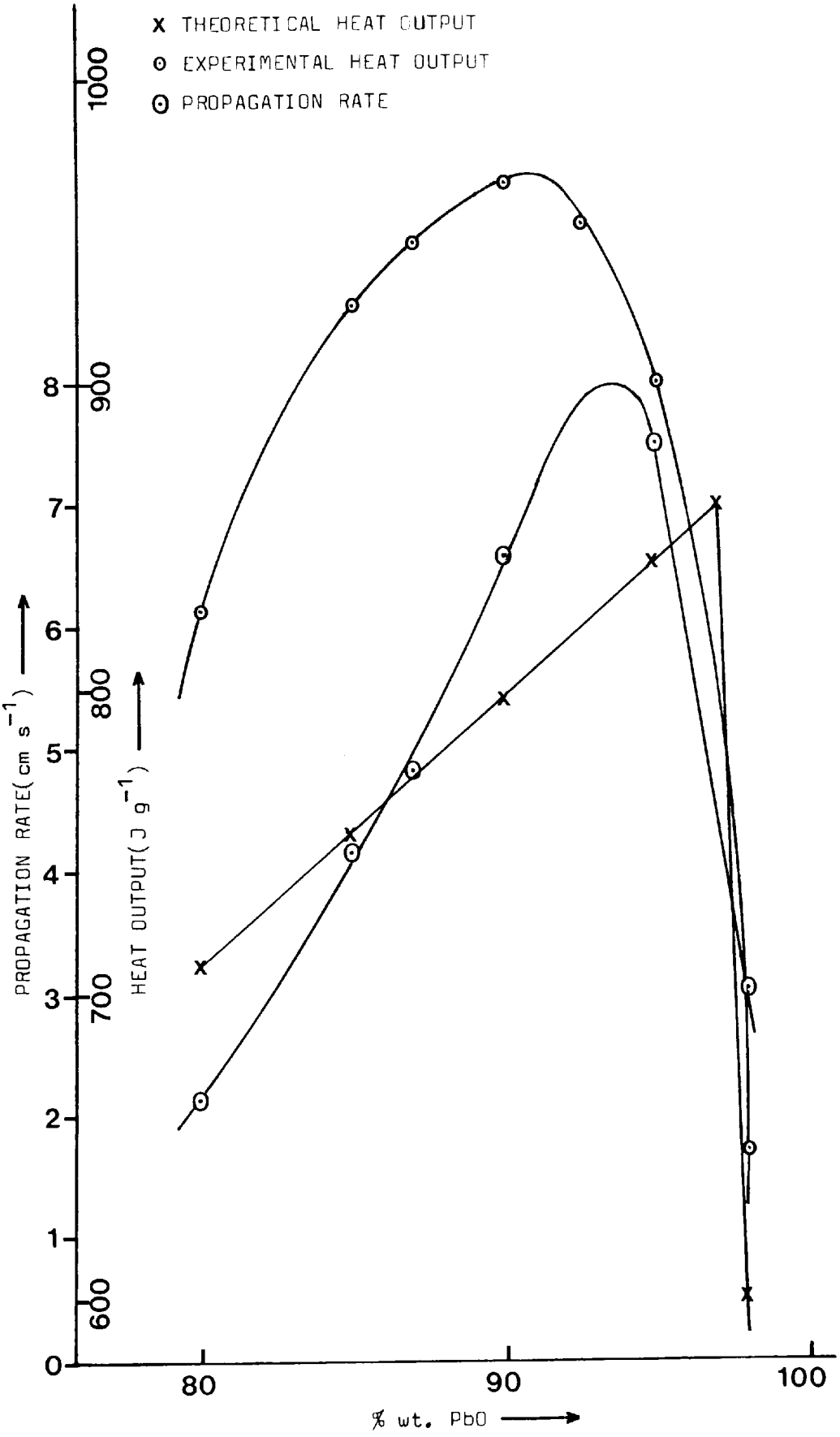

FIGURE 6.4

RELATIONSHIP BETWEEN HEAT OUTPUT AND PROPAGATION RATE IN THE SnO_2/B SYSTEM

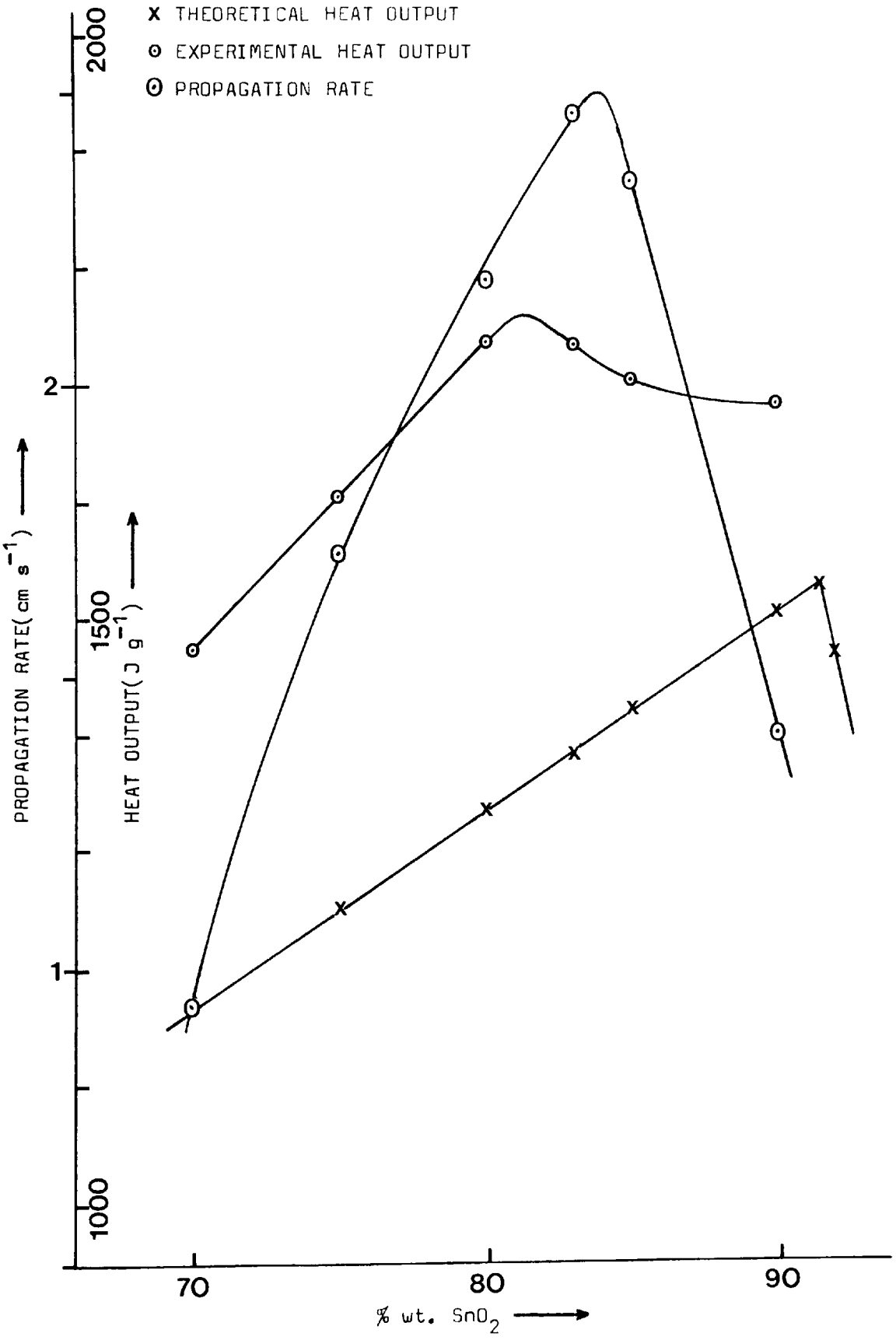

FIGURE 6·5

RELATIONSHIP BETWEEN HEAT OUTPUT AND PROPAGATION RATE

IN THE PbO/Si SYSTEM

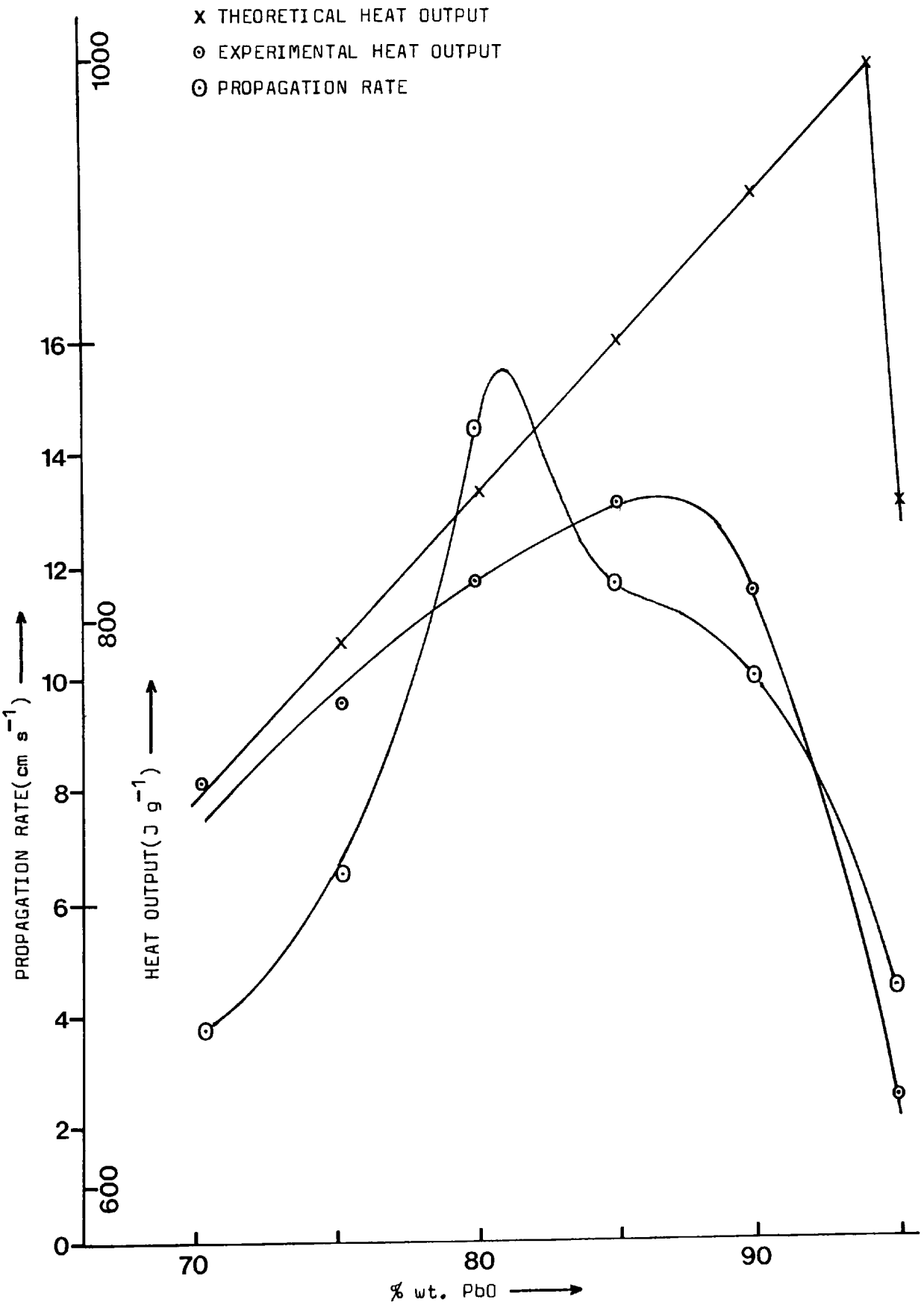

FIGURE 6.6

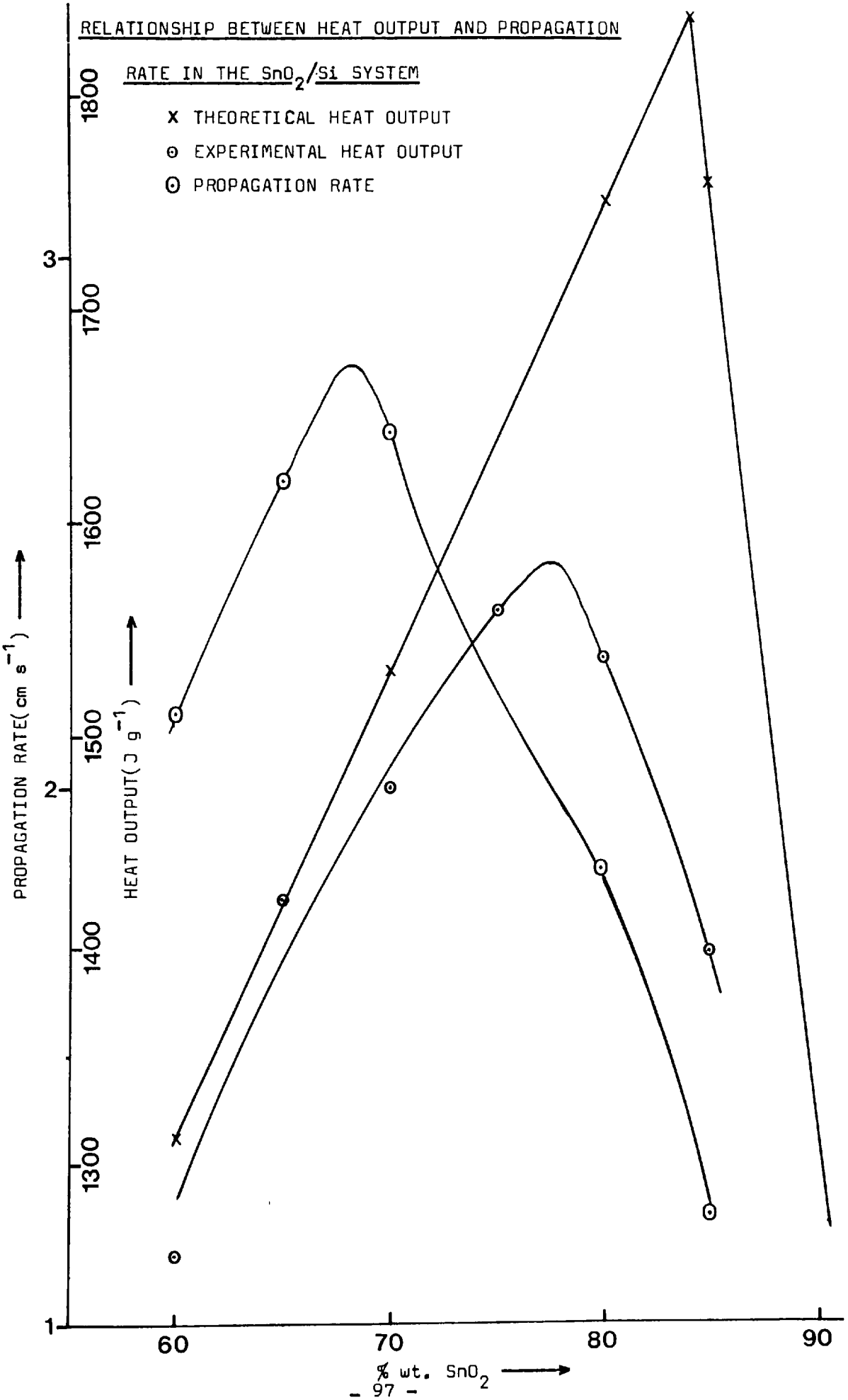
RELATIONSHIP BETWEEN HEAT OUTPUT AND PROPAGATION
RATE IN THE SnO2/Si SYSTEM
X THEORETICAL HEAT OUTPUT
⊙ EXPERIMENTAL HEAT OUTPUT
⊙ PROPAGATION RATE
PROPAGATION RATE(cm s-1)
HEAT OUTPUT(J g-1)
% wt. SnO2
1
2
3
1300
1400
1500
1600
1700
1800
60
70
80
90

reactions in the overall heat outputs of the compositions. This means that the available oxidiser can be consumed, to a large extent, in the surface reaction. The reduction in the importance of the 'bulk' reaction means that the product layer formed by the surface reaction will not significantly contribute to a reduction in the overall rate of the reaction because of its diffusion resistance.

The overall rate of reaction in compositions containing fuel levels in excess of the stoichiometric level would therefore be expected to be greater than that of stoichiometric compositions. This effect would lead to a consequent increase in the rate of heat evolution and of the propagation rate. Obviously this effect must eventually be outweighed by the decrease in the heat outputs of the compositions and the degree to which the contribution of the surface reaction to the total heat output can be increased, which will lead to a reduction in the rate of heat evolution and the propagation rate. If this were not the case no maximum would be observed in the propagation rate versus oxidiser level curve.

In the case of the two silicon fuelled compositions, Figures 6.5 and 6.6, it can be seen that the propagation rate curves exhibit a degree of shouldering at high oxidiser levels. It is proposed that the partially resolved maximum at high oxidiser levels reflects the achievement of the maximum in the heat output curve, while the subsequent maximum at lower oxidiser levels reflects the influence of the rate of heat evolution(enhanced surface reaction) on the propagation rate.

FIGURE 6·7

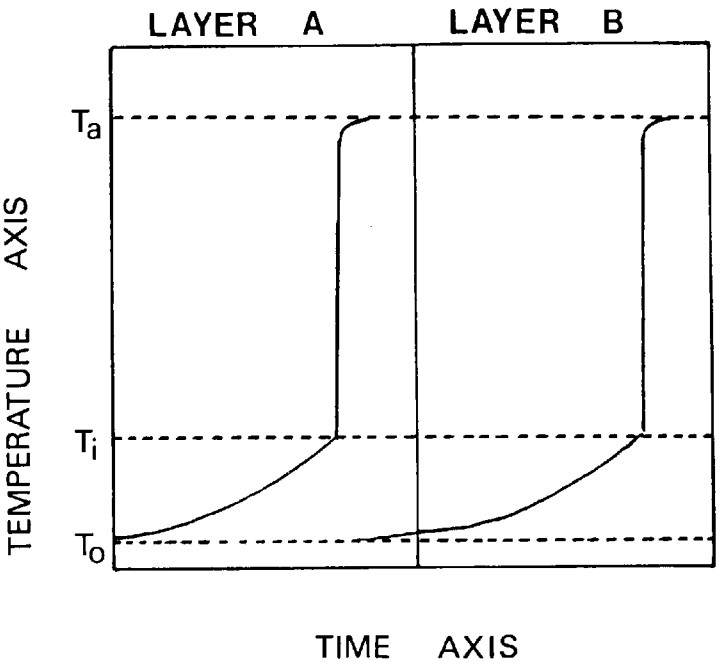

T_o INITIAL TEMPERATURE

T_i IGNITION TEMPERATURE

T_a ADIABATIC REACTION TEMPERATURE

A SCHEMATIC REPRESENTATION OF THE TEMPERATURE-TIME REGIME, IMMEDIATELY AHEAD OF THE REACTION ZONE, IN TWO ADJACENT LAYERS OF UNREACTED COMPOSITION

An examination of Figures 6.3 and 6.4 for the two boron fuelled systems would appear to indicate that the propagation rate curves do not follow the pattern described by Spice and Staveley which is discussed above. However, it is believed that this is not actually the case and that the true relationship of propagation rate to heat output is obscured by various factors in these systems.

If it is assumed, as would appear to be the case, that the heat output curves obtained for these systems are the result of the addition of the heat outputs of vapour phase, boron suboxide producing reactions to the heat output of the probably somewhat reduced B_2O_3 producing reaction, it is possible to explain the pattern of the curves quite simply.

If the assumption is made that a layer-to-layer propagation mechanism is appropriate to these systems, which is the accepted view at the present time, then Figure 6.7 provides a schematic representation of the temperature-time regime, immediately ahead of the reaction zone, in two adjacent layers of unreacted composition.

In Figure 6.7 layer A is at first heated slowly, by the conduction of heat from the reaction zone, from the initial temperature, T_o, to the ignition temperature, T_i. As soon as the temperature in layer A reaches the ignition temperature the chemical reaction between the oxidiser and the fuel takes place, proceeding to completion in a very short time and heating the layer to the adiabatic reaction temperature, T_a, very quickly.

Under the conditions described in Figure 6.7 when layer A reaches the ignition temperature the temperature in layer B is still at, or very close to, the initial temperature. The temperature in layer B does not begin to rise towards the ignition temperature until the temperature in layer A approaches the adiabatic reaction temperature.

In the description of layer-to-layer propagation given above it is assumed that only thermal conduction contributes to the transfer of heat from layer A to layer B. It is known that the thermal conductivities of consolidated pyrotechnic compositions are generally very low (68), much lower in fact than the thermal conductivities of the individual components. This is due to the rather poor contact between the reactant particles in the consolidated compositions which consequently contain significant voidage.

Compositions of low thermal conductivity can be considered to possess a low degree of thermal coupling between the theoretical, adjacent layers of composition. If the thermal coupling between the layers is for any reason increased it would be possible for the temperature in layer B to reach the ignition temperature before the temperature in layer A reaches the adiabatic reaction temperature, particularly if the system possesses a relatively low ignition temperature.

The thermal coupling in pyrotechnic compositions can be increased in various ways. One way in which the coupling can be deliberately increased is by the addition of chemically inert material which will form a liquid phase of high thermal conductivity

at or below the ignition temperature of the particular composition. Al-Kazraji(68) has demonstrated this phenomenon by the addition of lead to Pb_3O_4/Si compositions. The main effect of the lead additions is to increase the propagation rates of the compositons.

In sealed delay assemblies the effect of electrical igniter fuse is to provide enough energy to ignite the consolidated, pyrotechnic composition in the delay element and bring about the propagation reaction. However, the igniter also produces considerable quantities of hot gases which cause a large increase in pressure at the igniter end of the delay assembly(68). This will set up a pressure gradient along the delay column which when coupled with the pressure rise at the reaction zone will cause any hot gases, vapour phase species and liquids generated in the reaction zone to be forced into the unreacted layers ahead of the reaction zone. The main effect of this process will be to increase the thermal coupling in the composition as this process will transport heat faster than would thermal conductivity alone.

As reaction in the boron fuelled systems begins at temperatures well below those at which the production of boron suboxides will reach a significant level, the reaction which causes the initial rapid rise in temperature, at the ignition temperature, will be the B_2O_3 producing reaction.

It is proposed that in the boron fuelled systems the thermal coupling in compositions is very high, due to the production of considerable amounts of liquid and vapour phase species at

moderate temperatures, before the high temperature vapour phase boron suboxide producing reactions take place. This will mean that before the reaction in one layer is completed, that is before the high temperature vapour phase reactions take place, the next layer will have ignited. It should be pointed out that this effect would operate over quite a short distance due to the large temperature gradients present in the delay column. Insufficient information is available at present to enable the relative efficiencies of heat transport by the liquid and vapour phases to be estimated.

The overall effect of the process described above would be to link the propagation rate very strongly to the B_2O_3 producing reaction, while the boron suboxide producing reactions would have very little effect on the propagation rate. It is believed that this process will explain the apparent failure of the boron fuelled systems to observe the relationship between heat outputs and propagation rates proposed by Spice and Staveley(7).

It might be imagined that because of the high degree of thermal coupling present the boron fuelled systems might possess much higher propagation rates than the corresponding silicon fuelled systems. However, this is not the case as many other factors must be taken into consideration when propagation rates are to be compared.

6.4 THE VARIATION OF PROPAGATION RATE WITH CONSOLIDATION PRESSURE

The propagation rates of compositions, containing various oxidiser/fuel ratios, have been determined for the four oxidiser/fuel systems of interest at various consolidation pressures. The consolidation pressures used varied from $1{\cdot}3 \times 10^4$ kN m^{-2} to $2{\cdot}6 \times 10^5$ kN m^{-2}. The results are displayed graphically in Figures 6.8 to 6.11 and are summarized in Tables 6.2 to 6.5.

The four figures show that there are significant differences between the response of the propagation rates of the two boron fuelled systems to increasing consolidation pressure and the response shown by the two silicon fuelled systems. It is believed that these differences indicate a difference in the nature of the mechanism of propagation in boron and silicon fuelled pyrotechnic systems under the experimental conditions used in this work.

Figures 6.8 and 6.9 show the variation of propagation rate with increasing consolidation pressure, at various oxidiser/fuel ratios, for the PbO/B and SnO_2/B systems respectively. As can be seen in both systems, at all the oxidiser/fuel ratios examined, the propagation rate decreases with increasing consolidation pressure.

These results would appear to indicate that the overall response of the propagation rate to increasing consolidation pressure is determined to a great extent by the fuel component present. However, the detailed form of the curves of Figures 6.8 and 6.9 would appear to be determined by the nature of the

FIGURE 6 8

VARIATION OF PROPAGATION RATE WITH CONSOLIDATION PRESSURE

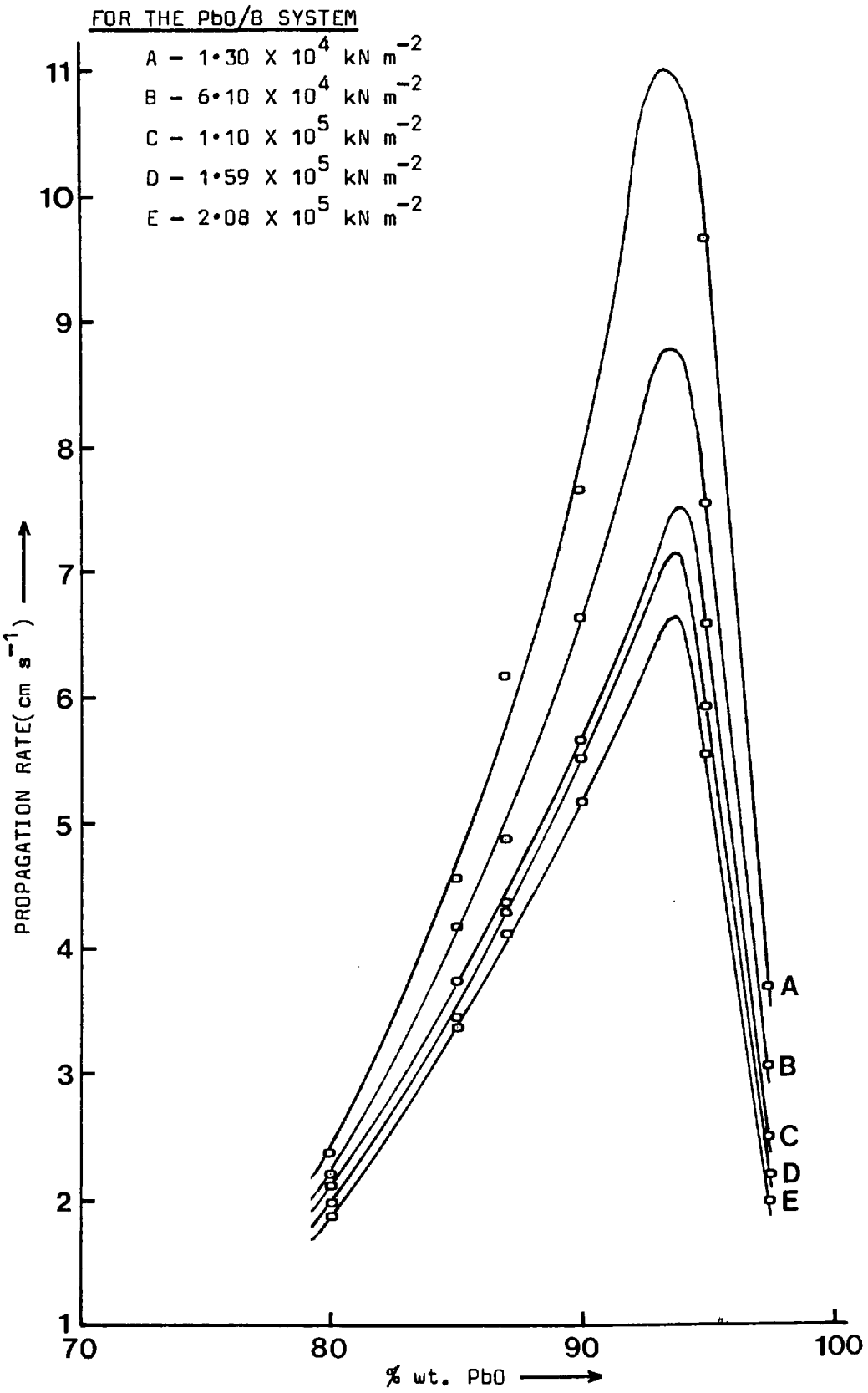

TABLE 6.2 VARIATION OF PROPAGATION RATE WITH CONSOLIDATION PRESSURE FOR THE PbO/B SYSTEM

PbO/B RATIO (% wt.)	CONSOLIDATION PRESSURE($kN\ m^{-2}$)	DELAY TIME(ms)	STANDARD DEVIATION(ms)	PROPAGATION RATE(cm/s)
80/20	$1{\cdot}30 \times 10^4$	423·6	57·4	2·4
	$6{\cdot}10 \times 10^4$	458·3	39·3	2·2
	$1{\cdot}10 \times 10^5$	476·7	37·9	2·1
	$1{\cdot}59 \times 10^5$	508·7	29·1	2·0
	$2{\cdot}08 \times 10^5$	534·5	39·5	1·9
85/15	$1{\cdot}30 \times 10^4$	220·9	28·2	4·5
	$6{\cdot}10 \times 10^4$	239·3	33·1	4·2
	$1{\cdot}10 \times 10^5$	268·5	14·0	3·7
	$1{\cdot}59 \times 10^5$	290·8	19·6	3·4
	$2{\cdot}08 \times 10^5$	296·3	16·2	3·4
87/13	$1{\cdot}30 \times 10^4$	162·4	12·4	6·2
	$6{\cdot}10 \times 10^4$	206·3	20·5	4·9
	$1{\cdot}10 \times 10^5$	230·2	17·3	4·3
	$1{\cdot}59 \times 10^5$	233·1	10·1	4·3
	$2{\cdot}08 \times 10^5$	244·1	10·0	4·1
90/10	$1{\cdot}30 \times 10^4$	130·9	20·0	7·6
	$6{\cdot}10 \times 10^4$	151·3	11·2	6·6
	$1{\cdot}10 \times 10^5$	177·8	8·3	5·6
	$1{\cdot}59 \times 10^5$	182·0	7·2	5·5
	$2{\cdot}08 \times 10^5$	193·0	7·4	5·2
95/5	$1{\cdot}30 \times 10^4$	103·3	6·5	9·7
	$6{\cdot}10 \times 10^4$	133·2	4·9	7·5
	$1{\cdot}10 \times 10^5$	152·1	13·8	6·6
	$1{\cdot}59 \times 10^5$	169·6	7·7	5·9
	$2{\cdot}08 \times 10^5$	180·9	8·8	5·5
98/2	$1{\cdot}30 \times 10^4$	272·7	18·7	3·7
	$6{\cdot}10 \times 10^4$	327·8	31·9	3·1
	$1{\cdot}10 \times 10^5$	408·8	37·8	2·5
	$1{\cdot}59 \times 10^5$	459·6	50·2	2·2
	$2{\cdot}08 \times 10^5$	507·6	36·2	2·0

FIGURE 6.9

VARIATION OF PROPAGATION RATE WITH CONSOLIDATION PRESSURE FOR THE SnO_2/B SYSTEM

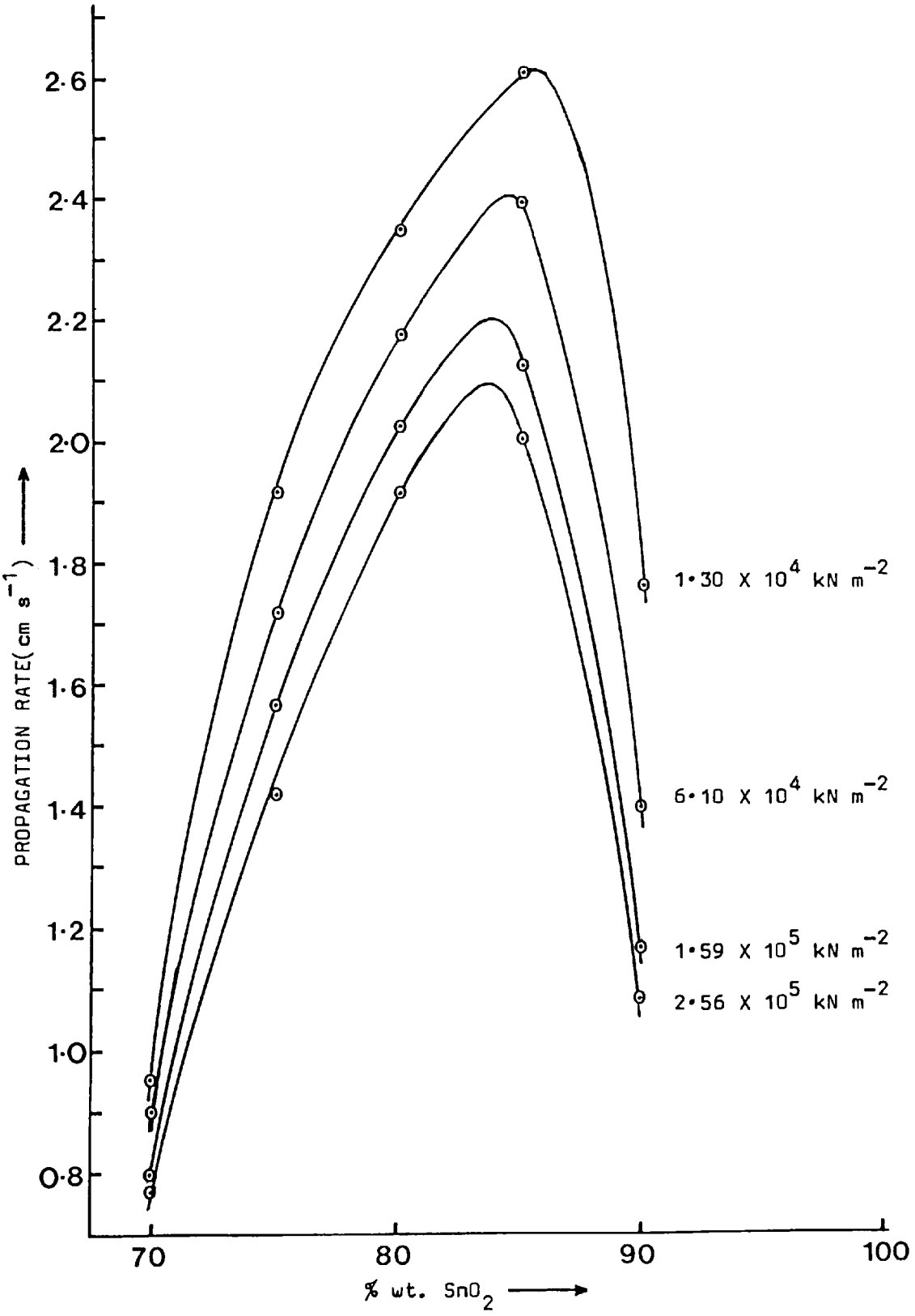

TABLE 6.3 VARIATION OF PROPAGATION RATE WITH CONSOLIDATION PRESSURE FOR THE SnO_2/B SYSTEM

SnO_2/B RATIO (% wt.)	CONSOLIDATION PRESSURE(kN m^{-2})	DELAY TIME(ms)	STANDARD DEVIATION(ms)	PROPAGATION RATE(cm/s)
70/30	$1{\cdot}30 \times 10^4$	1055·1	55·4	0·95
	$6{\cdot}10 \times 10^4$	1066·1	43·0	0·94
	$1{\cdot}59 \times 10^5$	1262·2	37·2	0·79
	$2{\cdot}56 \times 10^5$	1307·8	65·2	0·77
75/25	$1{\cdot}30 \times 10^4$	521·5	29·9	1·92
	$6{\cdot}10 \times 10^4$	581·9	25·9	1·72
	$1{\cdot}59 \times 10^5$	636·7	29·4	1·57
	$2{\cdot}56 \times 10^5$	702·6	40·6	1·42
80/20	$1{\cdot}30 \times 10^4$	425·4	18·5	2·35
	$6{\cdot}10 \times 10^4$	458·6	12·5	2·18
	$1{\cdot}59 \times 10^5$	493·7	16·8	2·03
	$2{\cdot}56 \times 10^5$	520·1	16·9	1·92
85/15	$1{\cdot}30 \times 10^4$	383·8	31·3	2·61
	$6{\cdot}10 \times 10^4$	425·7	25·2	2·35
	$1{\cdot}59 \times 10^5$	470·3	32·9	2·13
	$2{\cdot}56 \times 10^5$	496·9	43·5	2·01
90/10	$1{\cdot}30 \times 10^4$	565·2	145·8	1·77
	$6{\cdot}10 \times 10^4$	712·4	79·5	1·40
	$1{\cdot}59 \times 10^5$	853·7	69·3	1·17
	$2{\cdot}56 \times 10^5$	916·9	60·5	1·09

FIGURE 6·10

VARIATION OF PROPAGATION RATE WITH CONSOLIDATION PRESSURE

FOR THE PbO/Si SYSTEM

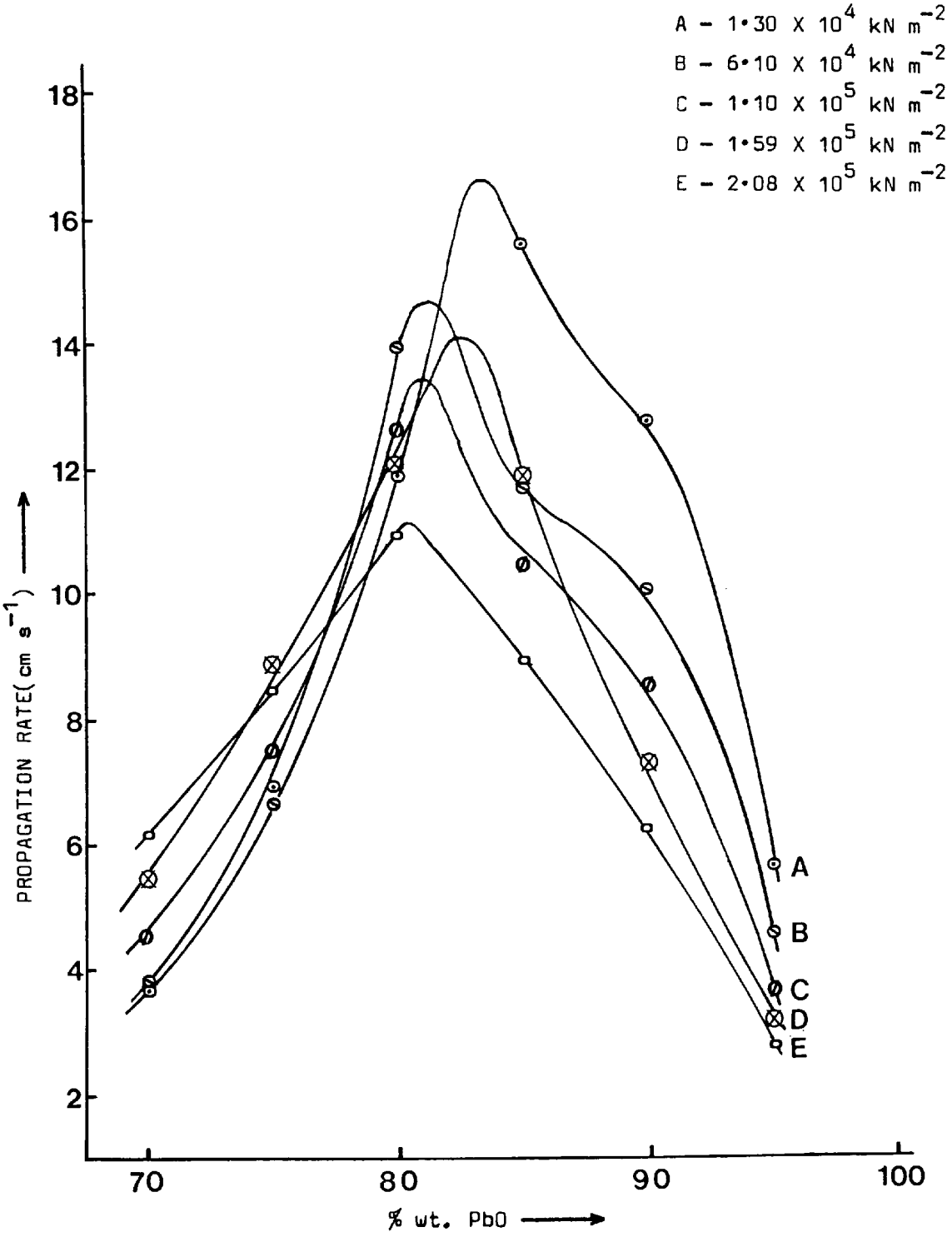

TABLE 6.4 VARIATION OF PROPAGATION RATE WITH CONSOLIDATION PRESSURE FOR THE PbO/Si SYSTEM

PbO/Si RATIO (% wt.)	CONSOLIDATION PRESSURE($kN\ m^{-2}$)	DELAY TIME(ms)	STANDARD DEVIATION(ms)	PROPAGATION RATE(cm/s)
70/30	$1{\cdot}30 \times 10^4$	259·2	6·5	3·9
	$6{\cdot}10 \times 10^4$	256·0	10·4	3·9
	$1{\cdot}10 \times 10^5$	218·7	19·9	4·6
	$1{\cdot}59 \times 10^5$	182·9	15·8	5·5
	$2{\cdot}08 \times 10^5$	161·6	20·2	6·2
75/25	$1{\cdot}30 \times 10^4$	144·3	16·8	6·9
	$6{\cdot}10 \times 10^4$	150·7	25·9	6·6
	$1{\cdot}10 \times 10^5$	134·2	29·3	7·5
	$1{\cdot}59 \times 10^5$	113·3	23·4	8·8
	$2{\cdot}08 \times 10^5$	118·7	23·7	8·4
80/20	$1{\cdot}30 \times 10^4$	84·0	15·2	11·9
	$6{\cdot}10 \times 10^4$	69·1	13·5	14·5
	$1{\cdot}10 \times 10^5$	79·3	12·1	12·6
	$1{\cdot}59 \times 10^5$	83·8	9·3	11·9
	$2{\cdot}08 \times 10^5$	91·0	11·1	11·0
85/15	$1{\cdot}30 \times 10^4$	64·1	18·0	15·6
	$6{\cdot}10 \times 10^4$	85·6	13·8	11·7
	$1{\cdot}10 \times 10^5$	96·0	13·3	10·4
	$1{\cdot}59 \times 10^5$	84·4	5·8	11·9
	$2{\cdot}08 \times 10^5$	111·5	20·5	9·0
90/10	$1{\cdot}30 \times 10^4$	78·5	5·5	12·7
	$6{\cdot}10 \times 10^4$	99·8	12·3	10·0
	$1{\cdot}10 \times 10^5$	117·5	10·0	8·5
	$1{\cdot}59 \times 10^5$	137·8	5·3	7·3
	$2{\cdot}08 \times 10^5$	160·7	9·5	6·2
95/5	$1{\cdot}30 \times 10^4$	178·2	7·8	5·6
	$6{\cdot}10 \times 10^4$	220·0	17·2	4·6
	$1{\cdot}10 \times 10^5$	276·3	34·5	3·6
	$1{\cdot}59 \times 10^5$	316·3	21·6	3·2
	$2{\cdot}08 \times 10^5$	360·5	42·3	2·8

FIGURE 6.11

VARIATION OF PROPAGATION RATE WITH CONSOLIDATION PRESSURE FOR THE SnO_2/Si SYSTEM

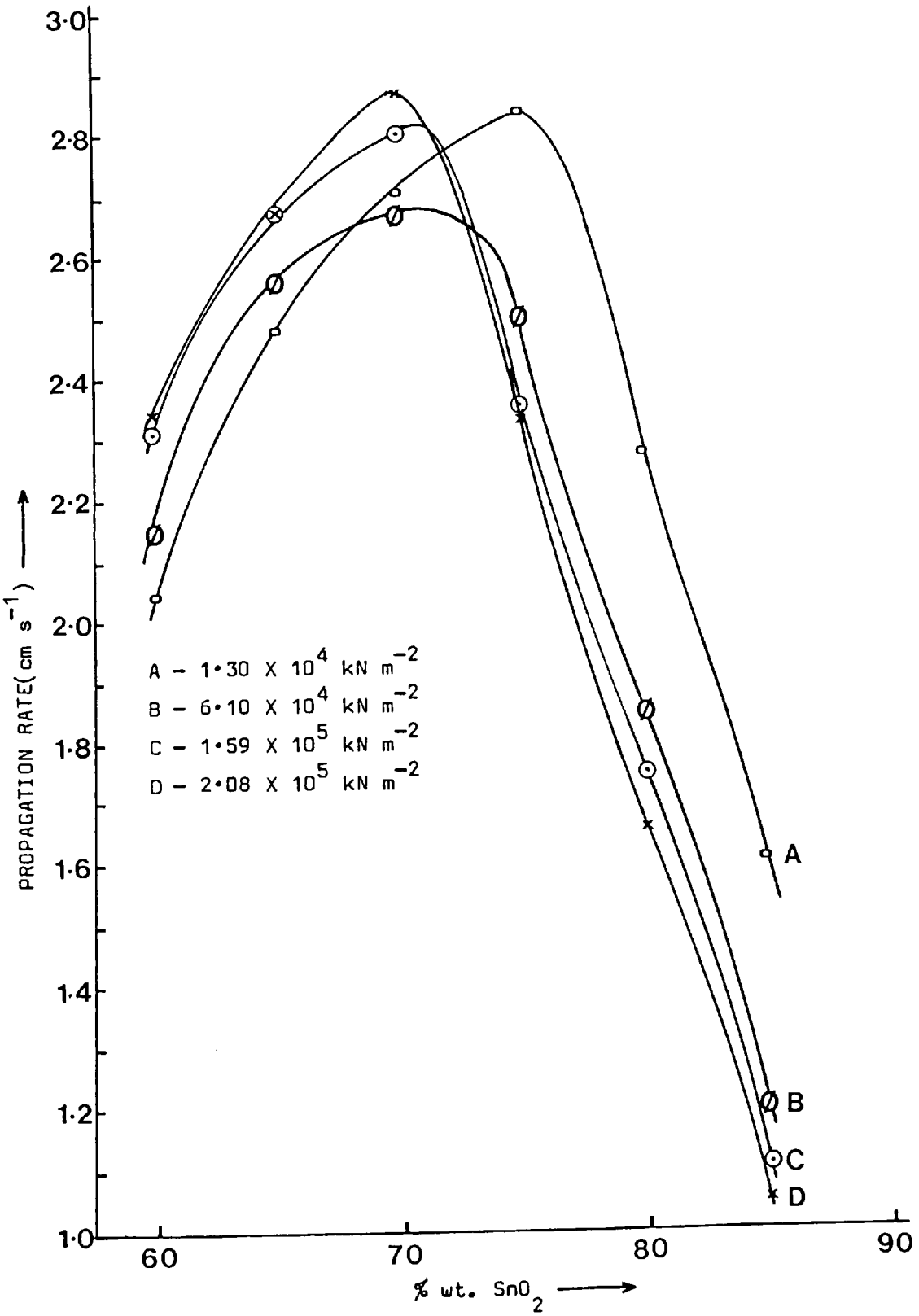

TABLE 6.5 VARIATION OF PROPAGATION RATE WITH CONSOLIDATION PRESSURE FOR THE SnO_2/Si SYSTEM

SnO_2/Si RATIO (% wt.)	CONSOLIDATION PRESSURE(kN m^{-2})	DELAY TIME(ms)	STANDARD DEVIATION(ms)	PROPAGATION RATE(cm/s)
60/40	$1{\cdot}30 \times 10^4$	490·0	4·7	2·04
	$6{\cdot}10 \times 10^4$	465·4	8·3	2·15
	$1{\cdot}59 \times 10^5$	430·6	14·3	2·32
	$2{\cdot}08 \times 10^5$	426·8	8·2	2·34
65/35	$1{\cdot}30 \times 10^4$	403·2	11·4	2·48
	$6{\cdot}10 \times 10^4$	388·1	7·4	2·56
	$1{\cdot}59 \times 10^5$	374·3	8·1	2·67
	$2{\cdot}08 \times 10^5$	374·7	10·1	2·67
70/30	$1{\cdot}30 \times 10^4$	368·5	28·6	2·71
	$6{\cdot}10 \times 10^4$	375·2	5·5	2·67
	$1{\cdot}59 \times 10^5$	355·6	8·9	2·81
	$2{\cdot}08 \times 10^5$	348·0	16·8	2·87
75/25	$1{\cdot}30 \times 10^4$	352·2	21·8	2·84
	$6{\cdot}10 \times 10^4$	398·6	13·9	2·50
	$1{\cdot}59 \times 10^5$	424·1	9·7	2·36
	$2{\cdot}08 \times 10^5$	426·6	8·7	2·34
80/20	$1{\cdot}30 \times 10^4$	439·2	28·0	2·28
	$6{\cdot}10 \times 10^4$	539·8	34·8	1·85
	$1{\cdot}59 \times 10^5$	570·5	11·5	1·75
	$2{\cdot}08 \times 10^5$	604·4	9·6	1·66
85/15	$1{\cdot}30 \times 10^4$	622·2	48·2	1·61
	$6{\cdot}10 \times 10^4$	835·0	37·7	1·20
	$1{\cdot}59 \times 10^5$	902·0	36·0	1·11
	$2{\cdot}08 \times 10^5$	947·9	85·4	1·05

oxidiser present in each particular case.

One point which is immediately apparent and which is observed in both Figure 6.8 and 6.9 is the trend in response at the extremes of the oxidiser/fuel ratio range over which propagation is obtained. In both cases a much larger decrease in the propagation rate with increasing consolidation pressure is obtained at high oxidiser levels.

In order to be able to explain both the overall trend in propagation rates with increasing consolidation pressures and the detailed form of the curves for the two boron fuelled systems it is neccessary to examine further the propagation mechanism described in the preceding section.

As mentioned previously the combustion of the electrical igniter in sealed delay assemblies produces a large rise in pressure at the igniter end of the delay assembly, which in turn will cause a pressure wave to move along the delay column forcing hot gases, vapour phase and liquid species produced in the reaction zone into the unreacted composition ahead of the reaction zone.

In the case of pyrotechnic systems in which one or more of the reaction products possess high vapour pressures and in which low temperature liquid phases are produced the main heat transfer process, causing propagation of the reaction zone, will be one of the transport of hot material from the reaction zone into the adjacent unreacted composition. The heat transferred by this process being sufficient to raise the temperature of the unreacted composition rapidly to the required ignition temperature. It is

proposed that heat transfer by mass transport is the dominant process in the propagation mechanism of the boron fuelled pyrotechnic systems studied.

The direct effect of an increase in the consolidation pressure in a pyrotechnic system is to increase the density of the composition in the delay column. There is also a consequent decrease in the voidage present in the consolidated composition. If the propagation mechanism proposed above is correct, then as the consolidation pressure is increased and the voidage in the delay column is decreased the ease, and therefore the speed, with which the pressure wave induced by the igniter travels along the delay column should be reduced and the propagation rate should decrease accordingly. The results presented in Figures 6.8 and 6.9 for the boron fuelled systems examined support the propagation mechanism proposed above.

It is worth stressing the point that in the boron fuelled systems it is the pressure gradient developed which is of importance in modifying the propagation rate. An initial high gas pressure along the entire length of the delay column,in a delay assembly vented at the igniter end,would produce a somewhat different result. This effect is demonstrated for the PbO/B system later in this chapter.

Figures 6.10 and 6.11 show the variation in propagation rate with increasing consolidation, at various oxidiser/fuel ratios, for the PbO/Si and SnO_2/Si systems respectively. As can be seen the response of the silicon fuelled systems to increasing consolidation pressure is significantly different

from the response exhibited by the boron fuelled systems.

The response of the silicon fuelled systems to increasing consolidation pressure can be divided into three distinct types of behaviour with regard to the oxidiser/fuel ratio range in which they are observed. At high oxidiser levels where the reaction temperature is high(see Chapter 7), the propagation rate decreases with increasing consolidation pressure, while at low oxidiser levels where the reaction temperature is lower the propagation rate increases with increasing consolidation pressure. Between these two regions of distinct and different behaviour there is a region at intermediate oxidiser levels where the response to increasing consolidation pressure is more complex.

At high oxidiser levels the response of the silicon fuelled systems is similar to that of the boron fuelled systems. It seems very likely, taking into account the high reaction temperatures achieved and the large amounts of relatively volatile metallic reaction products evolved, that the transfer of heat by mass transport processes dominates the propagation mechanism in this region.

At low oxidiser levels, where the mass transport processes will be considerably reduced because of the lower reaction temperatures achieved, it seems likely that heat transfer by conduction will be the dominant process in the propagation mechanism. This seems even more likely when the refractory nature of the SiO_2 produced is taken into account and compared with the volatility of the B_2O_3 produced and the ease of liquid

phase production at analogous oxidiser levels in the boron fuelled systems.

If the interpretation of the results given above is correct, then the behaviour at intermediate oxidiser levels can be explained on the assumption that neither heat transfer process dominates the propagation mechanism, over the entire range of consolidation pressures examined.

6.5 A BRIEF DISCUSSION OF THE EFFECT OF VENTED DELAY ASSEMBLIES AND VARYING ATMOSPHERIC PRESSURE ON PROPAGATION RATES

In the preceding section the effect of varying consolidation pressure on the propagation rates of pyrotechnic compositions in sealed delay assemblies was examined. As was indicated the use of delay assemblies vented at the igniter end would produce quite different results. When the delay times of compositions are measured in vented delay assemblies the results obtained are of poor quality, the delay times exhibiting large scatters about the mean value.

Because of the poor quality of the results only those for selected PbO/B compositions are shown to demonstrate the effect of venting and varying atmospheric pressure on propagation rates. Figure 6.12 shows the delay times for three PbO/B compositions in 10mm delay columns at a consolidation pressure of $6{\cdot}1 \times 10^4$ kN m^{-2} measured in:

A - sealed delay assemblies initially at a pressure of 1 atm

B - vented delay assemblies in N_2 at a pressure of 1 atm

C - vented delay assemblies in N_2 at a pressure of 7 atm

The barred and arrowed lines both represent one standard deviation unit above and below the mean value obtained.

As can be seen the effect of a moderate increase in atmospheric pressure in the vented systems is to increase the propagation rate which is the expected result(32).

The interesting feature of the results are the relatively small scatters of the delay times obtained in sealed delay

FIGURE 6·12

THE EFFECT OF VENTED DELAY ASSEMBLIES AND VARYING ATMOSPHERIC PRESSURE ON PROPAGATION RATES IN THE PbO/B SYSTEM

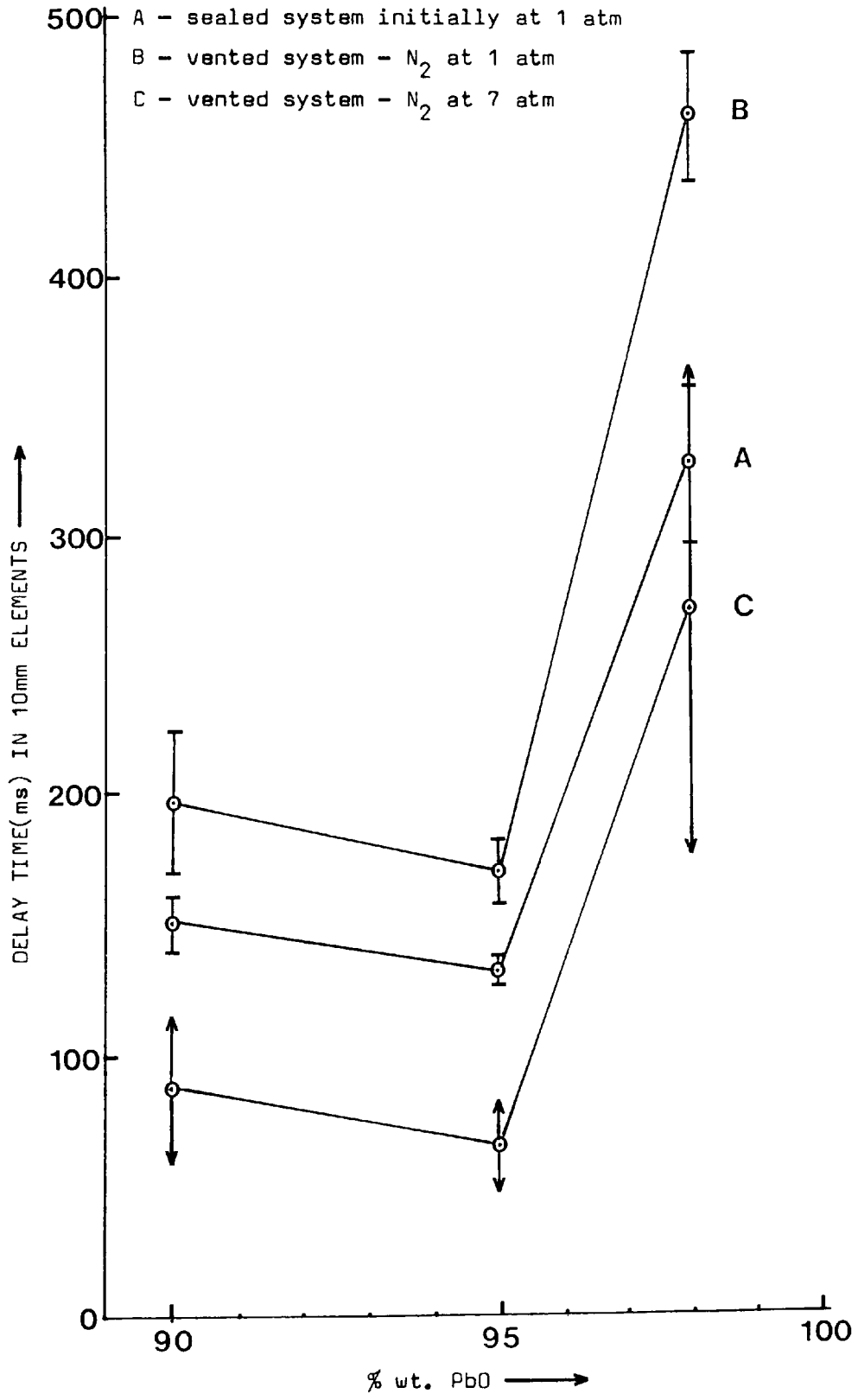

assemblies when compared with the results for the vented assemblies at 7 atm of pressure. The normal trend for delay time standard deviations is for them to become smaller the faster a composition propagates. It is believed that the opposite trend observed here is further evidence of the modifying effect on propagation of the directional pressure pulse generated by the igniter.

CHAPTER 7

REACTION TEMPERATURE MEASUREMENTS

7.1 INTRODUCTION

The measurement of the reaction temperatures of pyrotechnic delay systems is of considerable practical, as well as theoretical, interest. The incendivity of certain compositions, especially those containing titanium(78), when used in an atmosphere containing potentially explosive gas mixtures, is,most likely, at least partly a function of the high reaction temperatures attained.

The aquisition of reaction temperature data is normally accomplished using a thermocouple system. This technique has been described by Al-Kazraji(68). In order to achieve the fast thermocouple response times required in this type of work, the junctions must be made as fine as possible making them prone to damage.

Viewed objectively, the thermocouple method is not ideally suited to the task of obtaining reaction temperature data on large numbers of prospective delay compositions in an industrial environment, although its value as an academic research method is significant.

The thermocouple junction problem is particularly acute with certain pyrotechnic compositions which are characterized by very fast reactions, approximately 100 ms duration, and transient high temperatures(2000K to 3000K).

In the present work an automatic recording radiation pyrometer, operating in the near infra-red region, has been used in an attempt to find a more convenient and practical method of reaction temperature measurement.

Pyrometers of the type used in this work have characteristics which make them attractive for this purpose. The silicon detectors which they contain have response times in the microsecond range, which should be adequate to follow the temperature rise times encountered in pyrotechnic systems. Silicon detectors are also not prone to interference by the infra-red absorption bands to atmospheric carbon dioxide and water vapour. An informative discussion of the advantages and disadvantages associated with the use of silicon detectors is given by Barber and Land(79).

The principal problem affecting the accuracy of temperature measurements made with pyrometers is that of determining the emittance of the target. With regard to the present work, no precise information is available on the emittance of the complex mixtures of reaction products obtained, at the wavelengths to which the silicon detector responds.

It is worth stressing that the emittance of a material, unlike its emissivity, does not have a unique value but is highly dependent on the surface properties of the material. The definitions of the two terms help to clarify the distinction.

EMISSIVITY —— 'A property of a material, measured as the emittance of a specimen of the material that is thick enough to be completely opaque and has an optically smooth surface.'(72)

EMITTANCE —— ' The ratio of the emitted radiant flux per unit area of a sample to that of a black body radiator at the same temperature and under the same conditions.'(72)

The emissivity of a substance is in fact related to the electrical conductivity(or resistivity) of that substance and the spectral wavelength at which it is measured. It can therefore be seen that emissivity will vary with the wavelength at which it is measured and if the electrical conductivity(or resistivity) varies with temperature, at any given wavelength the emissivity will also vary with temperature. However, changes of emissivity, and therefore of emittance, with temperature are generally small enough to be ignored for practical purposes(80).

Initial measurements of the emittance values of the reaction products of the four pyrotechnic systems examined indicated that there was a sharp drop in emittance at approximately 1000K. Subsequently, this drop was found to be due to the experimental method described in Chapter 4. Using this method there is a considerable discrepancy between furnace wall temperature and sample temperatures close to and above 1000K(indicated sample temperature). Further work has shown that at lower temperatures, where the discrepancy between furnace wall temperature and sample temperature is much smaller, much more realistic emittance values are obtained. Consequently, all reaction temperatures quoted in this thesis have been determined using emittance values measured at 883K.

Theoretical adiabatic reaction temperatures have only been calculated for the lead monoxide/silicon system which provide a direct comparison with those calculated previously for the red lead/silicon system(68). The adiabatic reaction temperatures were calculated by the method described by Harris(33) and Al-Kazraji(68), while the heat outputs were the theoretical ones presented in Chapter 5.

FIGURE 7·1

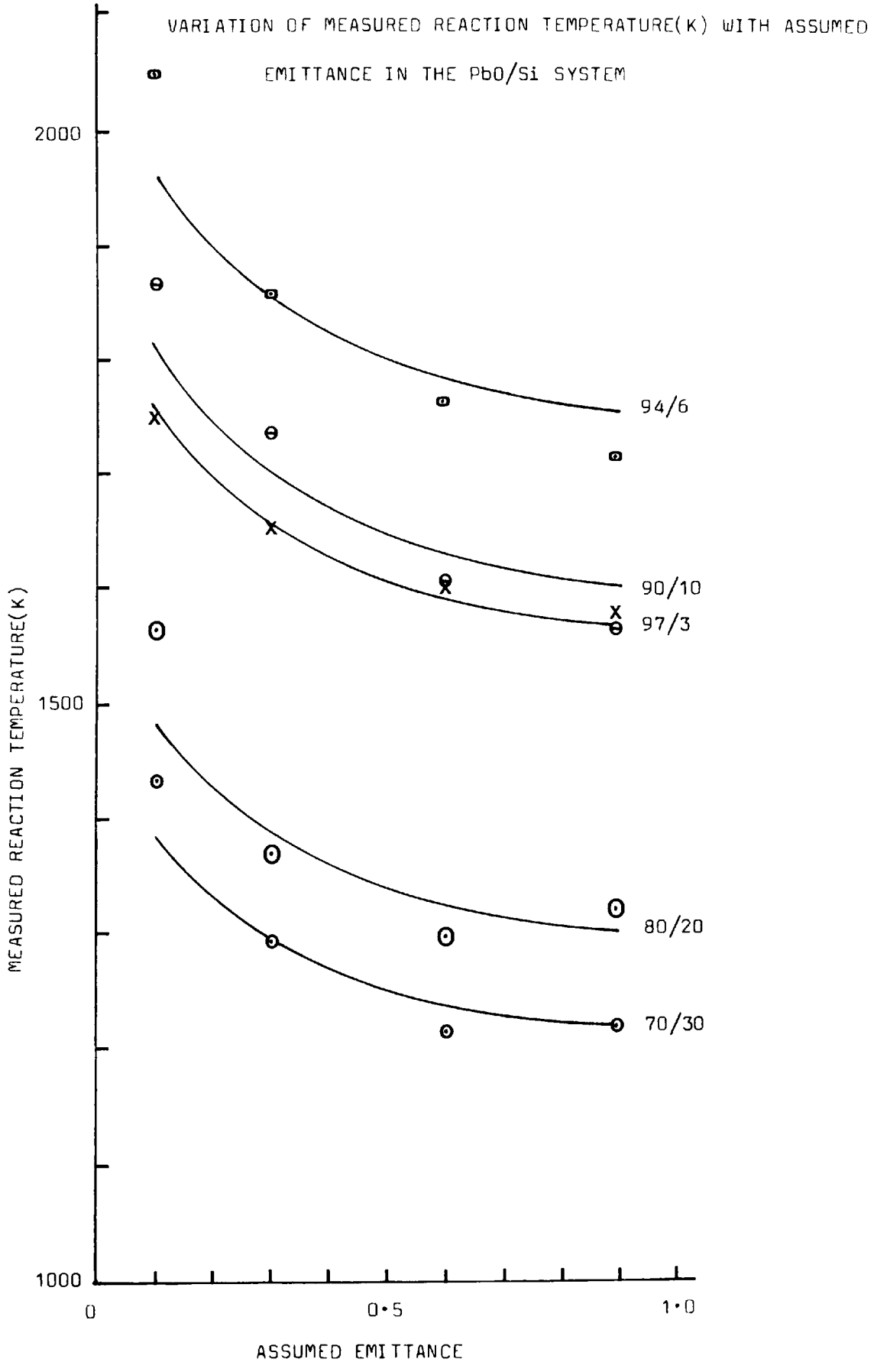
VARIATION OF MEASURED REACTION TEMPERATURE(K) WITH ASSUMED EMITTANCE IN THE PbO/Si SYSTEM
MEASURED REACTION TEMPERATURE(K)
2000
1500
1000
0
0·5
1·0
ASSUMED EMITTANCE
94/6
90/10
97/3
80/20
70/30

TABLE 7.1 VARIATION OF MEASURED REACTION TEMPERATURE(K) WITH ASSUMED EMITTANCE IN THE PbO/Si SYSTEM

ASSUMED EMITTANCE	PbO/Si RATIO (% WT)				
	70/30	80/20	90/10	94/6	97/3
0·1	1432 +/- 5%	1564 +/- 12%	1866 +/- 1%	2044 +/- 12%	1747 +/- 3%
0·3	1293 +/- 10%	1370 +/- 4%	1737 +/- 3%	1855 +/- 6%	1651 +/- 15%
0·6	1217 +/- 6%	1298 +/- 9%	1607 +/- 4%	1762 +/- 7%	1601 +/- 3%
0·9	1221 +/- 5%	1322 +/- 7%	1569 +/- 4%	1714 +/- 4%	1577 +/- 1%

ERROR LIMITS ARE DISPLAYED AS +/- 2 STANDARD DEVIATION UNITS ABOUT THE MEAN VALUE

The effect of the assumed emittance value on the measured reaction temperature is shown in Figure 7.1, the data being summarized in Table 7.1. In this figure the variation of the measured reaction temperature with assumed emittance value for several lead monoxide/silicon compositions is shown. As can be seen the trend in the measured reaction temperature with decreasing assumed emittance is, as would be expected, similar for all compositions.

Inspection of the data contained in Table 7.1 indicates that the maximum error in the measured temperature, linked to a maximum error in emittance setting, which should be expected is of the order of 20%. However, the occurence of emittance values lower than 0·5 in other than specially prepared materials, where the emittance value approaches the emissivity value, is quite rare. Therefore it should be expected that the error in the measured temperature should be much lower than 20%, probably of the order of 5%.

Table 7.2 presents the emittance values for several materials, and demonstrates the change in emittance value with changes in surface properties(80).

All reaction temperatures quoted in this thesis have been recorded using an emittance setting, adjusted for window material radiation losses, of 0·55.

TABLE 7.2

EMITTANCE VALUES FOR POLISHED AND OXIDISED METALS *

MATERIAL	Smooth Polish	Smooth Oxide
Alumel	0.32	0.90
Aluminium	0.15	0.25
Brass	0.20	0.70
Carbon Steel	0.33	0.75
Chromel	0.33	0.90
Chromium	0.40	0.70
Cobalt	0.33	0.75
Copper	0.10	0.70
Graphite (Smooth)	0.80	-
Iron	0.33	0.70
Lead	0.25	0.70
Manganese	0.45	0.90
Molybdenum	0.38	-
Nichrome	0.36	0.90
Nickel	0.32	0.90
Platinum	0.27	-
Silver	0.05	0.80
Silicon	0.70	-
Stainless Steel	0.33	0.85
Tantalum	0.27	0.70
Tin	0.35	0.60
Tungsten	0.40	0.60
Vanadium	0.36	0.75
Zinc	0.20	0.50
Zirconium	0.30	0.40

* The values listed refer to flat polished specimens and to the oxides formed on these surfaces.

7.2 REACTION TEMPERATURES IN THE PbO/B AND PbO/Si SYSTEMS

The measured reaction temperatures of PbO/B and PbO/Si compositions, containing various oxidiser/fuel ratios, are shown in Figures 7.2 and 7.3. The data displayed in these figures are summarized in Tables 7.3 and 7.4. In addition, Figure 7.3 also shows the calculated adiabatic reaction temperatures for the PbO/Si system.

The theoretical reaction temperatures for the PbO/Si system shown in Figure 7.3 have been calculated assuming constant pressure conditions, thus limiting the maximum attainable temperatures for the 90/10 and 94/6 compositions to the boiling point of lead. There will obviously be a pressure rise, of unknown magnitude, in the delay assembly due to gas production by the igniter composition and the temperature rise produced by the composition. This pressure rise will act to suppress the vapourisation of the lead allowing the reaction temperature to rise considerably above that obtained under constant pressure conditions(68). The same arguement applies to the reaction temperature of the 97/3 composition, which under constant pressure conditions is limited to the boiling point of lead monoxide. The reaction temperature of the 80/20 composition is limited by the melting point of the excess silicon present and should therefore be unaffected by any pressure increase which occurs.

No theoretical reaction temperatures have been calculated for the PbO/B system, or for the SnO_2/B and SnO_2/Si systems described in the following section, as the discrepancy between the theoretical temperatures and those obtained in practice is so great as to make the calculated temperatures of very little interest. In addition,

FIGURE 7·2

VARIATION OF REACTION TEMPERATURE WITH OXIDISER LEVEL

IN THE PbO/B SYSTEM

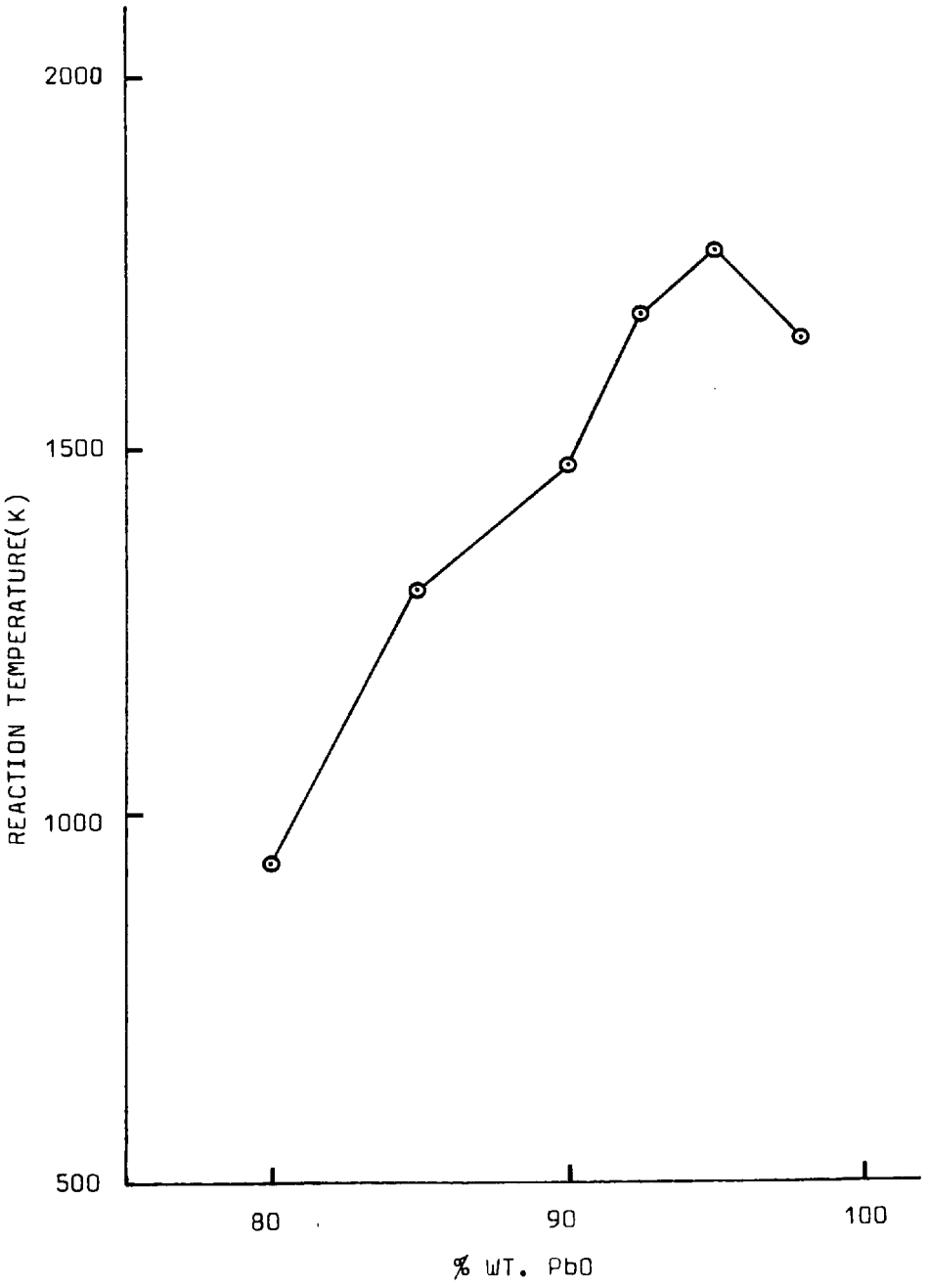

FIGURE 7.3

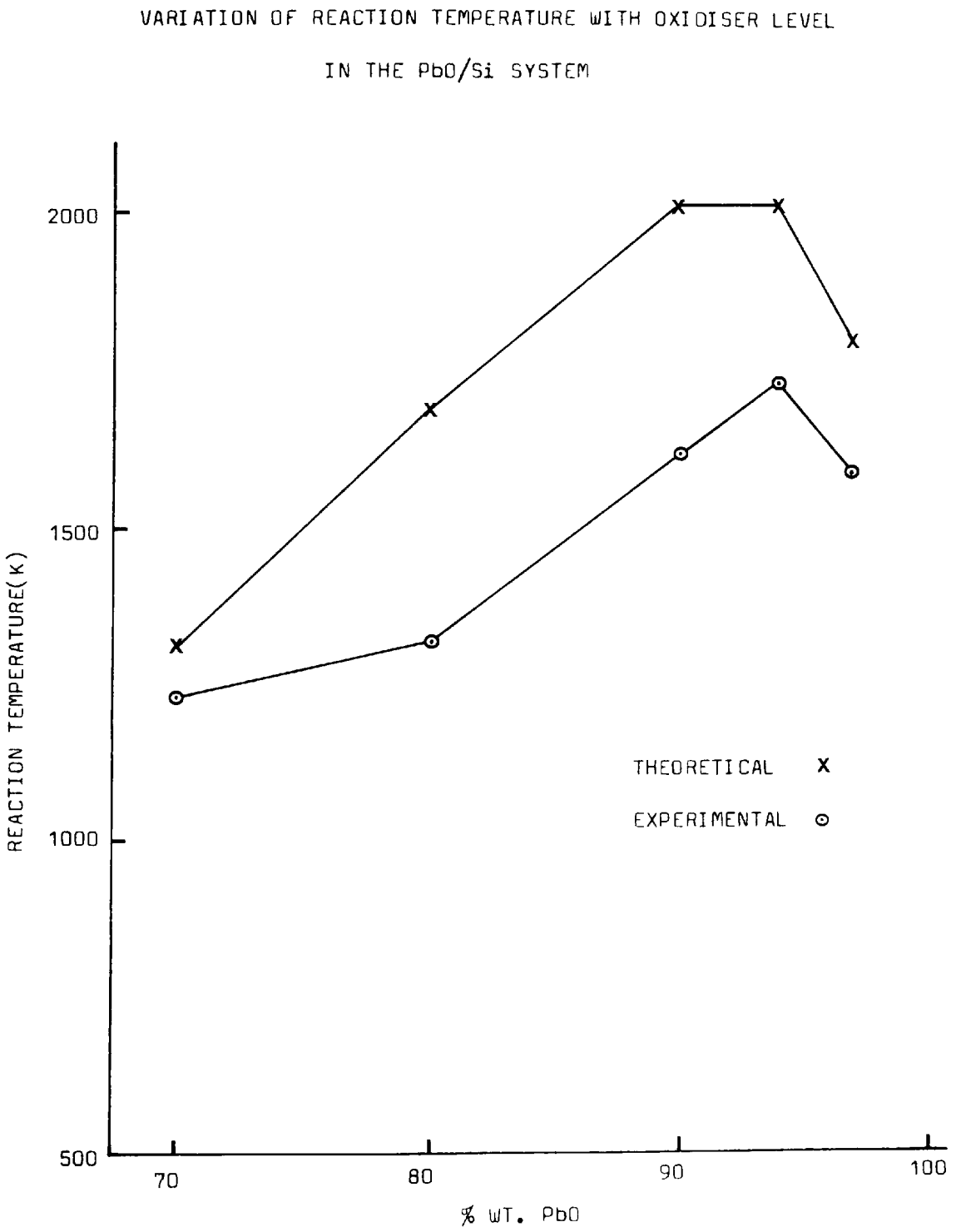
VARIATION OF REACTION TEMPERATURE WITH OXIDISER LEVEL
IN THE PbO/Si SYSTEM
REACTION TEMPERATURE(K)
2000
1500
1000
500
70
80
90
100
% WT. PbO
THEORETICAL X
EXPERIMENTAL ⊙

TABLE 7.3 REACTION TEMPERATURES IN THE PbO/B SYSTEM

SYSTEM	% WT. OXIDE	MEASURED REACTION TEMPERATURE(K) *
PbO/B	80	934 +/- 2·0%
	85	1306 +/- 9·3%
	90	1479 +/- 3·7%
	92·5	1680 +/- 2·3%
	95	1764 +/- 7·3%
	98	1642 +/- 4·4%

TABLE 7.4 REACTION TEMPERATURES IN THE PbO/Si SYSTEM

SYSTEM	% WT. OXIDE	MEASURED REACTION TEMPERATURE(K) *	THEORETICAL REACTION TEMPERATURE(K)
PbO/Si	70	1225 +/- 2·6%	1310
	80	1315 +/- 4·2%	1683
	90	1620 +/- 3·8%	2013
	94	1735 +/-10·3%	2013
	97	1590 +/- 3·4%	1800

* +/- 2 STANDARD DEVIATION UNITS

in the cases of the boron containing systems insufficient information is available on the nature and the relative amounts of the reaction products to be able to carry out any meaningful calculations.

A comparison of the data presented in Figures 7.2 and 7.3 shows that the reaction temperatures observed in the PbO/Si system are very similar to those observed in the PbO/B system. This may seem suprising when the relative heat outputs of the two systems are compared(Chapter 5), as the PbO/B system possesses a higher overall heat output than the PbO/Si system. However, the heat capacities of the boron compounds produced as reaction products are higher than those of the analogous silicon compounds. This means that the effectiveness of the higher heat output of the boron system in raising the reaction temperature is negated.

7.3 REACTION TEMPERATURES IN THE SnO_2/B AND SnO_2/Si SYSTEMS

The measured reaction temperatures of SnO_2/B and SnO_2/Si compositions, containing various oxidiser/fuel ratios, are shown in Figures 7.4 and 7.5 respectively. The data displayed in these figures are summarized in Tables 7.5 and 7.6.

Several points are worth commenting on with respect to the two stannic oxide systems. Probably the most obvious feature that both curves have in common is that they do not peak. This is a reflection of the heat output-reaction product heat capacity relationships in these two systems and the oxidiser/fuel ratios over which they propagate.

Another feature worth commenting on is the larger decrease in reaction temperatures in the boron fuelled system, when compared with the silicon fuelled system, as the fuel level increases. This is due to the higher heat capacity of the excess boron, which acts as a heat sink, relative to the heat capacity of the excess silicon.

The other interesting aspect of both of the curves is the apparent presence of an inflexion point. Although the inflexion point occurs at a different oxidiser level in each curve, the reaction temperature at which it occurs is very similar in each case(approx. 1450K). The inflexion is also more pronounced in the silicon fuelled system. The similarity of the temperatures at which the inflexion point occurs in both the boron and silicon fuelled systems indicates that the phenomenon is caused by the stannic oxide present in both systems.

FIGURE 7.4

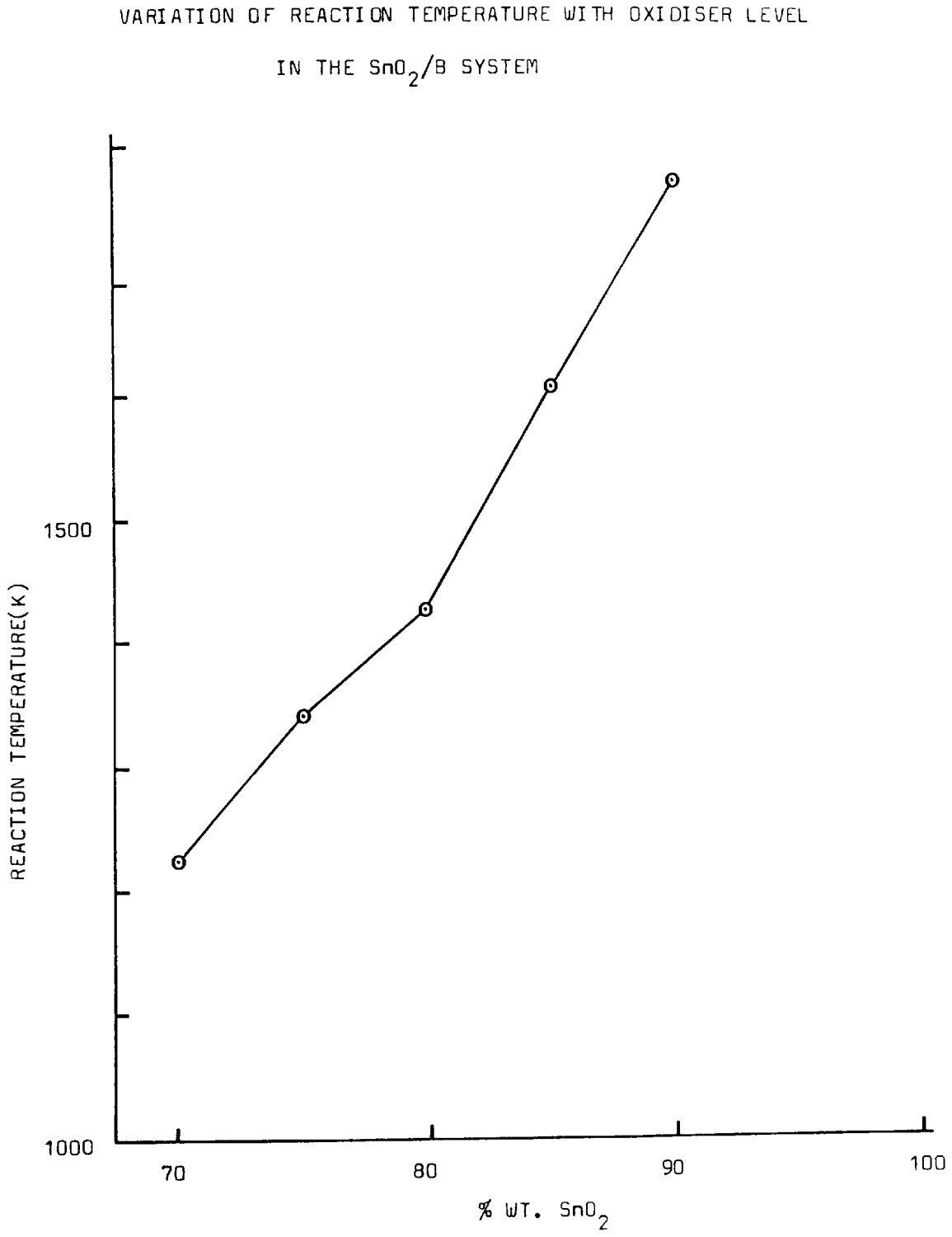
VARIATION OF REACTION TEMPERATURE WITH OXIDISER LEVEL
IN THE SnO_2/B SYSTEM
REACTION TEMPERATURE(K)
1500
1000
70
80
90
100
% WT. SnO_2

FIGURE 7.5

VARIATION OF REACTION TEMPERATURE WITH OXIDISER LEVEL IN THE SnO_2/Si SYSTEM

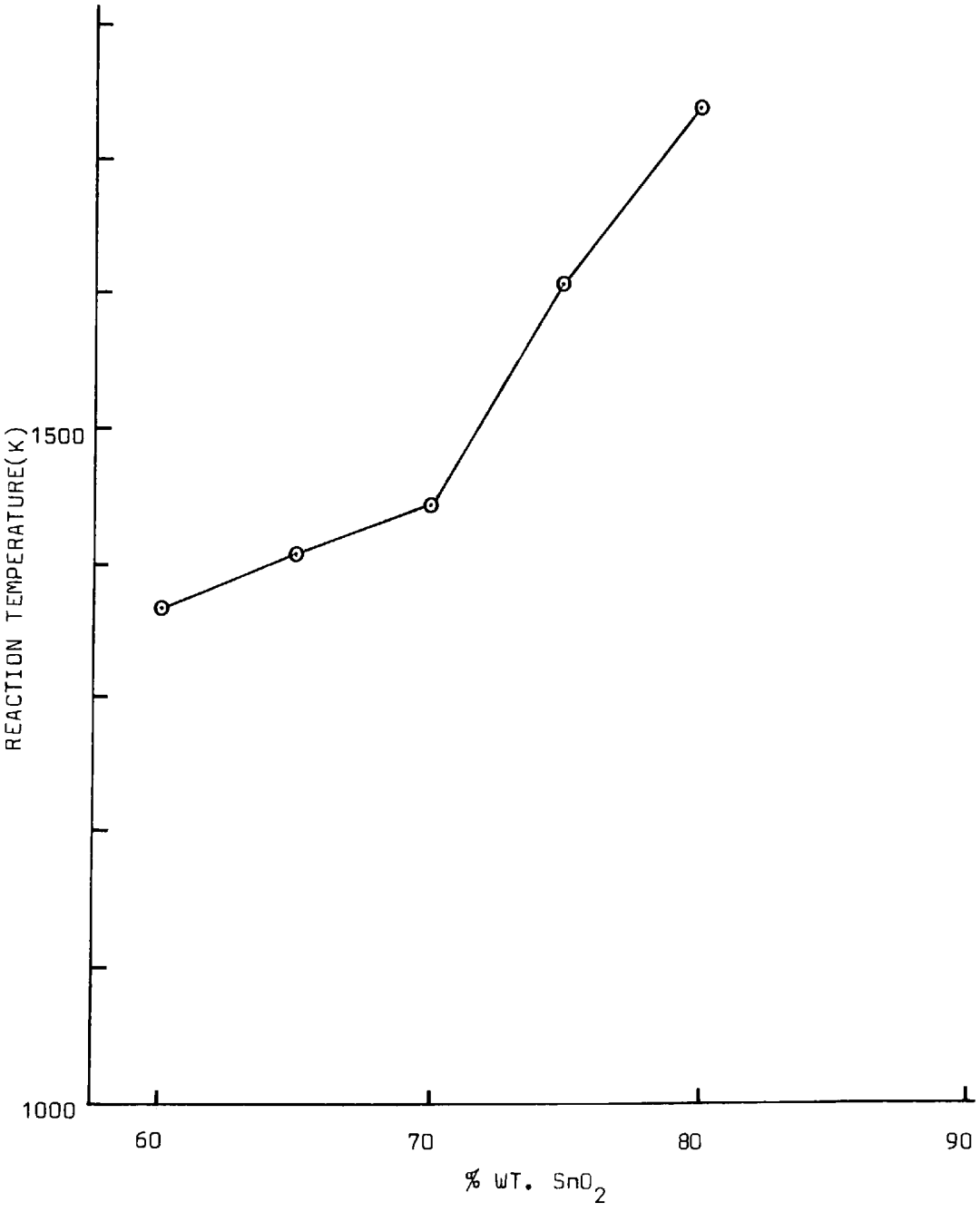

TABLE 7.5 REACTION TEMPERATURES IN THE SnO_2/B SYSTEM

SYSTEM	% WT. OXIDE	MEASURED REACTION TEMPERATURE(K)*
SnO_2/B	70	1224 +/- 3·2%
	75	1342 +/- 2·9%
	80	1424 +/- 9·7%
	85	1607 +/- 3·6%
	90	1772 +/- 5·1%

TABLE 7.6 REACTION TEMPERATURES IN THE SnO_2/Si SYSTEM

SYSTEM	% WT. OXIDE	MEASURED REACTION TEMPERATURE(K)*
SnO_2/Si	60	1367 +/- 2·2%
	65	1405 +/- 2·0%
	70	1442 +/- 6·0%
	75	1606 +/-13·3%
	80	1738 +/-10·0%

* +/- 2 STANDARD DEVIATION UNITS

Examination of Figure 7.3 indicates the presence of an inflexion point in the reaction temperature curve of the PbO/Si system. If the oxidiser/fuel ratios at which the inflexion is observed in the reaction temperature curves of the PbO/Si and SnO_2/Si systems are compared with the oxidiser/fuel ratios at which a change in response to loading pressures is observed in these two systems (Figures 6.10 and 6.11), reasonable agreement is obtained.

It is proposed that the temperature of the inflexion points observed reflect either the onset of a significant amount of, or an increase in, vapour phase activity in the systems examined. In the PbO/B system no inflexion is observed in the reaction temperature curve and it is believed that a relatively high degree of vapour phase activity occurs over the entire oxidiser/fuel ratio range examined.

CHAPTER 8

THERMAL ANALYSIS STUDIES

8.1 INTRODUCTION

The choice of oxidiser/fuel system for detailed study was determined by several factors which were, for the most part, concerned with the operating characteristics of the available thermal analysis equipment. The Perkin-Elmer DSC-2 differential scanning calorimeter has a working temperature range from room temperature to 1000K. Many pyrotechnic systems containing metal oxides exhibit reactions at the top end of this range or above. Although these reactions would be accessible to differential thermal analysis equipment with a working temperature range from room temperature to approximately 1600K, the inferior resolution and sensitivity of DTA, when compared with that of DSC, makes the technique unsatisfactory for any detailed study of a pyrotechnic system.

The first constraint is, therefore, that the pyrotechnic reaction should occur within the DSC temperature range. The second constraint is that the reaction should occur at as low a temperature as possible in the DSC temperature range, where the instrument baseline linearity and reproducibility are at a maximum. These are the main constraints and only the lead monoxide/boron system meets them fully.

Before discussing in detail the thermal analysis results obtained it is worth commenting on the general characteristics of pyrotechnic reactions with respect to thermal analysis techniques.

Due to the nature of solid state reactions it is necessary for various mass transport processes to be operative, to bring the reactants

into close enough proximity for chemical reaction to take place. This means that no reaction will be detected by thermal analysis techniques until temperatures are reached at which these processes achieve measurable rates, even though under homogeneous conditions the reactions would be detectable at much lower temperatures. It should also be pointed out that the first departure of a thermal analysis trace from the 'no reaction' baseline does not necessarily correspond to a unique temperature at which reaction begins, but that this point will depend on the sensitivity and noise level of the instrument(81).

The mass transport processes can be thought of as forming two general groups; those which achieve a substantial rate at relatively low temperatures such as surface, grain boundary and dislocation diffusion and those which will be detected at higher temperatures, such as lattice(volume or bulk) diffusion, achieved by various mechanisms and diffusion through a product layer with a high diffusion resistance.

It is doubtful whether thermal analysis techniques(dynamic methods) would be able to detect reaction brought about by the low temperature processes as these would become operative immediately the composition was prepared and would proceed at such relatively low rates and involve so little material as to be virtually undetectable. These reactions would probably be more amenable to study by isothermal techniques. However, it is fairly certain that it is these low temperature processes which are at least partly responsible for the 'ageing' of compositions in storage.

TABLE 8.1

SUBSTANCE	MELTING POINT(K)	TAMMANN TEMPERATURE(K)	
		α =0•3	α =0•52
PbO	1161	348	604
SnO_2	1400	420	728
B	2573	772	1338
Si	2873	862	1494

THE TAMMANN TEMPERATURES OF THE OXIDISERS AND FUELS EXAMINED

With respect to any given component in a reacting system, an approximate estimate of the temperatures at which the two groups of processes become of importance can be obtained from the TAMMANN temperature, α. This is equal to the ratio of the temperature of a solid to its melting temperature, where both temperatures are expressed as absolute temperatures. At α equal to approximately 0·3 the surface diffusion group of processes are operative, while at α equal to approximately 0·52 the lattice diffusion group of processes are operative. The Tammann temperatures for the two oxides and two fuels examined are given in Table 8.1.

* The experimental conditions for all the thermal analysis traces presented in this chapter can be found in the appendix.

8.2 REACTIONS IN THE PbO/B SYSTEM

Previous work has shown that oxidation - reduction reactions of the type found in the lead monoxide/boron system give DSC traces consisting of two overlapping peaks in the absence of side reactions between reaction products and the initial reactants(58). Figure 8.1 shows a typical DSC trace, in this case of a 55/45 PbO/Si composition. This type of peak pattern is in accord with the reaction model described by Komatsu(82) which provides a description of reactions taking place in powder mixes containing spherical particles. In this model the first stage of the reaction involves the reaction product phase growing spherically from each point of interparticle contact, eventually the growing spheres of product phase will come into contact with one another to form a spherical shell entraining the unreacted material. The second stage of the reaction involves the spherical shell of product advancing towards the interior of the particle as the reaction proceeds to completion.

The reaction model described above is extremely simplistic, however it does provide a framework of concepts within which the reactions taking place in the lead monoxide/boron system can be discussed.

Moghaddam(77) has shown that the reactions in the Pb_3O_4/Si and PbO/Si systems are very similar in terms of the DSC peak patterns obtained and the temperature range of the reactions, indicating that the main reaction in the Pb_3O_4/Si system is between lead monoxide and silicon. At higher temperatures in DTA apparatus Al-Kazraji(68) has shown that the Pb_3O_4/Si system does show evidence of PbO-SiO_2 reaction. Therefore by implication it should be expected that the

FIGURE 8.1

DSC TRACE OF A 50/50 PbO/Si COMPOSITION

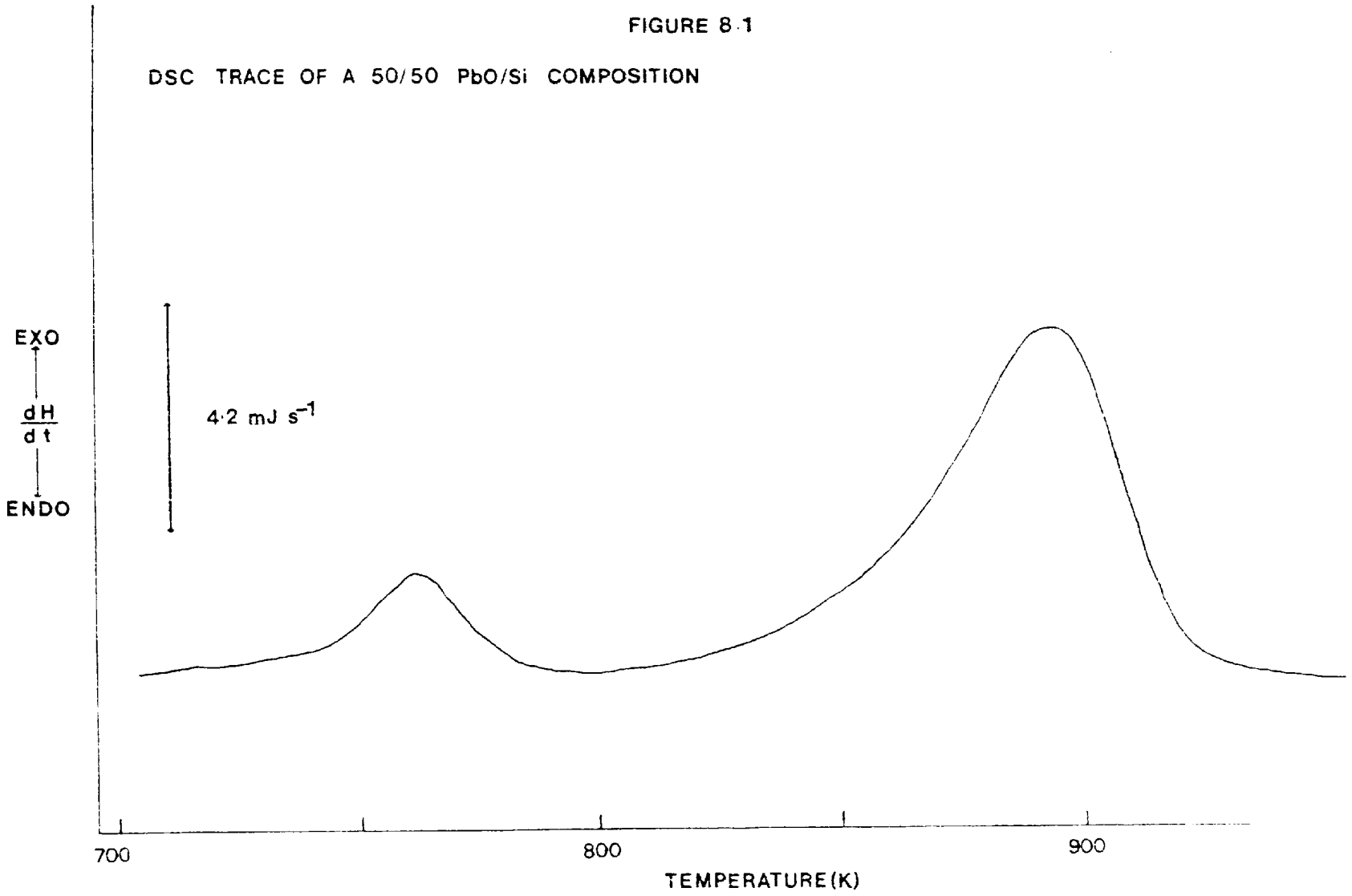

same reaction would occur in the PbO/Si system with compositions containing PbO at levels higher than the stoichiometric level.

The minimum temperature at which a liquid phase can be obtained in the PbO/SiO_2 system is indicated by Cooper et al(83) to be approximately 995K, high enough to ensure that liquid phase production (by way of $PbO-SiO_2$ reaction) will have minimal participation in and effect on the reaction between PbO and Si. Therefore in the PbO/Si system the $PbO-SiO_2$ reaction will not compete, as a concurrent reaction, for the available PbO but will only occur as a consecutive reaction consuming any remaining PbO after the main oxidation - reduction reaction has taken place.

The production of a low temperature liquid phase, relative to the temperature range of the oxidation-reduction reaction, in which one or both of the reactants are soluble can have a profound effect on the rate of the reaction. Welch(84) describes the acceleratory effect of impurities on the rate of solid-solid reactions by the introduction of a small amount of liquid phase.

The DSC peak pattern obtained for the PbO/B system is somewhat more complicated than that obtained for the PbO/Si system, giving a trace containing a maximum of four exothermic peaks. The relative peak areas, resolution and overlap of the peaks vary with heating rate, particle size of the reactants, source of the lead monoxide and oxidiser/fuel ratio.

Figure 8.2 illustrates the maximum of four peaks which can be obtained under ideal conditions. To explain this multiple peak pattern it is necessary to consider the possibility of reactions other than

FIGURE 8.2

DSC TRACE OF A 50/50 PbO/B COMPOSITION

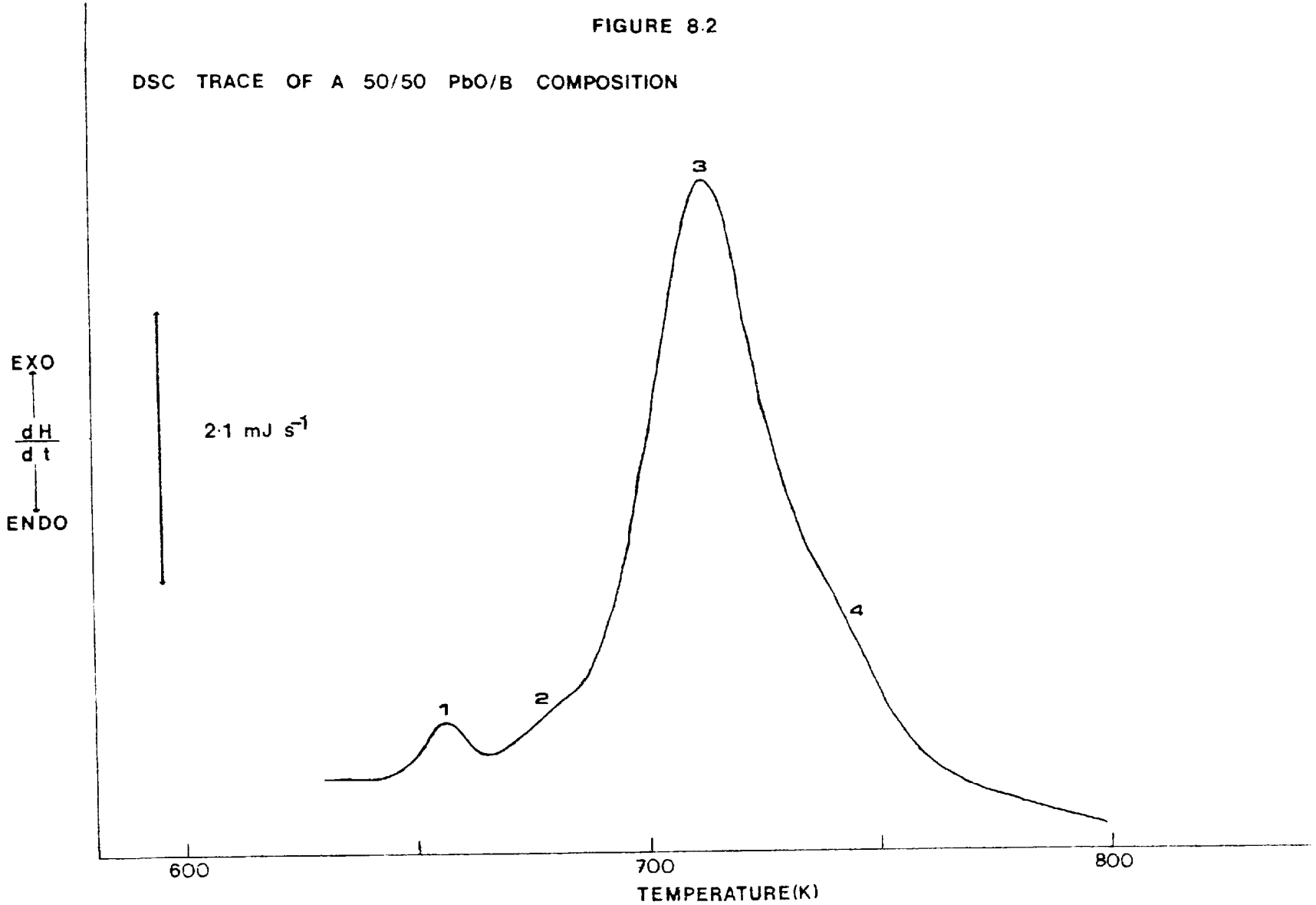

the main PbO-B oxidation-reduction reaction. Under the controlled temperature conditions obtained in DSC power compensation equipment the oxidation product of boron will be B_2O_3. As it is known that lead does not form a boride(71) and that no reaction between boron and B_2O_3 occurs in the DSC temperature range, this leaves the reaction between PbO and B_2O_3 as the origin of the two extra peaks in the DSC trace.

The solubility of PbO in B_2O_3 is well established(75), glasses being formed over a wide range of compositions with the viscosity of the melts tending to decrease as the lead monoxide content increases. Figure 8.3 shows the DSC trace of the reaction between PbO and B_2O_3 (1:1 w/w) over the temperature range of the PbO-B reaction. Mellor(74) indicates that the minimum temperature for the transition from a glass to a very viscous phase in the PbO/B_2O_3 system occurs at approximately 590K (Figure 8.4.A); which is in reasonable agreement with the temperature at which reaction is first detected in the DSC trace of Figure 8.3. The PbO/B_2O_3 reaction shows other exothermic peaks at temperatures above the PbO/B temperature range.

It is worth discussing the question of minimum temperatures for liquid phase production and their relation to the first signs of of reactivity in multi-component powder mixes examined in thermal analysis equipment. Figure 8.4.B shows the melting point curve for the PbO/SiO_2 system(100-40 eq.% PbO) adapted from Cooper et al(83). The solid and broken curve indicates the melting points of pre-fused PbO/SiO_2 mixes whereas the points away from this curve indicate the temperatures at which reaction is first detected in thermal analysis equipment using PbO/SiO_2 powder mixes. Figure 8.4.B emphasises the

FIGURE 8.3

DSC TRACE OF A 1:1 PbO/B_2O_3 MIX

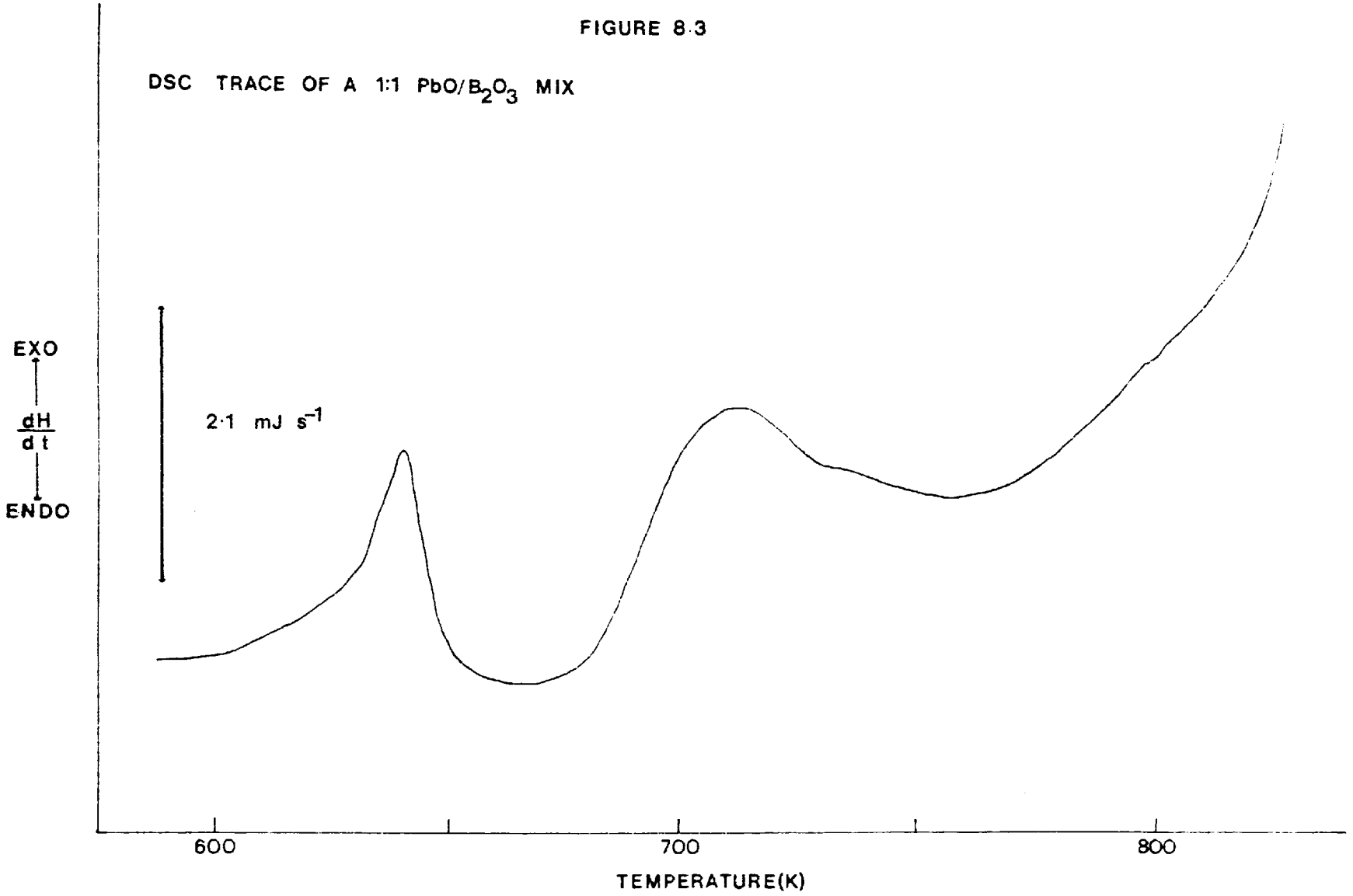

fact that the initial reactions which take place in powder mixes in thermal analysis equipment are independent of the overall composition of the mix but depend on the prevailing conditions at the points of inter-particle contact. If a melting point curve indicates a minimum solid-liquid transition temperature at a 70/30 composition it should be expected that an 80/20 composition would show its first sign of reaction at the same temperature. At that temperature a liquid phase of 70/30 composition will form at the points of inter-particle contact with consequent lowering of diffusion barriers and subsequent increase in reaction rate.

A comparison of the DSC traces of Figures 8.2 and 8.3 helps to clarify the peak pattern of the PbO/B system. The initial peak of Figure 8.3 corresponds very well in temperature with the small initial peak of Figure 8.2. The final peak in Figure 8.3 with a T_{MAX} of just over 700K corresponds very well with the final peak of Figure 8.2 which appears as a shoulder. This then leaves the second and third peaks of Figure 8.2 as those due to the oxidation-reduction reaction between lead monoxide and boron.

Further evidence of the importance of the PbO-B_2O_3 in the PbO/B system is supplied by a comparison of the DSC trace of a composition in which the boron has been treated to remove B_2O_3 and that of a composition in which the boron has had no pretreatment.

Figure 8.5 shows the DSC traces of two 50/50 PbO/B compositions. 50/50 compositions have been used to enhance the peak area corresponding to the initial PbO-B_2O_3 reaction. Trace A is of a composition in which the boron has been refluxed with ethyl alcohol(95% by volume)

FIGURE 8.4.A

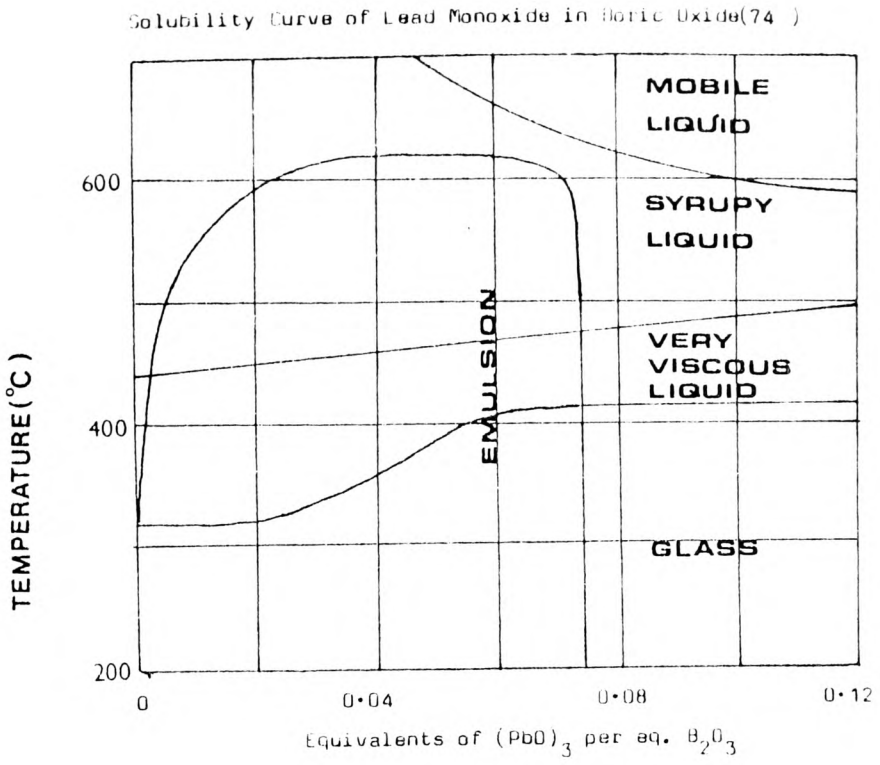

FIGURE 8.4.B

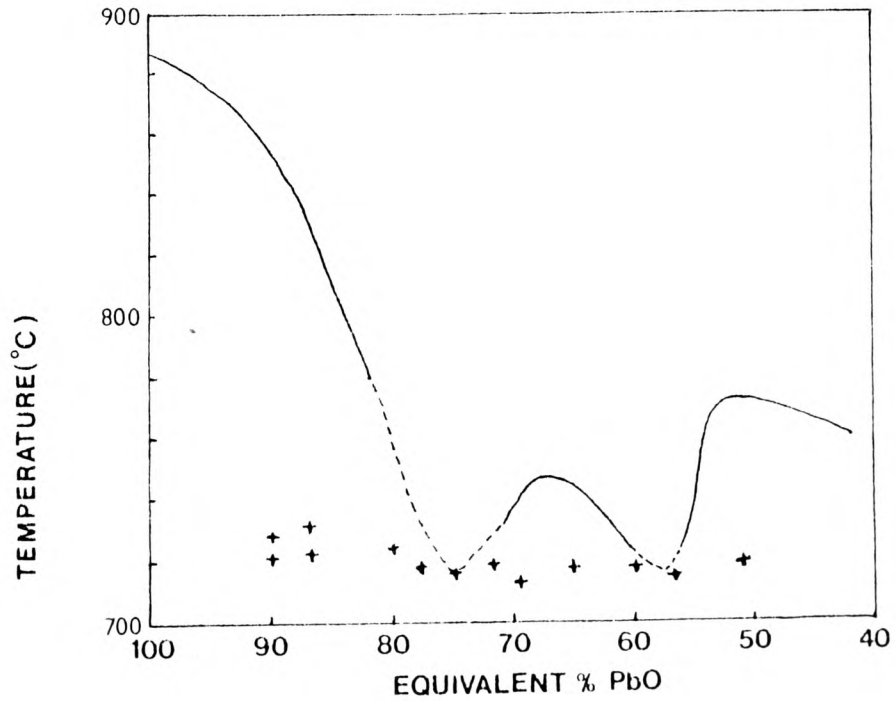

for one hour, then washed with fresh alcohol and dried prior to mixing. Trace B is of a composition, containing the same lead monoxide as in Trace A, in which the boron has had no pretreatment prior to mixing. The alcohol washing serves to remove contaminating B_2O_3 from the boron particles.

One noticeable feature of the DSC traces of Figure 8.5 is that the initial rise from the 'no reaction' baseline occurs at a lower temperature with 'washed' boron than with untreated boron. In the case of the untreated boron the initial reaction will be between PbO and B_2O_3 which has a lower heat output than the reaction between PbO and boron. Therefore it would be intuitively expected that the occurrence of the more exothermic oxidation-reduction reaction as a primary step in the 'washed' boron composition would push the detectability limit of the reaction to lower temperatures.

As stated above, in the case of the composition containing untreated boron the initial reaction between PbO and B_2O_3 will produce a viscous liquid phase, the viscosity of which will decrease as the PbO content increases. The rate of the ensuing oxidation-reduction reaction, at the liquid-boron interface will depend on the rate of transport of lead monoxide through the liquid phase to the liquid-boron interface, assuming that the oxidation-reduction reaction is a fast non-rate controlling step. The first two peaks of Trace B(Figure 8.5) represent consecutive reactions, the overlap of the two peaks being due to the particle size distribution of the reactants. Much sharper, better separated peaks would be obtained if reactants with very narrow particle size distibutions could be obtained.

FIGURE 8.5

DSC TRACES OF 50/50 PbO/B COMPOSITIONS

A - WASHED BORON

B - UNTREATED BORON

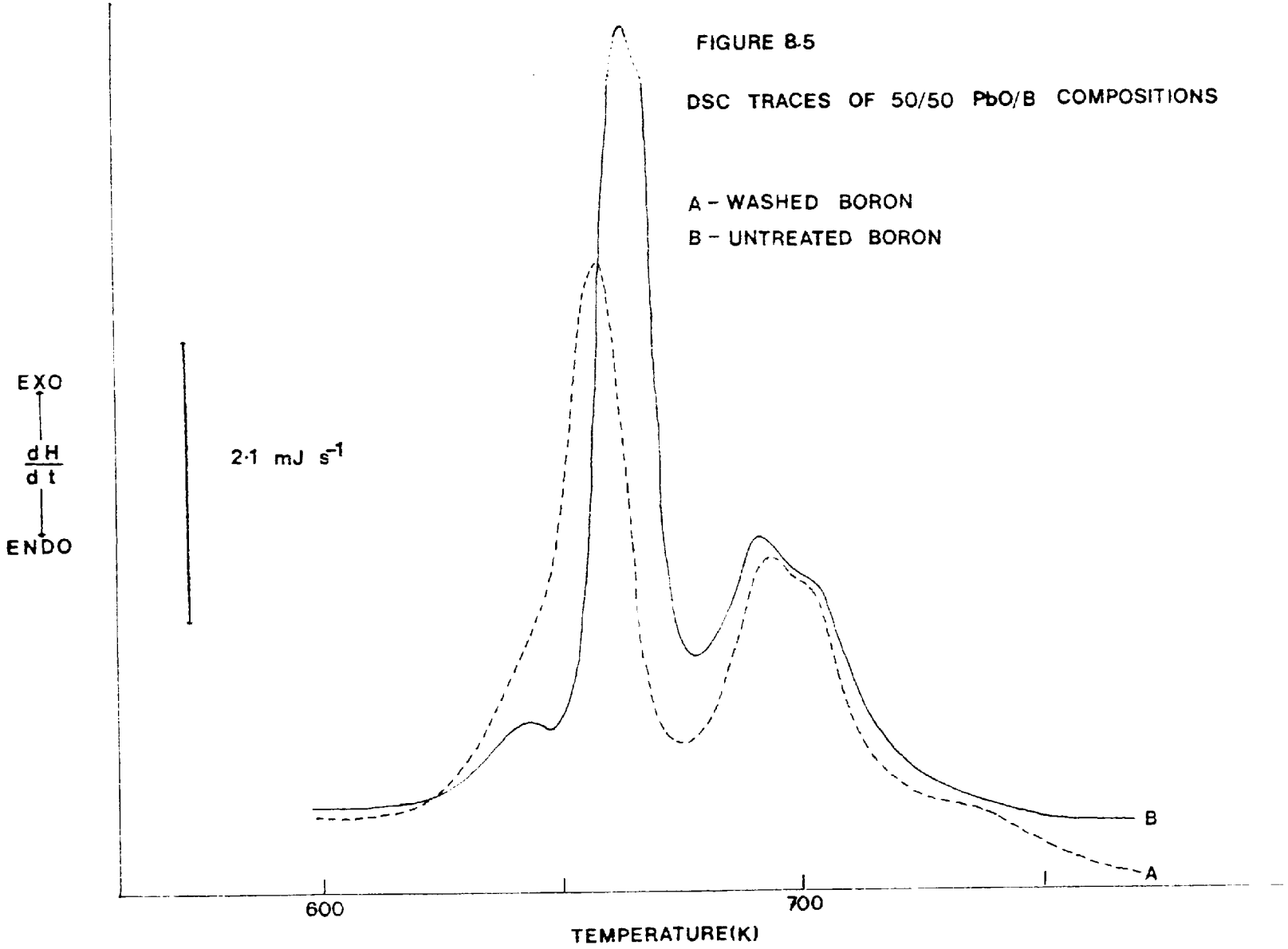

In the case of the composition containing the 'washed' boron no B_2O_3 is initially present to form a liquid phase as the primary reaction, therefore initially reaction must be between PbO and boron with solid phase diffusion providing the reactant flux. As soon as B_2O_3 has been formed it is available for reaction with PbO and two concurrent rections are established. The initial diffusion in the solid state explains why the reaction rate(proportional to $\frac{dH}{dt}$) is never as great as that achieved in the reaction with untreated boron where the reaction will be controlled throughout by liquid phase diffusion.

Where the metal oxide - fuel reaction is a single stage process i.e. it does not involve sequential reduction of the oxide as described by Charsley et al(53) in the MoO_3/B system, the two peak DSC trace is typical. However this peak pattern is only typical providing, as stated earlier, that no side reactions between initial reactants and reaction products occur within the oxidation - reduction reaction temperature range, as is the case in the PbO/B system.

Moghaddam(77) has shown, very simply, that the first peak relates to the production of a complete shell of product around the reactant particles, while the second peak relates to the consumption of the remainder of the reactants by way of diffusion through the encapsulating product layer.

Considering the case of the PbO/B system the first two peaks of Trace B(Figure 8.5) represent firstly reaction at the points of interparticle contact to produce a liquid PbO-B_2O_3 phase; secondly initiation of the oxidation - reduction reaction. This reaction then spreads from the initial points of contact, over the surfaces

of the reactant particles, with some penetration of the particles, until the edges of the reaction zones touch when the initial reaction will slow and stop. This stage in the reaction is similar to the nucleation and growth of nuclei processes which are familiar in solid state decomposition reactions(81) and forms a complete shell of product around the reactant particles.

The completion of the first stage of the reaction represents the initiation of a contracting interface, phase boundary reaction which consumes the remainder of the reactants to give the third peak. As this reaction proceeds and the temperature rises, the product layer thickens, the interface area for the oxidation - reduction reaction decreases and the $PbO-B_2O_3$ will tend to be favoured producing the final peak(shoulder) in Trace B(Figure 8.5).

The PbO/B system, where $PbO-B_2O_3$ liquid phase production occurs, is in sharp contrast to the PbO/Si system where no $PbO-SiO_2$ liquid phase production can occur within the temperature range of the oxidation - reduction reaction and where consequently reaction takes place by way of solid state diffusion processes.

8.3 EFFECT OF OXIDISER-FUEL RATIO ON DSC PEAK PATTERN

The DSC peak pattern of the PbO/B system changes on moving from a 50/50 composition towards the stoichiometric oxidiser - fuel ratio and beyond. As the boron level is decreased the amount of B_2O_3 initially present also decreases and the first small peak of Trace B, Figure 8.5 disappears. This does not imply that the initial PbO-B_2O_3 reaction does not occur simply that it is no longer resolvable as a separate peak. Figure 8.6, Trace B shows the DSC peak pattern of a 97/3 PbO/B composition recorded at the same temperature scan rate as used for the traces of Figure 8.5.

Another noticeable feature of the DSC traces of Figure 8.6 is the prominence of the final peak due to the PbO-B_2O_3 reaction. Although the amount of B_2O_3 initially present has been reduced, relative to the 50/50 composition, the PbO-B reaction produces B_2O_3 which is able to react with the increased PbO content.

The PbO-B_2O_3 reaction assumes greater importance at PbO levels above the stoichiometric level as there will always be excess PbO available for reaction when all the boron has been consumed.

FIGURE 8.6

DSC TRACES OF A 97/3 PbO/B COMPOSITION
EFFECT OF HEATING RATE

A - 5° MIN^{-1}
B - 10° MIN^{-1}
C - 20° MIN^{-1}

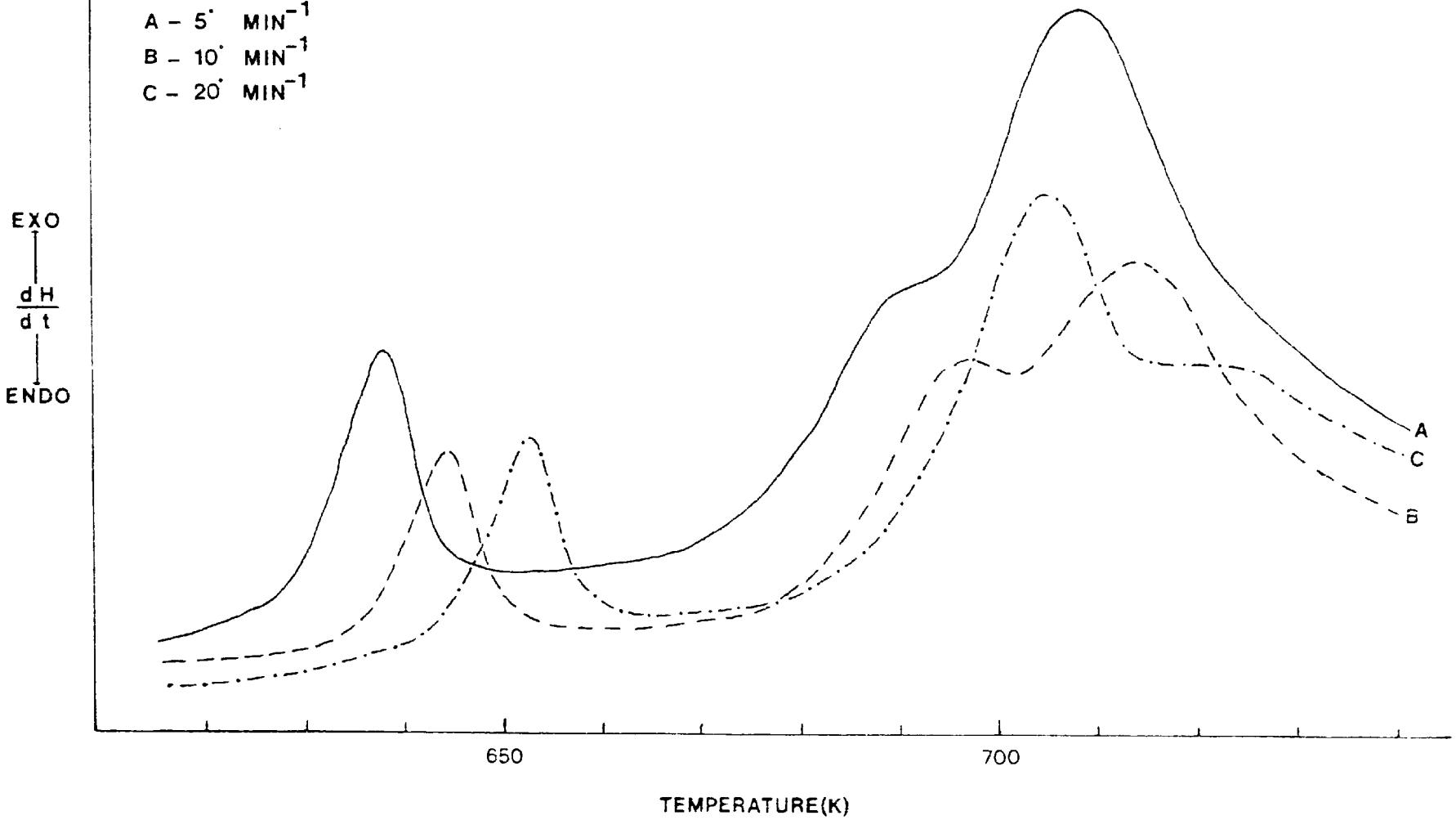

8.4 EFFECT OF HEATING RATE ON DSC PEAK PATTERN

Figure 8.6 as a whole illustrates the effect of increasing temperature scan rate(heating rate) on the DSC peak pattern. One obvious effect of the increase in heating rate is that the peak maximum temperature, T_M, increases as the heating rate increases. This phenomenon is well documented in the literature and has been used as the basis of a method for the determination of activation energies(62).

An effect which is not obvious from Figure 8.6, because of the different sensitivities used to record the traces, is that as the heating rate is increased the peak height, at T_M, is also increased. The peak height, in mJ s^{-1}, is proportional to the reaction rate which increases with increasing heating rate, illustrating the role of the heating rate as an energy regulator in thermal analysis studies. This effect is of great importance when examining highly exothermic reactions which possess an 'explosion' limit i.e. a heating rate above which the reaction proceeds uncontrollably, heat being generated faster than it can be conducted away.

The most interesting aspect of the traces in Figure 8.6 is the effect of increasing heating rate on the final peak. This composition(97/3) is very close to the stoichiometric ratio(96·9/3·1) with very little excess PbO but in Figure 8.6, Trace A the third peak representing PbO-B_2O_3 reaction is very prominent. However, as can be seen from Traces B and C, Figure 8.6, as the heating rate is increased the final PbO-B_2O_3 reaction is suppressed. Under propagative conditions the rate of self-heating is very high.

FIGURE 8.7

A SCHEMATIC REPRESENTATION OF THE EFFECT OF HEATING RATE ON THERMAL ANALYSIS CURVES ADAPTED FROM (81)

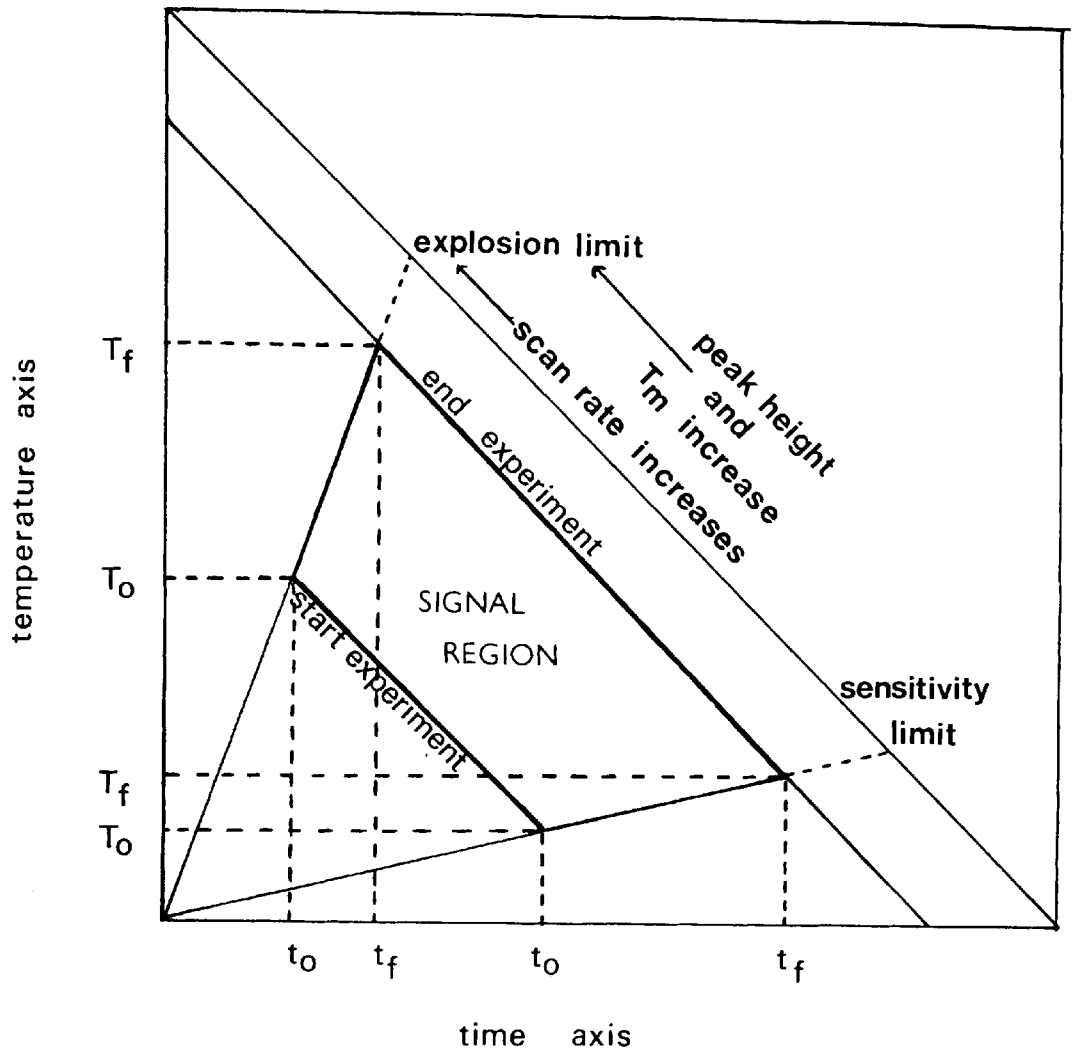

Charsley et al.(48) state that self-heating rates can approach one million degrees per minute and suppression of the $PbO-B_2O_3$ reaction should be total in compositions containing less than and up to the stoichiometrically required level of lead monoxide. The good agreement between the theoretical and experimentally determined heat outputs at the stoichiometric ratio appears to support this conclusion.

It has been found that under the conditions of low compaction, density and heating rate obtained in thermal analysis equipment reaction is never complete, with regard to the oxidation - reduction reaction, but that as the heating rate is increased the degree of completion of the reaction inceases. This effect can be seen by monitoring the heat output per gram of composition in DSC equipment as the heating rate is increased.

Figure 8.7 shows schematically the major effects of heating rate on thermal analysis traces.

FIGURE 8.8

DSC TRACES OF A NOMINAL 97/3 PbO/B 'COPRECIPITATED' COMPOSITION

A - FRESHLY PREPARED

B - AGED 1 YEAR AT 25°C

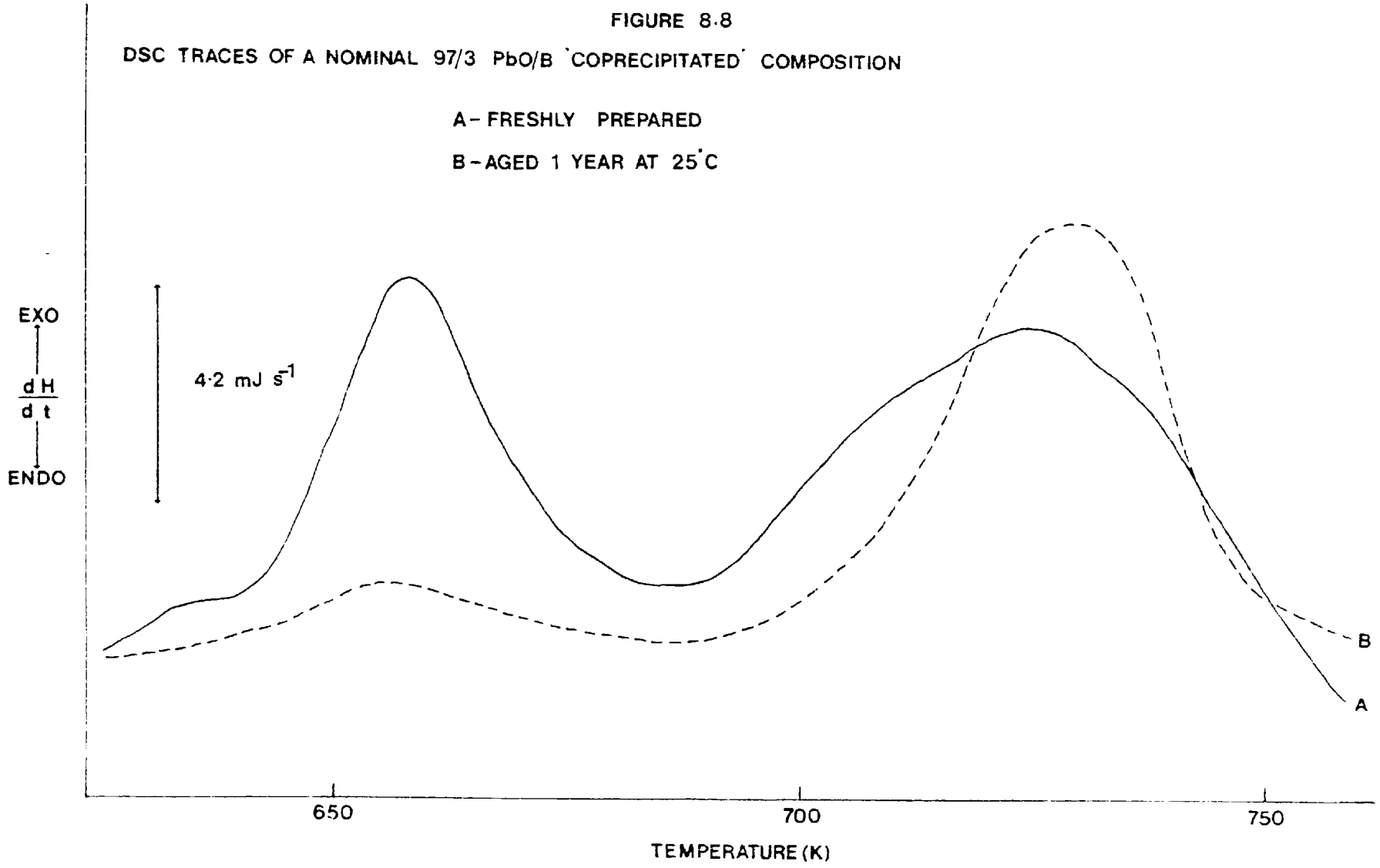

8.5 EFFECT OF INCREASED SURFACE CONTACT AND SOURCE OF OXIDISER ON DSC PEAK PATTERN

If the oxidiser in a pyrotechnic system is chemically or physically precipitated from a solution containing a suspension of the fuel so that the oxidiser crystals form on the surface of the fuel particles, the temperature at which reaction is first detected in thermal analysis equipment is expected to be considerably lowered. This method of preparation is loosely known as 'coprecipitation' and reductions of fifty degrees or more in the initial reaction temperature have been reported(35) which are explained in terms of improved surface contact of the reactants.

In the PbO/B system the reduction in the initial reaction temperature is not observed. Figure 8.8 shows the DSC traces of a nominal 97/3 PbO/B composition(freshly prepared and aged) prepared by the 'coprecipitation' method described by Holloway et al.(85). The two traces illustrate how the occurrence of surface reactions at ambient temperatures contribute to the 'ageing' effects in compositions, the initial peak being considerably reduced in size in the 'aged' compositon.

The temperature at which reaction is first detected in both the PbO/B(washed) system(Figure 8.5, Trace A) and the PbO/B_2O_3 system(Figure 8.3) are very similar and correspond very well with the Tammann temperature(α =0·52) for PbO. This temperature is in turn related to the amplitude of vibrations taking place within the PbO crystal lattice and thus, the general reactivity of the compound(32). This would seem to indicate that the onset of reaction in the PbO/B system is determined principally by the the properties

FIGURE 8.9

PRESSURE-TEMPERATURE RELATIONSHIP IN THE LITHARGE-MASSICOT SYSTEM ADAPTED FROM (88)

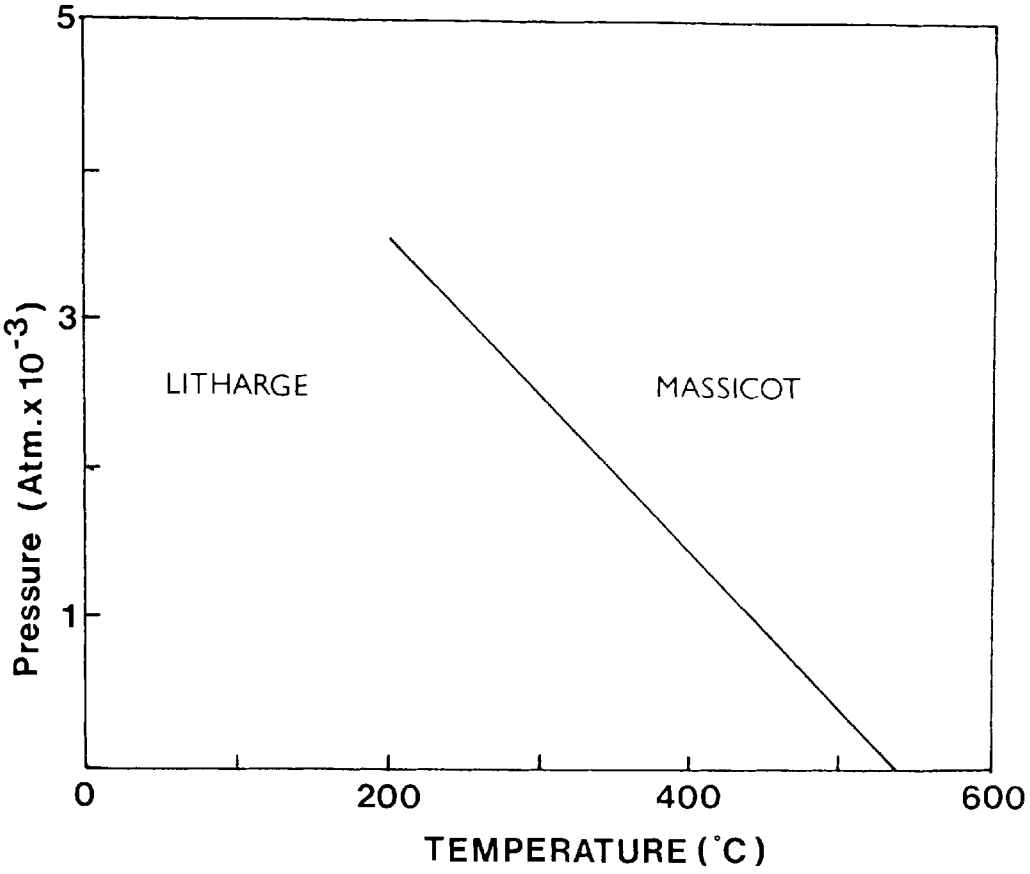

of the oxide component.

In Figure 8.8 reaction begins at a somewhat higher temperature than that observed in Figures 8.5 and 8.6. The most likely explanation of this fact is that the discrepancy in reaction onset temperature is due to a difference in crystal structure between the lead monoxide used in the mechanical mixes and that produced during the 'coprecipitation'.

Lead monoxide occurs in two polymorphic forms, an orthorhombic form known as massicot and a tetragonal form known as litharge. Figure 8.9 shows the temperature - pressure equilibrium curve of the massicot - litharge system.

Greninger et al.(86) state that although pure litharge is red in colour and pure massicot is yellow, colour can be an unreliable indicator of crystal type. In addition, although the red form, litharge, is the polymorph of greater stability at low temperatures and pressures the yellow form, massicot, can be stabilised in the litharge temperature - pressure region by the inclusion of low levels of impurities in the crystal lattice. However, the yellow form is only kinetically stabilised and on standing for long periods of time it gradually converts to the red form.

The 'coprecipitation' procedure produces exclusively orthorhombic lead monoxide whereas the lead monoxide used for the mechanical mixes contains mixture of both polymorphs. McLain(32) quotes evidence which indicates that the chemical reactivity of the red form of lead monoxide is greater than that of the yellow form. An examination of the crystal lattice structures of the two forms also indicates this, the lattice of the yellow form containing shorter and therefore stronger chemical bonds than the lattice of the red form(71). This would tend

FIGURE 8.10

DSC TRACE OF A 50/50 PbO/B COMPOSITION

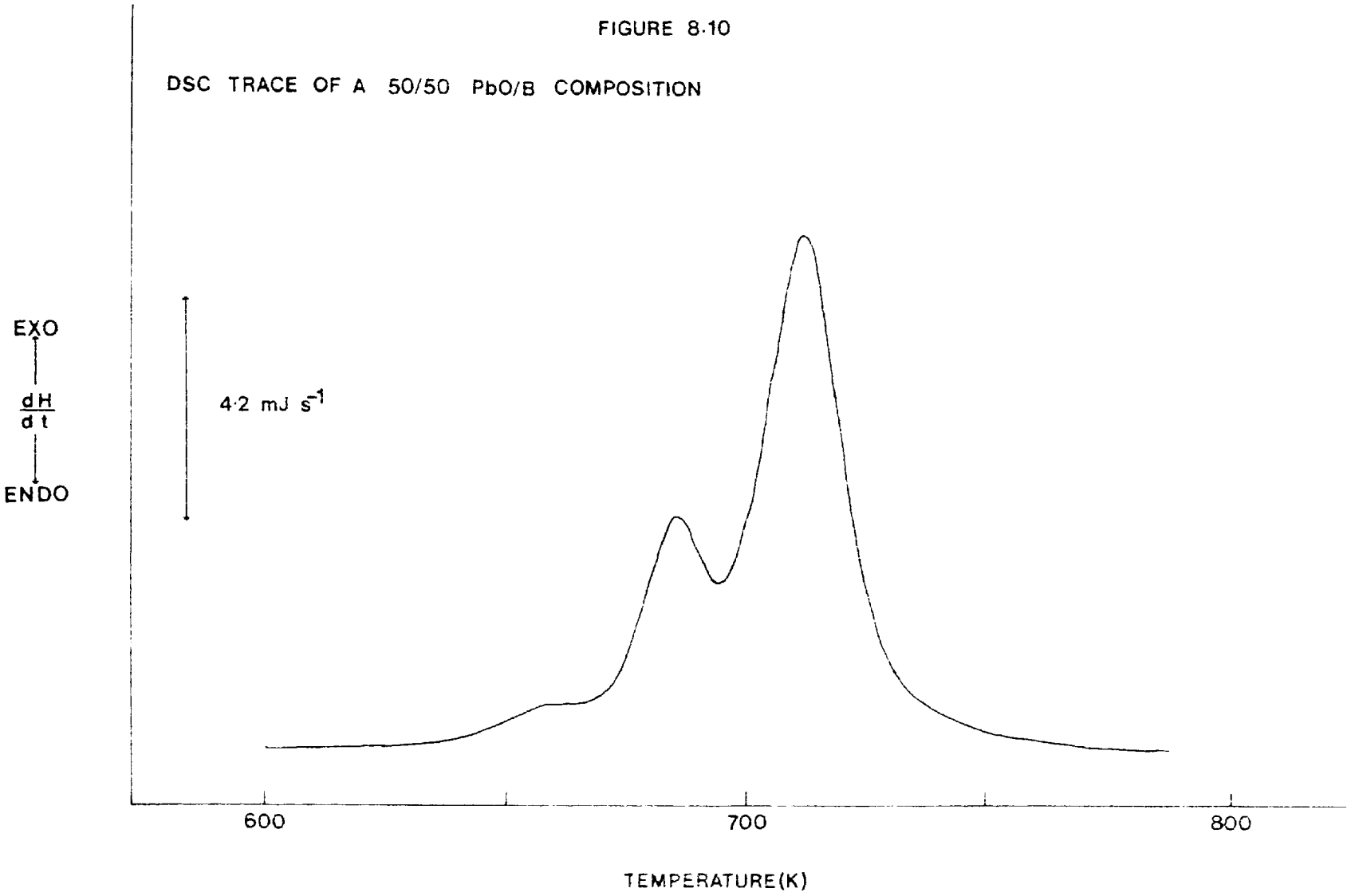

to make the red form more reactive. These facts can explain the shift to higher temperature of the reaction onset with pure orthorhombic lead monoxide, the increased reactivity due to improved surface contact being offset by the lower reactivity of this polymorph.

The situation is not actually as uncomplicated as described above as particle size and surface reactivity can exert a large influence on the reaction onset temperature, in addition to the effects of crystal type and the degree of interparticle contact. The interplay of these factors makes the prediction of the peak pattern and reaction onset temperature to be expected in any particular case extremely difficult.

A comparison of the DSC traces of Figures8.2, 8.5, 8.10, and 8.11, which are all of 50/50 PbO/B compositions, gives some idea of the variety of peak patterns which can be obtained as the source of the lead monoxide is varied.

Figure 8.10 is of a 50/50 composition prepared using PbO containing predominantly the yellow crystal form, while Figure 8.2 is of a 50/50 composition prepared using the same PbO which has been treated to increase the red PbO content. This pretreatment also increases the effective particle size of the PbO, indicated by the increased magnitude of the high temperature PbO-B_2O_3 reaction (peak 4, Figure 8.2). In compositions containing less than the stoichiometrically required amount of PbO the high temperature PbO-B_2O_3 reaction will only be resolved if the particle size of the PbO is large enough for significant amounts of unreacted PbO to be present at temperatures greater than approximately 725K, which is the temperature at which the PbO-B_2O_3 reaction achieves a significant rate.

FIGURE 8·11

DSC TRACES OF 50/50 PbO/B COMPOSITIONS

EFFECT OF BALL MILLING OF PbO ON DSC PEAK PATTERN

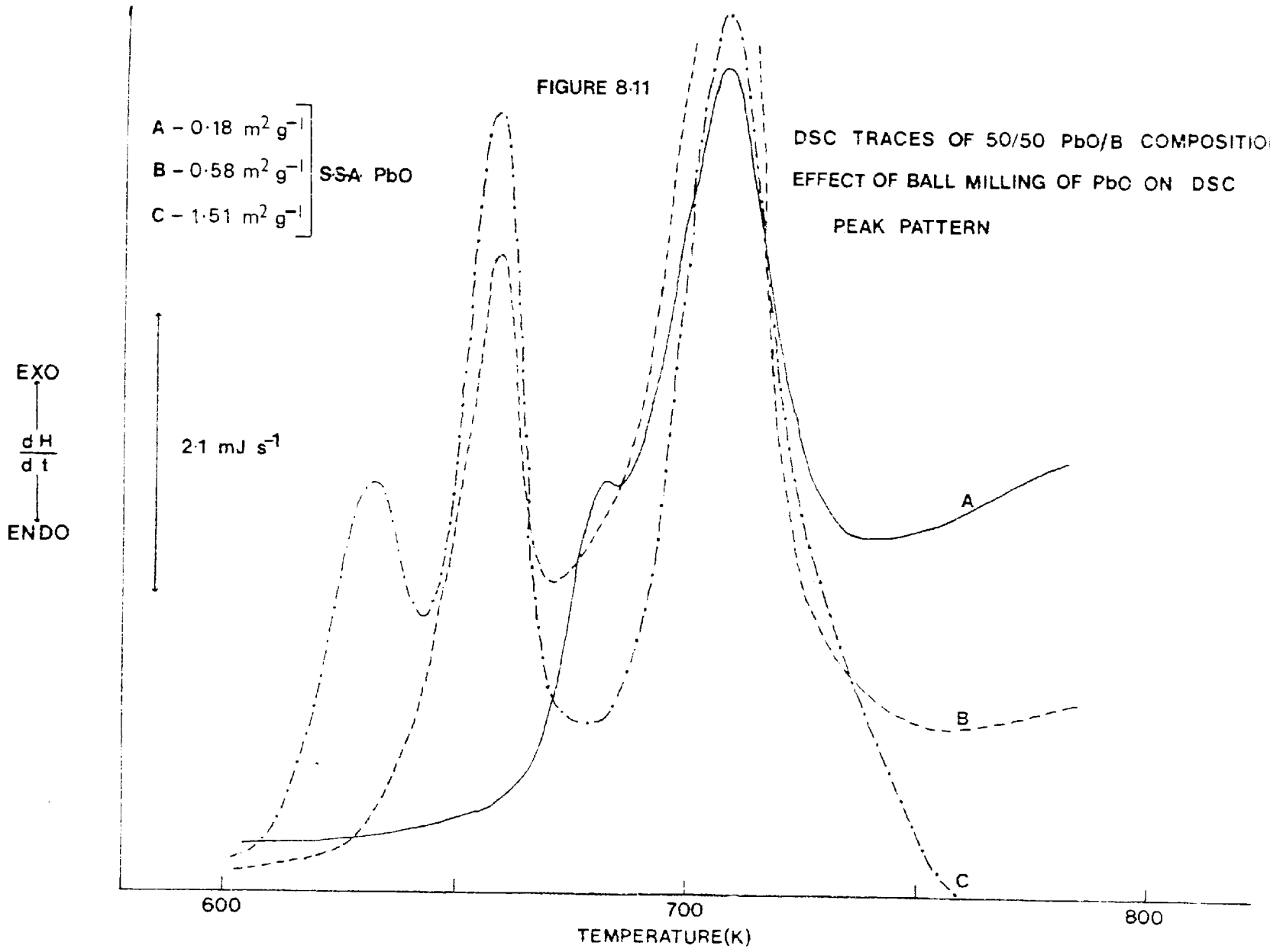

The PbO used to obtain the trace in Figure 8.5 was prepared by the decomposition of Pb_3O_4 which gives a product of high surface reactivity(87). This enhanced surface reactivity is reflected in the much increased peak area of the second peak and the much reduced size of the two remaining peaks. This peak pattern would seem to indicate that the surface reaction forming the complete shell of product also involves considerable penetration of the particles. The final peak is well resolved due to the reduction in size of the third peak. The final PbO-B_2O_3 reaction must take place to maintain the PbO flux for the reaction with boron.

The traces of Figure 8.11 illustrate the effect that the reduction of the oxidiser particle size has on the DSC peak pattern. On passing from Trace A to Trace C the specific surface area of the PbO has been increased by an order of magnitude. However, ballmilling not only reduces the mean particle size of the PbO but also brings about the conversion of yellow(massicot) PbO to red(litharge)(88). The opposite conversion can also occur and an equilibrium mixture of the two crystal types results. The composition of the mixture obtained will depend on the conditions prevailing in the ballmill. Therefore Figure 8.11 not only demonstrates the effect of reduction in oxidiser particle size but also of varying oxidiser crystal type.

8.6 HOT STAGE MICROSCOPY OF PbO/B POWDER MIXES

Hot stage microscopy is an important complementary technique to the conventional thermal analysis techniques of Differential Thermal analysis and Differential Scanning Calorimetry. It is able to provide useful, complementary information on the nature of the reactions taking place in pyrotechnic powder mixes which might not be obvious or unambiguously defined in conventional thermal analysis traces. For example, it is possible to identify with certainty fusions or changes of phase taking place, which might be masked in conventional thermal analysis traces by highly exothermic oxidation-reduction reactions taking place at the same time.

In this section hot stage microscopy results are presented for two representative PbO/B compositions, 97/3 and 80/20, which illustrate the complementarity of hot stage microscopy and DSC traces, in addition to providing general information on ignition temperatures and their variation as instrument operating and sample parameters are changed.

Figure 8.12 shows the reflected light intensity vs. temperature trace for a 10mg. sample of a 97/3 PbO/B composition recorded on the hot stage microscope(HSM) at a heating rate of 20 degrees/minute. One important difference between DSC and HSM traces is that the HSM trace is not a differential trace. It is in fact analogous to the weight vs. temperature trace obtained in thermogravimetry. Because of the form of the traces obtained from the hot stage microscope, described above, identification of the various stages of the reaction is not as easy as it is in DSC traces. However, the two main stages in the PbO-B oxidation-reduction reaction stand out very clearly. The first stage of the reaction is represented by the large decrease in reflected light intensity which

FIGURE 8·12

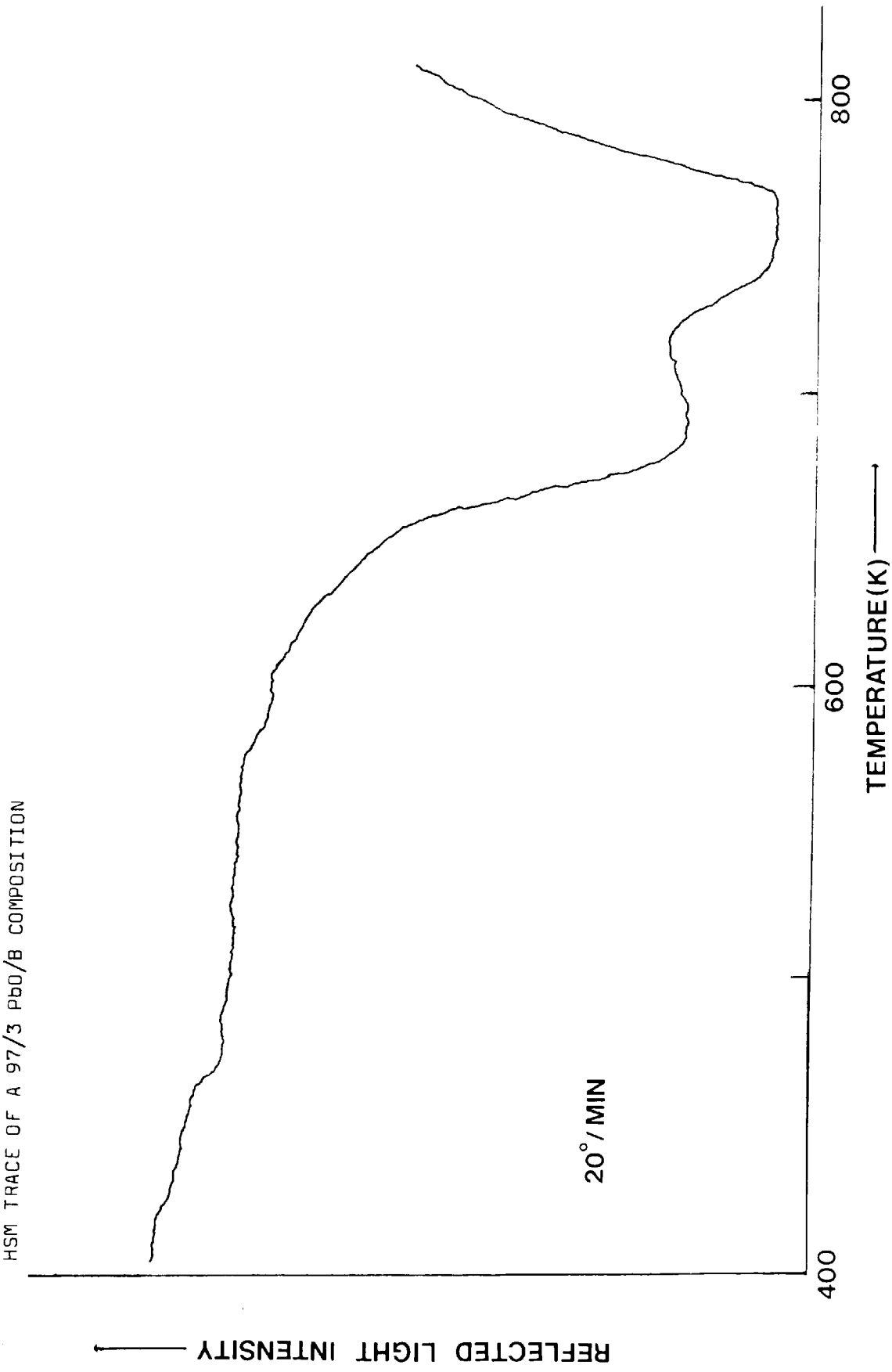
HSM TRACE OF A 97/3 PbO/B COMPOSITION
REFLECTED LIGHT INTENSITY
20°/MIN
400
600
800
TEMPERATURE(K)

begins at around 600K, while the second stage of the reaction is represented by the much smaller decrease in reflected light intensity which begins at approximately 725K. The small increase in reflected light intensity(RLI), which separates the two regions of decreasing RLI, represents the separation of liquid lead as a distinct product phase. The final, large increase in RLI represents the agglomeration of small globules of liquid lead into large globules with large highly reflective surfaces. This final agglomeration of the liquid lead globules is possible because the reaction products are all in the liquid state. This composition contains slightly less than the stoichiometrically required amount of boron which is therefore totally converted to B_2O_3, while the remaining slight excess amount of lead monoxide is completely dissolved in the B_2O_3 produced.

It is interesting to note that the relative magnitudes of the first and second stages of the PbO-B reaction, as indicated by the HSM trace, is in complete contradiction to that indicated by the DSC traces of the reaction. This apparent contradiction is quite easy to explain and depends entirely on the nature of the effects measured in the HSM and the DSC. The first stage of the reaction represents reaction at the surface of particles to form a shell of reaction product. In the HSM, where the intensity of reflected light is measured and recorded the magnitude of this effect is entirely dependant on the nature of the surfaces of the particles being examined, their colour and reflectivity, and not on the relative amount of material being reacted to produce the changes in colour and reflectivity. Therefore,it is possible for the reaction of relatively small amounts material to produce large changes in reflected light intensity.

FIGURE 8.13

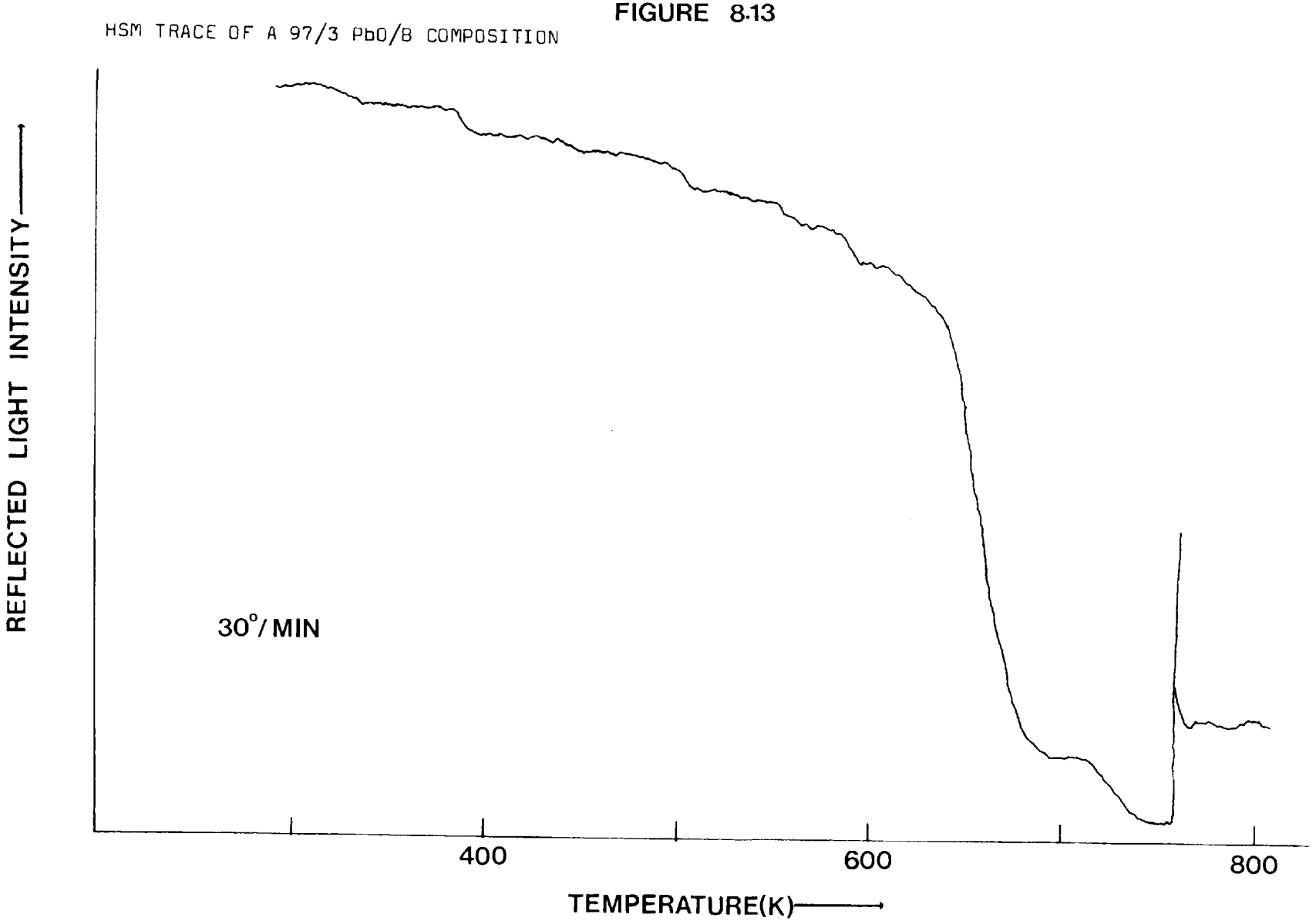
HSM TRACE OF A 97/3 PbO/B COMPOSITION
REFLECTED LIGHT INTENSITY
30°/MIN
400
600
800
TEMPERATURE(K)

It can therefore be seen that RLI traces obtained from the hot stage microscope will always tend to exaggerate surface reactions at the expense of the final 'bulk' reaction, while DSC traces, where rates of enthalpy change are measured, will more honestly represent the relative amounts of material consumed in the different stages of the reaction.

Figure 8.13 illustrates the effect of increased heating rate on the reaction in a 97/3 PbO/B composition. All conditions are the same as in Figure 8.12 except that the heating rate has been increased from 20 to 30 degrees/minute. It can be seen that the traces of Figures 8.12 and 8.13 are very similar except that in Figure 8.13 an ignition reaction has taken place, indicated by the discontinuity in the RLI trace at around 750K.

In general terms it can be stated that in thermal analysis equipment a pyrotechnic composition will exhibit an 'ignition' type reaction when the rate at which heat is supplied by the furnace,plus the rate at which heat is generated by the composition exceeds the rate at which heat can be conducted away from the composition. Under these conditions the composition will experience an uncontrolled rise in temperature, in other words an ignition reaction.

Figures 8.14 and 8.15 show the RLI traces for two samples of a 97/3 PbO/B composition. The sample weight in each case is 20mg., twice that used to obtain the traces of Figures 8.12 and 8.13. It can be seen that at both heating rates, 10 and 20 degrees/minute, an ignition reaction is obtained, again indicated by the discontinuity in each RLI trace. Therefore, it can seen that when the sample weight is increased,

FIGURE 8.14

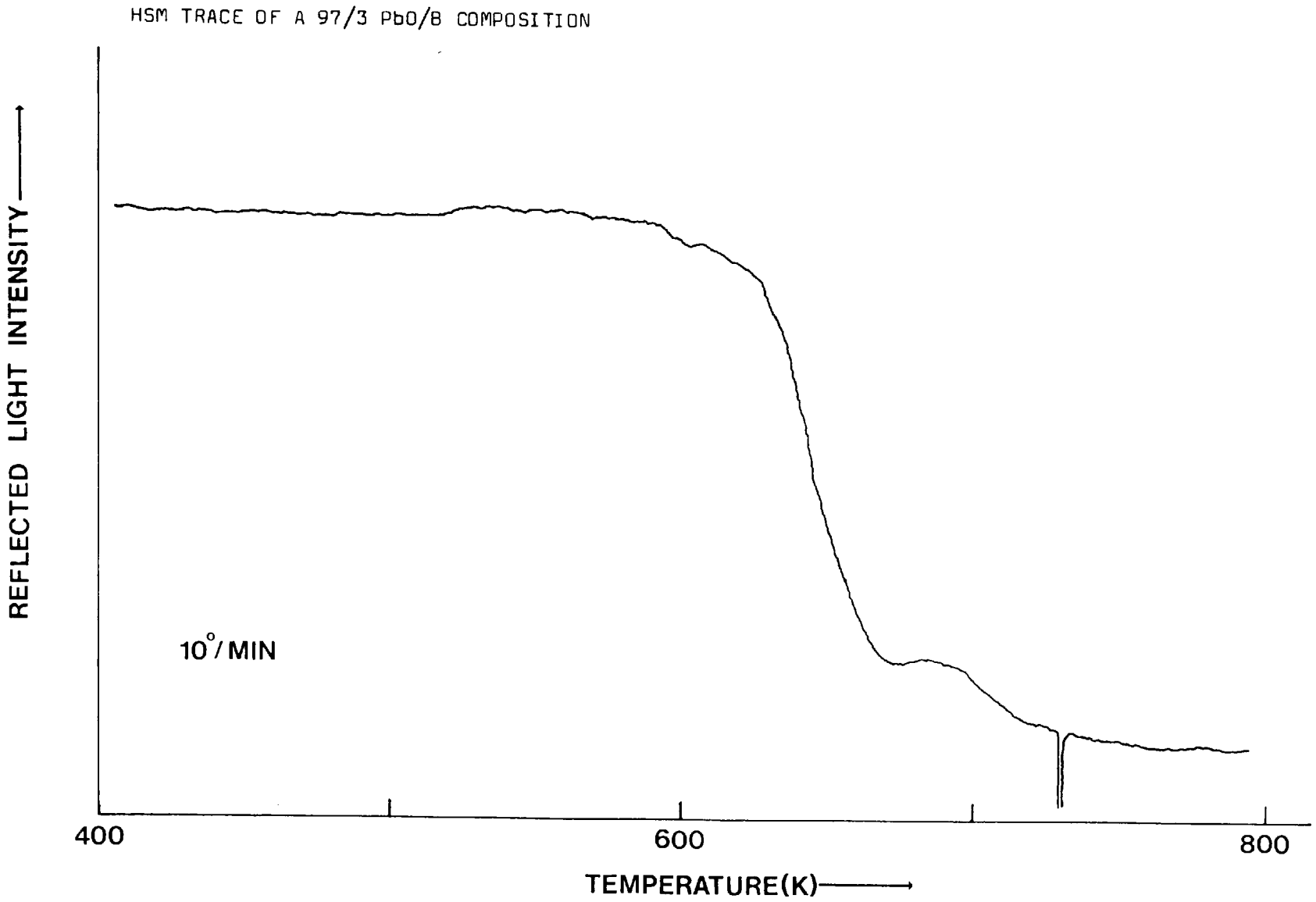
HSM TRACE OF A 97/3 PbO/B COMPOSITION
REFLECTED LIGHT INTENSITY
10°/MIN
400
600
800
TEMPERATURE(K)

FIGURE 8.15

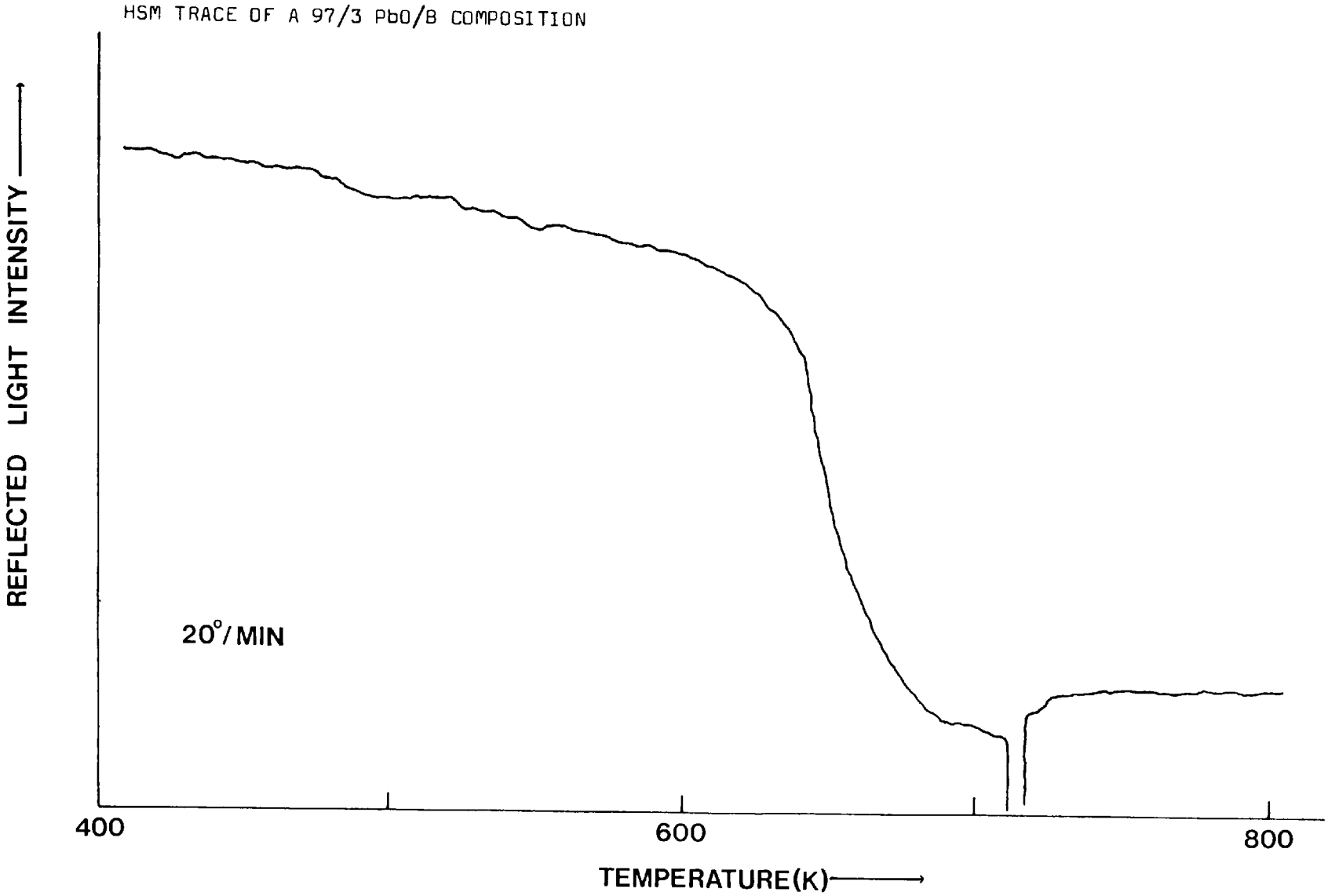
HSM TRACE OF A 97/3 PbO/B COMPOSITION
REFLECTED LIGHT INTENSITY
20°/MIN
400
600
800
TEMPERATURE(K)

consequently increasing the overall rate of heat evolution by the sample at any given temperature, the heating rate at which an ignition reaction is obtained is reduced. This result is in agreement with the conditions for ignition reactions in thermal analysis equipment proposed above.

The opposite trend can be demonstrated by examining a composition in which the overall rate of heat output of the sample has been reduced, either by the reduction of the sample weight or by providing an excess of one of the components.

Figures 8.16 and 8.17 show the RLI traces of two 10mg. samples of an 80/20 PbO/B composition. Because of the reduced rate of heat evolution of this composition, relative to that of the previous 97/3 composition, an ignition reaction is not obtained until a heating rate of 50 degrees/minute is used.

One important point that should be noted in Figure 8.17 is that the ignition reaction corresponds with the first stage of the PbO-B oxidation-reduction reaction. However, in the case of the 97/3 PbO/B composition the ignition reaction corresponded with the second stage of the oxidation-reduction reaction. Therefore, although in the case of the 80/20 PbO/B composition a higher heating rate is required for ignition, the effective ignition temperature is lower than that required for the 97/3 PbO/B composition.

In general terms it can be stated that in a two stage pyrotechnic reaction, the temperature at which ignition is observed will correspond to the first stage of the reaction only if that reaction is capable of increasing the temperature of the composition to that at which the second stage of the reaction takes place.

FIGURE 8.16

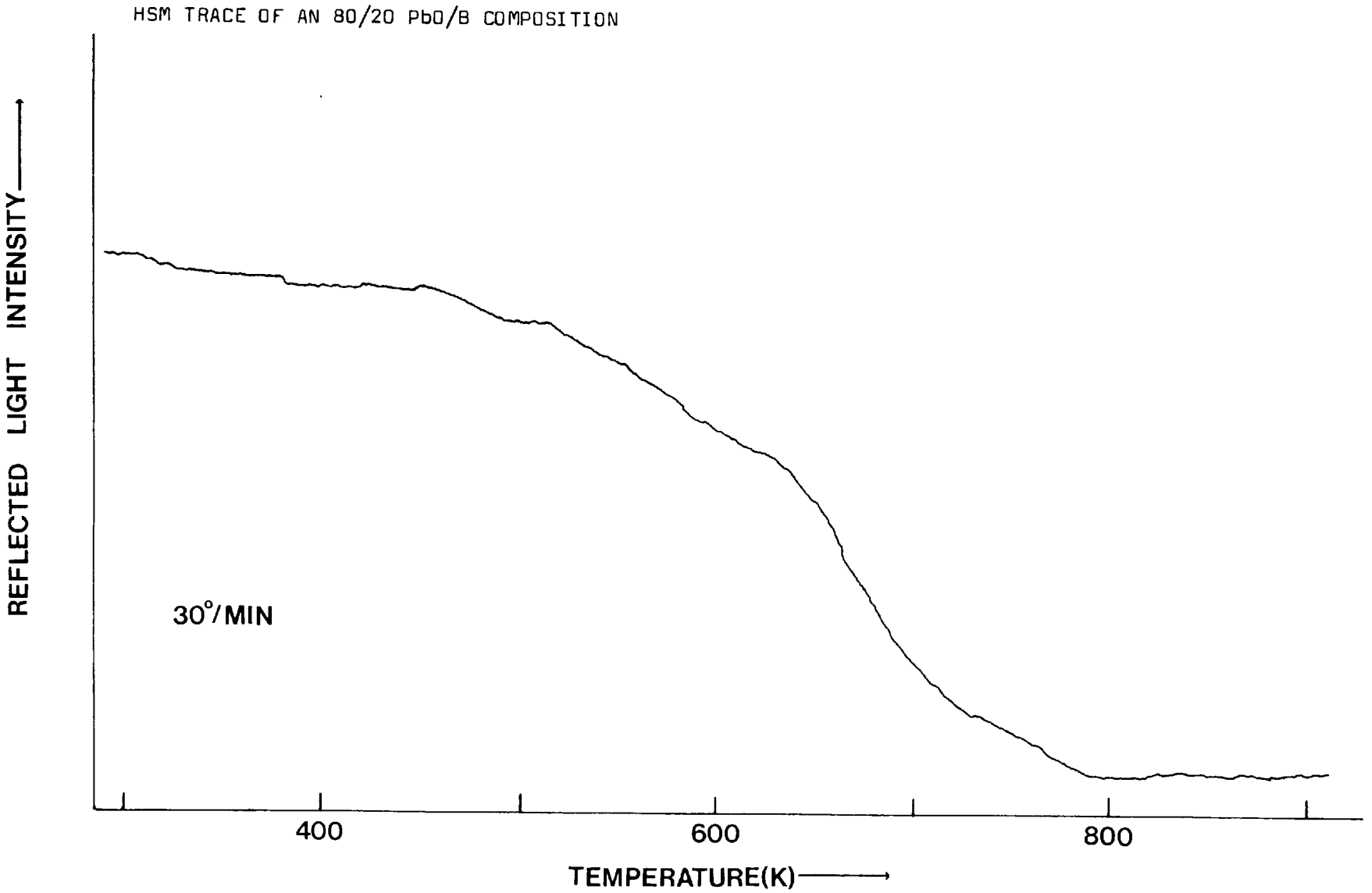
HSM TRACE OF AN 80/20 PbO/B COMPOSITION
REFLECTED LIGHT INTENSITY
30°/MIN
400
600
800
TEMPERATURE(K)

FIGURE 8.17

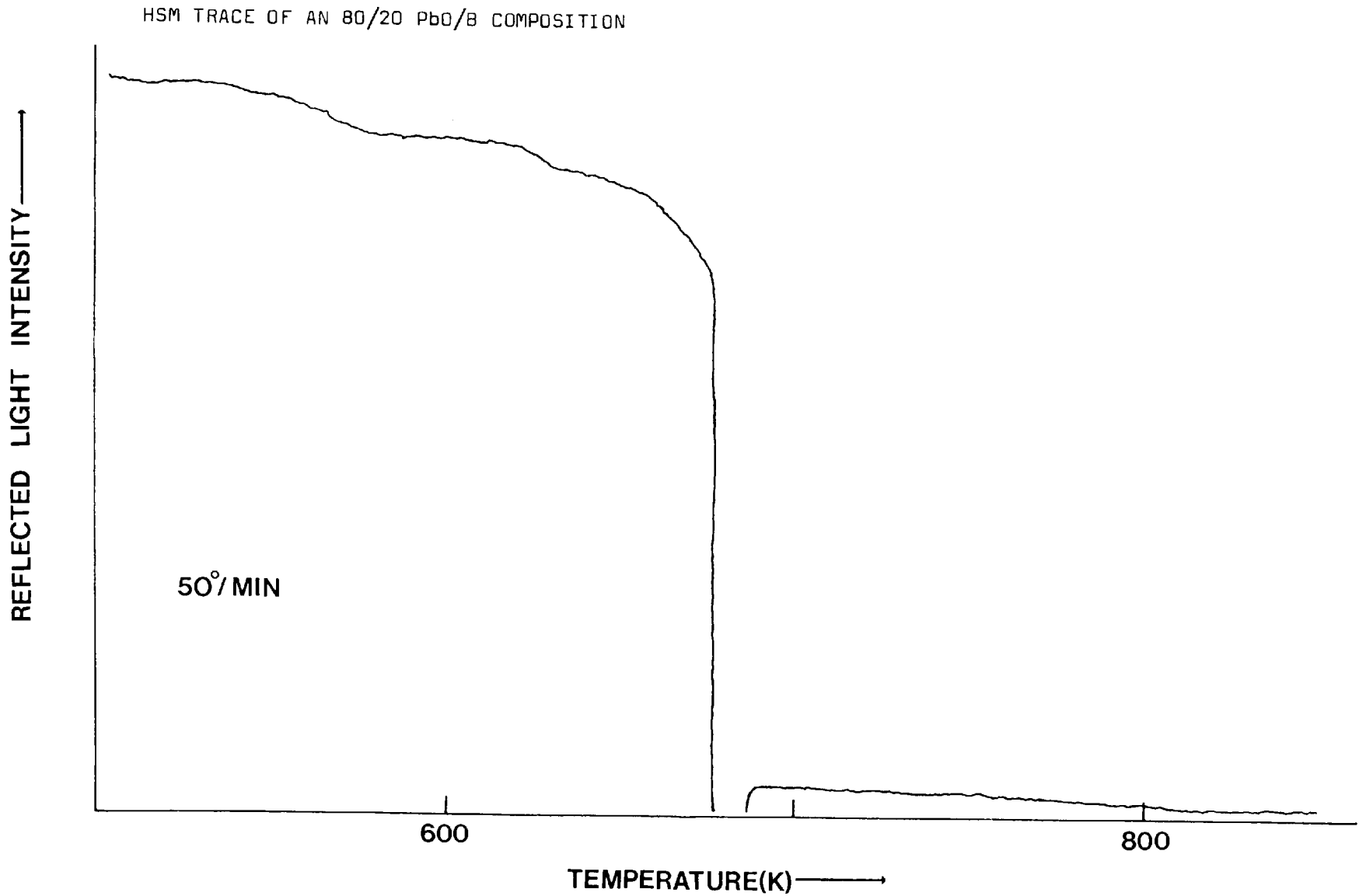
HSM TRACE OF AN 80/20 PbO/B COMPOSITION
REFLECTED LIGHT INTENSITY
50°/MIN
600
800
TEMPERATURE(K)

It is worth pointing out that in Differential Thermal Analysis equipment and in the Hot Stage Microscope the temperature of the sample being investigated will depart from the programmed temperature whenever a reaction takes place within that sample. However, in a Differential Scanning Calorimeter of the power compensation type, such as the Perkin-Elmer DSC-2, whenever a reaction takes place which begins to cause a departure of the sample temperature from the programmed temperature, the rate of heat supply to the sample is either increased or decreased to keep the sample at the programmed temperature. This means that in DSC equipment, that for any given sample weight, it should be possible to use higher heating rates,than in DTA or HSM equipment,before 'ignition' type reactions are observed. Previous work has shown this to be the case(77).

8.7 PbO/B PELLET-PELLET REACTIONS IN THE HOT STAGE MICROSCOPE

Although PbO/B powder mixes can be examined quite adequately in the hot stage microscope by means of visual observations and recording reflected light intensity changes, additional information can be obtained by examining the reactions occuring between consolidated pellets of the individual in the HSM, recording the progress of the reaction photographically.

Because of the small size of the hot stage furnace and consequently of the crucibles used to contain the reactants(6mm. diameter), it is very difficult to obtain pelleted materials with planar surfaces which when butted together give good, void free contact zones. In addition, because of the reduced contact area between reactants, when compared with powder mixes, it is necessary to carry out the reactions at considerably higher temperatures than those at which reaction is normally observed with powder mixes, to ensure that an adequate rate of reaction is obtained. Nevertheless, this technique can provide useful information on the mechanism of the reaction taking place between much smaller particles in powder mixes.

Figures 8.18.A to 8.18.H are photographs of the reaction between pellets of lead monoxide and boron at 757K taken at approximately two minute intervals(approx. X6·5 total magnification). The photographs clearly show the development of the reaction interface with time. It is worth noting that even in an inert atmosphere, as used in this study, it is possible to obtain an ignition reaction between the pelleted materials if the rate of

FIGURE 8.18

HOT STAGE PHOTOMICROGRAPHS OF THE PbO/B PELLET-PELLET REACTION AT 757K, TAKEN AT APPROXIMATELY TWO MINUTE INTERVALS

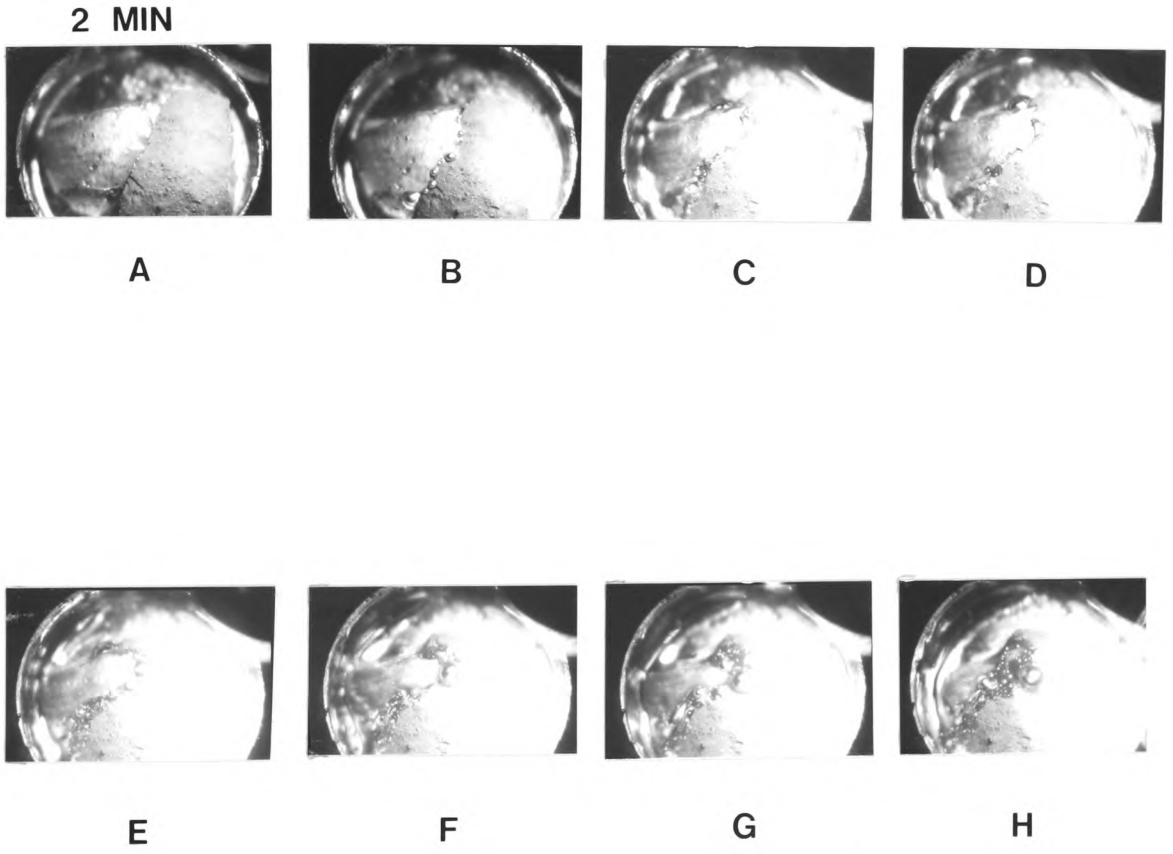

heating up to the final reaction temperature is too rapid. Ignitions in this system have been obtained at heating rates of 100^{0} min^{-1}. The occurrence of ignition reactions between pelleted reactants illustrates very clearly the ease with which reaction takes place between lead monoxide and boron.

Figure 8.19 is an enlargement of Figure 8.18.G showing the reaction in more detail(approx. X20 total magnification). The nature and orientation of the phases in Figure 8.19 are illustrated diagramatically in Figure 8.20. The orientation of the phases illustrated also applies to Figures 8.18.A to 8.18.H.

Visual observations of the reaction with the microscope at higher magnifications(X40) show clearly that as soon as the reaction interface has formed and the lead monoxide and boron are separated by a liquid phase, lead monoxide dissolves at the lead monoxide - liquid interface and that the oxidation - reduction reaction takes place at the boron - liquid interface. The occurrence of the oxidation - reduction at this interface is indicated by the appearance of very small globules of lead at the interface.

Figure 8.21 represents schematically the proposed mechanism of the reaction between lead monoxide and boron.

A serious problem associated with the photomicroscopy of pellet-pellet reactions is the small depth of field of the microscope optical system, the depth of field decreasing as the magnification increases. Figure 8.19 illustrates the problem quite well. It is possible to overcome this difficulty by dispensing with the microscope completely and photographing the reaction in

FIGURE 8.19

AN ENLARGEMENT OF FIGURE 8.18.G

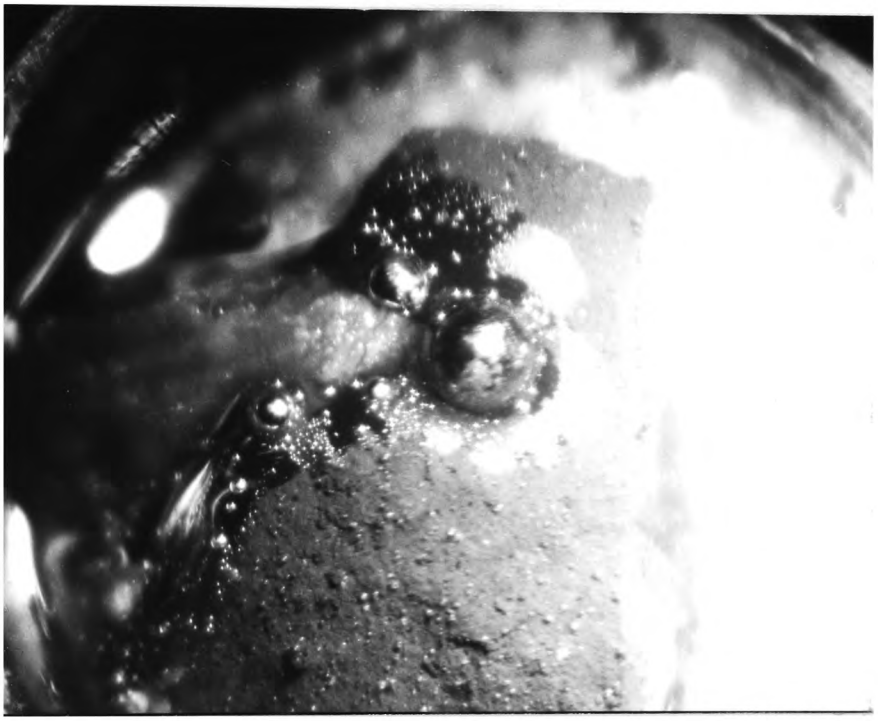

FIGURE 8.20

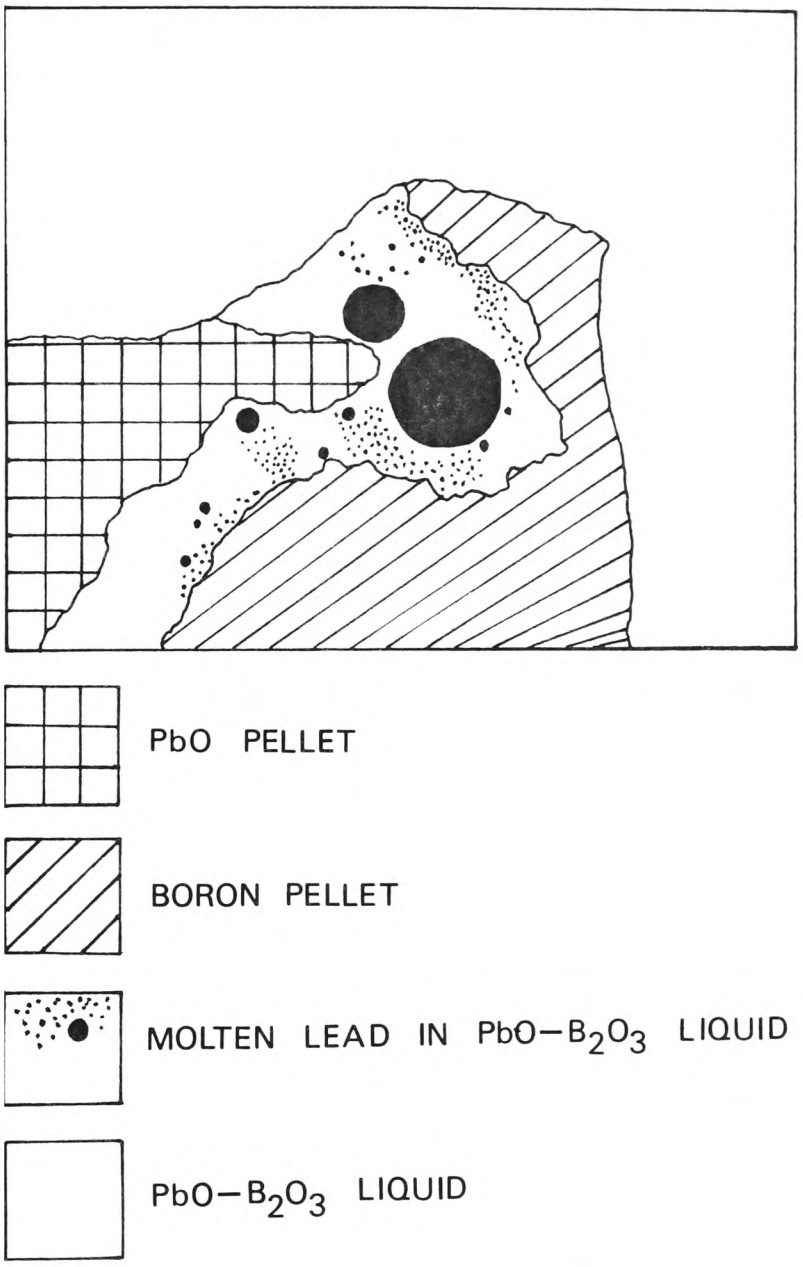

A SCHEMATIC REPRESENTATION OF THE NATURE AND ORIENTATION OF THE PHASES IN FIGURE 8.19

FIGURE 8.21

A SCHEMATIC REPRESENTATION OF THE PROPOSED REACTION MECHANISM IN THE PbO/B SYSTEM

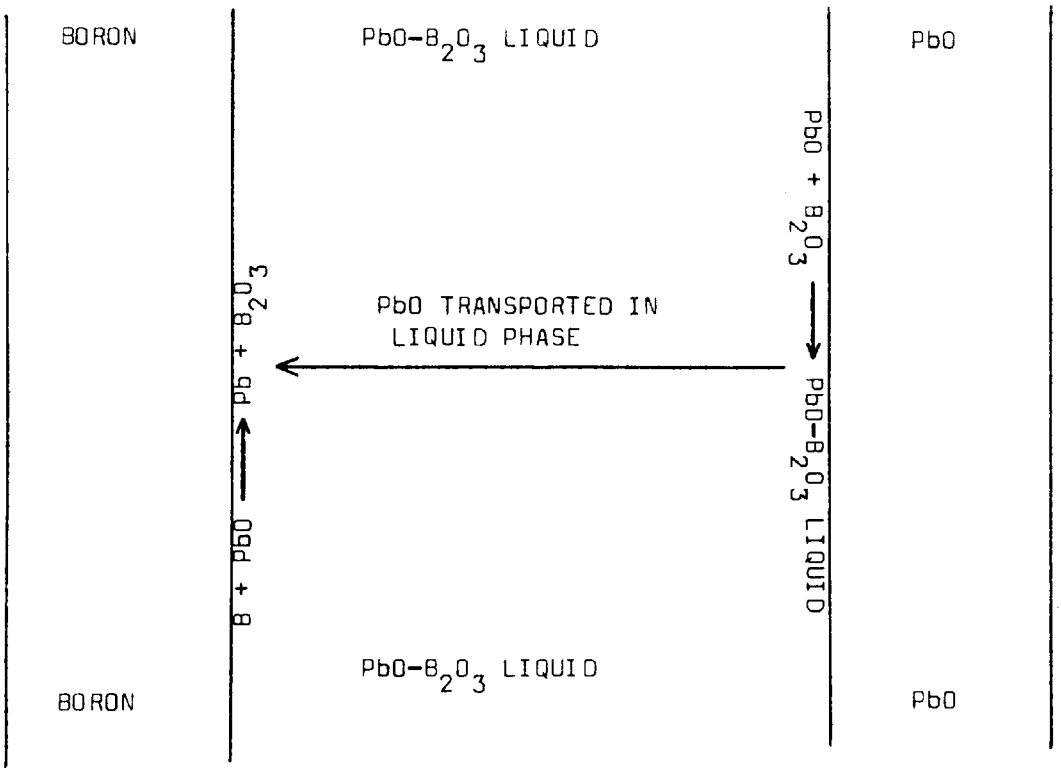

FIGURE 8.22

HOT STAGE PHOTOGRAPHS OF THE PbO/B PELLET-PELLET REACTION AT 757K

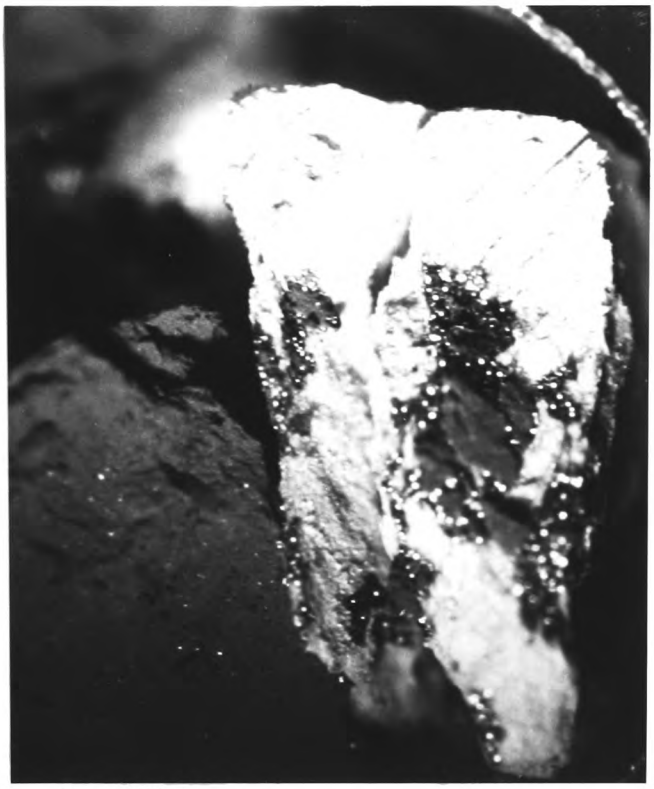

A - 2 MIN

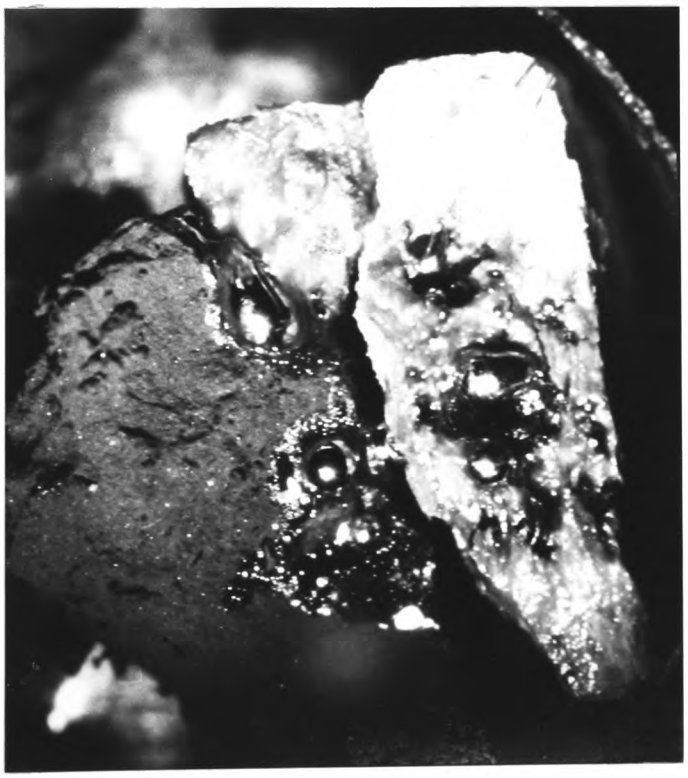

B - 12 MIN

FIGURE 8.22

HOT STAGE PHOTOGRAPHS OF THE PbO/B PELLET-PELLET REACTION AT 757K

C -14 MIN

D -16 MIN

the hot stage furnace directly. This technique requires the camera to be fitted with a close focus lens system. Unfortunately this technique forces the reaction to be observed with virtually no magnification, making immediate visual observation and interpretation very difficult. However, the quality of the photographic record obtained is much improved. Figures 8.22.A to 8.22.D illustrate this point. These photographs were obtained using the same experimental conditions as Figure 8.19 except that the reaction times correspond to 2, 12, 14 and 16 minutes respectively.

CHAPTER 9

KINETICS

9.1 INTRODUCTION

Classically kinetics studies have been carried out in the gas phase or in solution where it is generally, relatively easy to follow changes in the concentration of the reactants or products, these changes usually being the result of unlocalized bulk reactions. The mechanism of the reaction can then be interpreted in terms of the concept of 'order of reaction' by the use of the Guldberg-Waage law of mass action. This law states that 'the rate of a chemical reaction is proportional to the molar concentration of the reacting substances'. The law is strictly applicable only to elementary processes which can be said to represent either the conversion of an individual molecule into one(isomerisation) or several other molecules(decomposition, fragmentation, elimination), or its simultaneous reaction with one or several other molecules(addition, dimerisation, disproportionation, recombination reactions etc.).

Such studies are also usually carried out under isothermal conditions, making it necessary to carry out a number of experiments at different temperatures before an Arrhenius plot can be constructed from which the kinetic parameters, activation energy and pre-exponential factor, can be obtained. In principle, it should be possible to obtain kinetic parameters by the analysis of the results of a single thermal analysis experiment, carried out under dynamic heating conditions. This, of course, would represent a considerable practical advantage over isothermal techniques.

It can be readily appreciated that homogeneous kinetics theory is not directly applicable to multiphase reactions in general and to pyrochemical reactions in particular. A fundamental difficulty is encountered immediately multiphase reactions are considered, this is that the concept of reactant or product concentration cannot be used to define a kinetic rate equation.

To overcome this problem a quantity, normally designated α, is defined representing the fraction of material reacted, or the extent of reaction, in terms of fractional peak area in DTA or DSC. Reaction rates can then be represented by a function, $f(\alpha)$, multiplied by the rate constant, k:

$$\frac{d\alpha}{dt} = k \cdot f(\alpha) \quad \text{--------} \quad (1)$$

When the effect of temperature on the rate of reaction is taken into account by the use of the Arrhenius equation, the basic thermal analysis equation is obtained:

$$\frac{d\alpha}{dt} = k_{\infty} \cdot f(\alpha) \cdot \exp(-E/RT) \quad \text{--------} \quad (2)$$

where k_{∞} = pre-exponential factor

E = activation energy

R = universal gas constant

T = absolute temperature

The commonest method for discovering which one of a group of commonly used $f(\alpha)$ functions(see Appendix) best describes the reaction in question is a trial and error 'best fit' method, whereby the function giving the best straight line in an Arrhenius plot, for the given set of data points, is adopted. This method

requires a considerable amount of mathematical manipulation of the data and consequently most trial and error methods use a computer in order to speed up data handling.

Even with the 'best fit' functions obtained with these techniques departures from linearity of the Arrhenius plot are normally found in portions of the plot corresponding to extreme values of α, the fraction reacted. In addition, it has been shown that where the mechanism of a reaction is known with its corresponding kinetic rate equation, it is possible for very convincing, linear Arrhenius plots to be obtained using incorrect rate equations(67). It is also worth commenting on the fact that the values for the activation energy obtained were not very different from the value obtained using the correct rate equation. These observations must cast some doubt on the validity of the 'best fit' approach and there is a trend towards the use of generalised $f(\alpha)$ functions(89).

When using thermal analysis techniques a problem which can be encountered is that the use of programmed heating, rather than isothermal conditions, can give rise to temperature gradients within the sample. Under these conditions it becomes impossible to relate a rate constant to a particular temperature in the Arrhenius equation. This condition will give rise to non-linearity of an Arrhenius plot, making determination of kinetic parameters very difficult.

Temperature gradients can be particularly pronounced in the case of highly exothermic, pyrochemical reactions and it is good policy to use compositions of as low a heat output as possible, and to programme at as low a heating rate as possible.

Even when the above considerations are taken into account, the determination of the kinetic parameters for predominantly solid state reactions from thermal analysis data is a contentious exercise. Pope(90) states that although 'the transition state theory provides us with a useful model for homogeneous reactions and for reactions occuring between adsorbed species, no corresponding treatment is available for' multiphase reactions. 'In fact, the so-called 'energy of activation' can really only be taken as the measure of the slope of the curve, when lnk is plotted against $1/T\ (K^{-1})$. As this will be influenced by both the history of a solid and its defect structure, published figures appear to be of limited value to other workers. Further, use of the term 'energy of activation' clearly implies that the nature of the rate determining step in the reaction is known. This is far from the truth in most cases where solids are involved.'

Garn(91) has also reviewed the situation, with regard to the determination of the kinetic parameters for solid state reactions, by way of a comparison of energy distributions in homogeneous liquid and gas systems and those in solids. His conclusions are generally in accord with those of Pope quoted above.

It can be seen that great caution must be exercised in the analysis of data obtained from thermal analysis experiments with a view to determining kinetic parameters.

9.2 THE EXTRACTION AND ANALYSIS OF DATA FROM THERMAL ANALYSIS CURVES

In this work only the extraction and analysis of data obtained from DSC equipment of the power compensation type will be considered. However, the principles applied here should be equally applicable to any differential type curve(DTA or DTG).

Figure 9.1 illustrates an idealised DSC curve. Before discussing in detail the ways in which useful data can be obtained from the curve, it is worth pointing out the ways in which this idealised curve differs from those obtained in practice.

The first point that should be made is that for the idealised curve the baseline segments, B_0-T_a and T_b-B_1, on either side of the peak are linear; in practice linear baselines are extremely difficult to achieve, especially at, or close to the upper temperature limit of the instrument. This difficulty is due to the mismatching of the radiation characteristics of the individual furnaces at high temperatures.

Figure 9.1 also indicates that the baseline segments, to either side of the peak, are co-linear across the peak; again in practice this is very rarely found to be the case. In the case of differential scanning calorimetry the deflection of the baeline, with sample in the instrument, from that obtained when the instrument contains no sample, is directly proportional to the heat capacity of the sample at the temperature at which the deflection is measured. Therefore, if there is a difference in heat capacity between the reactants and the products, which is normally the case, the baseline segments will not be co-linear across the peak. Wilburn(92) has

shown, by the use of an electronic analogue model, that the baseline across the peak is actually sigmoid in form, the inflection being centred on the peak maximum temperature.

With regard to the points T_a and T_b which represent the start and finish of the reaction respectively, Figure 9.1 shows them to be relatively well defined; however, in practice these points are usually much less clearly defined. This lack of definition can introduce a small, but finite, error into peak area measurements which is analogous to the zero time error encountered in isothermal experiments.

Although Figure 9.1 shows only one peak, DSC curves of pyrochemical reactions normally exhibit multiple peak patterns. This not only makes peak assignment difficult but also complicates the extraction of useful data from the curves. This problem will be discussed in more detail in the following section.

There are two main methods for extracting useful data from DSC curves, either peak heights can be measured at regular temperature intervals across the peak as far as the peak maximum temperature, the peak height being proportional to the rate constant, or partial peak areas can be measured at regular temperature intervals across the peak; when these partial areas are divided by the total peak area, the resulting fractional peak area is equivalent to the fraction of material reacted at the temperature at which the partial peak area is measured.

With reference to Figure 9.1 the peak height, B_i-T_i, is proportional to the rate constant at that particular temperature.

FIGURE 9.1

AN IDEALISED DSC TRACE

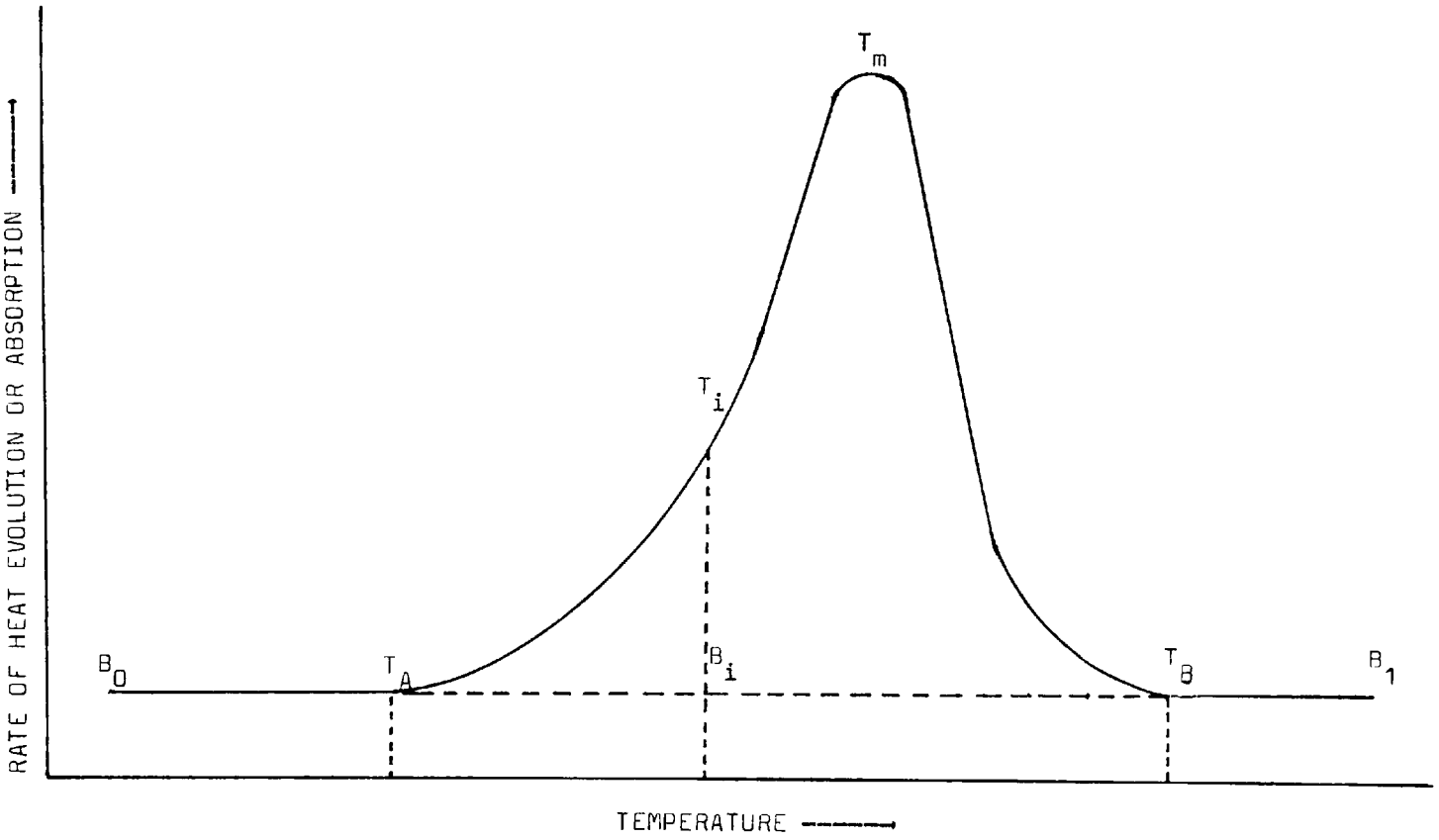

If the peak height is expressed as a rate of heat evolution and the sample size(in g) and the heat of reaction(in J g^{-1}) are known the rate constant can be calculated.

With regard to peak area measurements in Figure 9.1 the total peak area can be defined by the points T_a, T_m and T_b and can be thought of as representing 100% of material reacted, while the partial peak area,defined by the points T_a, T_i and B_i, represents the amount of material reacted up to the temperature at which the partial peak area is measured. The result of dividing the partial peak area by the total peak area is the fraction of material reacted at the temperature T_i. From this method fraction reacted versus time, or temperature, data are obtained which can be analysed by the standard kinetics techniques. A survey of current methods is presented in Chapter 2.

In order to demonstrate the practical difficulties associated with the kinetic analysis of the DSC curves obtained with pyrochemical systems a composition of very low heat output per unit volume was chosen in an attempt to minimise sample temperature non-uniformity. To this end the reaction between boron and the thin oxide layer on lead particles was examined. It is known that this oxide layer is lead monoxide(93) and it was found that a 200:1(wt:wt) Pb:B mix gave a suitable level of heat output, the peak pattern obtained being similar to that of a 97/3 PbO/B composition. The peak pattern obtained is illustrated in Figure 9.2.

The low temperature peak of this system appeared to be quite suitable for kinetic analysis, exhibiting very little apparent

FIGURE 9.2

DSC TRACE OF A 200:1(WT./WT.) Pb(PbO)/B MIX

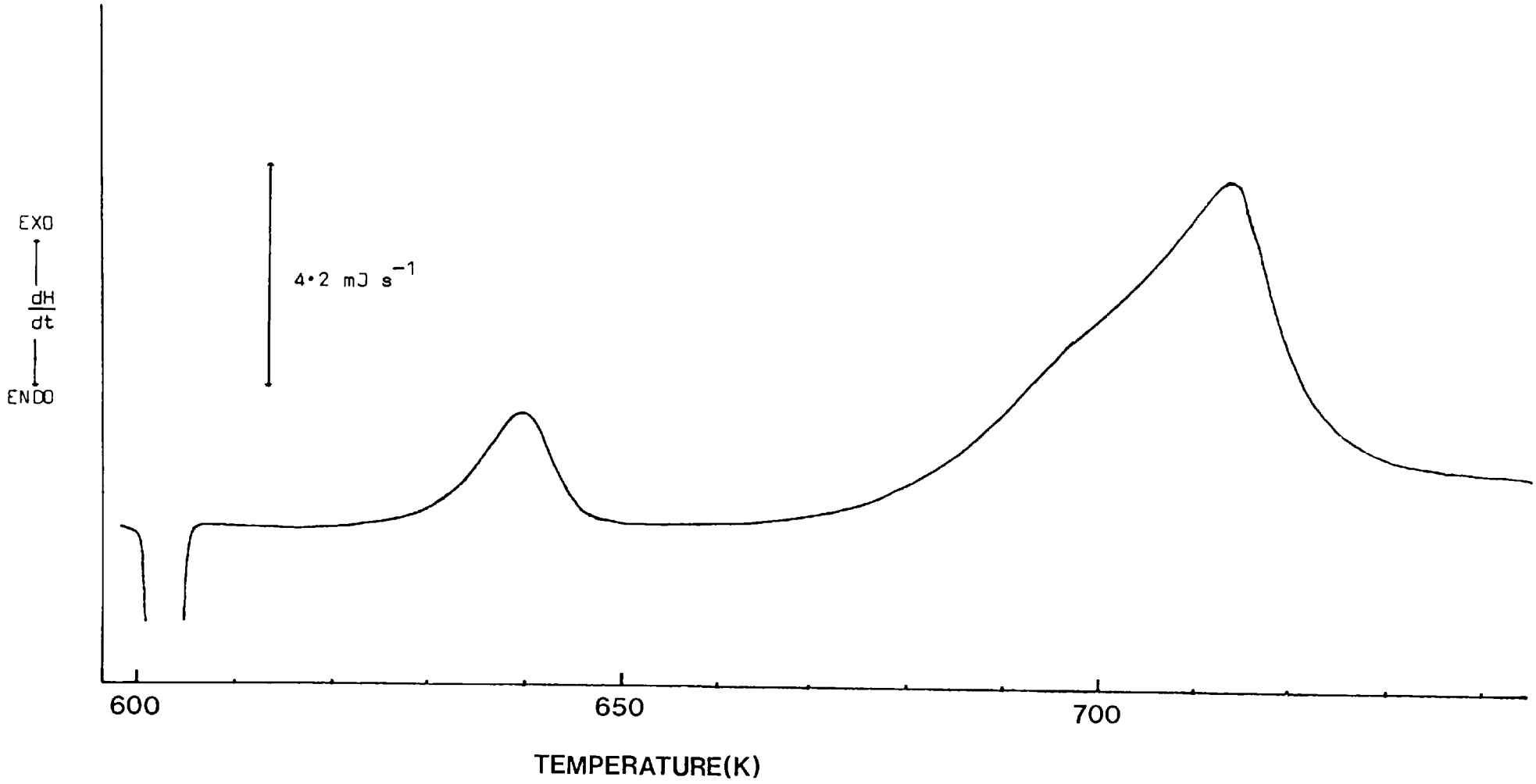

overlap with the higher temperature peak. A typical example of the low temperature peak, which was reproducible in freshly prepared mixes, is illustrated in Figure 9.3.

The first step in the analysis of this peak involves the measurement of partial peak areas at regular time(or temperature) intervals across the peak by the use of a planimeter. To achieve this it is necessary to decide on the position of the baseline under the peak. As pointed out earlier the position of the baseline is dependant on the heat capacity of the sample. If there is no difference in the heat capacities of the reactants and the products the baseline under the peak can be obtained by simply drawing a straight line between the peak start and peak finish positions on the DSC trace. However, if a difference in heat capacities does exist between the reactants and the products, which is normally the case, then the pre- and post-peak baselines will not be co-linear across the peak. In this case the baseline will be a curve, the shape of which will depend on the relative amounts of reactants and products present at any particular time during the reaction. To determine the position of the baseline accurately in this case it is necessary to know the fraction of material reacted at any particular time, for which fractional peak areas are required which makes it necessary that the baseline be known.

This paradoxical situation means that any baseline drawn must, of necessity, be arbitary. To illustrate the effect baseline position has on fraction reacted versus time data, two baselines, one stepped and the other straight, both illustrated in Figure 9.3,

FIGURE 9.3

THE INITIAL DSC PEAK OF THE 200:1(WT./WT.) Pb(PbO)/B SYSTEM

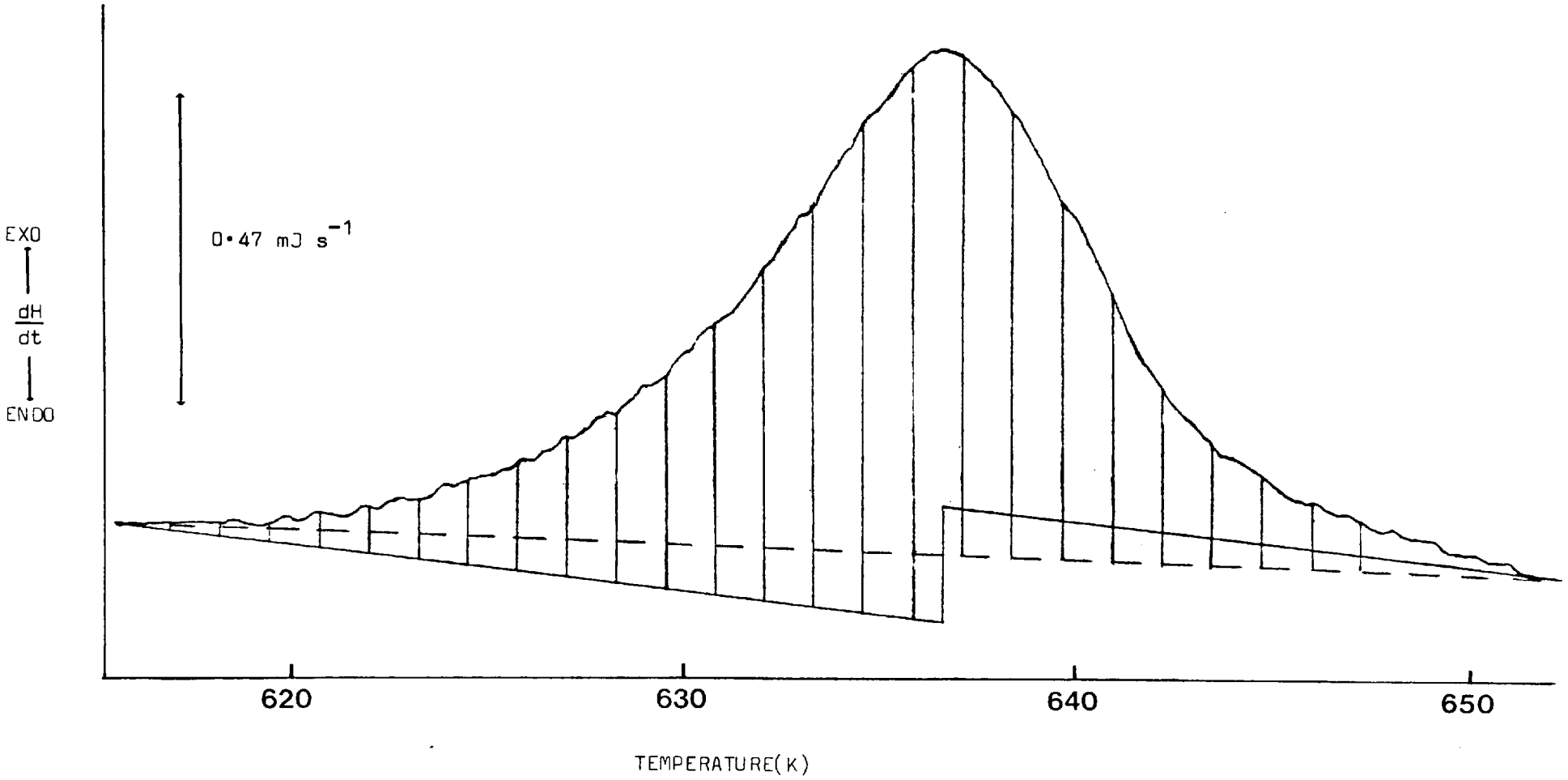

have been drawn. The results obtained are illustrated in Figure 9.4, and summarized in Table 9.1.

It can be seen from Figure 9.4 that changing the baseline from stepped to straight does not substantially alter the form of the fraction reacted versus time plot, although some small changes in detailed form do occur. The detailed changes in form can more easily be seen if the fraction reacted versus time plots are converted to reduced time plots. In these plots the fraction reacted is plotted against $t/t_{0.5}$ (where $t_{0.5}$ is the time at fraction reacted = 0·5)(94). These plots are shown in Figure 9.5 the results being summarized in Table 9.1.

Tang and Chaudhri argue that the form of $f(1-\alpha)$, where α represents the fraction reacted, should be the same in dynamic studies as in isothermal studies, on the basis that the dynamic process can be considered as the limiting case of a series of time intervals, during which the reaction proceeds isothermally, but at the end of each time interval the temperature is altered, in a time so short that the sample remains unchanged(67).

If the Tang and Chaudhri arguement is accepted it should be possible to analyse the fraction reacted versus time data, obtained from dynamic studies, in terms of the reaction equations developed for isothermal studies. Sharp et al(94) have provided standard fraction reacted and $t/t_{0.5}$ values calculated from a comprehensive selection of commonly used reaction equations. In this data the dependence of the rate constant on temperature, pressure and other variables is absorbed in the scale factor.

FIGURE 9.4 VARIATION OF FRACTION REACTED WITH TIME WITH CHANGING BASELINE POSITION ACROSS THE FIRST PEAK OF THE 200:1 Pb(PbO)/B DSC TRACE

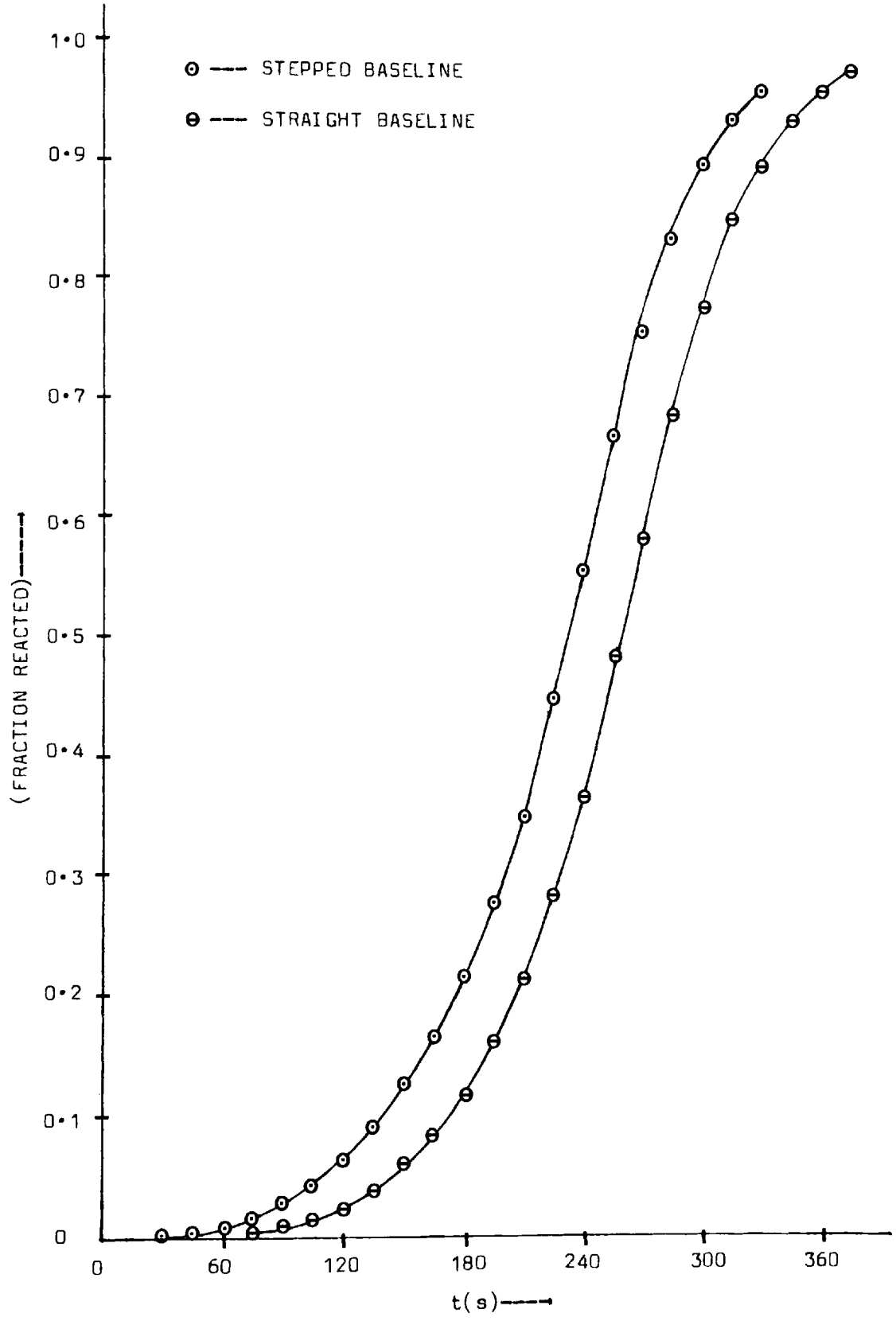

FIGURE 9.5 VARIATION OF FRACTION REACTED WITH REDUCED TIME WITH CHANGING BASELINE POSITION ACROSS THE FIRST PEAK OF THE 200:1 Pb(PbO)/B DSC TRACE

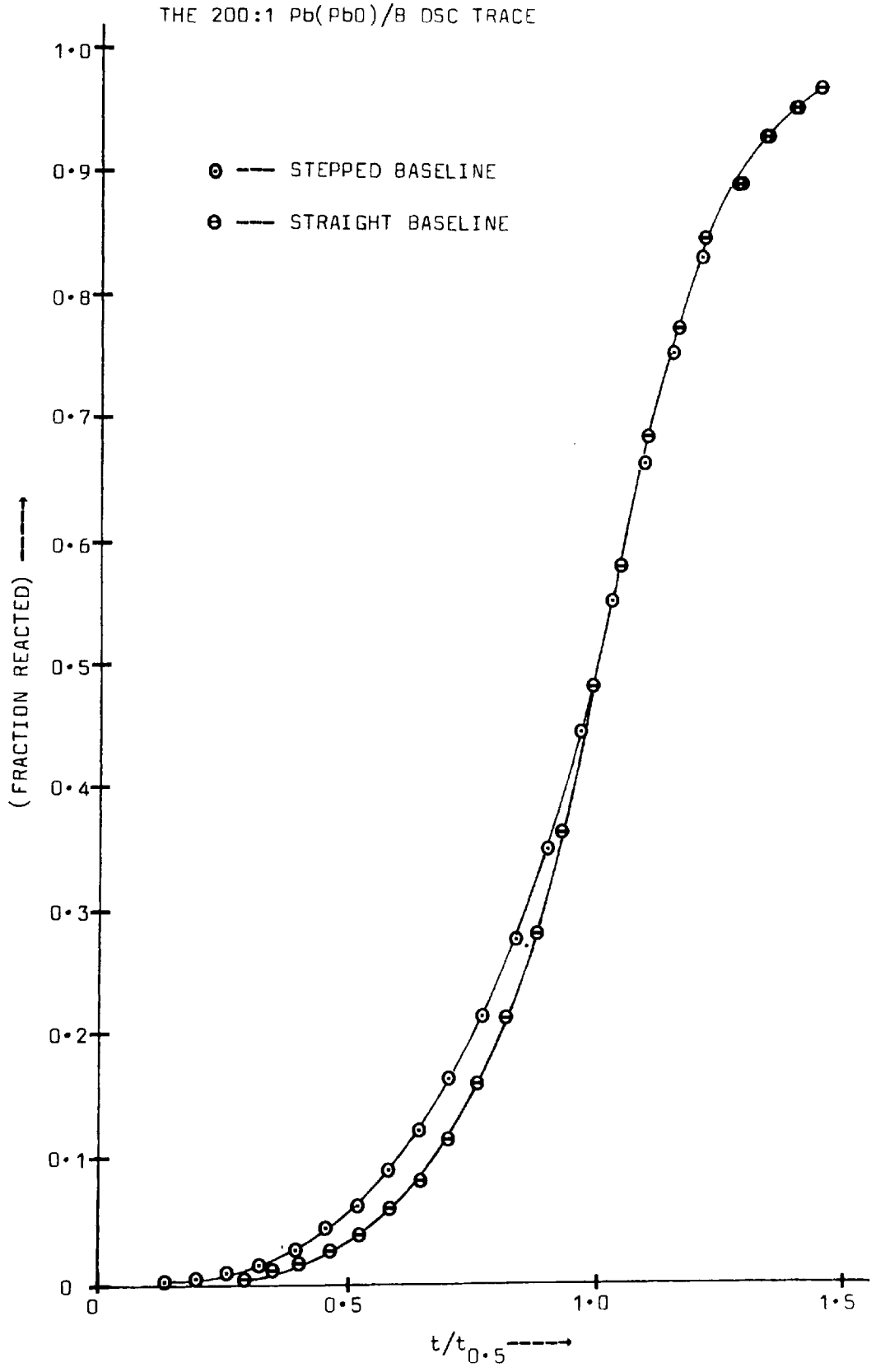

TABLE 9.1 FRACTION REACTED VERSUS TIME AND REDUCED TIME DATA FOR TWO BASELINE POSITIONS ACROSS THE FIRST PEAK OF THE 200:1 Pb(PbO)/B DSC TRACE

	BASELINE TYPE			
	STEPPED*		STRAIGHT**	
t(s)	α	$t/t_{0.5}$	α	$t/t_{0.5}$
15	0·001	0·064	———	———
30	0·002	0·129	———	———
45	0·004	0·193	———	———
60	0·010	0·257	———	———
75	0·015	0·322	0·004	0·292
90	0·029	0·387	0·012	0·350
105	0·044	0·451	0·015	0·409
120	0·064	0·515	0·024	0·467
135	0·091	0·579	0·040	0·525
150	0·124	0·644	0·062	0·584
165	0·166	0·708	0·083	0·642
180	0·215	0·773	0·117	0·701
195	0·279	0·837	0·160	0·759
210	0·350	0·901	0·213	0·817
225	0·447	0·965	0·282	0·876
240	0·555	1·031	0·366	0·934
255	0·669	1·094	0·481	0·992
270	0·755	1·158	0·582	1·050
285	0·834	1·224	0·687	1·108
300	0·894	1·288	0·778	1·168
315	0·932	1·353	0·849	1·225
330	0·955	1·416	0·895	1·284
345	———	———	0·931	1·343
360	———	———	0·953	1·401
375	———	———	0·971	1·459

* $t_{0.5}$ = 233s

** $t_{0.5}$ = 257s

Unfortunately, the plots of the standard data are non-linear and although the technique does enable experimental data to be compared with standard data and the correct reaction equation to be identified, extreme accuracy of the data is required in order to be able to distinguish between some of the similar reaction equations. For example, members of the diffusion controlled group of reaction equations can hardly be distinguished below $\alpha = 0{\cdot}7$.

Doulah(95,96) has suggested a method whereby fraction reacted versus time(or temperature) data may be linearised, based on a generalised rate equation:

$$\frac{d\alpha}{dt} = (\beta/\gamma)(t/\gamma)^{\beta-1}(1-\alpha) \qquad \text{---------(1)}$$

Integration of equation (1), and conversion of the resulting equation into logarithmic form gives:

$$\ln\ln\left[1/(1-\alpha)\right] = \beta \ln t - \beta \ln \gamma \qquad \text{---------(2)}$$

A plot of $\ln\ln\left[1/(1-\alpha)\right]$ versus $\ln t$ (or $\ln(t/t_{0{\cdot}5})$) should be linear. Doulah states that the slope, β, of this plot carries mechanistic significance. This statement can be tested by use of the standard reduced time data provided by Sharp et al.(94).

Table 9·2 shows the result of linear regression analysis on the standard reduced time data($\alpha = 0{\cdot}1$ to $\alpha = 0{\cdot}9$) of Sharp et al. treated according to equation(2) above. All the data used were to the same precision and if the plots are indeed linear it would be expected that the correlation coefficients and the sum of the remaining squares obtained in each case would also be similar.

TABLE 9.2 RESULTS OF LINEAR REGRESSION ANALYSIS ON STANDARD REDUCED TIME DATA TREATED ACCORDING TO THE METHOD DESCRIBED BY DOULAH

	REACTION EQUATION TYPE***								
	D_1	D_2	D_3	D_4	F_1	R_2	R_3	A_2	A_3
SLOPE	0·678	0·618	0·557	0·612	1·000	1·178	1·110	2·000	3·002
INTERCEPT	−0·237	−0·273	−0·321	−0·205	−0·366	−0·283	−0·322	−0·366	−0·364
RSS*	$1·640_{1} \times 10^{-1}$	$8·630_{2} \times 10^{-2}$	$1·918_{2} \times 10^{-2}$	$4·182_{1} \times 10^{-1}$	$3·922_{6} \times 10^{-6}$	$4·429_{2} \times 10^{-2}$	$2·170_{2} \times 10^{-2}$	$4·846_{6} \times 10^{-6}$	$9·316_{5} \times 10^{-5}$
r**	0·989	0·994	0·999	0·975	1·000	0·997	0·999	1·000	1·000

* - residual sum of squares

** - correlation coefficient

*** - for full description of reaction equation types see Appendix

Table 9.2 shows that although the first order(F_1), and the two Avrami-Erofe'ev type equations(A_2 and A_3) give excellent correlation coefficients and very low residual sums of squares the remaining reaction equation types fall some way below this standard. The results would appear to indicate that not all reaction equations give absolutely linear plots when the data is plotted in the form indicated by equation (2).

It can be seen, however, that the slopes of the plots are sufficiently different, on the whole, to enable discrimination between the various groups of reaction equations. Some difficulties could be anticipated in discriminating between the members of the diffusion controlled group of reaction equations for instance. To avoid such difficulties experimental data of as high a quality as possible is required.

Although the standard reaction equation data(α = 0·1 to 0·9) give reasonably good linear plots when plotted according to equation (2), the experimentally obtained data, presented in Table 9.1, give a somewhat more complicated plot.

Figure 9.6 shows the plots of $\ln\ln(1/1-\alpha)$ versus $\ln(t/t_{0.5})$ for the two alternative baselines. The derived data used for these plots are summarized in Table 9.3.

FIGURE 9.6 PLOT OF $\ln\ln(1/1-\alpha)$ VS $\ln(t/t_{0.5})$ FOR TWO BASELINE POSITIONS ACROSS THE FIRST PEAK OF THE 200:1 Pb(PbO)/B OSC TRACE

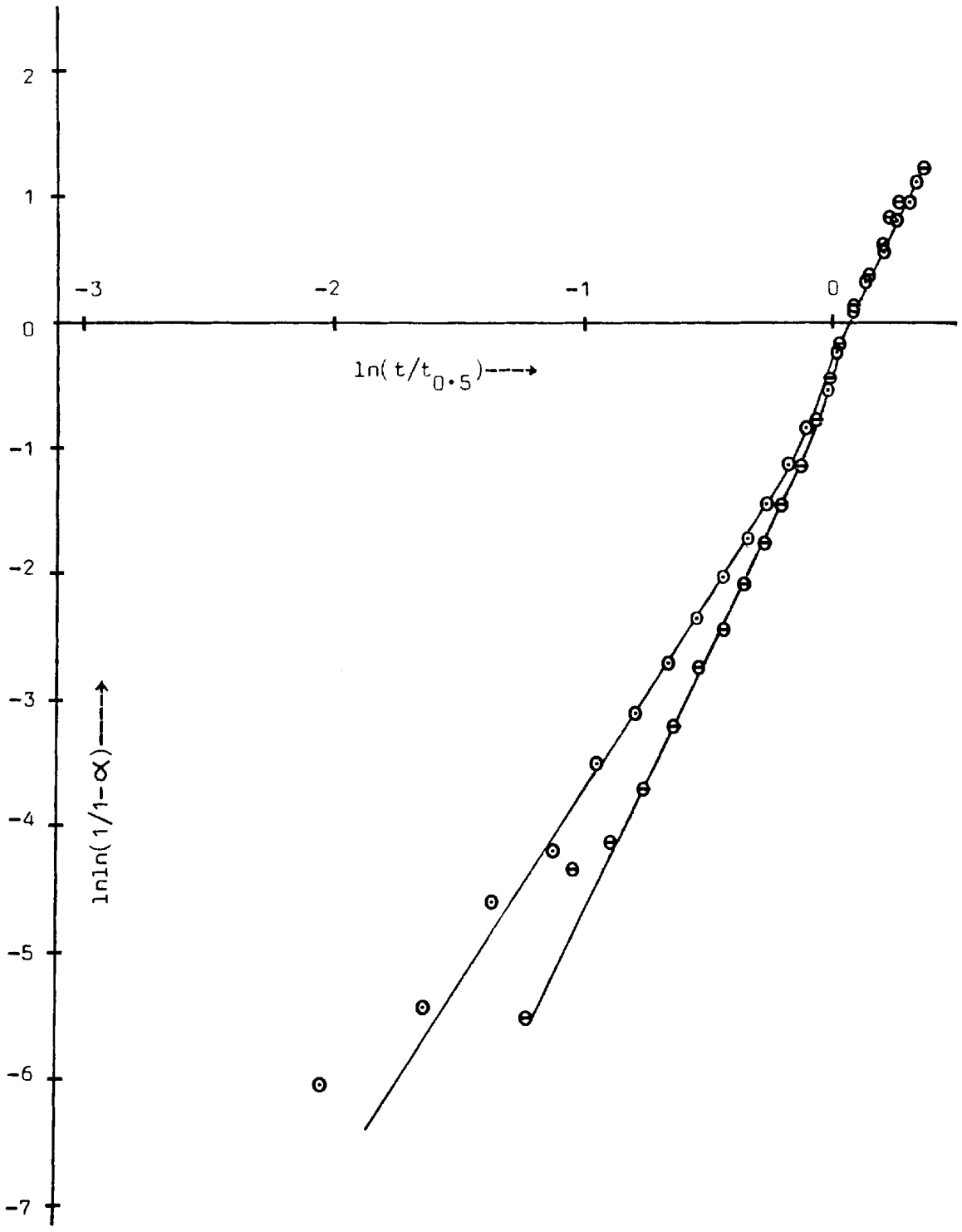

TABLE 9.3 DERIVED DATA FOR TWO BASELINE POSITIONS ACROSS THE FIRST PEAK OF THE 200:1 Pb(PbO)/8 OSC TRACE

	BASELINE TYPE			
	STEPPED		STRAIGHT	
t(s)	$\ln\ln(1/1-\alpha)$	$\ln(t/t_{0.5})$	$\ln\ln(1/1-\alpha)$	$\ln(t/t_{0.5})$
15	-7·131	-2·743	———	———
30	-6·074	-2·050	———	———
45	-5·495	-1·644	———	———
60	-4·621	-1·357	———	———
75	-4·206	-1·134	-5·545	-1·232
90	-3·526	-0·950	-4·392	-1·049
105	-3·113	-0·797	-4·179	-0·895
120	-2·713	-0·664	-3·735	-0·762
135	-2·352	-0·546	-3·201	-0·644
150	-2·020	-0·440	-2·756	-0·538
165	-1·709	-0·345	-2·443	-0·443
180	-1·417	-0·258	-2·085	-0·356
195	-1·120	-0·178	-1·745	-0·276
210	-0·843	-0·104	-1·428	-0·202
225	-0·523	-0·035	-1·107	-0·133
240	-0·212	0·030	-0·785	-0·068
255	0·100	0·090	-0·422	-0·008
270	0·340	0·147	-0·136	0·049
285	0·587	0·202	0·150	0·103
300	0·810	0·253	0·408	0·155
315	0·987	0·302	0·638	0·203
330	1·128	0·348	0·813	0·250
345	———	———	0·983	0·295
360	———	———	1·120	0·337
375	———	———	1·261	0·378

Figure 9.6 shows that the experimental data, plotted according to equation (2), exhibit a fairly high degree of non-linearity. One criticism levelled against the use of double logarithmic plots, of the type required by equation (2), is that it is very easy to obtain linear plots with any data, whatever the relative quality. Linear regression analysis of standard data(94) treated according to equation (2) and inspection of plots of experimental data treated in the same way would seem to indicate that this assumption is not necessarily true.

Before discussing Figure 9.6 further it is worth examining the type of plot obtained with data from the DSC study of a somewhat less complex reaction, namely the decomposition of potassium permanganate(97). Figures 9.7 and 9.8 are plots of fraction reacted versus time and $\ln\ln(1/1-\alpha)$ versus $\ln(t/t_{0.5})$ respectively, for an 8.90 mg sample of potassium permanganate heated at $2{\cdot}5^{o}$ min^{-1} in a dynamic argon atmosphere(a full description of experimental conditions is given in the appendix). A straight baseline has been used and the data is summarized in Table 9.4.

Linear regression analysis of the data of Figure 9.8 gives a correlation coefficient of 0·998, a better result than is obtained with some of the standard reaction equation data. A visual inspection of the plot in Figure 9.8 indicates much less curvature than is present in the plots of Figure 9.6. It can be seen in Figure 9.8 that the curvature of the plot is greatest for low values of fraction reacted. It is in this portion of the plot that any errors in partial peak area measurements, due either to the measuring technique used, or to an incorrectly positioned baseline will be greatest. It

FIGURE 9.7 PLOT OF FRACTION REACTED VERSUS TIME FOR THE DSC PEAK OF THE DECOMPOSITION OF POTASSIUM PERMANGANATE*

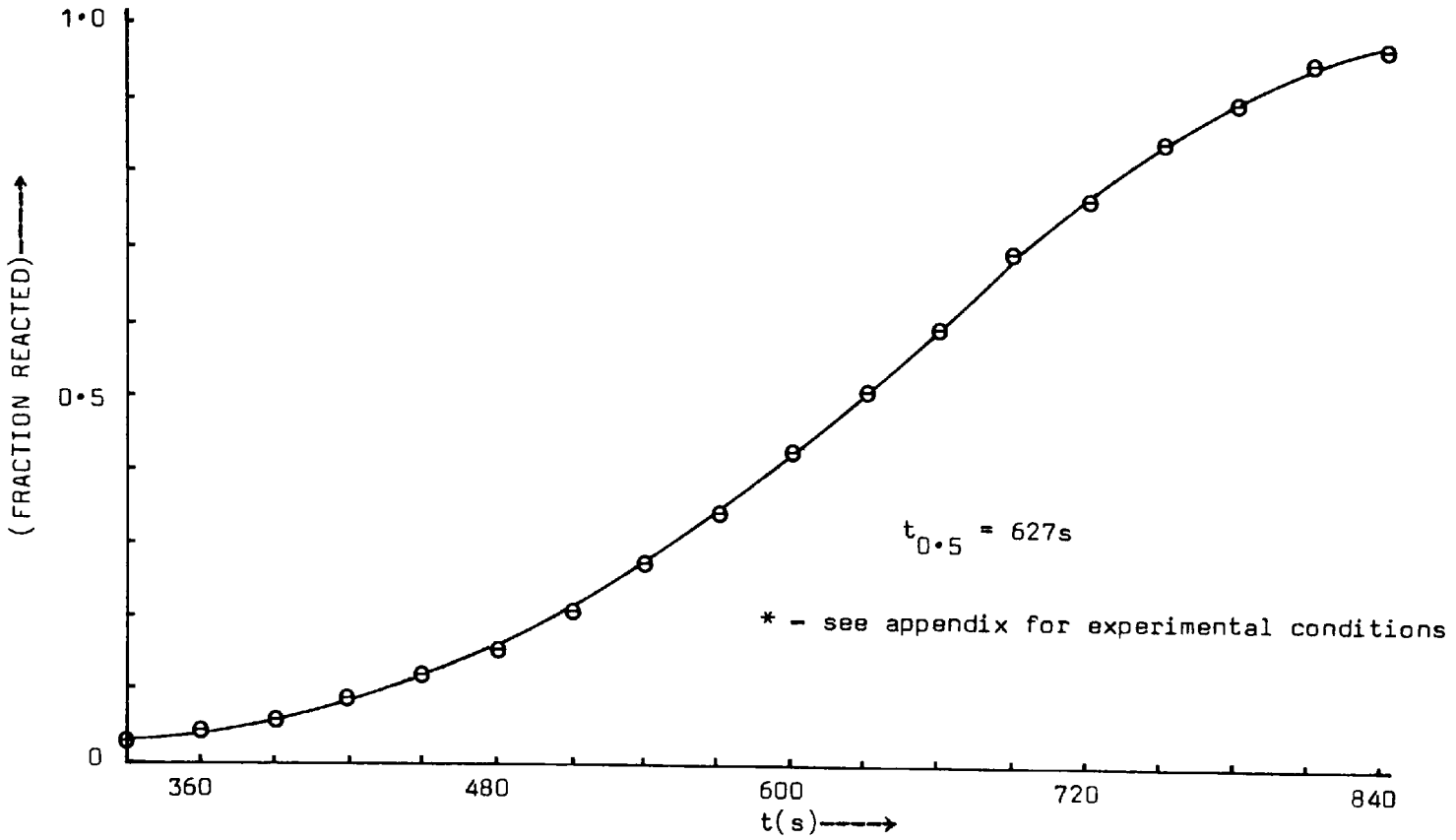

FIGURE 9.8 PLOT OF $\ln\ln(1/1-\alpha)$ VS $\ln(t/t_{0.5})$ FOR THE DSC PEAK OF THE DECOMPOSITION OF POTASSIUM PERMANGANATE*

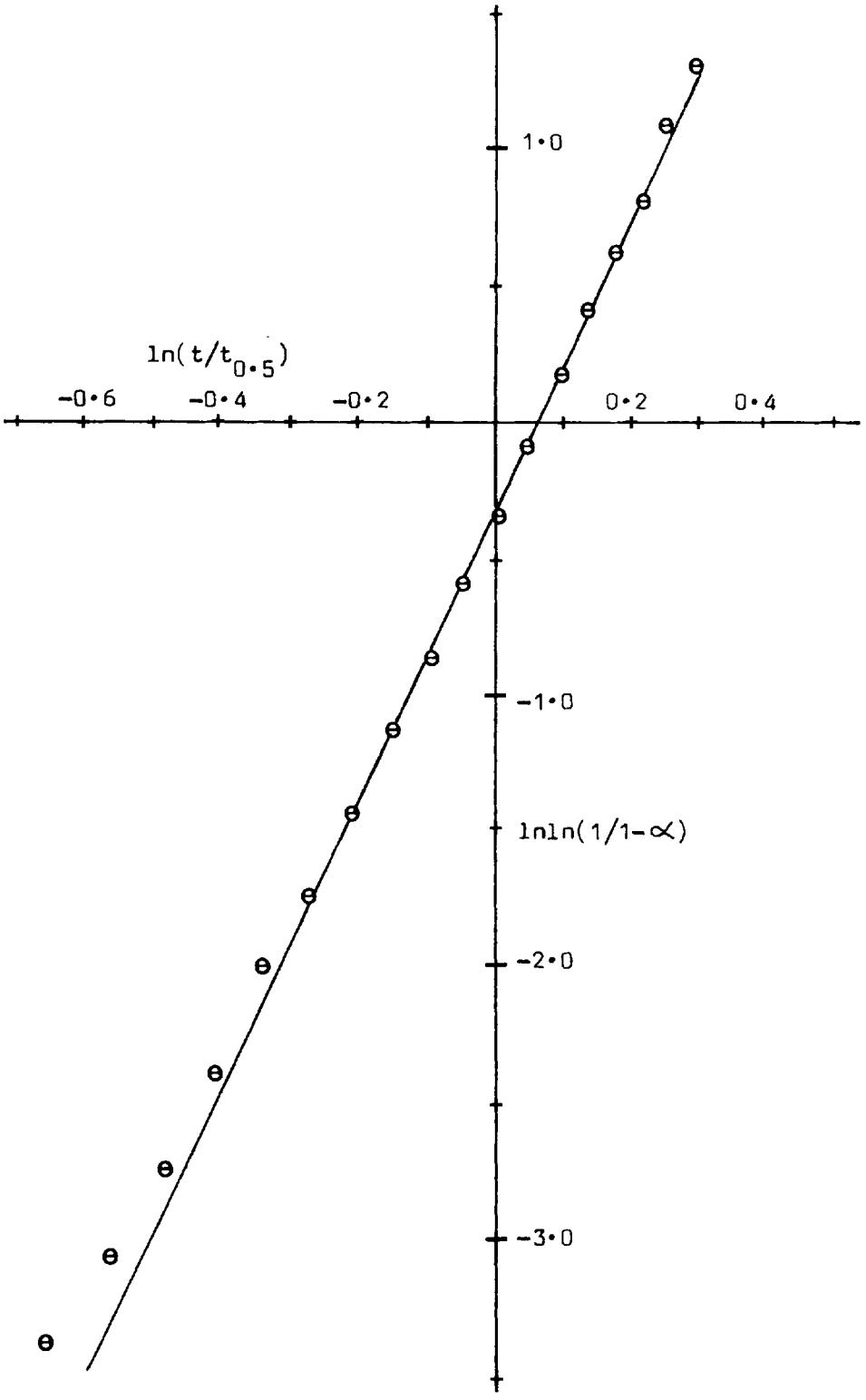

* - see appendix for experimental conditions

TABLE 9.4 FRACTION REACTED VERSUS TIME AND DERIVED DATA FOR THE DSC PEAK OF THE DECOMPOSITION OF POTASSIUM PERMANGANATE*

* - see appendix for experimental conditions

$t_{0.5}$ = 627s

t(s)	FRACTION REACTED (α)	ln ($t/t_{0.5}$)	lnln ($1/1-\alpha$)
330	0·035	-0·642	-3·335
360	0·047	-0·555	-3·034
390	0·064	-0·475	-2·716
420	0·089	-0·401	-2·373
450	0·127	-0·332	-1·996
480	0·160	-0·267	-1·747
510	0·210	-0·207	-1·445
540	0·279	-0·149	-1·117
570	0·344	-0·095	-0·864
600	0·426	-0·044	-0·589
630	0·510	0·005	-0·338
660	0·600	0·051	-0·087
690	0·699	0·096	0·183
720	0·777	0·138	0·406
750	0·847	0·179	0·630
780	0·900	0·218	0·834
810	0·950	0·256	1·097
840	0·975	0·292	1·305

seems likely that the small amount of curvature observed in Figure 9.8 can be attributed to these causes.

Returning to the discussion of Figure 9.6 it can be seen that in this case there is a much greater degree of non-linearity present than in Figure 9.8. It is believed that the non-linearity in Figure 9.6 cannot be totally accounted for by errors in peak area measurement and an incorrectly positioned baseline, as in this case the non-linearity is not concentrated in the low fraction reacted portion of the plots.

The qualitative analysis of the DSC traces, presented in Chapter 8, for the PbO/B system indicates that although there are two low temperature reactions present, $PbO-B_2O_3$ and PbO-B, they need not necessarily be resolved into two peaks. It is suggested that this phenomenon of unresolved reactions gives a reasonable explanation of the non-linearity observed in the plots of Figure 9.6.

Inspection of the straight baseline plot of Figure 9.6 indicates the presence of two linear portions, one from $\ln(t/t_{0.5}) = -1.232$ to -0.068($\alpha = 0.004$ to 0.366) and the other from $\ln(t/t_{0.5}) = 0.103$ to 0.378($\alpha = 0.687$ to 0.971), separated by a non-linear portion. The fact that the structure of the plot is essentially the same with the two different baselines used would seem to indicate that the non-linearity of the plot is a real effect and not due simply to baseline errors.

Evidence for this analysis of the fraction reacted versus time data being correct is provided by the observation that on low temperature($-5^{o}C$) storage of the mix for six weeks the apparently

FIGURE 9.9

THE EFFECT OF LOW TEMPERATURE STORAGE ON THE INITIAL DSC PEAK OF THE 200:1 Pb(PbO)/B SYSTEM

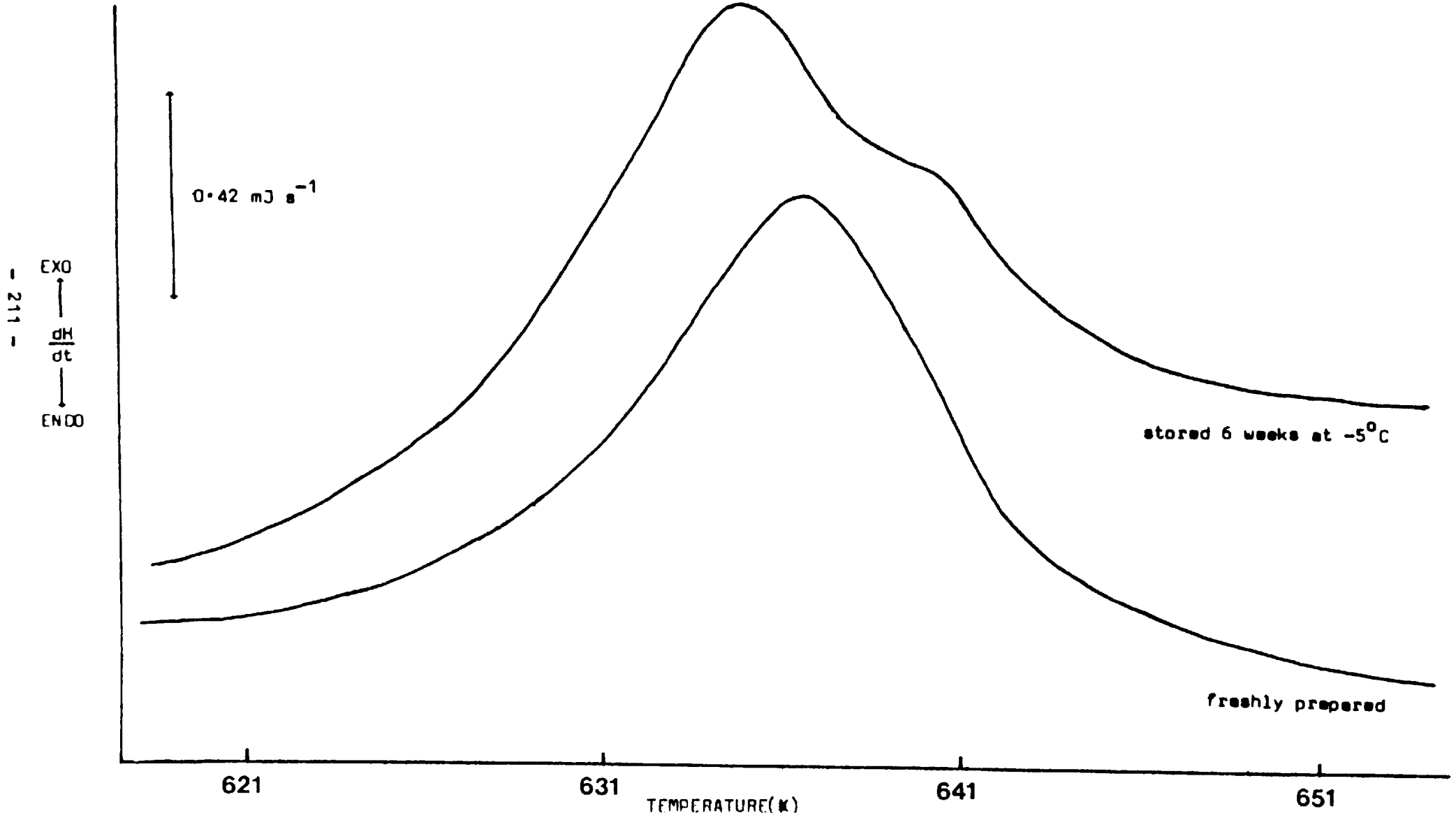

single initial peak splits into two. Figure 9.9 illustrates the structure of the peak obtained before and after storage.

Any additional analysis of the data is extremely difficult, if not impossible, as it becomes impossible to identify the $\alpha = 0$ and $\alpha = 1$ points for the individual reactions.

The second peak of this system is also double and therefore it can be appreciated that a complete kinetic analysis of the dynamic data obtained for the PbO/B system is virtually impossible.

CHAPTER 10

CONCLUSIONS

The heat output results presented illustrate several points quite clearly. Probably the most important point is the difference in behaviour between the boron and silicon fuelled pyrotechnic systems. It would appear that the difference arises from differences between their oxidation products.

Boron gives rise to a low melting point, high volatility oxide, B_2O_3, while silicon gives rise to a high melting point, low volatility oxide, SiO_2. It can be appreciated that in the case of boron the boric oxide produced, because of its physical characteristics relative to those of silicon dioxide, will tend to favour the occurrence of vapour phase side reactions to a greater extent than is found in the silicon fuelled systems at any given temperature.

A comparison of the heat output curves obtained for the four oxide/fuel systems examined would seem to indicate that the oxide component only contributes to the detailed form of the experimental curves. The overall form of the experimental curves and their relationships to the theoretical curves would appear to be determined, for the most part, by the nature of the fuel component and its oxidation products.

With regard to the kJ mol^{-1} of oxide versus oxidiser level plots, the main conclusion that can be drawn from the results is that although the inflexion point, corresponding to the stoichiometric point of the reaction, is an important and easily identified

point in the theoretical plot, it is poorly defined in the experimental plot. This lack of definition, due to physical as well as chemical reasons, means that the inflexion point loses much of its interpretive significance. Under these circumstances it is believed that more attention should be paid to the experimental heat outputs obtained in the plateau region of the curve at high fuel levels. It is believed that the heat output values approached at high fuel levels, in systems such as those examined in this work, give a much better indication of the main oxidation-reduction reaction taking place than does an attempted interpretation of the position of the inflexion point.

The main conclusions regarding the overall energetics of the boron fuelled systems can be summarized as follows:

(1) the main oxidation-reduction reaction produces B_2O_3

(2) at fuel levels above the stoichiometric level(of the B_2O_3 producing reaction) vapour phase, suboxide producing secondary reactions take place which produce heat outputs in excess of those expected solely from the B_2O_3 producing reaction. However, at fuel levels considerably in excess of the stoichiometric level the vapour phase reactions become of less importance

(3) at fuel levels below the stoichiometric level(of the B_2O_3 producing reaction) it is possible for the excess oxidiser present to react with B_2O_3 produced in the main oxidation-reduction reaction, again giving rise to heat outputs in excess of those expected.

The main conclusions drawn from the propagation studies can be summarized as follows:

(1) the silicon fuelled systems follow the heat output-propagation

rate relationship described by Spice and Staveley(7),

(2) the boron fuelled systems present a more complicated heat output-propagation rate relationship and appear not to follow the relationship described by Spice and Staveley(7). However, it is proposed that the propagation rate is strongly linked to the initial B_2O_3 producing reaction, following the Spice and Staveley pattern, with the vapour phase suboxide producing secondary reactions obscuring the true heat output-propagation rate relationship,

(3) the propagation rates of the silicon fuelled systems display a complex response to an increase in consolidation pressure, as the oxidiser/fuel ratio changes, indicating a change in the dominant heat transfer mechanism as this ratio changes,

(4) the propagation rates of the boron fuelled systems display a consistent response to an increase in consolidation pressure, as the oxidiser/fuel ratio changes, indicating a virtually unchanging heat transfer mechanism as this ratio changes.

The results presented in Chapter 7 indicate that reasonably accurate non-contact reaction temperature measurements can be made using an infra-red recording brightness pyrometer. Although all the results presented have been obtained using an assumed effective emittance of 0·55, it is possible to generate from any of the results obtained a plot, similar to those of Figure 7.1, showing the variation of recorded temperature with assumed emittance. This means that adjustments to the results obtained can be made, in the light of any improvement in the measurement of emittance values for instance, without it being necessary to repeat the

measurements.

It is worth mentioning that it is possible to overcome the emittance difficulties associated with infra-red brightness pyrometers by the use of an infra-red 'two colour' pyrometer. This instrument measures the ratio of the spectral radiance of a body at two different, but very close, infra-red wavelengths, the ratio being a unique function of the temperature of the body, independent of its emittance. This technique makes it necessary to assume that the **spectral** emittance of the body is the same at both wavelegths, the graybody assumption.

The thermal analysis study, coupled with the attempted kinetic analysis, of the PbO-B reaction has demonstrated the complex reaction pattern that can be obtained with an apparently simple oxidation-reduction reaction. The thermal analysis study has also demonstrated the important role that the reaction product B_2O_3 plays in the PbO-B reaction mechanism, the high solubility of PbO in B_2O_3 meaning that PbO can easily be transported via the liquid phase.

Overall, the results presented indicate that although it is possible to draw some general conclusions as to the pattern of reaction in metal oxide/metal pyrotechnic systems, the individual characteristics of each system must be taken into account if a detailed description of the reaction is to be provided.

In conclusion it can also be said that some of the oxidiser/fuel compositions examined possess propagation rates and 10mm column length delay time standard deviations which would make them suitable for practical use as time delay compositions.

REFERENCES

1. R.M. Blunt,
Proc. of The Seventh Int. Pyrotechnics Seminar, 1, 1-12, (1980).

2. A.A. Shidlovskii,
Symp. Chem. Prob. Connected Stab. Explos.(Proc), 3rd,
315-319, (1974).

3. G. Hale,
U.S. Patent 1805214, (1931).

4. C. Campbell and A.J. Beardell,
Thermochimica Acta, 8, 27-33, (1974).

5. H. Ellern, Military and Civilian Pyrotechnics,
Chemical Publishing Company Inc., New York, (1968).

6. J.E. Spice and L.A.K. Staveley,
J. Soc. Chem. Ind., 68, 313-319, (1949).

7. J.E. Spice and L.A.K. Staveley,
J. Soc. Chem. Ind., 68, 348-355, (1949).

8. R.A.W. Hill, L.E. Sutton, R.B. Temple and A. White,
Research, 3, 569-576, (1950).

9. R.A.W. Hill and T.L. Cottrell,
4th Int. Symp. on Combustion(Proc), 349-352, (1953).

10. R.A.W. Hill,
Proc. Royal Society, 226A , 455-471, (1954).

11. R.A.W. Hill and A.A. Wallace,
Nature, 178 , 692-693, (1956).

12. R.A.W. Hill,
Trans. Faraday Soc., 53 , 1136-1144, (1957).

13. R.A.W. Hill,
Proc. Royal Society, 239A , 476-486, (1957).

14. R.A.W. Hill and J.N. Welsh,
Trans. Faraday Soc., 55 , 299-305, (1959).

15. E. Maillard and Le Chatelier,
Ann. Mines, 4, 274, (1895).

16. F. Booth,
Trans. Faraday Soc., 49 , 272-281, (1953).

17. S. Nakahara and T. Hikita,
Jnl. Ind. Explos. Soc.(Japan), 20 , 275-279, (1959).

18. S. Nakahara and T. Hikita,
Jnl. Ind. Explos. Soc.(Japan), 20 , 356-360, (1959).

19. S. Nakahara and T. Hikita,
Jnl. Ind. Explos. Soc.(Japan), 21 , 2-8, (1960).

20. S. Nakahara and T. Hikita,
Jnl. Ind. Explos. Soc.(Japan), 21 , 86-92, (1960).

21. S. Nakahara,
Jnl. Ind. Explos. Soc.(Japan), 21 , 238-243, (1960).

22. S. Nakahara,
Jnl. Ind. Explos. Soc.(Japan), 21 , 363-374, (1960).

23. G.J. Rees,
Ph.D. Thesis(London Univ.), (1958).

24. G.J. Rees,
Fuel, 52 , 138-142, (1973).

25. G.J. Rees,
Fuel, 52 , 226-229, (1973).

26. G.J. Rees,
Fuel, 53 , 110-113, (1974).

27. A.P. Hardt and P.V. Phung,
Combustion and Flame, 21 , 77-89, (1973).

28. A.P. Hardt and R.W. Holsinger,
Combustion and Flame, 21 , 91-97, (1973).

29. A.P. Hardt and P.V. Phung,
Combustion and Flame, 22 , 323-335, (1974).

30. S. Patai and E. Hoffmann,
J. Appl. Chem., 2 , 8-11, (1952).

31. J.H. McLain,
Pyroteknikdagen, Stockholm, 1-16, (1973).

32. J.H. McLain,
Pyrotechnics, The Franklin Institute Press, (1980).

33. R.C. Harris,
Symp. Chem. Prob. Connected Stab. Explos.(Proc), 2nd,
356-373, (1970).

34. R.C. Harris,
Symp. Chem. Prob. Connected Stab. Explos.(Proc), 3rd,
275-283, (1974).

35. C.H. Miller,
Symp. Chem. Prob. Connected Stab. Explos.(Proc), 3rd,
285-301, (1974).

36. R.J. Benge,
Pyrochem International(Proc), 22·1-22·17, (1975).

37. S.S. Al-Kazraji and G.J. Rees,
Fuel, 58 , 139-143, (1979).

38. J.N. Bradley, W.D. Capey and J.F. Shere,
Nature, 277 , 291-292, (1979).

39. L.W. Collins, L.D. Haws and A. Gibson,
Combustion and Flame, 38 , 155-158, (1980).

40. L.W. Collins,
Proc. of The Seventh Int. Pyrotechnics Seminar, 1 ,
107-117, (1980).

41. L.W. Collins,
Combustion and Flame, 41 , 325-330, (1981).

42. A.Z. Moghaddam and G.J. Rees,
Fuel, 59 , 42-44, (1980).

43. B.J. Thomson and A.M. Wild,
Pyrochem International(Proc), 11·1-12·1, (1975).

44. D.M. Speros and J.R. Debresis,
Combustion and Flame, 45 , 235-250, (1982).

45. W.C. Roberts-Austen,
Proc. Inst. Mech. Eng., 35-41, (1899).

46. G. Urbain and C. Boulanger,
Compt. Rend., 154 , 347, (1912).

47. K. Honda,
Sci. Rep. Tohoku Imp. Univ., Ser. 1, 4 , 97-103, (1915).

48. T. Boddington, P.G. Laye, H. Morris, C.A. Rosser,
E.L. Charsley, M.C. Ford and D.E. Tolhurst,
Combustion and Flame, 24 , 137-138, (1975).

49. T. Boddington and P.G. Laye,
Pyrochem International(Proc), 12·1-12·6, (1975).

50. T. Boddington and P.G. Laye,
Pyrochem International(Proc), 24·1-24·4, (1975).

51. P.G. Laye and J. Tipping,
Proc. of The Seventh Int. Pyrotechnics Seminar, 2,
651-654, (1980).

52. E.L. Charsley and D.E. Tolhurst,
Microscope, 23 , 227-237, (1975).

53. E.L. Charsley and M.R. Ottaway,
Pyrochem International(Proc), 17·1-17·16, (1975).

54. E.L. Charsley and M.R. Ottaway,
8th Int. Symp. on The Reactivity of Solids(Proc), 737-741, (1977).

55. S.L. Howlett and F.G.J. May,
Thermochimica Acta, 9 , 213-216, (1974).

56. S.S. Al-Kazraji and G.J. Rees,
Combustion and Flame, 31 , 105-113, (1978).

57. S.S. Al-Kazraji and G.J. Rees,
Jnl. of Thermal Analysis, 16 , 35-39, (1979).

58. A.Z. Moghaddam and G.J. Rees,
Fuel, 60 , 629-632, (1981).

59. L. Sulacsik,
Jnl. of Thermal Analysis, 5 , 33-42, (1973).

60. P. Murray and J. White,
Trans. Brit. Ceram. Soc., 54 , 190, (1955).

61. P. Murray and J. White,
Trans. Brit. Ceram. Soc., 54 , 204, (1954).

62. H.E. Kissinger,
Anal. Chem., 29 , 1702-1706, (1957).

63. H.J. Borchardt and F. Daniels,
Jnl. Am. Chem. Soc., 79 , 41-46, (1957).

64. T. Ozawa,
Bul. Chem. Soc. Jap., 38 , 1881-1886, (1965).

65. R.N. Rogers and E.D. Morris,
Anal. Chem., 38 , 412-414, (1966).

66. T.B. Tang and M.M. Chaudhri,
Jnl. of Thermal Analysis, 17 , 359-370, (1979).

67. T.B. Tang and M.M. Chaudhri,
Jnl. of Thermal Analysis, 18 , 247-261, (1980).

68. S.S. Al-Kazraji,
Ph.D. Thesis(Polytechnic of Wales), (1979).

69. G. Lombardi,
For Better Thermal Analysis, ICTA, (1980).

70. P.H. Kemp,
The Chemistry of Borates-A Review, Part 1,
Borax Consolidated Ltd., London, (1956).

71. J.C. Bailar, H.J. Emeleus, R. Nyholm, A.F. Trotman-Dickenson(Eds.),
Comprehensive Inorganic Chemistry, 1,
Pergamon Press, Oxford, (1973).

72. C.R.C. Handbook of Chemistry and Physics, 61st Edition,
C.R.C. Press Inc., Florida, (1981)

73. V.M. Gremyachkin, A.G. Istratov and O.I. Leipunskii,
Fizika Goreniya I Vzryva, 15 , 6, 5-13, (1979).

74. J.W. Mellor,
A Comprehensive Treatise On Inorganic And Theoretical
Chemistry, 5 , Longman, London, (1961).

75. L. Shartsis and E.S. Newman,
Jnl. Res. Nat. Bur. Standards, 40 , 471-478, (1948).

76. I.E. Campbell and E.M. Sherwood(Eds.),
High-Temperature Materials And Technology,
John Wiley & Sons Inc., New York, (1967).

77. A.Z. Moghaddam,
M.Phil. Thesis(Polytechnic of Wales), (1980).

78. Unpublished Research Report, Nobels' Explosives Co. Ltd..

79. R.Barber and T. Land,
Temperature-Its Measurement And Control In Science And
Industry, Advantages Of Silicon Detectors, 3 , Part 2,
Reinhold Publishing Corp., (1962).

80. Technical Note TN 56, Sirius Instruments Ltd..

81. E. Koch,
Non-Isothermal Reaction Analysis,
Academic Press Inc.(London) Ltd., (1977)

82. W. Komatsu,
5th Int. Symp. on The Reactivity of Solids(Proc), 182-191, (1964).

83. H.C. Cooper, E.H. Kraus and A.A. Klein,
Am. Chem. Jnl., 47 , 273-285, (1912).

84. W.E. Garner(Ed.),
Chemistry of the Solid State, Butterworth, London, (1955).

85. K.J. Holloway, G.W.C. Taylor and A.T. Thomas,
U.S. Patent 3954530, (1977).

86. D. Greninger, V. Kollonitsch, C.H. Kline and L.C. Willemsens,
Lead Chemicals, International Lead Zinc Research Organization Inc.,
New York, (1973).

87. M.E. Brown, D. Dollimore and A.K. Galwey,
1st European Symp. on Thermal Analysis(Proc), 248-251, (1976).

88. I.J. Lin, S. Nadiv and D.J.M. Grodzian,
Minerals Sci. Engng. (S. Africa), 7 , 4, 313-336, (1975).

89. V.M. Gorbachev,
Jnl. Thermal Analysis, 18 , 193-197, (1980).

90. M.I. Pope,
Analytical Division of the Chemical Soc.(Proc), 236-239, (1980).

91. P.D. Garn,
Jnl. Thermal Analysis, 13 , 581-593, (1978).

92. F.W. Wilburn,
Analytical Division of the Chemical Soc.(Proc), 221-223, (1980).

93. J.W. Matthews, C.J. Kircher and R.E. Drake,
Thin Solid Films, 47 , 95-108, (1977).

94. J.H. Sharp, G.W. Brindley and B.N.N. Achar,
Jnl. Am. Ceram. Soc., 49 , 7, 379-382, (1966).

95. M.S. Doulah,
Thermochimica Acta, 35 , 263-265, (1980).

96. M.S. Doulah,
Thermochimica Acta, 42 , 373-375, (1980).

97. A.Z. Moghaddam,
private communication, (1982).

APPENDIX

FIGURE 8.1

LEAD MONOXIDE S.S.A. ——— 0·58 $m^2\ g^{-1}$ (FISONS) BALLMILLED 4 HOURS

SILICON S.S.A. ——————— 10·6 $m^2\ g^{-1}$

OXIDISER/FUEL RATIO ——— 50/50(% wt.)

SAMPLE SIZE ——————— 4·97 mg

HEATING RATE ——————— $20^o\ min^{-1}$

CHART SPEED ——————— 20 mm min^{-1}

SENSITIVITY ——————— 21 mJ s^{-1} FULL SCALE DEFLECTION(F.S.D.)

ATMOSPHERE ——————— 20 ml min^{-1} DRY N_2

FIGURE 8.2

LEAD MONOXIDE S.S.A. ——— 0·38 $m^2\ g^{-1}$ PRODUCED BY Pb_3O_4 DECOMPOSITION

BORON S.S.A. ——————— 7·96 $m^2\ g^{-1}$

OXIDISER/FUEL RATIO ——— 50/50(% wt.)

SAMPLE SIZE ——————— 4·74 mg

HEATING RATE ——————— $10^o\ min^{-1}$

CHART SPEED ——————— 10 mm min^{-1}

SENSITIVITY ——————— 8·4 mJ s^{-1} F.S.D.

ATMOSPHERE ——————— 20 ml min^{-1} DRY N_2

FIGURE 8.3

REACTANTS ——————— PbO(BDH) AnalaR USED AS RECEIVED

B_2O_3(BDH) AnalaR USED AS RECEIVED

REACTANT RATIO ——————— 50/50(% wt.)

SAMPLE SIZE ——————— 16·3 mg

HEATING RATE ——————— $10^o\ min^{-1}$

CHART SPEED ——————— 10 mm min^{-1}

SENSITIVITY ——————— 8·4 mJ s^{-1}

ATMOSPHERE ——————— 20 ml min^{-1} DRY ARGON

FIGURE 8.5

LEAD MONOXIDE S.S.A. ——— 0·38 m^2 g^{-1} BOTH TRACES

BORON S.S.A.(ORIGINAL) ——— 7·96 m^2 g^{-1} BOTH TRACES

OXIDISER/FUEL RATIO ——— 50/50(% wt.) BOTH TRACES

SAMPLE SIZE ——— 4·5 mg BOTH TRACES

HEATING RATE ——— 10^{o} min^{-1} BOTH TRACES

CHART SPEED ——— 10 mm min^{-1} BOTH TRACES

SENSITIVITY ——— 8·4 mJ s^{-1} BOTH TRACES

ATMOSPHERE ——— 20 ml min^{-1} DRY ARGON

FIGURE 8.6

LEAD MONOXIDE S.S.A. ——— 1·51 m^2 g^{-1} ALL TRACES

BORON S.S.A. ——— 7·96 m^2 g^{-1} ALL TRACES

OXIDISER/FUEL RATIO ——— 97/3(% wt.) ALL TRACES

SAMPLE SIZE ——— TRACE A —— 4·11 mg

TRACE B —— 4·05 mg

TRACE C —— 4·06 mg

HEATING RATE ——— TRACE A —— 5^{o} min^{-1}

TRACE B —— 10^{o} min^{-1}

TRACE C —— 20^{o} min^{-1}

CHART SPEED ——— TRACE A —— 10 mm min^{-1}

TRACE B —— 20 mm min^{-1}

TRACE C —— 40 mm min^{-1}

SENSITIVITY ——— TRACE A —— 8·4 mJ s^{-1} F.S.D.

TRACE B —— 21 mJ s^{-1} F.S.D.

TRACE C —— 42 mJ s^{-1} F.S.D.

ATMOSPHERE ——— 20 ml min^{-1} DRY ARGON - ALL TRACES

FIGURE 8.8

LEAD MONOXIDE ———— PRECIPITATED FROM $Pb(NO_3)_2$ SOLUTION

BORON S.S.A. ———— $7{\cdot}96\ m^2\ g^{-1}$

OXIDISER/FUEL RATIO ———— NOMINAL 97/3(% wt.) 'COPRECIPITATE' BOTH TRACES

SAMPLE SIZE ———— 4·0 mg BOTH TRACES

HEATING RATE ———— $10^o\ min^{-1}$ BOTH TRACES

CHART SPEED ———— 20 mm min^{-1} BOTH TRACES

SENSITIVITY ———— 21 mJ s^{-1} BOTH TRACES

ATMOSPHERE ———— 20 ml min^{-1} DRY ARGON - BOTH TRACES

FIGURE 8.10

LEAD MONOXIDE S.S.A. ———— $0{\cdot}42\ m^2\ g^{-1}$ (BDH) UNTREATED

BORON S.S.A. ———— $7{\cdot}96\ m^2\ g^{-1}$

OXIDISER/FUEL RATIO ———— 50/50(% wt.)

SAMPLE SIZE ———— 7·25 mg

HEATING RATE ———— $10^o\ min^{-1}$

CHART SPEED ———— 10 mm min^{-1}

SENSITIVITY ———— 21 mJ s^{-1}

ATMOSPHERE ———— 20 ml min^{-1} DRY ARGON

FIGURE 8.11

LEAD MONOXIDE S.S.A. ———— TRACE A —— $0{\cdot}18\ m^2\ g^{-1}$ UNTREATED(FISONS)

TRACE B —— $0{\cdot}58\ m^2\ g^{-1}$ BALLMILLED 4 HOURS

TRACE C —— $1{\cdot}51\ m^2\ g^{-1}$ BALLMILLED 19 HOURS

BORON S.S.A. ———— $7{\cdot}96\ m^2\ g^{-1}$ ALL TRACES

OXIDISER/FUEL RATIO ———— 50/50(% wt.) ALL TRACES

SAMPLE SIZE ———— TRACE A —— 3·39 mg

TRACE B —— 6·02 mg

TRACE C —— 8·38 mg

HEATING RATE ———— $10^o\ min^{-1}$ ALL TRACES

FIGURE 8.11 CONTINUED

CHART SPEED ——————— 10 mm min^{-1}

SENSITIVITY ——————— 8·4 mJ s^{-1} F.S.D.

ATMOSPHERE ——————— 20 ml min^{-1} DRY N_2

FIGURE 8.12

LEAD MONOXIDE S.S.A. ——— 0·42 m^2 g^{-1}(BDH) UNTREATED

BORON S.S.A. ——————— 7·96 m^2 g^{-1}

OXIDISER FUEL RATIO ——— 97/3(% wt.)

SAMPLE SIZE ——————— 10·0 mg

HEATING RATE ——————— 20° min^{-1}

CHART SPEED ——————— 10 mm min^{-1}

ATMOSPHERE ——————— 20 ml min^{-1} N_2

FIGURE 8.13

LEAD MONOXIDE S.S.A. ——— 0·42 m^2 g^{-1}(BDH) UNTREATED

BORON S.S.A. ——————— 7·96 m^2 g^{-1}

OXIDISER/FUEL RATIO ——— 97/3(% wt.)

SAMPLE SIZE ——————— 10·0 mg

HEATING RATE ——————— 30° min^{-1}

CHART SPEED ——————— 10 mm min^{-1}

ATMOSPHERE ——————— 20 ml min^{-1} N_2

FIGURE 8.14

LEAD MONOXIDE S.S.A. ——— 0·42 m^2 g^{-1}(BDH) UNTREATED

BORON S.S.A. ——————— 7·96 m^2 g^{-1}

OXIDISER/FUEL RATIO ——— 97/3(% wt.)

SAMPLE SIZE ——————— 20 mg

HEATING RATE ——————— 10° min^{-1}

CHART SPEED ——————— 10 mm min^{-1}

ATMOSPHERE ——————— 20 ml min^{-1} N_2

FIGURE 8.15

LEAD MONOXIDE S.S.A. ——— $0{\cdot}42\ m^2\ g^{-1}$ (BDH) UNTREATED

BORON S.S.A. ——————— $7{\cdot}96\ m^2\ g^{-1}$

OXIDISER/FUEL RATIO ——— 97/3(% wt.)

SAMPLE SIZE ——————— 20·0 mg

HEATING RATE ——————— $20^{o}\ min^{-1}$

CHART SPEED ——————— 5 mm min^{-1}

ATMOSPHERE ——————— 20 ml min^{-1} N_2

FIGURE 8.16

LEAD MONOXIDE S.S.A. ——— $0{\cdot}42\ m^2\ g^{-1}$ (BDH) UNTREATED

BORON S.S.A. ——————— $7{\cdot}96\ m^2\ g^{-1}$

OXIDISER/FUEL RATIO ——— 80/20(% wt.)

SAMPLE SIZE ——————— 10.0 mg

HEATING RATE ——————— $30^{o}\ min^{-1}$

CHART SPEED ——————— 10 mm min^{-1}

ATMOSPHERE ——————— 20 ml min^{-1} N_2

FIGURE 8.17

LEAD MONOXIDE S.S.A. ——— $0{\cdot}42\ m^2\ g^{-1}$ (BDH) UNTREATED

BORON S.S.A. ——————— $7{\cdot}96\ m^2\ g^{-1}$

OXIDISER/FUEL RATIO ——— 80/20(% wt.)

SAMPLE SIZE ——————— 10·0 mg

HEATING RATE ——————— $50^{o}\ min^{-1}$

CHART SPEED ——————— 30 mm min^{-1}

ATMOSPHERE ——————— 20 ml min^{-1} N_2

FIGURE 9.2

LEAD ---------- BDH POWDER 43μm TO DUST

BORON S.S.A. ---------- 7·96 $m^2\ g^{-1}$

SAMPLE SIZE ---------- 50 mg

HEATING RATE ---------- $5^o\ min^{-1}$

SENSITIVITY ---------- 21 mJ s^{-1} F.S.D.

ATMOSPHERE ---------- 20 ml min^{-1}

FIGURE 9.3

LEAD ---------- AS FOR FIGURE 9.2

BORON ---------- AS FOR FIGURE 9.2

SAMPLE SIZE ---------- 33·3 mg

HEATING RATE ---------- $5^o\ min^{-1}$

SENSITIVITY ---------- 2·1 mJ s^{-1} F.S.D.

CHART SPEED ---------- 40 mm min^{-1}

ATMOSPHERE ---------- 20 ml min^{-1} DRY N_2

TABLE 9.2 REACTION EQUATION TYPES

D_1 -- One-dimensional diffusion processes with constant diffusion coefficient: $\alpha^2 = (k/x^2)t$ where 2x is the thickness of the reacting layer

D_2 -- Two-dimensional diffusion controlled reaction into a cylinder of radius r: $(1-\alpha)\ln(1-\alpha) + \alpha = (k/r^2)t$

D_3 -- Jander equation for a diffusion controlled reaction in a sphere: $(1-(1-\alpha)^{\frac{1}{3}})^2 = (k/r^2)t$ where r is the radius of the sphere

D_4 -- Ginstling and Brounshtein equation for a diffusion controlled reaction starting on the exterior of a spherical particle of radius r: $(1-2\alpha/3) - (1-\alpha)^{2/3} = (k/r^2)t$

F_1 -- First order reaction: $\ln(1-\alpha) = -kt$

R_2 — For a circular disc reacting from the edge inward, or for a cylinder, where the reaction is controlled by movement of an interface at a constant velocity u:
$(1 - (1 - \alpha)^{\frac{1}{2}}) = (u/r)t$ where r is the radius of the disc or cylinder

R_3 — For a sphere of radius r reacting from the surface inward, where the reaction is controlled by movement of an interface at a constant velocity

A_2 — Reaction controlled by nucleation of the reactant, followed by two-dimensional growth of nuclei. As nuclei grow they must eventually impinge on one another, so that growth ceases where they touch: $(-\ln(1 - \alpha))^{\frac{1}{2}} = kt$

A_3 — As for A_2 but with three-dimensional growth of nuclei:
$(-\ln(1 - \alpha))^{\frac{1}{3}} = kt$

FIGURE 9.7

$KMnO_4$	BDH LIGHTLY CRUSHED AND ALL MATERIAL LARGER THAN 43μm SIEVED OUT
HEATING RATE	$2{\cdot}5^{o}$ min^{-1}
SAMPLE SIZE	8·9 mg
CHART SPEED	20 mm min^{-1}
SENSITIVITY	4·2 mJ s^{-1} F.S.D.
ATMOSPHERE	10 ml min^{-1} DRY ARGON

FIGURE 9.9

LEAD	AS FOR FIGURE 9.2
BORON	AS FOR FIGURE 9.2
SAMPLE SIZE	35 mg
HEATING RATE	5^{o} min^{-1}
SENSITIVITY	2·1 mJ s^{-1} F.S.D.
CHART SPEED	40 mm min^{-1}
ATMOSPHERE	20 ml min^{-1} DRY N_2